CAMURE 12 & ISMR 11

8-11 SEPTEMBER 2024

Ghent, Belgium

12th International Symposium on
Catalysis in Multiphase Reactors
&
11th International Symposium on
Multifunctional Reactors

WHAT IS CAMURE 12 & ISMR 11?

The CAMURE (Catalysis in Multiphase Reactors) meeting was initiated in 1994 in Lyon, France, followed by subsequent gatherings in Toulouse (1998), Naples (2000), Lausanne (2002), and Portorose (2005). In 2005, CAMURE merged with ISMR (International Symposium on Multifunctional Reactors) during the Portorose Symposium. Prior ISMR meetings were held in Amsterdam (1999), Nuremberg (2001), and Bath (2003). The combined symposia took place in Pune (2007), Montreal (2009), Naantali (2011), Lyon (2014), Quindao (2017), and Milano (2021). The merger aimed to foster interdisciplinary discussions on multiphase catalytic systems and multifunctional reactors, covering areas such as catalysis, kinetics, heat/mass transfer, hydrodynamics, process intensification, catalyst design, and sustainable chemical processes. The International Scientific Committee is led by prof. dr. Claude De Bellefon (France) and prof. dr. Faiçal Larachi (Canada).

THANK YOU TO OUR SPONSORS:

Cargill™
fwo
Flanders
State of the Art
B.I.P.
elneo
ShARP Engineering
inter science
ExxonMobil

WITH THE SUPPORT OF

ACS ENGINEERING Au
AN OPEN ACCESS JOURNAL OF THE AMERICAN CHEMICAL SOCIETY

I&EC research
Industrial & Engineering Chemistry Research

AWARDS & SPECIAL ISSUE

BEST PRESENTATION AND POSTER AWARD

We are proud to announce also that CAMURE 12 & ISMR 11 will award the best 3 oral presentations and the best 2 poster presentations, which will be selected by the Scientific Commitee. The eligibility criteria will consider the excellence and originality of the research presented as well as the quality of the presentation. The awards, which are sponsored by ACS Engineering Au, will be presented during the Closing Ceremony.

SPECIAL ISSUE

We are pleased to announce that ACS Engineering and I&EC Research will feature a special issue dedicated to the CAMURE 12 & ISMR 11 conference. We welcome all presenters and their research teams to submit their work, provided it aligns with the journal's scope and was presented at the conference. The deadline for submission is 31st of October, 2024.

ACS ENGINEERING Au
AN OPEN ACCESS JOURNAL OF THE AMERICAN CHEMICAL SOCIETY

I&EC research
Industrial & Engineering Chemistry Research

© Travelinmotion

© Cedric Verhelst

© Boy Martin

GHENT

As one of Belgium's most vibrant cities, Ghent offers a unique cultural fusion, where ancient traditions blend harmoniously with modern ideas. With a rich heritage spanning over centuries, Ghent's story has been shaped by diverse influences, leaving an indelible imprint on its character.

Ghent embraces its role as a hub of creativity, attracting artists, researchers, and young innovators who thrive within its progressive atmosphere. Ghent is a city where people enjoy life: a chilled-out place where anything goes and a city that feels human.

Ghent is located at the intersection of the E17 and E40 and is therefore easily accessible by car and bus. With two train stations in the city and the international airport of Zaventem 'Brussels Airport' less than an hour away, train and plane are certainly an option.

THE VENUE

Academiestraat 1, 9000 Ghent

Thagaste is a unique venue in a magnificent monastery where fathers live and work. Besides a wide choice of characterful event rooms, there are special art treasures, a beautiful interior garden, the historic library and the baroque church with its valuable organs.

MAP OF THAGASTE

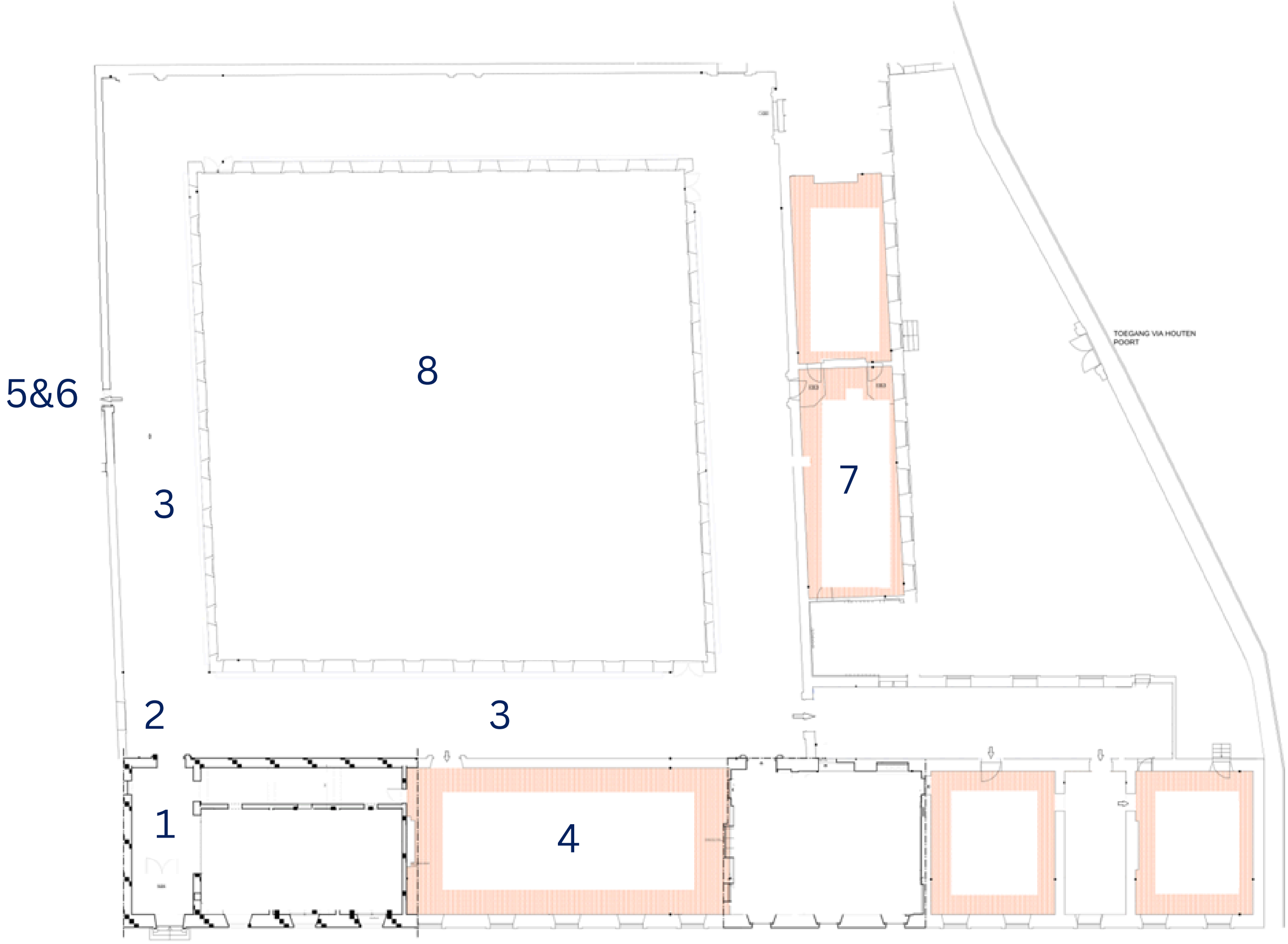

1. Entrance
2. Registration desk
3. Coffee break and poster area
4. Augustinus room
5. Stairs to Bibliotheek room
6. Rest room
7. Hippo room
8. Garden

SYMPOSIUM THEMES

Multidisciplinary program covering more traditional themes as well as very latest issues and novel developments in the field of multiscale modeling and experimentation.

REGULAR SESSIONS

- CATALYSIS AND KINETICS
- REACTOR DESIGN
- PROCESS DEVELOPMENT

THEMATIC SESSIONS

- LOW CARBON TECHNOLOGY
- RENEWABLE CHEMICALS
- PROCESS INTENSIFICATION

PLENARY SPEAKERS

Prof. Jesus Santamaria – Universidad de Zaragoza
Can heterogeneous catalysis change the way we treat cancer?

Prof. Louise Olsson – Chalmers University of Technology
The importance of catalysis for future biorefineries

Prof. Enrico Tronconi – Politecnico di Milano
Advancing catalytic processes for the energy transition

PROGRAMME

SUNDAY SEPTEMBER 8	MONDAY SEPTEMBER 9	TUESDAY SEPTEMBER 10	Wednesday SEPTEMBER 11
	Plenary session *Louise Olsson*	Plenary session *Enrico Tronconi*	**Process Development** **Low Carbon Technology**
	Break	Break	Break
	Catalysis and Kinetics **Renewable Chemicals**	**Reactor Design** **Renewable Chemicals**	**Catalysis and Kinetics** **Renewable Chemicals**
	Lunch break	Lunch break	
	Catalysis and Kinetics **Process Intensification**	**Reactor Design** **Plastic Recycling**	Closing Ceremony & Awards
	Break	Break	
Registration	**Catalysis and Kinetics** **Process Intensification**	**Low Carbon Technology** **Panel Debate**	
Opening Ceremony Plenary session *Jesus Santamaria*	Poster session with beer tasting	Boat trip in Ghent	
Welcome Reception		Conference dinner	

SUNDAY, SEPTEMBER 8

15:30-17:30 Registration

Augustinus
17:30-18:00 Opening Ceremony

18:00-19:00 **PLENARY SESSION I**
session chair: Joris Thybaut
Can heterogeneous catalysis change the way we treat cancer?
Jesus Santamaria – Universidad de Zaragoza

Corridors
19:00-21:00 Welcome Reception

◆ ◆ ◆ ◆ ◆ ◆ ◆ ◆

MONDAY, SEPTEMBER 9

Augustinus
9:00-10:00 **PLENARY SESSION II**
session chair: Mark Saeys
The importance of catalysis for future biorefineries
Louise Olsson – Chalmers University of Technology

Corridors
10:00-10:20 Coffee break

Augustinus **CATALYSIS AND KINETICS I**
session chair: Tapio Salmi and Jeriffa De Clercq

10:20-11:00 KEYNOTE Solid acid catalysts for esterification reactions – challenges with stability of acid sites
Josephine Hill – The University of Calgary

11:00-11:20 Cu/Al_2O_3 as a selective catalyst for (de)methylation of anisole and guaiacol
Snehasis Dutta, Setal A/P Govi Nair, Kateřina Pacultová, David Kubička

11:20-11:40 Reactions in three phase CO_2 methanation using LOHC as liquid phase
Mathias Held, Siegfried Bajohr, Thomas Kolb

11:40-12:00 The effect of mesopores in platelike H-ZSM-5 zeolites in the 1-butanol dehydration reaction
Phebe Lemaire, Arno de Reviere, Dhanjay Sharma, Joris W. Thybaut, Maarten K. Sabbe, An Verberckmoes

Bibliotheek RENEWABLE CHEMICALS I

session chair: Leon Lefferts and Robin Varghese

10:20-10:40 Insights into the mild catalytic reductive depolymerization of Soda lignin: link between the catalytic properties of Pd and PdCu catalysts and the derived product pools
Boyana Atanasova, Tibo De Saegher, Joeri Vercammen, An Verberckmoes, Jeriffa De Clercq, Jeroen Lauwaert

10:40-11:00 Metal sulfates-catalyzed depolymerization of cellulose to alkyl levulinates
Viktória Flóra Csendes, Karine Thomas, Sébastien Leveneur

11:00-11:20 Magnetically heated Ru-catalyst for levulinic acid HDO in electrified slurry reactor
Miha Grilc, Darko Makovec, Blaž Likozar, Sašo Gyergyek

11:20-11:40 Commercial polymeric waste mix characterization and pyrolysis in a lab-scale setup for gas and liquid fractions products valorization
Andrea Pastorino, Marcello Pagliero, Giancarlo Bruni, Renzo Di Felice, Antonio Comite

11:40-12:00 Catalytic Oxidation of Glucose: A Heterogeneous Pathway to Glucuronic Acid Production
Maher Elhallal, Vitaly Ordomski V., Mickael Capron

12:00-13:30 Lunch break

Augustinus CATALYSIS AND KINETICS II

session chair: Elio Santacesaria and An Verberckmoes

13:40-14:00 Optimization of temperature profile for di-methyl ether synthesis by CO_2 hydrogenation
Laura Duran Martinez, Isabelle Pitault, Isabelle Polaert

14:00-14:20 Kinetic study of CO_2 hydrogenation to formate over a solid micellar catalyst: unveiling the role of the base
Catarina Mendes, Javiera Rubio, Francisca Rebelo, Vitaly Ordomsky, Mark Saeys

14:20-14:40 Shining light on sustainability: CuInxGa1-xSe (CIGS) solar cells drive selective photocatalytic oxidation of methane
Duc Manh Nguyen, Chunyang Dong, Thomas Tom, Negar Naghavi, Vitaly V. Ordomsky, Andrei Y. Khodakov

14:40-15:00 Kinetics and modelling of direct CO_2 hydrogenation into liquid hydrocarbons
Antoinette Maarawi Chidraoui, Carlotta Panzone, Alban Chappaz, Geneviève Geffraye, Albin Chaise

15:00-15:20 Kinetic assessment of the heterogeneous catalyzed hydroformylation over a nanoparticle rhodium catalyst
Maria Herrero Manzano, Jeroen Poissonnier, Sébastien Siradze, Joris W. Thybaut

Bibliotheek PROCESS INTENSIFICATION I

session chair: Hannsjörg Freund and Yi Ouyang

13:40-14:20 KEYNOTE Process intensification: The potential and challenges of acoustic droplet based reactor systems
Leen Braeken – KU Leuven

14:20-14:40 Sorption-Enhancement with in-situ water removal for an intensified methanol production from carbon dioxide
Enrico Antonuccio, David Edouard, Pascal Fongarland

14:40-15:00 Development of semi-batch process for the synthesis of methyl pentanone
Nitin Sharma, Sumit Kamal

15:00-15:20 Study of heterogeneous enzymatic reactive distillation: from experiment to comprehensive modeling
Nicolas Chaussard, Clémence Nikitine, David Rouzineau, Michel Meyer, Pascal Fongarland

Corridors

15:20-15:40 Coffee break

Augustinus CATALYSIS AND KINETICS III

session chair: Leen Braeken and Jeroen Lauwaert

15:40-16:00 Transient techniques in the investigation of three-phase catalytic processes: epoxidation of alkenes in trickle bed reactor
Tapio Salmi, Vincenzo Russo, Matias Alvear Cabezón, Michele Emanuele Fortunato, Christoph Schmidt, Christopher Stäglich, Kari Eränen

16:00-16:20 Solid foam catalyst for three-phase sugar hydrogenation: semi-batch and continuous operation
German Araujo-Barahona, Alberto Goicoechea-Torres, Maria Ciaramella, Miriam Cavaliere, Kari Eränen, Dmitry Y. Murzin, Juan García-Serna, Vincenzo Russo, Tapio Salmi

16:20-16:40 Transient reaction kinetics for CO hydrogenation: Combining periodic experimentation with microkinetic modeling
Max Gäßler, Simon Hermann, Jens Friedland, Robert Güttel

16:40-17:00 Mechanistic insights into r-WGS reaction on Rh and Pt via a combined experimental and structure-dependent microkinetic analysis
Gabriele Spanò, Luca Nardi, Gabriele Contaldo, Raffaele Cheula, Chiara Negri, Matteo Maestri

17:00-17:20 Unravelling the liquid-phase oxidation of cyclohexane by computer-aided kinetic model development with ‘ALKIMO’
Kevin De Ras, Gust Popelier, Lander Nelis, Connor Huntwork, Robin Vercauteren, Unni Kurumbail, Joris W. Thybaut, Ive Hermans, Kevin M. Van Geem

Bibliotheek **PROCESS INTENSIFICATION II**
session chair: Tilman Schildhauer and Georgios Bellos

15:40-16:20 KEYNOTE
The Urgent Energy-Efficient Transition Towards an Electrified Chemical Sector for Reduced CO_2 Emissions
Patrice Perreault – Universiteit Antwerpen

16:20-16:40
Intensification of mass-transfer limited catalytic applications through POCS structured supports with optimized cell and streamlined strut shape
Claudio Ferroni, Mauro Bracconi, Matteo Ambrosetti, Matteo Maestri, Gianpiero Groppi, Enrico Tronconi

16:40-17:00
Model development of gas-liquid vortex reactor for process intensification of CO_2 capture
Afroditi Kourou, Gozde Gecim, Siyuan Chen, Geraldine J. Heynderickx, Yi Ouyang, Kevin M. Van Geem

17:00-17:20
Photodegradation of phenol in rotating disk reactor and 3D modelling
Ewan Westgate, Dom Johnson, Farid Aiouache

Augustinus

17:30-19:15 Poster session with beer tasting
17:30-17:45 Introduction to the secrets of Belgian beer (in Augustinus)
17:45-19:15 Poster session (in the corridors)

* * *

TUESDAY, SEPTEMBER 10

Augustinus
9:00-10:00 **PLENARY SESSION III**
session chair: Kevin Van Geem
Advancing catalytic processes for the energy transition
Enrico Tronconi – Politecnico di Milano

Corridors
10:00-10:20 Coffee break

Augustinus **REACTOR DESIGN I**
session chair: Jan Kopyscinski and Patrice Perreault

10:20-11:00 KEYNOTE
The complexity of kinetics of plasma-catalytic reactions
Leon Lefferts – University of Twente

11:00-11:20
InterPOCS for in operando adjustment of fluid flow and mass transport characteristics in heterogeneous catalysis
Lisa Eckendörfer, Hannsjörg Freund

11:20-11:40 Measurement of Bubble Property Distributions for Better Description of Mass Transfer Limitations in Chemical Reactors
Philipp Riechmann, Lukas Schlagenhauf, Evert C. Wagner, J. Ruud van Ommen, Tilman Schildhauer

11:40-12:00 Validity of the generalized film-model criteria for instantaneous gas-liquid reactions in Higbie's penetration model
Pieter Janssens, Jeroen Poissonnier, René Bos, Joris W. Thybaut

Bibliotheek RENEWABLE CHEMICALS II

session chair: Miha Grilc and Jeriffa De Clercq

10:20-11:00 KEYNOTE Heterogeneous Catalysis as Key Technology for Circular Economy – A Spotlight on Renewable Feedstocks and Hydrogen
Regina Palkowits – RWTH Aachen University

11:00-11:20 (Un)catalyzed depolymerization of hydrolysis lignin: experimental assessment and kinetic modelling
Lucas I. Garbarino, Matteo Deroma, Dhanjay Sharma, Jeriffa De Clercq, An Verberckmoes, Jeroen Lauwaert, Joris W. Thybaut

11:20-11:40 Reaction kinetics prediction and modeling in the 5-HMF solvolysis to alkyl levulinate aided by structure reactivity relationships
Erny Encarnacion Munoz, Jean-Christophe Buvat, Sébastien Leveneur

11:40-12:00 Exploring Selective Glucose Oxidation: Monometallic versus Bimetallic Catalysts
Žan Lavrič, Janvit Teržan, Ana Kroflič, Janez Zavašnik, Matej Huš, Miha Grilc, Blaž Likozar

12:00-13:30 Lunch break

Augustinus REACTOR DESIGN II

session chair: Robert Güttel and Patrice Perrault

13:40-14:20 KEYNOTE Multifunctional fluidized bed reactors: overview and case studies
Pedro Castano - KAUST

14:20-14:40 LOGIC 2,0: Characterisation of a natural convection driven methanol reactor
Tim van Schagen, Wim Brilman

14:40-15:00 Development of an improved one-dimensional fixed-bed catalytic reactor model through CFD simulations
Liantsoa Randriambololona, Arnaud Cockx, Philippe Schmitz, Marie-José Huguet, Olivier Peruch

15:00-15:20 Pilot scale methanation and PtG of (simulated) wood gasification
Tilman Schildhauer, Chiara Berretta, Lukas Schlagenhauf, Tanja Wieseler, Martin Künstle, Julian Indlekofer, Robert Janz, Daniel Erne

Bibliotheek

PLASTIC RECYCLING

session chair: Marvin Kusenberg and Kevin Van Geem

13:40-14:00 A combined experimental and modeling study of a 3D printed gyroidal copper structure for post-plasma chemical process intensification in non-reactive conditions

Victor Rosa, Fabio Cameli, Kevin M. Van Geem, Georgios Stefanidis

14:00-14:20 Maximizing Olefin Yields for Steam Cracking of Plastic Waste Pyrolysis Oils: An Experimental and Modeling Study

Tamás Buzogány, Ismaël Amghizar, Marvin Kusenberg, Lin Chen, David J. Brown, Guy B. Marin, Geraldine J. Heynderickx, Kevin M. Van Geem

14:20-14:40 Unlocking Radical Insights: Integrating Detailed Kinetic Modeling and Method of Moments for Pyrolysis of Polystyrene

Daniël Withoeck, Florence Vermeire, Oğuzhan Akin, Robin John Varghese, Kevin Van Geem, Steven De Meester, Paul Van Steenberge

14:40-15:00 Characterization and Pyrolysis Analysis of PVC Waste: Insights into Composition, Degradation Products, and HCl Emissions

Mohammadhossein Havaei, Robin John Varghese, Florent Minette, Eric Romers, Kevin Van Geem

15:00-15:20 Sustainable Waste Polypropylene Recycling: Enhancing Catalyst Stability and Selectivity in Light Olefin Production

Oğuzhan Akin, Qing He, Parviz Yazdani, Robin John Varghese, Kevin Van Geem

Corridors

15:20-15:40 Coffee break

Augustinus

LOW CARBON TECHNOLOGY I

session chair: Gunther Kolb and Yi Ouyang

15:40-16:20 KEYNOTE CO2 capture and utilization. From catalyst development and kinetic assessment to reactor design

Jan Kopyscinski – McGill University

16:20-16:40 Evaluation of the relevant mass and heat transfer phenomena in a packed bed membrane reactor for the direct conversion of CO_2 to dimethyl ether

Serena Poto, Huub van den Bogaard, Fausto Gallucci, Fernanda Neira D'Angelo

16:40-17:00 Design and construction of a large-scale GDE-based electrolyzer for sustainable formate production using CO_2 as feedstock

Jose Antonio Abarca, Axel Arruti, Esther Santos, Guillermo Díaz-Sainz, Angel Irabien

17:00-17:20 Alternative to Claus process through COS as intermediate: CO_2 and H_2S competitive adsorption and reaction on sodium zeolites

Marco Fabbiani, Syeda Rabia Batool, Ludovic Pinard, Alexey Novikov, Helene Retot, Igor Shlyapnikov, Valentin Valtchev

Hippo **PANEL DEBATE**
moderators: Annick Meersman and Erik Paredis

15:40-17:20 “Innovations and technical challenges: Expected future for plastics recycling”
Kevin Van Geem, Jeremias Michal, Azd Zayoud, Geoff Brighty, Steven De Meester

“Towards a circular economy: Social acceptance of chemical recycling”
Kevin Van Geem, Rémi Tilkin, Alexander Röder, Saskia Walraedt, Werner Bosmans

17:50-19:00 Boattrip in Ghent
Meeting point: Sint-Antoniuskaai, 9000 Ghent

19:00-24:00 Conference dinner in Café Theatre
Schouwburgstraat 7, 9000 Ghent

* * *

WEDNESDAY, SEPTEMBER 11

Augustinus **PROCESS DEVELOPMENT**
session chair: Pedro Castano and Georgios Bellos

09:00-09:40
KEYNOTE
From kinetic model to process simulation: production of levulinate
Sébastien Leveneur – INSA Rouen

09:40-10:00 Electrothermal Fluidized Bed Reactor model for high temperature endothermic reactions: The case of COS decomposition
Klaus Jacobs, Soroush Zareghorbaei, Jeroen Lauwaert, Igor Shlyapnikov, Miha Grilc, Gleb Veryasov, Joris W. Thybaut

10:00-10:20 Techno-economic analyses of NETmix-based facilities for the production of CO_2 hydrates
Isabel S. Fernandes, Mariana G. Domingos , Marcelo F. Costa, Ricardo J. Santos, José C. B. Lopes

Bibliotheek **LOW CARBON TECHNOLOGY II**
session chair: Isabelle Polaert and Joris Thybaut

08:40-09:00 Intensifying the catalytic process via the conservative perturbed equilibrium (CPE): methane tri-reforming as an example
Mykhailo O. Vilboi, Vitaly R. Trishch, Gregory S.Yablonsky

09:00-09:20 CFD design of photocatalytic mesostructured reactors for green ammonia production
Isabel S.O. Barbosa, M. Teresa Oliveira, Margarida S.C.A. Brito, Cláudia G. Silva, Ricardo J. Santos

09:20-09:40 Spatially resolved measurements and reactive CFD modelling of the selective catalytic reduction of nitrogen oxides in the context of future hydrogen engines
Lisa Nordhausen, Marie Richter, Marion Börnhorst

09:40-10:00 Ni-decorated $BiVO_4/WO_3$ photoanodes for an enhanced photoelectrochemical response under solar light
Ivan Merino-Garcia, Sara Crespo, Jose Antonio Abarca, Jonathan Albo

10:00-10:20 Catalyst coatings for hydrogen generation by ammonia decomposition at high temperatures and elevated pressure
Gunther Kolb, Tobias Weissenberger, Ralf Zapf, Helmut Pennemann

Corridors
10:20-10:40 Coffee break

Augustinus

CATALYSIS AND KINETICS IV

session chair: Pascal Fongarland and Mark Saeys

10:40-11:00 Impact of mild hydrothermal aging on NH_3, NO, CO, and SO_2 oxidation kinetics on a Cu/SSZ-13 catalyst
Tetyana Zheleznyak, Petr Kočí, William Epling

11:00-11:20 Upscaling of a debenzylation reaction in pharmaceutical synthesis: the mass transfer paradox
Wout Callewaert, Jeroen Lauwaert, Mairtin McNamara, Joris W. Thybaut

11:20-11:40 Transient methods to overcome the thermodynamic limits of the levulinic acid esterification
Vincenzo Russo, Francesco Taddeo, Riccardo Tesser, Martino Di Serio

11:40-12:00 Elucidating the Effect of Hydrocarbon Structure and Zeolite Topology on the β-Scission Activation Energy
Yannick Ureel, Konstantinos Alexopoulos, Maarten K. Sabbe, Kevin M. Van Geem

Bibliotheek

RENEWABLE CHEMICALS III

session chair: Josephine Hill and Jeroen Lauwaert

10:40-11:00 Novel superbases as organocatalysts in low temperature depolymerization of polyethylene terephthalate (PET)
Ali Harlin, Henri Olander, Erno Karjalainen

11:00-11:20 Evaluation of piston reactor to produce hydrogen from methane via gas-phase SMR and ATR routes
Aya Abousrafa, Mary Anna Katebah, Patrick Linke, Ma'moun Al-Rawashdeh

11:20-11:40 Kinetic modelling and packed bed reactor technology in the catalytic oxidation of furfural to valuable products
Enrico Marchi, Wander Perez Sena, Kari Eränen, Johan Wärnå, Dmitry Murzin, Tapio Salmi

11:40-12:00 Levulinate esters valorization: the production of γ-valerolactone and ethyl pentenoates through an innovative gas-phase continuous flow process
Luca Visentin, Pietro Zappalorti, Stefania Albonetti, Nikolaos Dimitratos, Leandro Ardemani, Nicola Scotti, Tommaso Tabanelli, Fabrizio Cavani

Augustinus
12:00-12:30 Closing Ceremony & Awards

* * *

POSTER SESSION

1 Process intensification for ammonia synthesis – Analyzing the potential of in situ product removal for high single-pass conversion
Theresa Kunz, Johannes Geri, Robert Güttel

2 Equations of state: The critical component of supercritical water-hydrocarbon mixtures
Gust Popelier, Maarten Sabbe, Florence Vermeire, Kevin M. Van Geem

3 Modeling of baker's yeast and ethanol production by *Saccharomyces Cerevisiae*
Elio Santacesaria, Riccardo Tesser, Martino Di Serio

4 Intelligent catalyst carrier concept with reversible wall contact in tubular reactors for an improved wall heat transfer
Dominik Rudolf, Hannsjörg Freund

5 Epoxidation of tall oil in the presence of metal doped SBA15 heterogeneous catalysts
Tommaso Cogliano, Angie Desgouliere, Wander Perez Sena, Kari Eränen, Vincenzo Russo, Laurence Pirault-Roy, Tapio Salmi

6 Thermocatalytic decomposition of methane over innovative ordered mesoporous Carbons and Carbon Black
Simon De Langhe, Soroush Zareghorbaei, Hilde Poelman, Vladimir Galvita, Dirk Poelman, Joris W. Thybaut, Kevin M. Van Geem

7 Microkinetic analysis of acid gas conversion to COS by zeolite 13X
Raman Ghassemi, Soroush Zare Ghorbaei, Jeroen Lauwaert, Marco Fabbiani, Ludovic Pinard, Valentin Valtchev, Joris W. Thybaut

8 Experimental and numerical assessment of radial thermal behavior of chemical looping packed bed reactor
Ahmed Aman Ismaeel Ali, Vincenzo Spallina

9 CO and O_2 solubility in different mixtures of ethanol, acetonitrile and water at high temperatures and pressures
Maan Al Jurdi, Assaad Zoughaib, Tetiana Krachko, Tawfiq Nasr Allah, Benoît Illy

10 DPA synthesis: a feasibility study towards the continuous application
Francesco Taddeo, Federica Orabona, Domenico Licursi, Claudia Antonetti, Vincenzo Russo, Anna Maria Raspolli Galletti, Martino Di Serio

25 Single pellet string reactors – Theoretical study on heat and mass transport limitations based on the CO_2 methanation
Christian Bauer, Tabea Gros, Olaf Hinrichsen

26 Coalescence and rebound of bubbles in gas-liquid dispersed systems: experiments and theory
Runci Song, Jie Chen, Luchang Han, Chao Yang

27 Comparative study of conventional and ozone-assisted catalytic oxidation of methane using Mn/Hydroxyapatite catalyst: introducing a novel setup
Reza Monjezi, Alexandra Bouriakova, Karen Leus, Philippe M. Heynderickx,
Pascal Van Der Voort, Rino Morent, Joris W. Thybaut

28 A facile biomass carbon-based composite for application in electrochemistry
Cristina M. S. G. Baptista, Christopher M. A. Brett, Marcelino L. Gimenes,
Mara Heloisa N. O. Scaliante, Wanderson da Silva, Wardleison M. Moreira

29 Characterization and modelling of an innovative elastic foam-bed Reactor (EFR) for gas-liquid(-solid) multiphase applications
Laura TRICAS, Pascal FONGARLAND, Régis PHILIPPE, David EDOUARD

30 Computational Benchmark for Vanadium Oxide clusters in oxidative dehydrogenation of propane
Dilan Tunçer, Elisabete Maria Tangerino Pinto, Sara Santos, Max Bols, Mark Saeys

31 MICS: Green and sustainable products & materials from non-critical and secondary raw sources
Martino Di Serio, Federica Orabona, Federica Recupido, Francesco Taddeo,
Giuseppe Cesare Lama, Letizia Verdolotti, Vincenzo Russo

32 GCM development to predict liquid organic hydrogen carrier properties and to evaluate energetically their hydrogenation/dehydrogenation cycle
Javier Álvarez-Valcarce, Antonio Tabernero, Eva M. Martín del Valle

33 Single Bubble Rise in Marinized Fluidized Beds
Athena Adabi, Ali Akbar Sarbanha, Seyed Mohammad Taghavi, Faïçal Larachi

34 Kinetics and reaction mechanism of limonene epoxidation with hydrogen peroxide promoted by Al_2O_3
Rosa Turco, Wander Perez Sena, Federica Orabona, Martino Di Serio, Kari Eränen,
Dmitry Murzin, Vincenzo Russo, Tapio Salmi

35 Post-Plasma Catalytic Toluene Abatement over Mn-Cu based Oxides Supported on Hydroxyapatite
Anastasiia Gromova, Jean-Marc Giraudon, Jean-Francois Lamonier, Maryam Nilkara
Karen Leus, Mikhail Gromov, Christophe Leys, Nathalie De Geyter, Rino Morent

36 Optimizing Photocatalytic Reactor Design for Enhanced Indoor VOC Decomposition
Hadis Mortazavi Milani, Ewoud Cosaert, Dirk Poelman

37 BHET hydrolysis kinetics in a batch reactor
Riccardo Tesser, Vincenzo Russo

38 CFD simulations and surrogate modeling approach of photocatalytic reactor for ethanol oxidation
Mohammad Rusydi Fatahillah, Quinten Nijs, Geraldine J. Heynderickx

CAMURE 12
ISMR 11

ABSTRACT BOOK

12th International Symposium on
Catalysis in Multiphase Reactors
&
11th International Symposium on
Multifunctional Reactors

PLENARY SESSION

Sun. 08/09 // 18:00-19:00

PLENARY SESSION I

Can heterogeneous catalysis change the way we treat cancer?

Jesus Santamaria[1,2,3]

[1]Instituto de Nanociencia y Materiales de Aragón (INMA), CSIC-Universidad de Zaragoza, Zaragoza 50009, Spain. [2]Department of Chemical and Environmental Engineering Universidad de Zaragoza Campus Rio Ebro, 50018 Zaragoza, Spain.[3]Networking Research Center on Bioengineering, Biomaterials and Nanomedicine (CIBER-BBN), 28029 Madrid, Spain

jesus.santamaria@unizar.es

Highlights

- Heterogeneous catalysis has the potential to be a game changer in oncology
- Generation of toxic species inside the tumor
- Destruction of key molecules needed for proliferation
- Selective catalyst delivery or selective activation inside the tumor is needed

Abstract

Catalysis is the obvious choice when the goal is to facilitate or to inhibit certain processes in complex reaction environments. Because of this, its huge potential to modify the tumor microenvironment chemistry towards a growth inhibition scenario has been recognized for some time. However, in spite of the exciting opportunities it affords, catalysis remains a scarcely explored tool in oncology, due to the huge challenges involved in developing suitable catalysts and delivering them selectively to a growing tumor.

This scenario could be about to change, thanks to recent developments in this field. A family of catalysts capable of working within the tumor environment has now emerged, enabling a range of new therapeutic strategies based on specific reactions: depletion of molecules key for tumor growth, such as glucose or amino acids, generation of reactive oxygen species in the tumor microenvironment, and fabrication of toxic drugs via de-protection chemistry are some of the possibilities afforded. Even more importantly, different methods to deliver catalysts to the tumor with sufficient selectivity are being actively developed. When this is not possible, on-site catalyst activation methods offer an elegant alternative to confine the catalytic action to the tumor. Last but not least, novel strategies to preserve the active life of the catalyst in a hostile environment teeming with deactivating (e.g. sulfur- containing) molecules are also needed.

In this talk, some of the most recent developments from our laboratory in this field will be presented, and the challenges that must be solved for the application of catalysis in oncology will be discussed.

References

[1] Sancho-Albero et al. Nature Catalysis 2, 864-72, (2019)
[2] Sancho-Albero et al. Nature Protocols 16, 131-63, (2021)
[3] Sancho-Albero et al. J. Extracellular Vesicles 11:e12193 (2022).
[4] Bonet-Aleta et al. Chemical Science, 13, 8307-20, (2022)
[5] Rubio-Ruiz et al. Nano Letters, 23, 804-11, (2023)
[6] Bonet-Aleta et al. Nano Letters, 24, 4091-4100, (2024)

Mon. 09/09 // 09:00-10:00

PLENARY SESSION II
The importance of catalysis for future biorefineries.

Louise Olsson *

Chemical Engineering, Chalmers University of Technology, Gothenburg, 41296, Sweden

**Corresponding author: louise.olsson@chalmers.se*

Highlights

- Catalysis will play a major role for the production of renewable fuels and chemicals
- Co-processing Kraft lignin with pyrolysis oil could suppress the solid char formation
- 5-HMF could effectively be upgraded using Ni catalyst, but it can be deactivated by residual DMSO
- Tests in a refinery unit for advanced biofuel production showed the contaminants Fe, P, K and Na

1. Introduction

Biorefineries will be critical for the future in order to produce chemicals and materials from biomass. Biomass is composed mainly of lignocellulose, which largely consist of cellulose (~40-50%), hemicellulose (~20-30%) and lignin (~20-30%) [1]. In order to produce chemicals and fuels from biomass it needs first to be depolymerized, which could be done for example by catalytic fast pyrolysis or reductive catalytic fractionation (RCF) to produce bio-oils. Another possibility is to first take out the cellulose and hemi-cellulose and make valuable products out of these, and thereafter depolymerize the lignin. Lignin is a highly branched complex 3D amorphous network of aromatic compounds and after depolymerization it results in very complex bio-oils, with hundreds and hundreds of components. In addition, during lignin depolymerization it forms unwanted char. The cellulose can be used to produce sugars, from which different platform chemicals can be produced by catalytic processes, such as e.g. 5-hydroxymethylfurfural (5-HMF) [2], 2,5-Furandicarboxylic acid (FDCA) and levulinic acid (LA). From these platform chemicals various chemicals can be produced.

2. Methods

Catalysts were prepared, both supported catalysts [2] as well as unsupported catalysts [3]. The catalysts were characterized using multiple methods such as BET, ICP, SEM, TEM, XRD, CO chemisorption and NH_3 TPD. The feedstock, e.g. sawdust, lignin, pyrolysis oil was upgraded in three-phase batch reactors at high hydrogen pressure. The produced bio-oils are examined using GCxGC/MS, NMR, Karl Fischer, TGA, FTIR and elemental analysis.

3. Results and discussion

Different catalytic reactions for producing renewable fuels and chemicals from biomass and waste feed stock will be shown. In this section a few examples are given. Reductive catalytic liquefication was examined for Kraft lignin depolymerization [3]. A major issue with lignin depolymerization is the formation of solid char formation, which reduces the bio-oil yield and also results in catalyst deactivation. When using a NiMoS catalyst at 400 ºC and 75 bar H_2 about 14 % char was observed (see Figure 1). We thereafter added small amount of pyrolysis oil and found an increase of char. Interestingly, when adding about 50% pyrolysis oil together with the Kraft lignin the char formation was suppressed and when using the same amount of pyrolysis oil and lignin no char was detected [3]. Based on several experiments with model compounds, we suggest that the reason for the char suppressing effect of pyrolysis oil is that the small molecules in the pyrolysis oil act as capping agents thereby blocking the lignin radicals and hindering the repolymerization. We also found that upgrading of hydrolysis lignin decreased the char formation compared to Kraft lignin and we suggest that this is due to that hydrolysis lignin contain less ash, has a more reactive structure and that the remaining cellulose compounds could act as capping agents [4].

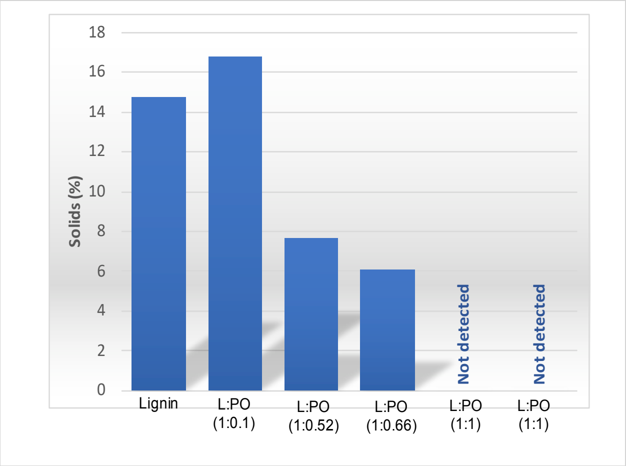

FiguFigure 1.. The solid residue formation from slurry-hydrocracking experiments using a NiMoS catalyst at 400 ºC and 75 bar H_2 using Kraft lignin (L), and co-processing Kraft lignin with different fractions of pyrolysis oil (PO).

The sugar platform from cellulose, opens up for very large possibilities to produce various renewable chemicals. We have studied the upgrading of 5-HMF to valuable products, such as 2.5-Bis (hydroxymethyl)furan (BHMF) [4]. We found that Ni/SiO_2 catalysts exhibited superior performance with a total yield of BHMF of up to 99 wt.% at 180 ºC, 75 bar H_2 for 2 h. This excellent performance might be attributed to the high Ni dispersion and low acidity of the support. Moreover, in some routes to prepare 5-HMF, DMSO is used, and we found that residues of DMSO was detrimental for the process.

We have prepared $NiMo/Al_2O_3$ catalysts at Chalmers and added these to a real refinery unit for advanced biofuel production for several months and the spent catalysts were thereafter recovered. We found contaminants such as Fe, P and alkalis (like Na and K) in the spent catalysts. Further model deactivation studies were conducted.

4. Conclusions

To summarize, catalysis will play a key role in a future bio-refinery. Catalysts can aid the depolymerization in for example RCF and catalytic fast pyrolysis. It is also crucial for the upgrading of the different components, for example for producing chemicals from the cellulose platform and upgrading the depolymerized bio-oils to produce different chemical compounds and renewable fuels. We have shown a catalytic process for HMF upgrading using a nickel-based catalyst and that it can be deactivated by residuals of DMSO from the 5-HMF production. Renewable fuel production can be enhanced by the usage of hydrolysis lignin compared to Kraft lignin. The char formation during Kraft lignin depolymerization could be completely suppressed by a co-process with pyrolysis oil. Moreover, results showed that contaminants such as Fe, P and alkalis (like Na and K) were present after experiments in a real refinery unit for advanced biofuel production.

References

[1] Y.H. Liao, S.F. Koelewijn, G. Van den Bossche, J. Van Aelst, S. Van den Bosch, T. Renders, K. Navare, T. Nicolai, K. Van Aelst, M. Maesen, H. Matsushima, J.M. Thevelein, K. Van Acker, B. Lagrain, D. Verboekend, B.F. Sels, 367 (2020) 1385

[2] A. Achour, D. Bernin, D. Creaser, L. Olsson, Chemical Engineering Journal, 453 (2023) 139829

[3] *Y*.W. Cheah, R. Intakul, M.A. Salam, J. Sebastian, P.H. Ho, P. Arora, O. Öhrman, D. Creaser, L. Olsson, 475 (2023) 146056.

[4] Ojagh, A. Achour, P.H. Ho, D. Bernin, D. Creaser, O. Pajalic, J. Holmberg, L. Olsson, Reaction Chemistry & Engineering, 7 (2021) 192-200

Keywords

Bio-refinery, heterogeneous catalysis, biofuel, renewable chemicals

Tue. 10/09 // 09:00-10:00

PLENARY SESSION III

Advancing Catalytic Processes for the Energy Transition: Joule-Heated Structured Reactors as a Key Solution for Decarbonization and Intensification..

Matteo Ambrosetti, Alessandra Beretta, Gianpiero Groppi, Enrico Tronconi*

LCCP, Dipartimento di Energia, Politecnico di Milano, via La Masa 34, 20156 Milano, Italy

**Corresponding author: enrico.tronconi@polimi.it*

Highlights

- Cellular catalyst substrates enable enhanced conductive heat transfer and direct ohmic heating
- SMR over Joule-heated washcoated SiSiC foams promises reduced process footprint and low-C H_2
- Same concept for electrification of CO_2 methane reforming and reverse water-gas shift

1. Introduction

The adoption of thermally conductive structured substrates in tubular reactors allows to shorten industrial multi-tubular reactors for non-adiabatic applications, as well as to operate heat-transfer limited catalytic processes at intensified conditions [1]. In Milano we have studied conductive cellular structures with interconnected cavities (open-cell foams, 3D printed periodic-open-cell-structures, aka POCS) applied to the intensification of e.g. the strongly exothermic Fischer-Tropsch synthesis [2] and the endothermic Steam Methane Reforming [3]. Further to exploiting the continuous matrix of cellular substrates for heat conduction, we are now exploring their electrical conductivity for direct ohmic heating of the catalyst in endothermic heat-transfer limited processes, in view of combined intensification and electrification [4] of key catalytic processes for the energy transition. Renewable electricity can be converted into heat and thermally drive chemical reactors. In this context, electrified steam methane reforming (eSMR) is a promising concept for low-carbon H_2 production, as it offers potential to utilize excess energy to produce either building blocks for chemical processes or clean fuels, while at the same time mitigating CO_2 emissions. Moreover, by bringing the heat source closer to the catalytic sites, it drastically reduces the heat transfer limitations, which are the bottleneck of the conventional SMR process, allowing for process intensification. Wismann et al. [5] have proposed direct Joule heating of a FeCrAl-alloy tube washcoated with Ni-catalyst for SMR. The performance of such a reformer configuration is controlled by external mass transfer limitations, which calls for the adoption of tubes with small diameters, leading eventually to the development of reactor solutions based on either honeycomb monoliths or micro-channel technologies. Compared to laminar flow in wall coated reactors, open cell foam catalysts could greatly reduce external mass transfer limitations. Along these lines, we have demonstrated the feasibility of direct electrification of SiSiC foam structures, washcoated with a Rh/ Al_2O_3 catalyst, for the strongly endothermic SMR reaction [6-8]. The application of the same approach to the direct electrification of the CO_2 reforming of methane (eCRM) and to the reverse water-gas shift (eRWGS) processes in washcoated structured reactors [9] will be also reported.

2. Methods

In our electrified tubular reactor, a SiSiC foam serves both as the catalyst support and as the Joule heating element connected to an external power supply via steel connectors (Figure 1(a)). 80% of the foam is washcoated with an active 1% Rh/Al2O3 catalyst formulation, while the 20% uncoated entry region is used to preheat the feed stream. Outlet temperatures (Tdown) and compositions are monitored by a thermocouple and a micro GC [6].

3. Results and discussion

A specific energy demand as low as 1.24 kWh/Nm$^3_{H2}$ and a high H_2 productivity of approx. 8200 Nm$^3_{H2}$//h/m$^3_{foam}$ were measured in eSMR tests on a washcoated SiSiC foam with a catalyst density of 88 g/L (GHSV = 150000 cm^3/h/g$_{cat}$, S/C = 4.1, ambient pressure, Figure 1(d)), accompanied by an unprecedented high energy efficiency of 81%. Preliminary scale up simulations promise high energy intensities and H_2 productivities in compact eSMR reactors.

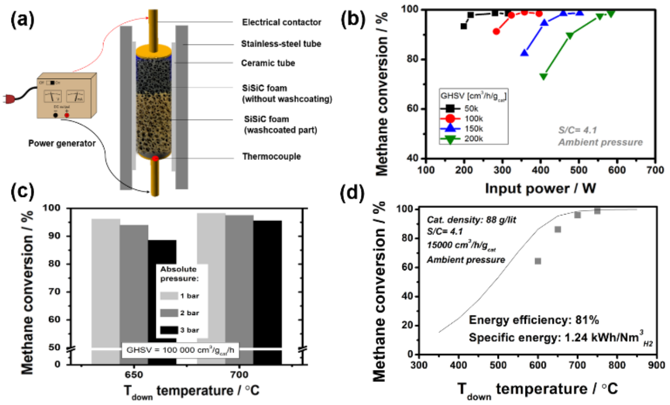

Figure 1.. (a) Electrified methane steam reforming (eSMR) reactor layout; (b) CH4 conversion vs. input power at different space velocities, 2.2 g of 1% Rh/Al2O3 washcoated (4/5) on SiSiC foam; (c) CH4 conversion vs. Tdown at different pressures, 2.5 g of 1% Rh/Al2O3 washcoated (4/5) on SiSiC foam; (d) Methane conversion vs. Tdown during runs at intensified conditions, 5.5 g of 1% Rh/Al2O3 washcoated (4/5) on SiSiC foam.

4. Conclusions

Direct Joule heating of cellular reactor internals removes the heat and mass transfer limitations affecting conventional packed-bed reactors for the SMR process and reduces drastically its footprint by eliminating the firebox. If electricity from RES is used, low-carbon hydrogen can be produced. The same concept paves the way for the intensification of other endothermic catalytic processes which are highly relevant for the ongoing energy transition.

Funding from European Research Council (ERC) (GA No. 694910 -'INTENT') and MIUR (PRIN Bando 2020, project "PLUG-IN") is gratefully acknowledged.

References

[1] E. Tronconi et al., Curr. Opin. Chem. Eng. 5 (2014) 55–67.
[2] L. Fratalocchi. et al., Cat. Today 383 (2022) 15-20.
[3] R. Balzarotti et al., Front. Chem. Eng. 3 (2022) 811439.
[4] K. Van Geem et al., Science 364 (2019) 734-735.
[5] S.T. Wismann et al., Science 364 (2019) 756-759.
[6] L. Zheng et al., ACS Eng. Au (2023) 4 (2024) 4-21.
[7] L. Zheng et al., AIChE J. 69 (2022) e17620.
[8] L. Zheng, et al., Int. J. Hydrog. Energy 48 (2023) 14681.
[9] L. Zheng, et al., Chem. Eng. J. 466 (2023) 143154.

Keywords
Process electrification, Joule heating, structured catalysts.

CATALYSIS AND KINETICS

Mon. 09/09 // 11:00-11:20

CK – I – 1

Cu/Al2O3 as a selective catalyst for (de)methylation of anisole and guaiacol col

Snehasis Dutta[1], Setal A/P Govi Nair[1,2], Kateřina Pacultová[3], David Kubička[1,4*]

[1]Department of Sustainable Fuels and Green Chemistry, University of Chemistry and Technology Prague, Technická 5, 166 28 Prague 6, Czech Republic

[2]Department of Fundamental and Applied Sciences, Universiti Teknologi PETRONAS, 32610, Bandar Seri Iskandar, Perak Darul Ridzuan, Malaysia

[3]Institute of Environmental Technology, CEET, VSB-Technical University of Ostrava, 17. listopadu 2172/15, 708 00 Ostrava, Czech Republic

[4]Technopark Kralupy, University of Chemistry and Technology Prague, nám. G. Karse 7, 278 01 Kralupy nad Vltavou, Czech Republic

**Corresponding author: kubickad@vscht.cz*

Highlights

- Cleavage of the O-CH_3 bond of anisole and guaiacol occurs on Lewis acid sites at elevated temperatures, which is followed by methylation of the aromatic ring and -OH group.
- Dimethoxybenzene formed by the methylation at the -OH group of guaiacol, may further undergo (de)methylation.
- Reaction conversion does not depend on the loading of Cu, however, it is enhanced by increasing the catalyst contact time.

1. Introduction

Studying of demethylation reactions of anisole and guaiacol is an important aspect of hydrodeoxygenation (HDO) of lignin-derived phenolics [1-3]. Cleavage of the O-CH_3 bond, followed by reattachment of the -CH_3 group to the aromatic ring is vital for improving 'HDO atom economy' by preventing the loss of C atoms from the feedstock. This work reports the use of Cu/Al_2O_3 as a selective catalyst for the (de)methylation of anisole and guaiacol. The effect of the wt.% of Cu in the catalyst has been studied to shed light on the relevant active sites. The reaction was carried out at various catalyst contact times allowing for the visualization of the reaction pathway.

2. Methods

We have synthesized Cu/Al_2O_3 catalysts of various Cu loading (3, 10, 15 wt.%) using wet impregnation of $Cu(NO_3)_2$ precursor on a commercially available ɣ-Al_2O_3. The materials were dried at 120 °C and calcined at 350 °C. The nature of the crystallites in the catalysts was studied by XRD and their acidic sites were analyzed by NH_3-TPD. Before testing for (de)methylation reaction of anisole and guaiacol, the catalysts were reduced in-situ in a flow-reactor at 220 °C. They were then tested at 270-300 °C, 5 bar H_2 pressure, H_2/feed molar ratio of 8, and various weight average space velocities (WHSV 4-30 h^{-1}). The spent catalysts were characterized by XRD and CHNS analysis.

3. Results and discussions

When Al_2O_3 and 10 wt.% Cu/Al_2O_3 were tested with anisole at 300 °C, 5 bar, and WHSV 30 h^{-1}, conversion of about 7 and 20%, respectively, was reached. The primary products were phenol, methyl phenol, dimethyl phenol, and methyl anisole. Guaiacol was found to be less reactive as compared to anisole and resulted in about 20% conversion over Cu/Al_2O_3 catalysts at 300 °C, 5 bar, and WHSV 4h^{-1}. When the Cu loading on the catalyst was increased from 1 to 3 wt.% the conversion was found to increase from 13 to about 20%. However, a further increase in Cu loading did not enhance guaiacol conversion (Figure 1a, top). This indicates that the reaction mainly occurs at the active sites provided by the alumina support and the activity is enhanced by Cu preventing coke formation on the surface. The coke formation on Al_2O_3 is visible from the spent catalysts (Figure 1a, bottom). Guaiacol conversion was found to increase with the catalytic contact time, which allowed the visualization of the reaction progress (Figure 1b, bottom).

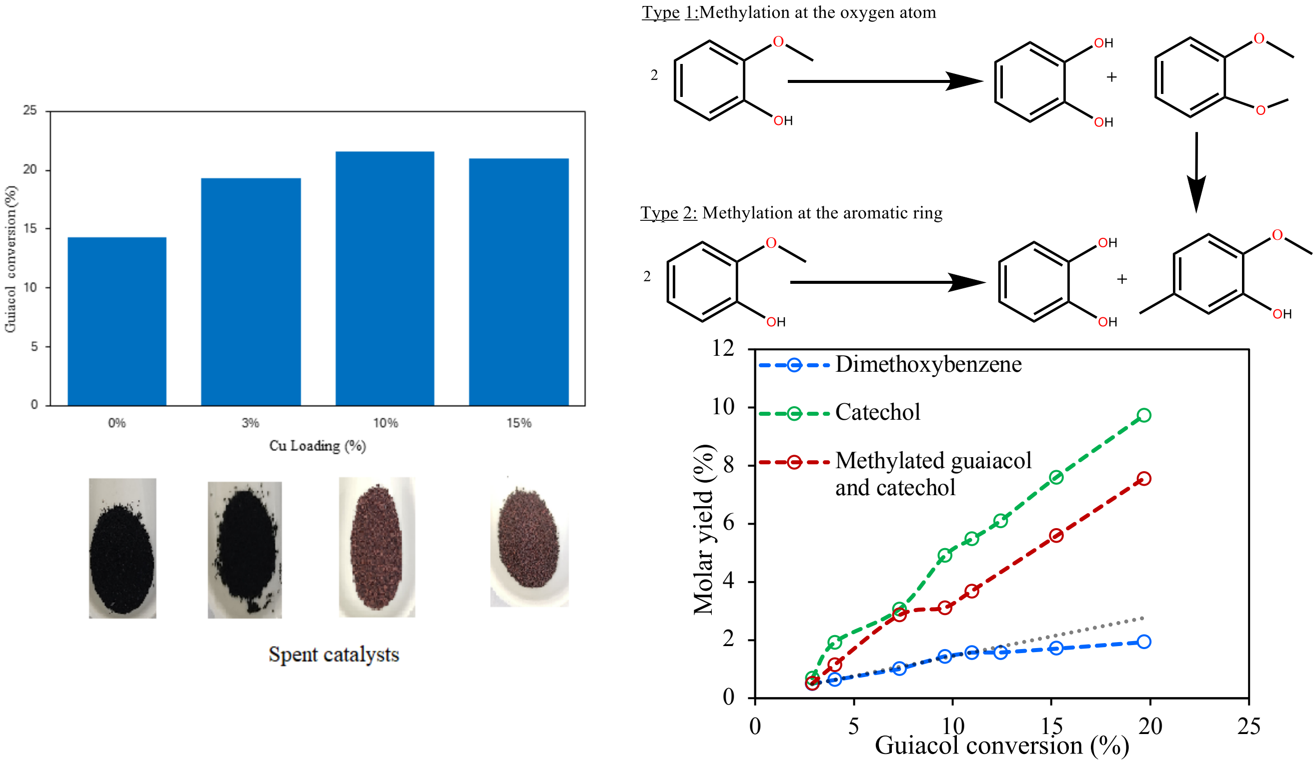

a

b

FigurFiguree 1.. **a**. Top- effect of guaiacol conversion (at 300 °C, 5 bar, WHSV $4h^{-1}$) on Cu loading, bottom- spent catalysts, **b**. Top- (de)methylation reaction pathway, bottom-yield of products vs conversion for reaction over 10% Cu/Al_2O_3

Figure 1b shows the methylation of guaiacol may occur at both the aromatic ring (to methylated catechols and guaiacols) as well as the -OH group (resulting in the formation of dimethoxybenzene). The yield of dimethoxybenzene was found to increase initially and then remained constant with further conversion of guaiacol. This suggests that dimethoxybenzene may undergo further (de)methylation to methyl guaiacol.

4. Conclusions

Cu/Al_2O_3 catalysts are selective towards (de)methylation of anisole and guaiacol. The reaction takes place on the Lewis acid sites provided by the alumina support, during adsorption at elevated temperatures. The presence of Cu enhances the reaction by providing stability to the active sites.

Referencesferences

[1] X. Zhu, L.L. Lobban, R.G. Mallinson, D.E. Resasco, J. Catal. 281 (2011) 21–29.
[2] S. Mukundan, M. Konarova, L. Atanda, Q. Ma, J. Beltramini, Catal. Sci. Technol. 5 (2015) 4422-4432.
[3] C. Li, Y. Nakagawa, M. Tamura, A. Nakayama, K. Tomishige, *ACS Catal.* 10 (2020) 14624–14639.

Keywords

(De)methylation; anisole; guaiacol; Cu/Al_2O_3 catalysts.

Mon. 09/09 // 11:20-11:40

CK – I – 2

Reactions in three phase CO2 methanation using LOHC as liquid phase

Mathias Held[1*], Siegfried Bajohr[1], Thomas Kolb[1]

1 Karlsruhe Institute of Technology, Engler-Bunte-Institut – Division of Fuel Technology, Engler-Bunte-Ring 1, 76131 Karlsruhe, Germany

**Corresponding author: mathias.held@kit.edu*

Highlights

- A combination of the LOHC process with three phase methanation is presented.
- The influence of degree of hydrogenation of the LOHC on CO_2 conversion in methanation reaction was determined.
- Reaction conditions were optimized to favor either hydrogenation or methanation reaction.
- Catalyst activation by reduction in the liquid phase is possible.

1. Introduction

The Power-to-Gas concept allows mid- and long-term storage of renewable energy in form of chemical energy carriers [1]. In this context methanation of carbon dioxide with hydrogen has been extensively discussed. Hydrogen can be provided by water electrolysis, carbon dioxode is captured from either ambient air or industrial streams. The main focus of methanation reactor concepts is put on efficient heat management since the reaction is highly exothermic [2].

By introducing a liquid phase with high heat capacity and thermal conductivity in three phase methanation, isothermal reaction conditions can be achieved in a slurry bubble column reactor. This is beneficent regarding the dynamic behavior of the reactor, even for high load changes in short time only small temperature increase of the reactor content is observed [3].

The liquid phase used in three phase methanation is dibenzyl toluene which can also be used as Liquid Organic Hydrogen Carrier (LOHC). LOHC offer an easy and safe way to store and transport hydrogen using the existing infrastructure for liquid energy carriers [4]. High storage capacities are achieved by chemically binding hydrogen to the carrier molecule under high pressure, dehydrogenation is performed using a suitable catalyst and low pressures.

In scope of the presentation a combination of LOHC and three phase methanation is proposed. Therefore the reaction rates for hydrogenation and methanation reaction with a nickel catalyst are determined. Further, catalyst reduction in the liquid phase was investigated.

2. Methods

To describe the hydrogenation and methanation reaction experiments were performed in a continuous stirred tank reactor (CSTR). The nickel catalyst used in methanation was suspended in dibenzyl toluene and educt gas was fed to the reactor. Temperature was varied from $T_R = 220$ °C to $T_R = 320$ °C, absolute reactor pressure was varied from $p_R = 5$ bar to $p_R = 20$ bar. Product gas analysis via gas chromatography was used to determine methanation reaction rates. Degree of hydrogenation was determined by density measurement of liquid samples using a linear correlation.

Methanation reaction rates were determined with product gas composition and modified residence time. Hydrogenation reactivity was determined by change in DoH, molar amount of dibenzyl toluene and catalyst mass.

To investigate catalyst reduction, two methods were used: For the first method the catalyst was reduced in a fixed-bed reactor according to the manufacturer instructions. The catalyst was then transferred to the CSTR in an inert atmosphere. For the second method the catalyst was suspended in the liquid phase in the CSTR in oxidized state. Subsequently it was reduced in the liquid phase by dosing hydrogen. In this case lower temperatures were set to avoid liquid phase decomposition and evaporation. After activation, catalyst activity was checked by methanation experiments.

3. Results and discussions

Hydrogenation of dibenzyl toluene takes place as a side reaction in three phase methanation. In the experiments almost full hydrogenation could be reached at low reactor temperatures. The change of DoH showed linear behavior at the beginning of each experiment, after several hours an influence of the chemical equilibrium was observed. Hydrogenation reactivity is high at low temperatures and decreases with increasing temperature. Catalyst deactivation is assumed to be the reason for this behavior. Further the hydrogenation shows a strong pressure dependence, reactivity increases with increasing pressure.

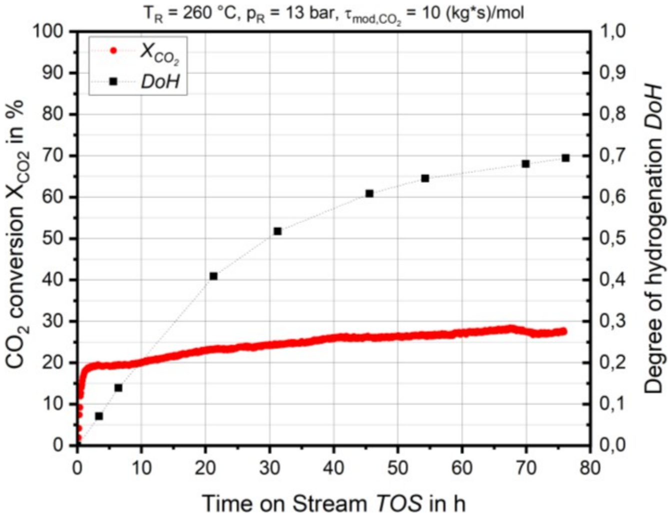

Figure 1. CO_2 conversion X_{CO2} and degree of hydrogenation *DoH* for a methanation experiment in the CSTR.

Methanation reaction rates were calculated using the CO_2 conversion X_{CO2}. X_{CO2} increases with increasing degree of hydrogenation. This can be explained by the decrease of hydrogenation reactivity over time due to the chemical equilibrium. When hydrogenation equilibrium is reached the methanation reaction is in steady-state. X_{CO2} is further influenced by liquid sampling, what leads to a change in modified residence time due to catalyst removal from the reactor. When methanation reaction rates were calculated this influence was considered and the modified residence time was adjusted accordingly. Methanation reaction rates increase with increasing temperature, but are less pressure dependent compared to hydrogenation reactivities.

Catalyst reduction was done in a fixed-bed reactor as well as in the CSTR. In both reactor similar activities could be reached. When reducing the catalyst in the liquid phase, high temperatures should be avoided, as they can lead to liquid phase decomposition and catalyst deactivation.

4. Conclusions

The hydrogenation of dibenzyl toluene in three phase methanation was investigated. The hydrogenation reactivities show a strong pressure dependence whereas methanation reaction rates show strong temperature dependence. By adjusting the reaction conditions accordingly, either of the reactions can be favored.

Catalyst reduction was possible both in a two-phase fixed-bed reactor as well as in a three-phase CSTR. Further research will focus on possible catalyst deactivation mechanisms.

References

[1] S. Rönsch, J. Schneider, S. Matthischke, M. Schlüter, M. Götz,J. Lefebvre, P. Prabhakaran, S. Bajohr, Fuel 2016, 166, 276–296.
[2] M. Götz, J. Lefebvre, F. Mörs, A. McDaniel Koch, F. Graf, S. Bajohr, R. Reimert, T. Kolb, Renewable Energy 2016, 85,1371–1390.
[3] Sauerschell, S. Bajohr, T. Kolb. Energy & Fuels 2022, 36(13), 7166-7176.
[4] M. Niermann, A. Beckendorff, M. Kaltschmitt, K. Bonhoff, International Journal of Hydrogen Energy 2019, Jg. 44, Nr. 13, S. 6631–6654.

Keywords
LOHC; CO_2 Methanation; three phase reaction kinetics, renewable gas

Mon. 09/09 // 11:40-12:00

CK – I – 3

The effect of mesopores in platelike H-ZSM-5 zeolites in the 1-butanol dehydration reaction

Phebe Lemaire[1,2], Arno de Reviere[1,2], Dhanjay Sharma[1], Joris W. Thybaut[2], Maarten K. Sabbe[1,2], An Verberckmoes[1]

[1] *Industrial Catalysis and Adsorption Technology (INCAT), Valentin Vaerwyckweg 1, 9000 Ghent, Belgium*

[2] *Laboratory for Chemical Technology (LCT), Technologiepark 125, 9052 Ghent, Belgium*

**Corresponding author: Phebe.Lemaire@UGent.be*

Highlights

- Platelike morphology improves the catalytic performance of ZSM-5
- Limited effect of large mesopores on the catalytic performance in the dehydration of 1-butanol
- Mesopores result in a small decrease in activity at higher temperatures

Introduction

In light of stepping away from fossil fuels, fermentation of biomass to bio-alcohols is a widely investigated and already implemented sustainable production route for platform molecules [1]. One such bio-alcohol is n-butanol, which can be catalytically dehydrated to butenes, important building blocks in the chemical industry [2]. H-ZSM-5 is well known as a catalyst, with high activity and selectivity to olefins for this reaction [3, 4], but it also shows drawbacks, e.g. diffusion limitations and deactivation due to coke formation [5]. Several strategies have been proposed in literature to overcome these problems. It is possible to add additional mesoporosity to the existing micropores using post-treatment, creating hierarchical H-ZSM-5. Another option is to change the morphology of H-ZSM-5 by limiting the b-axis to the nanoscale during synthesis, creating platelike H-ZSM-5 [5, 6].

In this work, both strategies are combined. For this, platelike H-ZSM-5 is first synthesized and mesopores are introduced through post-synthesis desilication using NaOH and TPAOH. Furthermore, the materials are thoroughly characterized by XRD, N_2-sorption, NH_3-TPD, ICP-OES, TEM and SEM and tested in the n-butanol dehydration reaction using a high throughput setup.

Methods

Platelike H-ZSM-5 (PL-ZSM-5) with a Si/Al ratio of 25 is obtained through hydrothermal synthesis where urea is added to inhibit growth along the b-axis, thus creating a platelike morphology [7]. Hierarchical platelike H-ZSM-5 (m-PL-ZSM-5) is obtained through desilication of PL-ZSM-5 with NaOH and TPAOH at 353 K for 1 hour. Here, TPAOH is added to the desilication mixture to prevent excessive extraction of silicon from the zeolite framework [8]. The structural and chemical properties of both catalysts are assessed using different characterization methods, and their performance in the n-butanol dehydration is tested in a high throughput kinetics screening setup at 483 K and 513 K at a total pressure of 5 bar and a butanol partial pressure of 29 kPa. Additionally, the performance of both materials is compared to that of commercial H-ZSM-5 (c-ZSM-5) with a similar Si/Al ratio.

Results and discussion

The TEM images of PL-ZSM-5 and m-PL-ZSM-5 ((Figure 1 (a) and (b), respectively) show the typical coffin-shaped morphology with a reduced b-axis of approximately 70 nm. For m-PL-ZSM-5, the presence of mesopores is also clearly visible. These mesopores are rather large compared to the crystal size and tend to merge into large cavities inside the zeolite crystals. Furthermore, N_2-sorption shows a decrease in the specific surface area and micropore volume, indicating a loss of microporosity upon desilication.

As shown in Figure 1 (c), PL-ZSM-5 reveals an improved activity per active site compared to c-ZSM-5, especially at higher temperatures. After modification, catalytic testing at 513 K displays a small decrease in activity for m-PL-ZSM-5 compared to PL-ZSM-5, yet still outperforming c-ZSM-5, whereas there is no difference in activity at 483 K. The selectivity analysis shows a slightly increased selectivity towards the 2-butenes at the cost of selectivity towards dibutyl ether for PL-ZSM-5 compared to its commercial counterpart. This effect is visible at both temperatures, although more pronounced at 483 K. After modification, the selectivities of m-PL-ZSM-5 align with those of the commercial material again. Additionally, stability tests were performed at 513 K for 60 hours time on stream. Here, the platelike morphology shows an enhanced stability compared to c-ZSM-5 and further improvement is obtained upon desilication.

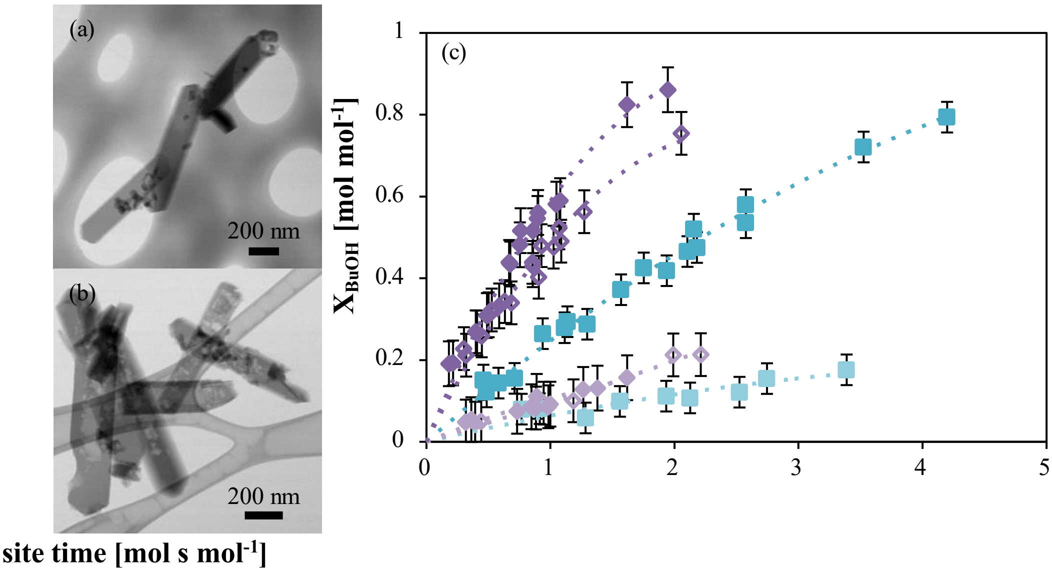

Figure 1: TEM-images of PL-ZSM-5 (a) and m-PL-ZSM-5 (b) and n-butanol conversion (X_{BuOH}) as function of site time for c-ZSM-5 (■), PL-ZSM-5 (♦) and m-PL-ZSM-5 (◊) at 483 K (light) and 513 K (dark), p_{tot} = 5 bar and p_{BuOH} = 29 kPa (c)

Conclusions

Desilication of the self-synthesized platelike H-ZSM-5 zeolite results in the formation of large mesopores within the zeolite crystals which tend to merge into large cavities. A loss of microporosity compared to the parent zeolite is also observed. Nevertheless, the large mesopores have a rather limited effect on the catalytic performance of platelike H-ZSM-5, whereas the platelike morphology itself notably improves the catalytic behaviour. These results indicate that the confinement in the micropores is essential in efficient catalysis for n-butanol dehydration.

References

[1] B.O. Abo, M. Gao, Y.L. Wang, C.F. Wu, Q.H. Wang, H.Z. Ma, Environ. Sci. Pollut. Res., 26 (2019) 20164-20182.
[2] G.W. Huber, A. Corma, Angew. Chem.-Int. Edit., 46 (2007) 7184-7201.
[3] A. de Reviere, D. Gunst, M.K. Sabbe, M.F. Reyniers, A. Verberckmoes, Catal. Sci. Technol., 11 (2021) 2540-2559.
[4] D. Gunst, K. Alexopoulos, K. Van der Borght, M. John, V. Galvita, M.F. Reyniers, A. Verberckmoes, Appl. Catal. A-Gen., 539 (2017) 1-12.
[5] D. Kerstens, B. Smeyers, J. Van Waeyenberg, Q. Zhang, J.H. Yu, B.F. Sels, Adv. Mater., 32 (2020) 47.
[6] W.J. Dai, C. Kouvatas, W.S. Tai, G.J. Wu, N.J. Guan, L.D. Li, V. Valtchev, Journal of the American Chemical Society, 143 (2021) 1993-2004.
[7] Y.F. Li, S.Q. Wang, S.X. Fan, B. Ali, X.C. Lan, T.F. Wang, ACS Sustain. Chem. Eng., 10 (2022) 3808-3816.
[8] N. Chaihad, Y.A. Situmorang, A. Anniwaer, I. Kurnia, S. Karnjanakom, Y. Kasai, A. Abudula, P. Reubroycharoen, G.Q. Guan, Renew. Energy, 169 (2021) 283-292.

Keywords
platelike H-ZSM-5; desilication; butanol dehydration

Mon. 09/09 // 13:40-14:00

CK – II – 1

Optimization of Temperature Profile for di-methyl ether synthesis by CO2 hydrogenation.

Laura Duran Martinez[1], Isabelle Pitault[2], Isabelle Polaert[1]*

1 INSA Rouen Normandie, Univ Rouen Normandie, Normandie Univ, LSPC UR 4704, F-76000 Rouen, France. 2 Université Claude Bernard de Lyon, CNRS, LAGEPP UMR5007, F-69100 Villeurbanne, France

**Corresponding author: isabelle.polaert@insa-rouen.fr*

Highlights

- Di-methyl ether can improve CO_2 hydrogenation compared to methanol synthesis.
- Optimal Temperature Profiles (OTP) increase CO_2 conversion into methanol and DME.
- Low residence times and optimal temperature profiles are recommended.
- Heat exchanger-reactor has to be compatible with low residence time and OTP.

1. Introduction

Harnessing renewable energies to produce green hydrogen capable of converting CO_2 into fuels and chemicals, with the potential to replace fossil feedstocks in the chemical industry, is a remarkable alternative for mitigating greenhouse gas emissions and reducing dependence on fossil fuels. Thermal catalytic *hydrogenation of CO_2*, efficient and easy to industrialize despite its energy consumption and the catalyst deactivation, refers to the process of converting carbon dioxide into value-added molecules, such as methanol and di-methyl ether (DME), using hydrogen (H_2). The hydrogenation of CO_2 to methanol (CTM) is a combined process of three reactions (1 -3), and in the direct hydrogenation of CO_2 to DME, methanol is formed as an intermediate and successively dehydrated (4) in a single reactor containing bifunctional catalysts or mixture of two catalysts optimized for both the reactions separately. The relative occurrence of these parallel or consecutive reactions is difficult to quantify under operating conditions and generally depends on the thermodynamic conditions and the catalysts chemical nature.

$$\mathrm{CO_2 + 3H_2 \rightleftharpoons CH_3OH + H_2O} \quad (1) \qquad \mathrm{CO_2 + H_2 \rightleftharpoons CO + H_2O} \quad (2)$$

$$\mathrm{CO + 2H_2 \rightleftharpoons CH_3OH} \quad (3) \qquad 2CH_3OH \rightleftharpoons CH_3OCH_3 + H_2O \quad (4)$$

All the reactions are, a priori, balanced, and thermodynamic limitations lead to low conversions and selectivities under acceptable kinetic conditions. The aim of this study was therefore to work on the operation of a catalytic reactor in order to improve the conversion per pass of a fixed-bed reactor, by examining its possible temperature control.

2.Methods

This study consisted of three parts: (i) calculation of the gas composition at thermodynamic equilibrium; (ii) estimate of the kinetic parameters from our experiments; (iii) assessment of the several scenarios for temperature profile optimization.

The gas composition and CO_2 conversion at thermodynamic equilibria were calculated by RGibbs under Aspen Plus V12 for the same conditions than the experimental ones. The equation of state used was SRK. The experiments were carried out in a 200mm x 4mm diameter stainless steel fixed-bed reactor in a furnace using a mechanical mixture of catalysts (0-200µm): $CuO\text{-}ZnO\text{-}Al_2O_3$ (Alfa Aesar) (CZA), and ZSM5 (ACS Material). The experimental set-up is precisely described in [1]. The ranges of pressure and temperature were [26-36 bar] and [463-593 K] for H_2/CO_2 inlet ratios of about 1, 3 and 9 with 10% N_2 added to calculate balances accurately. The outlet gas was analyzed by gas chromatography. Kinetic modeling was classically carried out, but considering the molecular contraction along the reactor and the existing deactivation on the CZA catalyst [2]. The kinetic laws were derived from Langmuir-Hinshelwood-type models, independent for each catalyst. The ODE system was solved using the *ode45* Matlab routine and the parameter estimate was performed using the *lsqnonlin* Matlab solver.

For the temperature profile optimization, a fixed bed piston reactor was simulated. When reversible exothermic reactions occur, the Arrhenius law suggests to begin at a high temperature to achieve higher rate and conversion (kinetic limitation), but due to the thermodynamics limitations, it is necessary to decrease the temperature to maximize the conversion. Thus, there is an optimum temperature profile to identify to attain a maximum conversion with a minimum volume by changing temperature as a function of a given reactant conversion (X_j). The compound mass balances were discretized into at least 100 cells to avoid numerical errors. In each cell, considering the upstream gas composition, the temperature required to achieve the target criteria was determined and fixed and the gas composition calculated. Several target criteria were used, either maximizing the extents of the reactions (X1) and (X4), the CO_2 conversion (X CO2) or the methanol and DME production (FMD) or minimizing the extent of the reaction (X2). The optimizations were performed for several reactor inlet temperatures [473-607 K], H_2/CO_2 inlet ratios from 1 to 9, pressures [31, 36 bar] and catalyst masses and inlet gas flow rates to vary the residence times [1-130 s].

3. Results and discussion

For the reactions taken place on the commercial CZA catalyst, the kinetic model developed by Quezada [2] was retained. For the reaction 4, the model proposed by Ortega et al. [3] assuming the reaction equilibrium was modified taking into account the slower rate of the reverse reaction than that expected assuming thermodynamic equilibrium. 13 kinetic parameters were estimated. A regression analysis validated the model on 39 experiments.

Figure 1 shows that the optimization of temperature profiles in the reactor allows a sharp increase of CO_2 conversion into methanol and DME (from 10 to 40% on fig. 1.c), minimizing the CO production. While without optimization, that is to say in isothermal conditions, the outlet CO_2 conversion is the conversion at the thermodynamic equilibrium of the inlet temperature, conversions keep on increasing when decreasing temperature along the bed. The choice of the target criteria led to different optimized temperature profiles and the optimization of X1 (proportional to FMD) led to better CO_2 conversion and methanol and DME production. Our set of optimizations demonstrated that if long residence times are chosen (small flowrates or/and high catalysts weights), working at low temperatures give the best results but for a bigger production minimizing the catalysts amounts, the best is to work with low residence times, enter the reactor at high temperature and follow the optimized temperature decreasing profile.

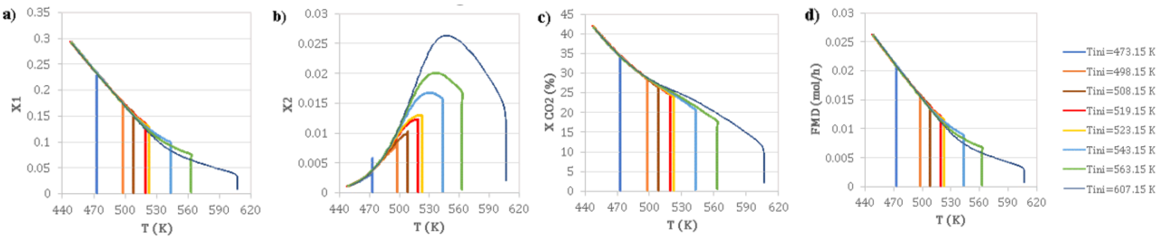

Figure 1. Effect of the inlet temperature on CO_2 conversion, X1, X2 reaction extents and value-added molecule production maximizing the target criteria X1. P=31.1 bar, H_2/CO_2=2.8, N_2=10%. Residence time 6 s.

4. Conclusions

A tool for scaling-up a reactor for the hydrogenation of CO_2 to DME and methanol has been developed, maximizing the conversion of CO_2 and/or the production of methanol and DME by optimizing the residence time and the optimal temperature profile to be followed. This tool needs to be improved by considering any limitations due to internal transfer in the catalyst grains. However, we assumed in our method that a perfect removal of the heat produced by the exothermic reactions can be performed, that could be unrealistic. Hence, designing a heat exchanger reactor from our kinetic models is our next goal.

References

[1] B. Alrafei, I. Polaert, A. Ledoux, F. Azzolina-Jury, Cat. Today. 346 (2020) 23-33
[2] M. J. Quezada, PhD of Normandie Université (2020) HAL NNT : 2020NORMIR12. tel-03215410.
[3] C. Ortega, M. Rezaei, V. Hessel, G. Kolb, Chem. Eng. J., 347 (2018) 741-753.

Keywords
Optimal Temperature Profile ; CO_2 Hydrogenation ; DME synthesis ; Kinetic model

Mon. 09/09 // 14:00-14:20

CK – II – 2

Kinetic study of CO2 hydrogenation to formate over a solid micellar catalyst: unveiling the role of the base lid micellar catalyst: unveiling the role of the base

Catarina Mendes[1], Javiera Rubio[1], Francisca Rebelo[1,2], Vitaly Ordomsky[3], Mark Saeys[1]*

1 Laboratory for Chemical Technology (LCT), Department of Materials, Textiles and Chemical Engineering, Ghent University, Technologiepark 125, 9052 Ghent, Belgium;

2 Chemical Engineering Department, Instituto Superior Técnico, Universidade de Lisboa, Av. Rovisco Pais, 1049-001 Lisbon, Portugal;

3 Univ. Lille, CNRS, Centrale Lille, ENSCL, Univ. Artois, UMR 8181 – UCCS – Unité de Catalyse et Chimie du Solide, F-59000 Lille, France;

**Corresponding author: mark.saeys@ugent.be*

Highlights

- $Ru^{(III)}$@MCM is a novel type of single-site heterogeneous catalyst, efficient for CO_2 hydrogenation to formate in the presence of triethylamine.
- Kinetic experiments show a second order dependence in H_2 and a first order dependence in triethylamine of the CO_2 hydrogenation rate.
- H_2-D_2 isotope exchange experiments demonstrate that triethylamine co-catalyzes heterolytic H_2 dissociation.

Introduction

Solid micellar catalysts (SOMICs) are a new class of catalytic materials that contain isolated metal ion sites incorporated in the walls of a silica matrix, stabilized by surfactant molecules in the pores [1-3]. The first example of this family, $Ru^{(III)}$@MCM, consists of $Ru^{(III)}$ single sites incorporated into the walls of MCM-41 via Ru-O-Si bonds, and stabilized by a cetyltrimethylammonium (CTA^+) surfactant. $Ru^{(III)}$@MCM (**Figure 1**) previously showed interesting performance for CO_2 hydrogenation to formate in the presence of triethylamine under mild conditions[1].

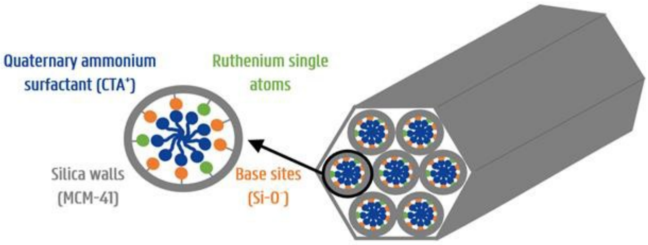

FiguFigure 1.. Schematic representation of the $Ru^{(III)}$@MCM catalyst.

Our study of the reaction kinetics of CO2 hydrogenation to formate demonstrates that the base not only improves the reaction thermodynamic, but also co-catalyzes heterolytic H_2 dissociation.

Methods

Catalytic tests were performed in a 45 mL stainless steel pressure reactor. After reaction, the gas phase was analyzed via gas chromatography (GC) or mass spectrometry (MS). Quantitative analysis of formate in the liquid product was performed via ^1H NMR using TSP-d_4 as internal standard.

Results and discussion

The dependence of formate concentration and productivity on the reaction time, temperature, H_2 and CO_2 partial pressures, amount of triethylamine (TEA) in the feed, and solvent were investigated.

Kinetic analysis at low CO_2 and TEA conversions determined an apparent activation energy of 56 kJ/mol, a quasi-second-order dependence on the H_2 partial pressure (**Figure 2(a)**), and a limited effect of the CO_2 partial pressure. The concentration of TEA significantly increases the formate productivity (**Figure 2(b)**).

H_2-D_2 isotope exchange at room temperature confirmed that $Ru^{(III)}$@MCM can activate H_2, but the presence of TEA increases the HD formation rate fourfold, showing that TEA co-catalyzes H_2 activation. Screening of different bases demonstrated that small and non-sterically hindered tertiary amines, with pKa above 10, are preferred as co-catalysts.

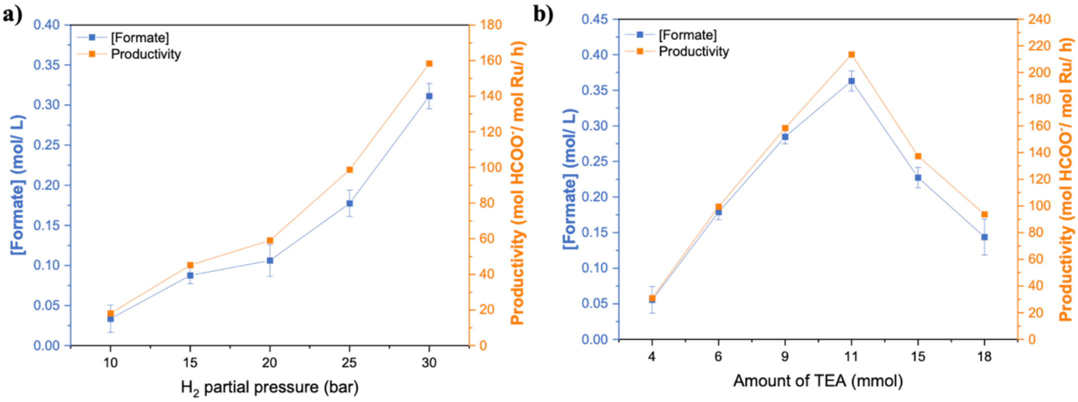

Figure 2. Dependence of catalyst productivity on H_2 partial pressure **(a)** and amount of TEA in the feed **(b)**. Conditions: 3.1 µmol Ru, 9 mmol TEA (Figure (a)), 6 mL H_2O, 20 bar of CO_2, 30 bar H_2 (Figure (b)), 90 °C and 4 h.

Conclusions

TEA co-catalyzes the sluggish heterolytic H_2 dissociation during CO_2 hydrogenation to formate over $Ru^{(III)}$@ MCM. Proper concentrations of TEA are required to achieve high formate productivity.

References

1. Q. Wang, S. Santos, C. A. Urbina-Blanco, W. Y. Hernández, M. Impéror-Clerc, E. I. Vovk, M. Marinova, O. Ersen, W. Baaziz, O. V. Safonova, A. Y. Khodakov, M. Saeys and V. V. Ordomsky, *Applied Catalysis B: Environmental*, 2021, **290**, 120036.
2. Q. Wang, S. Santos, C. A. Urbina-Blanco, W. Zhou, Y. Yang, M. Marinova, S. Heyte, T.-R. Joelle, O. Ersen, W. Baaziz, O. V. Safonova, M. Saeys and V. V. Ordomsky, *Applied Catalysis B: Environmental*, 2022, **300**, 120730.
3. Q. Wang, C. M. De Brito Mendes, O. V. Safonova, W. Baaziz, C. A. Urbina-Blanco, D. Wu, M. Marinova, O. Ersen, M. Capron, A. Y. Khodakov, M. Saeys and V. V. Ordomsky, *Journal of Catalysis*, 2023, **426**, 336-344.

Keywords
CO_2 hydrogenation, formate, triethylamine, H_2 activation

Mon. 09/09 // 14:20-14:40

CK – II – 3

Shining Light on Sustainability: CuInxGa1-xSe (CIGS) Solar Cells Drive Selective Photocatalytic Oxidation of Methane

Duc Manh Nguyen[1], Chunyang Dong[1], Thomas Tom[2], Negar Naghavi[2*], Vitaly V. Ordomsky[1*], Andrei Y. Khodakov [1*]

[1] University of Lille, CNRS, Centrale Lille, University of Artois, UMR 8181, UCCS – Unité de Catalyse et Chimie du Solide, F-59000 Lille, France; [2] CNRS, UMR 9006, Institut Photovoltaique d'Ile-de-France (IPVF), 91120 Palais, France

**Corresponding author:negar.naghavi@chimieparistech.khodakov@univ-lillepls.eu.fr , vitaly.ordomsky@univ-lille.fr,*

Highlights

- The different CIGS-based photocatalysts were prepared via well-established methods.
- The oxidation of methane over CIGS-based photocatalysts under different conditions was studied.

*1. Introduction

Methane is used as a fuel for transportation, heating, and power generation, which corresponds to a major emission of CO_2 into the atmosphere. Furthermore, methane is itself a greenhouse gas (GHG) with an effect on the climate 30 times more significant than CO_2. Therefore, methane activation and its selective conversion to value-added products presents an appealing prospect from both economic and environmental aspects. Photocatalysis, which uses sunlight, has been shown as a very promising alternative to high temperature-required routes for methane conversion into platform molecules such as syngas, olefins, methanol, etc. [1]. In addition, the advancements in solar cells based on the photovoltaics effect [2] open up new possibilities to combine these two technologies for the development of sustainable and eco-friendly photocatalytic systems utilizing solar irradiation and operating at ambient temperature.

Herein, we report selective oxidation of methane over CIGS-based photocatalysts at ambient conditions under light irradiation. In the absence of added water, the standard CIGS thin film enables a stable synthesis of 0.16 mmol $g_{cat.}^{-1}$ h^{-1} of carbon monoxide with the carbon-based CO selectivity over 80%. The presence of water facilitates 100% production of methanol with an activity of 0.087 mmol $g_{cat.}^{-1}$ h^{-1} over CIGS/ZnO nanowires decorated with Au nanoparticles.

2. Methods

The standard CIGS plate was prepared by depositing CIGS layer via a co-evaporation method under high vacuum of 10^{-5} Pa on 800 nm DC sputtered Mo layer coated over soda lime glass. The ZnO nanowires (ZnO NWs) were grown on the top of CIGS layer using electrodeposition. Gold was loaded on nanowires by illuminating an aqueous solution consisting of chloroauric acid ($HAuCl_4$) and CIGS/ZnO NWs glass with a 500 W Xe lamp.

Typically, the 250mL-photocatalytic reactor containing photocatalyst in the bottom is first evacuated using a vacuum pump and then is filled with reagents. The catalytic tests were conducted without water and with catalyst immersed in water added to the reactor. Before irradiated by a 500 W Xe lamp with full spectra (λ, 200 ~ 1100 nm), the light intensity of 0.45 mW cm^{-2}, the reactor was kept in the dark for 30 min to obtain the adsorption desorption equilibrium. After the photocatalytic reaction, the gaseous products were analyzed by a gas chromatography (PerkinElmer Clarus 580 GC) equipped with a thermal conductive detector and a flame ionized detector. The liquid products were analyzed by nuclear magnetic resonance spectroscopy (300 MHz Brucker Advance NMR).

3 Results and discussions

Fig. 1a shows photocatalytic performance of standard CIGS under different air/CH_4 ratios. Under the optimal partial pressures of methane and air (9.75/0.25), CO production and selectivity reaches 0.16

mmol $g_{cat.}^{-1}$ h^{-1} and 80% , respectively. Pure CH_4 treatment with light irradiation leads to H_2 production and carbon deposition over CIGS surface (Fig. 1b). The subsequent air treatment under light facilitates CO_2 production, suggesting oxygen-assisted activation of methane over the surface of standard CIGS (Fig. 1c). Accordingly, the reaction proceeds by sequential CH_4 dissociation and coupling into hydrocarbons followed by dehydrogenation into carbon on the surface with further partial oxidation of these carbon species to CO.

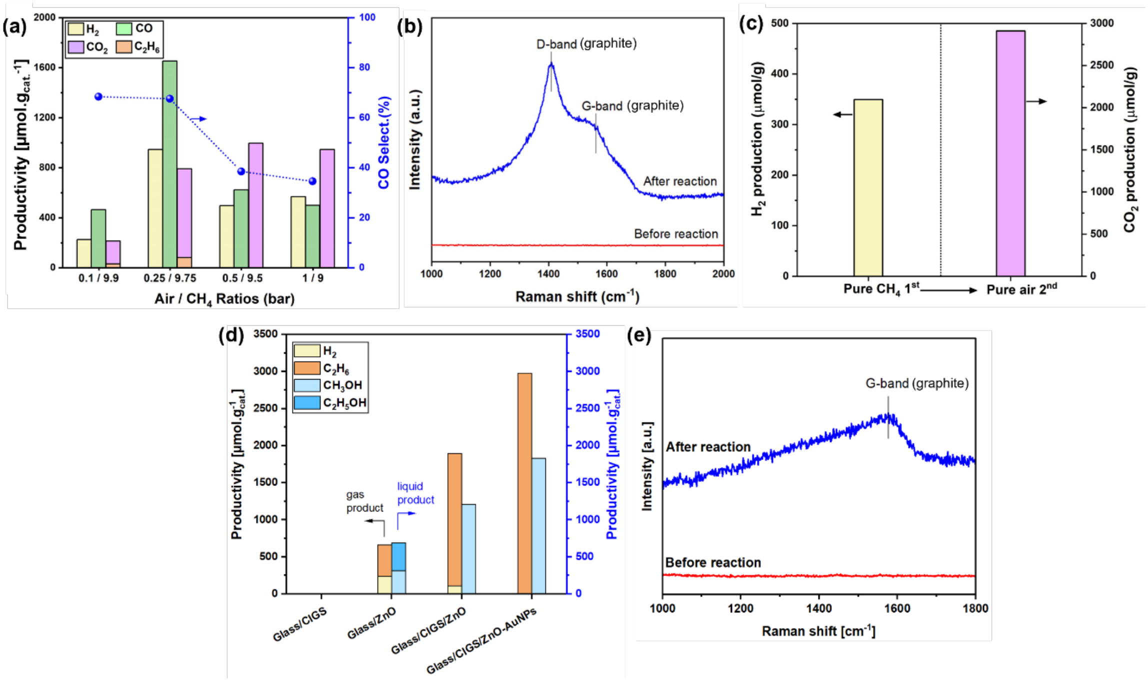

Figure 1.. The photocatalytic performance of (a) the standard CIGS plate under different air/CH_4 ratios, 20 °C, 15h, (c) of the standard CIGS plate under sequential pure CH_4 and air conditions, and (d) of different modified CIGS plates under 10 bar CH_4, 20 mL H_2O, 20 °C, 21h; (b,e) Raman spectra of fresh/spent standard CIGS plate under 10 bar CH_4 treatment with light irradiation, and fresh/spent Glass/CIGS/ZnO-AuNPs plate under 10 bar CH_4, 20 mL H_2O with light irradiation.

In the aqueous phase, CIGS with ZnO nanowires on the top efficiently catalyze highly selective oxidation of methane to methanol without any CO_2 production (Fig. 1d). This enhancement may be due to, first, the pn-junction between CIGS and ZnO which facilitates separation of photogenerated charge carriers. Second, the presence of water plays a role in promoting the desorption of products from active sites to avoid unexpected overoxidation [3]. The plate decorated with Au NPs exhibits a promising activity of 0.087 mmol $g_{cat.}^{-1}$ h^{-1} of CH_3OH with 100% selectivity in liquid phase. Furthermore, the methane coupling also improved in this condition, corresponding to the ethane production rate of 0.142 mmol $g_{cat.}^{-1}$ h^{-1}. After reaction, a small amount of disordered carbon contributing to the catalyst deactivation was detected on the CIGS surface (Fig. 1e). The partially deactivated catalyst can be regenerated by exposure to air under light irradiation.

4. Conclusions

In summary, the prepared CIGS-based photocatalysts show promising performances for selective oxidation of methane either to CO or methanol in the absence of added water or in aqueous conditions, respectively under the simulated sunlight and very mild reaction conditions.

References

[1] D. Hu, V. V. Ordomsky, A. Y. Khodakov, Appl. Catal., B 286 (2021) 119913.
[2] P.K. Nayak, S. Mahesh, H.J. Snaith, D. Cahen, Nat. Rev. Mater. 4 (2019) 269-285.
[3] A.A. Latimer, A. Kakekhani, A.R. Kulkarni, J.K. Norskov, ACS Cat. 8 (2018) 6894-6907.

Keywords
CIGS; methane; selective oxidation; photocatalysis

Mon. 09/09 // 14:40-15:00

CK – II – 4

Kinetics and modelling of direct CO2 hydrogenation into liquid hydrocarbons

Antoinette Maarawi Chidraoui[1]*, Carlotta Panzone[1], Alban Chappaz[1], Geneviève Geffraye[1], Albin Chaise[1] *1 Univ Grenoble Alpes, CEA, Liten, DTCH, Laboratoire Réacteurs et Procédés (LRP), 38000 Grenoble, France*

**Corresponding author: antoinette.maarawi@cea.fr*

Highlights

- Performances of catalysts with different K/Fe ratio in direct CO_2 hydrogenation are compared.
- 40% of CO_2 conversion and less than 10% CO and CH_4 selectivity are obtained.
- Experimental kinetic study with the optimal catalyst is conducted.
- Effect of reactor design on the reaction is studied numerically and a novel technology is proposed.

1. Introduction

The direct hydrogenation of CO_2 into hydrocarbons through the Fischer-Tropsch (FT) pathway has emerged as a versatile approach for producing a variety of gaseous and liquid hydrocarbons. This process involves the reverse water-gas shift (RWGS) and FT synthesis conducted within the same reactor. Due their effectiveness in facilitating both of these reactions, iron-based catalysts are widely used. Despite advancements in catalyst development, limited attention is given to the reaction kinetics[1-3]. Our research group[3] recently provided new experimental data using a Fe-K/Al_2O_3 catalyst (achieving 30% CO_2 conversion to mainly short olefins C_2-C_4, with a non-negligible methane formation) and proposed a macro-kinetic model that outlines the production of linear alkanes, 1-alkenes, and alcohols up to 20 carbon atoms. Building upon this previous research, the present study aims to assess upscaled catalysts, refine the kinetic model of the reaction, and explore the impact of reactor design on reaction performance.

2. Methods

Our experimental work is divided into two parts: 1) testing catalysts with different compositions to choose the most performant and 2) performing tests campaign with the chosen catalyst to determine reaction kinetics. The reaction takes place in a stainless steel fixed-bed reactor with an inner diameter of 10.2 mm and a total length of 210 mm. Prior to each test, the catalyst undergoes *in-situ* reduction at 310°C for 24 hours under H_2/N_2 flow. Non-condensed gases and liquid products are analyzed using an online μ-GC system and an offline GC-MS system, respectively. For part 1), iron-based catalysts with varying K/Fe mass ratios (0.77, 0.43, and 0.41) and corresponding potassium contents of 8.7%, 5.7%, and 6.8% by weight are synthesized following the protocol outlined in our previous work[3]. For each catalyst, operating conditions include a temperature of 300°C, pressure of 15 bars, and H_2/CO_2 ratio of 3. The contact time (τ_{mod}), defined as the catalyst mass divided by the total inlet gas volume flow, is varied (0.36, 0.53, and 1.33 $g \cdot s \cdot Nml^{-1}$). For part 2), the effects of several operating parameters are investigated: temperature (250 – 300°C), total pressure (10 – 25 bars), H_2/CO_2 ratio (3 – 24) and τ_{mod} (0.36 – 1.33 $g \cdot s \cdot Nml^{-1}$). Two- and three-dimensional (2D/3D) fixed-bed reactor models that incorporate the kinetic model of the FT-CO_2 reaction are developed using COMSOL Multiphysics.

3. Results and discussion

Each catalyst's response to contact time variation is investigated by altering the total inlet gas volume flow. As anticipated, augmenting the contact time leads to a nearly linear increase in CO_2 conversion (from around 25% to 40%). Additionally, CO selectivity progressively diminishes (from 50% to 10%). At lower contact times, higher quantities of CO, methane, and short hydrocarbons are generated at the expense of longer-chain hydrocarbons. A comparison of the performance of the catalysts at iso-τ_{mod} reveals no significant differences in CO_2 conversions, as seen in Figure 1a for τ_{mod} = 0.53 $g \cdot h \cdot Nml^{-1}$. However, catalyst 2 led to higher CH_4 selectivity (13%) compared to catalysts 1 and 3 (~6%). The latter have higher K content that is able to limit the H_2 adsorption, resulting in less methane formation. On another hand, 32% of CO selectivity is obtained with catalyst 3, vs 23% and 20% for catalysts 1 and 2, respectively. This may be due to lower K content, leading to a promotion of the CO desorption instead of its dissociation. Therefore, the choice is made for the first catalyst, which led to higher selectivity toward C_{2+} hydrocarbons, to be used in the kinetic tests. The experimental kinetic study is in progress and the impact of contact time on CO_2 conversion, CO selectivity, and CH_4 selectivity is depicted in Figure1b. At low contact time (<0.72 g·s·Nml^{-1}), no significant effect is observed on the CO_2 conversion and CO selectivity. However, the CH_4 selectivity increased by around 10%. At higher contact time, the CH_4 selectivity remains stable (~18%). Nevertheless, a progressive increase in CO_2 conversion with contact time and a decrease of the CO selectivity is observed. These results suggest that FT is a slow reaction and increasing the contact time favors the conversion of CO towards the hydrocarbons. When the kinetic study will be completed, the kinetic model proposed in our previous work[3] will be adjusted with the obtained data.

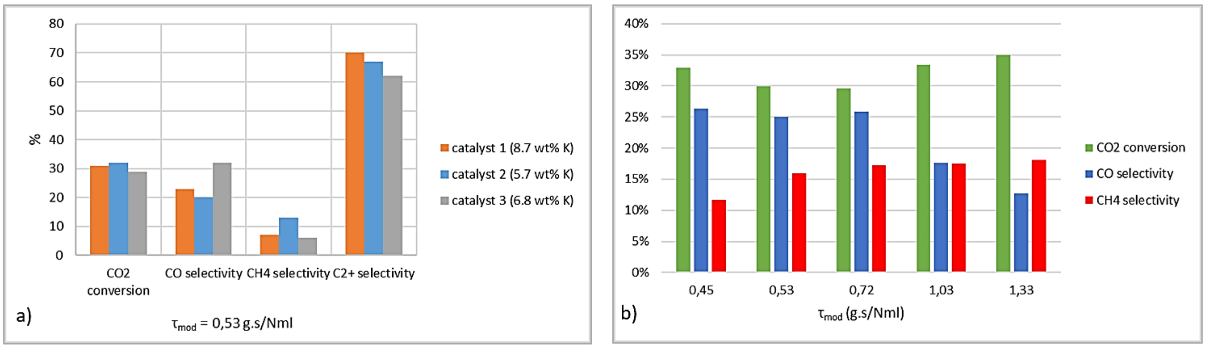

Figure 1. Conversion and selectivities a) at τ_{mod} = 0.53 g·h·Nml^{-1} for the tested catalysts and b) vs τ_{mod} in the kinetic study.

Simultaneously, a 2D model is constructed for the tubular reactor, incorporating the kinetic model[3] and validated using experimental data. Additionally, experimental thermal profiles within the catalytic bed reveal a temperature increase (ΔT) of up to 15°C, a relatively high value that could potentially negatively impact the selectivity towards long-chain hydrocarbons[6]. To address this thermal constraint, a novel structured reactor is designed and its performance for this reaction is assessed through 3D simulation. The results indicate a significant reduction in ΔT within the catalytic bed (less than 1°C) while maintaining desirable performance metrics (40% CO_2 conversion and 7% CO selectivity). Subsequently, the reactor is simulated with doubled catalyst thickness. At iso-τ_{mod}, performance metrics are upheld, achieving a ΔT of 3°C and doubling production. Although promising, further investigations are warranted. Sensitivity analyses are conducted by varying geometric parameters of the reactor to optimize its design for optimal efficiency in FT-CO_2 synthesis.

4 Conclusions

Advancements have been achieved in catalyst development for direct CO_2 hydrogenation reactions; however, to our knowledge, no research has explored the impact of reactor design on performance. To facilitate process intensification for CO_2 valorization, this study introduces a novel reactor technology tailored to this reaction.

References

[4] T. Riedel, G. Schaub, K. Jun, K. Lee, Ind. Eng. Chem. Res. 40 (2001) 1355-1363
[5] S. Najari, G. Grof, S. Saeidi, F. Gallucci, Int. J. Hydrog. Energy. 44 (2019) 4630-4649
[6] C. Panzone, R. Philippe, C. Nikitine, L. Vanoye, A. Bengaouer, A. Chappaz, P. Fongarland, Ind. Eng. Chem. Res. 60 (2021) 16635–16652
[7] R. Philippe, M. Lacroix, L. Dreibine, C. Pham-Huu , D. Edouard, S. Savin, F. Luck, D. Schweich, Catal. Today. 147S (2009) S305-S312

Keywords

Direct CO_2 hydrogenation; reaction kinetics; iron-based catalyst; reactor design.

Mon. 09/09 // 15:00-15:20

CK – II – 5

Kinetic assessment of the heterogeneously catalyzed hydroformylation over a nanoparticle rhodium catalyst .

Maria Herrero Manzano, Jeroen Poissonnier, Sébastien Siradze, Joris W. Thybaut*

Laboratory for Chemical Technology, Ghent University, Technologiepark 125, 9052 Gent, Belgium

**Corresponding author: Joris.Thybaut@UGent.be*

Highlights

- Higher activation energy for hydrogenation (82 kJ/mol) than hydroformylation (37 kJ/mol).
- A negative reaction order for CO suggested its inhibitory role at low temperatures.
- Evidence suggesting C_2H_4 hydrogenation to C_2H_5 as rate-determining step (RDS) for hydroformylation.
- Ethyl hydrogenation towards ethane is proposed as the RDS for ethane hydrogenation.

1 Introduction

Hydroformylation accounts for the production of around 10 million ton of aldehydes per year, by contacting olefins and syngas over a cobalt- or rhodium-based catalyst. Industrially, it is mainly performed using homogeneous catalysts due to their high olefin conversion and aldehyde selectivity, although this is equivalent with a difficult separation and recycling of the catalyst. Heterogenous catalysis in hydroformylation could overcome these disadvantages of homogeneous catalysts, but the associated aldehyde yields are still not competitive . In this work, heterogeneously catalyzed ethylene hydroformylation over a rhodium nanoparticle catalyst was performed. The aim is to probe the reaction kinetics to propose a suitable reaction mechanism which provides a comprehensive understanding of the reaction and serves to tune the reaction conditions into an optimal hydroformylation performance.

2 Methods

The commonly accepted Wilkinson mechanism describes the homogenously catalyzed hydroformylation, whereas the mechanism for heterogeneously catalyzed hydroformylation is still a subject of active research. In gas-phase heterogeneous catalysis, Langmuir-Hinshelwood mechanisms are generally used to describe the surface adsorption and surface reaction, assuming a certain rate-determining step. The major hydroformylation products are the desired product propanal and the hydrogenation product ethane, along with trace amounts of propanol depending on the reaction conditions. To get first indications on the kinetic relevance of the elementary steps involved, a power law model was developed and regressed to the data, accounting for hydroformylation (HF) and hydrogenation (HY). The detailed reaction mechanism and employed power law equations are shown in Figure 1. In the detailed reaction mechanism, propanal is formed in three steps: (1) ethylene hydrogenation (2) CO insertion and (3) propionyl hydrogenation. Ethane, on the other hand, is formed via ethylene hydrogenation (1) followed by ethyl hydrogenation (4).

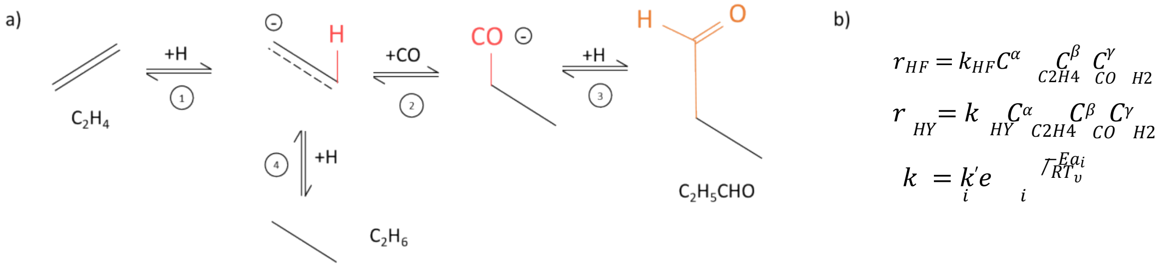

$$r_{HF} = k_{HF} C^{\alpha}_{C2H4} C^{\beta}_{CO} C^{\gamma}_{H2}$$

$$r_{HY} = k_{HY} C^{\alpha}_{C2H4} C^{\beta}_{CO} C^{\gamma}_{H2}$$

$$k_i = k'_i e^{-\frac{Ea_i}{RT_v}}$$

Figure 1. a) Reaction mechanism for hydroformylation and hydrogenation of ethylene and b) the power law model equations

Results and discussions

A power law model was employed to determine the apparent activation energies for hydroformylation and hydrogenation and the reaction orders of the components. The regression of 50 experiments at temperatures ranging from 120 °C to 175 °C, total pressures from 10 to 60 bar and molar ratios (C_2H_4:CO:H_2) of 1-4:1:1 and 1:1:1-4 was carried out using a plug flow reactor model and resulted in an accurate reproduction of the data, see Figure 2 b). The parameter estimates obtained in the regression are provided in Figure 2 a). A higher apparent activation energy was obtained for hydrogenation (82 kJ/mol) compared to hydroformylation (37 kJ/mol). The values, in agreement with the literature [1], explain the increased ethylene selectivity at higher temperatures. Hence, lower temperatures enhance propanal productions over ethane. For both, hydroformylation and hydrogenation, a negative reaction order was found for CO, indicating that it acts as an inhibitor for both reactions. This can be explained by the high surface coverage of CO due to its high heat of adsorption, resulting in almost total coverage of CO at low temperatures, leading to very low ethylene conversions (<10%).

a)

i	HF	HY
Ea_i	3.69E+04	8.23E+04
k'_i	3.31E-05	3.18E-05
α_i	0.82	1.02
β_i	-1.39	-2.03
γ_i	0.88	1.24

b)

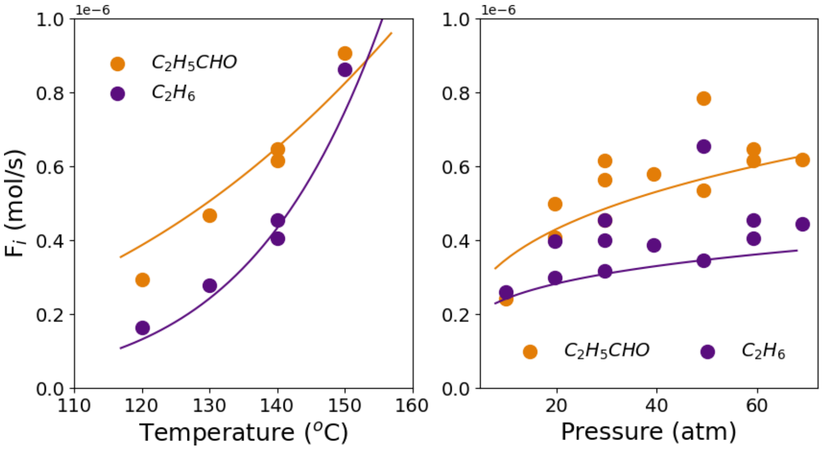

Figure 2. a) Regressed parameters for ethylene hydroformylation over rhodium nanoparticles catalyst and b) simulated using a power law model and experimentally measured flow rates of propanal and ethane during ethylene hydroformylation as a function of temperature (P_{tot} = 60 bar) and total pressure (T = 140 °C). W_{cat} = 3 g, C_2H_4/CO/H_2 = 1:1:1, Dilution = 22 % N_2.

Analysis of the reaction orders indicates a positive effect of H_2 and C_2H_4 on both hydroformylation and hydrogenation reactions, suggesting their involvement in the kinetically most relevant reactions. On one hand, for hydroformylation, ethylene hydrogenation (1) involves adsorbed H and C_2H_4, showing to be a promising candidate for the rate-determining step. On the other hand, the lower total reaction order of hydrogenation (0.23) compared to hydroformylation (0.31) could suggest a different kinetically most relevant reaction, such as the H-addition to ethyl (4), in which ethylene and H_2 also both play a role.

Conclusions

The proposed kinetic model for the heterogeneously catalyzed ethylene hydroformylation in a plug flow reactor describes the temperature and total pressure effect. Initial findings indicate that low temperature has a twofold opposing impact on hydroformylation. While it favors steering the reactions towards the production of propanal over ethane, it also results in elevated CO surface coverage which inhibits the reaction. The H-additions to ethylene and ethyl were suggested as the kinetically most relevant reactions for hydroformylation and hydrogenation, respectively. Moving forward, its essential to explore alternative reaction conditions that limit the partial pressure of CO ensuring a more balanced distribution of the reactants on the catalyst surface.

References

[1] N. Navidi, J. W. Thybaut, and G. B. Marin, “Experimental investigation of ethylene hydroformylation to propanal on Rh and Co based catalysts,” Appl. Catal. Gen., vol. 469, pp. 357–366, Jan. 2014.

Keywords

Heterogeneous hydroformylation ; kinetic assessment ; rhodium catalyst ; ethylene

Mon. 09/09 // 15:40-16:00

CK – III – 1

Transient techniques in the investigation of three-phase catalytic processes: epoxidation of alkenes in trickle bed reactor

Tapio Salmi[1*], Vincenzo Russo[1,2], Matias Alvear Cabezón[1], Michele Emanuele Fortunato[1,2], Christoph Schmidt[1], Christopher Stäglich[1], Kari Eränen[1]

1 Laboratory of Industrial Chemistry and Reaction Engineering (TKR), Johan Gadolin Process Chemistry Centre (PCC), Åbo Akademi University, FI-20500 Turku/Åbo Finland; 2 Department of Chemical Sciences, Università di Napoli "Federico II", IT-80126 Napoli, Italy
**Corresponding author: tapio.salmi@abo.fi*

Highlights

- Epoxidation of alkenes under transient conditions was studied in a laboratory-scale trickle bed reactor.
- The effect of process parameters on the product formation was illustrated.
- The influence of the catalyst particle size was elucidated in the experiments.
- Mathematical modelling was successfully applied to describe the transient behavior of the three-phase system.

Introduction

Experimental investigations and mathematical modelling of transient states of continuous catalytic reactors are important activities because of many reasons, e.g. to describe and predict reactor start-up and shut-down behavior, process disturbances, periodic operation of chemical reactors, to describe systems which are transient per se (self-oscillating processes, deactivating catalysts). Last but not least, transient methods are very strong tools in in the investigation of catalytic surface reaction mechanisms, since the surface concentrations of the active species change during the transient period of operation. The common way to apply transient techniques is to introduce pulse or step changes of at the inlet of a chemical reactor filled with catalyst particles or structured catalyst elements. The concentration responses at the reactor outlet are measured with rapid analytical techniques, such as quadrupole mass spectrometry, micro gas chromatography, infrared spectroscopy or with specific online sensors of chemical compounds. A particularly powerful approach is to combine transient studies in conventional laboratory reactor studies (tubular and tank reactors) with in situ investigations of active and spectator species on catalyst surfaces by applying in situ FT-ATR technique. Transient investigations of catalytic three-phase systems are still rather scarce, even though three-phase processes, such as hydrogenation, oxidation, epoxidation and isomerization reactions, are of enormous practical importance. The very important issue to be kept in the mind when applying transient techniques in catalytic three-phase systems is the dynamics of the different processes involved: surface processes (adsorption, surface reaction, desorption), diffusion processes in catalyst pores and liquid films around the catalyst layer and at the gas-liquid interphase as well as the fluid dynamics. The time constants of these processes are highly different; therefore, the selection of the process parameters is of crucial importance. In this work, the power of transient approach is illustrated with an exciting three-phase process, epoxidation of alkenes on TS-1 catalyst. The overall reaction is **Epoxide + Hydrogen peroxide →Epoxide + Water.** The role of ring-opening side reactions is minor.

Methods

The step response experiments, for investigating the kinetics and the fluid dynamics of the system, were conducted in a laboratory-scale trickle bed reactor. The catalyst bed was composed of the titanium silicate (TS-1) catalyst diluted in of quartz beads used as inert material. Experiments were conducted both with very small solid particle sizes (125 μm) and pressed catalyst pellets to compare the conditions of intrinsic kinetics and diffusion-affected kinetics. Epoxidation of ethylene and propylene we investigated at temperatures and pressures 15-75°C and 2.5-8.5 bar, respectively at a wide range of gas and liquid flow rates. The gas-phase composition was determined with on line gas chromatography (GC), whereas the samples were taken the reactor outlet for off line GC analysis.

Results and discussions

The very important issue to be kept in the mind when applying transient techniques in catalytic three-phase systems is the dynamics of the different processes involved: surface processes (adsorption, surface reaction, desorption), diffusion processes in catalyst pores and liquid films around the catalyst layer and at the gas-liquid interphase as well as the fluid dynamics. The time constants of these processes are highly different and easily masked; therefore, the selection and systematic variation of the process parameters, such as concentrations, temperature, pressure and flow rates are of crucial important. Therefore, the approach to mathematical modelling was kept very general in this work.

Some experimentally recorded step responses and model predictions are displayed in Figure 1. The interpretation of the step responses was based on the following mechanistic hypothesis: hydrogen peroxide interacts with the site on TS-1 and transforms it to an active form, after which the alkene molecule available in the pores reacts to epoxide. Besides this main reaction, some ring opening of the epoxide appears as a side reaction. Based on these hypotheses, rate equations for the elementary steps were formulated. Two approaches were compared: 'real' rate equations with surface concentrations 8or coverages) and rate equations, where the surface concentrations were eliminated with quasi- equilibrium hypotheses of adsorbed species and the surface reaction was presumed to be rate determining. The dynamic, time-dependent mathematical models for the trickle bed reactor and the catalyst particles consisted of partial parabolic differential equations (PDEs) which described the gas and liquid bulk phases as well as the liquid phase inside the catalyst pores as well as and ordinary differential equations (ODEs) which described adsorbed species on the active sites in the catalyst pores. The flow pattern was assumed to follow the axial dispersion model, where the dispersion coefficient was obtained from the step change experiments with inert tracers. The PDEs were converted to ODEs by discretization of the axial coordinate with finite differences and the ODE system created was solved numerically with stiff ODE solvers implemented in gPROMS and Modest software. A combined simplex-Levenberg-Marquardt method was used in parameter estimation. A comparison of the model predictions with experimental data is provided in Figure 1, which indicates a reasonable agreement between observed and predicted concentrations.

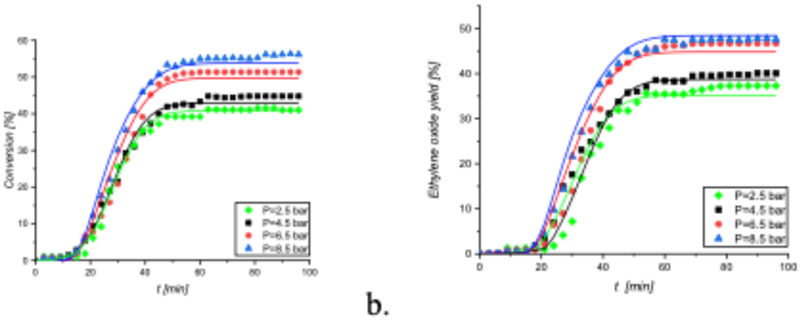

Figure 1. Effect of the pressure on the a) ethylene conversion and b) ethylene oxide yield.

Conclusions

The step response method was successfully applied to study the trickle bed reactor dynamics and catalytic surface processes in the epoxidation of ethylene and propylene on TS-1 catalyst. Kinetic models were derived and verified for the reaction systems. The effect of intraparticle diffusion on the overall dynamics was illustrated with catalyst particles of different sizes.

References

[1] Matias Alvear Cabezn, Epoxidation of light olefins on titanium silicates, Doctoral thesis, *Acta technologiae chemicae Aboensia* 2023 A/3

Keywords
transient techniques; three-phase system; trickle bed; mathematical modelling

Mon. 09/09 // 16:00-16:20

CK – III – 2

Solid foam catalyst for three-phase sugar hydrogenation: semi-batch and continuous operation

German Araujo-Barahona[1,2]*, Alberto Goicoechea-Torres[1,2], Maria Ciaramella[1,3], Miriam Cavaliere[1,3], Kari Eränen[1], Dmitry Y. Murzin[1], Juan García-Serna[2], Vincenzo Russo[3], Tapio Salmi[1]

1 Laboratory of Industrial Chemistry and Reaction Engineering (TKR), Åbo Akademi University, FI-20500 Turku/Åbo Finland; 2 Grupo de Tecnologías a Presión (PressTech), Instituto de Bioeconomía de la Universidad de Valladolid (BioEcoUVa), Universidad de Valladolid, ES-47011 Valladolid, Spain; Chemical Sciences Department, 3 Università di Napoli "Federico II", IT-80126 Naples, Italy
** german.araujobarahona@abo.fi*

Highlights

- An active Ru/C foam catalyst for selective sugar hydrogenation was prepared.
- The catalyst was successfully applied on continuous and semi-batch production of sugar alcohol.
- Advanced kinetic models based semi-competitive adsorption described the experimental data.

Introduction

Structured catalysts display attractive features for chemical reactors, such as a high void fraction, lower pressure drop compared to conventional packed beds of pellets, and low flow resistance. Solid foam catalysts stand out among structured catalysts because their structure provides a disruptive and tortuous flow path; hence, they exhibit exceptional mixing properties for gases and liquids along with a good mechanical stability [1]. Because of the thin catalyst layers used, solid foams are superior to conventional large catalyst pellets, which often suffer from heavy internal diffusion limitations. These characteristics render solid foam catalysts an interesting solution for three-phase reactions in fine chemical production, such as sugar alcohols. Sugar alcohols such as sorbitol and xylitol are utilized for alimentary, cosmetic, and pharmaceutical products, with a market value of three billion euro in 2023 [2]. Although the production process of these polyols is relatively well established, the finely dispersed nickel catalyst used for sugar hydrogenation is pyrophoric, susceptible to deactivation, and limited to semi-batch operation [3]. In this sense, Ru/C solid foam catalysts represent promising alternatives for continuous and stable production of sugar alcohols because they combine the high activity and stability of the Ru/C system with a low pressure drop, suppressed diffusion resistance inside the catalyst layer, and improved gas-liquid mixing provided by the foam structure coated with a thin catalyst layer. The objective of this study was to develop a Ru/C solid foam catalyst for the selective hydrogenation of sugar monomers and dimers, i.e., xylose, arabinose, galactose, and lactose and test their activity, selectivity, and durability in semi-batch and continuous operation.

Methods

Solid foam catalysts were synthesized by coating cylindrical foam pieces (porosity=96%) with polyfurfuryl alcohol through a controlled polymerization process in the presence of oxalic acid as the polymerization catalyst and polyethylene glycol (PEG; molar mass= 80 kDa) as the pore former (0-20 wt. %) to tailor the porosity of the resulting carbon layer. The formed polymer was pyrolyzed, thereafter activated with oxygen, and functionalized with dilute nitric acid. Ruthenium nanoparticles were deposited on the carbon layer by incipient wetness impregnation followed by direct reduction with hydrogen.

Catalyst screening in semi-batch mode was performed to identify the best catalyst preparation conditions. The most active catalyst was utilized in a systematic kinetic study, exploring the effect of temperature (60-120°C), hydrogen pressure (20-60 bar), and sugar concentration (0.065-0.26 M) on the intrinsic hydrogenation kinetics. Continuous operation experiments were conducted in a parallel screening reactor provided consisting of six isothermal beds, varying the process parameters such as temperature (60-120°C), liquid flow rate (0.25-1.25 ml/mol), and feed concentration (0.065-0.39 M). The liquid flow pattern was characterized using step-response experiments using xylitol as the tracer. The liquid hold-up under different reaction conditions was determined using a close-loop gravimetric method, employing helium as testing gas.

Results and discussion

The foam catalyst prepared with 5 wt. % of PEG displayed a carbon coating with a meso-to-micropore volume ratio of 1, in contrast to the value of 0.12 observed for the catalyst prepared without PEG. The introduction of mesoporosity into the 5 wt.% PEG catalyst enabled a higher dispersion of the Ru nanoparticles, yielding a twofold increase in both the initial rate and the stability for xylose hydrogenation. The Ru loading was 1.7 wt. % with an average nanoparticle size of 3 nm, maintaining stable activity for over 200 hours.

Selectivity values with the best catalyst exceeded 98% in the semi-batch experiments, while the sugar conversions ranged from 50% to 99%, depending on the temperature. A kinetic model based on the assumption of semi-competitive adsorption behavior among sugar molecules and hydrogen was successfully implemented to describe the intrinsic kinetic data and the effect of the process parameters along with insights on the complex mode of adsorption of sugars on the active sites of the catalyst.

Figure 1 displays the effect of temperature, liquid flow, and feed concentration on continuous xylose hydrogenation. The xylitol selectivity values were higher than 92%. The catalyst exhibited excellent stability throughout the time-on-stream (TOS). A slight decrease in the selectivity was observed with increasing temperature due to by-products formation. As expected, the decrease in the liquid flow rate and feed concentration enhanced sugar conversion.

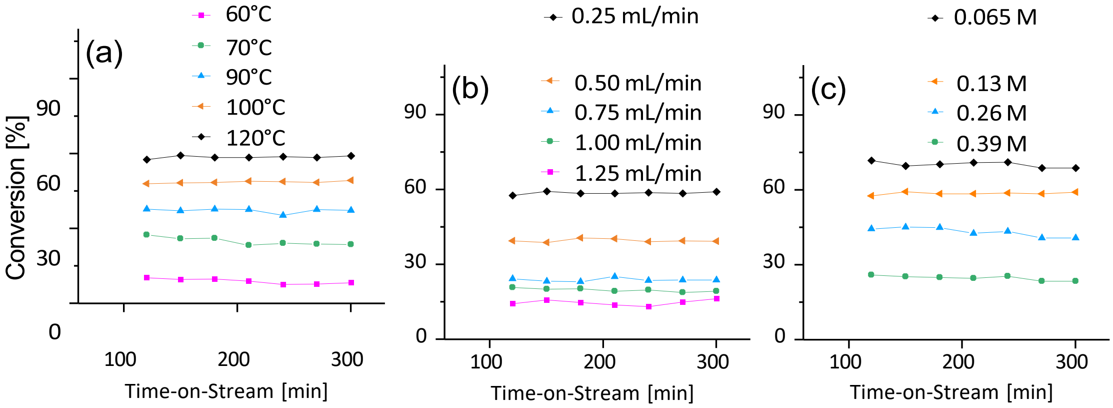

Figure 1. Continuous xylose hydrogenation using Ru/C solid foam catalysts: (a) effect of temperature, (b) liquid flow, and (c) feed concentration. Conditions: 0.013gRu (three foams), 30 mL/min H_2.

Conclusions

This study complied the development, optimization, and application of Ru/C foam catalysts for hydrogenation of primary sugars from biomass in continuous and semi-batch operation modes. The performance demonstrated by this solid foam catalyst presents a promising alternative to the conventional semi-batch production process based on dispersed catalysts.

References

[1] K. Pangarkar, T.J. Schildhauer, J.R. Van Ommen, J. Nijenhuis, F. Kapteijn, J.A. Moulijn, Structured packings for multiphase catalytic reactors, Ind. Eng. Chem. Res. 47 (2008).

[2] A. Kumar, Global markets for non-sugar sweeteners, pp. 113, BCC Research LLC, 2019.

[3] B.W. Hoffer, E. Crezee, P.R.M. Mooijman, A.D. Van Langeveld, F. Kapteijn, J.A. Moulijn, Carbon supported Ru catalysts as promising alternative for Raney-type Ni in the selective hydrogenation of D-glucose, Catal. Today 79–80 (2003) 35–41.

Keywords
Structured catalyst, three-phase reaction, solid foam, sugar alcohol

Mon. 09/09 // 16:20-16:40

CK – III – 3

Transient reaction kinetics for CO hydrogenation: Combining periodic experimentation with microkinetic modeling

Max Gäßler[1], Simon Hermann, Jens Friedland, Robert Güttel[1]*

1 Institute of Chemical Engineering, Ulm University, 89081 Ulm, Germany

**Corresponding author: robert.guettel@uni-ulm.de*

Highlights

- Transient periodic experimentation methods are applied to CO hydrogenation
- Insights into transient kinetics for CH_4 and H_2O formation are derived
- Micro-kinetic modelling considers the involved surface processes
- Additional surface phase with H_2O storage capacity is also included

Introduction

The catalytic CO/CO2 hydrogenation is key in synthesis of hydrocarbons via Power-to-X processes. However, mechanistic aspects of involved reactions are still under debate due to their complex nature. In addition, reaction kinetics valid under transient conditions are not yet available. In recent years, sophisticated transient experimental methods have been developed to elucidate kinetic and mechanistic effects on the catalyst surface [1,2]. These methods provide the data basis to deduce transient reaction kinetics valid in a broad range of realistic operation conditions. In particular, transient microkinetic models appear promising.

Methods

In this contribution, the periodic transient kinetics (PTK) method is employed, which is based on periodic switching between two feed gas mixtures and measuring the product gas compositions with high temporal resolution via calibrated mass spectrometry (MS) [3,4]. Ar is used as internal standard, for in situ measurement of the residence time distribution (RTD). The external standard Ne allows to derive molar flow rates of involved gaseous species. Therefore, the transient responses of the gaseous species, e.g., CO, CO_2, H_2O and CH_4, are measured and evaluated to derive transient molar flow rates for model-based kinetic analysis. The developed microkinetic model considers the surface reaction and the ad-/desorption steps as well as the RTD in the reactor setup. Furthermore, surface species are implemented, which are most probably participating in the reaction mechanism. The reaction mechanism was derived by systematic fitting of kinetic parameters to the experimental data and subsequent simplification.

Results and discussion

Fig. 1 shows the measured step responses for CH_4 and H_2O during build-up (switch from H_2 to syngas) and back-transient phase (switch back to H_2) together with the RTD. For CH_4 an overshoot followed by a characteristic decrease is observed after both switching events. In addition, deviations between the measured CH_4 response and that expected from RTD are visible. These observations are caused by transient kinetic effects at the surface. For instance, after switching from H_2/He to H_2/CO/Ar, which corresponds to the build-up phase, a raising CO fraction in the gas phase is contacted with a surface saturated with H_2. This leads to instantaneous CO dissociation and hydrogenation up to the observed maximum. Further raising CO fractions lead to saturation of the surface with CO and probably also O-species, which decelerates the hydrogenation rate. Hence, CH_4 formation rate approaches steady-state values asymptotically.

Interestingly, the H_2O response is retarded compared to CH_4, even though both compounds are formed simultaneously based on stoichiometry. Kruse et al. assume that CO dissociates into C* and O* surface species [5]. O* is subsequently hydrogenated to H_2O, with a lower rate than C* hydrogenation to CH_4. We assume that the H_2O formed even spills over to the support and remains adsorbed for a certain period of time. Hence, the support acts as a H_2O storage, which retards the respective response.

In our microkinetic model we included several mechanistic pathways known from literature and fitted the respective kinetic parameters for different mechanisms. We ensured global optimization by using the basin-hopping approach proposed by Deutschmann et al. [6]. The comparison between measured and predicted transient responses in Fig. 1 exhibits a good agreement for CH_4 in the shown mechanism. Even though a certain discrepancy for H_2O still exists, it appears plausible that H_2O (or other O species) are adsorbed at the support after spill-over from the active metal. In this scenario the support provides a significant storage capacity. Hence, the focus of our ongoing work is to understand the mechanism and reaction-transport trajectory of H_2O.

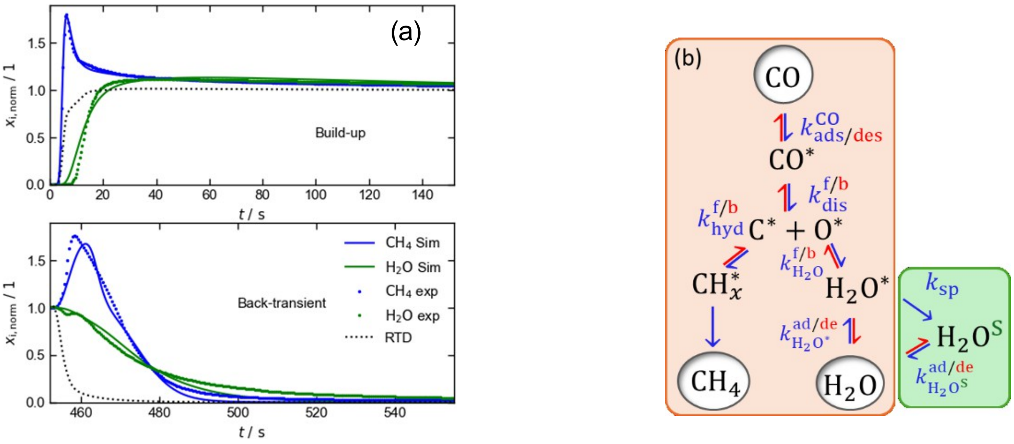

Figure 1. (a) Measured and simulated step response of CH_4 and H_2O and residence time distribution (RTD); 280 °C, 4 bar, H_2:CO = 4:1, 100 mg 10 wt% Co/TiO_2. (b) Proposed reaction mechanism for CH_4 and H_2O formation and H_2O storage on support.

Conclusions

We developed a transient microkinetic model for CO hydrogenation on Cobalt-catalysts based on sophisticated experimental data under technical relevant conditions, which will be extended to Fischer-Tropsch synthesis. We are able to show that the reaction-transport trajectory of H_2O involves storage at the support. These insights open the door to improve catalysts for CO hydrogenation under steady-state and dynamic operation conditions.

References

[1] R. Zhang, Y. Wang, P. Gaspard, N. Kruse Science 382 (2023) 99-103.
[2] W. Chen, I. A. W. Filot, R. Pestman, E. J. M. Hensen ACS Catal. 12 (2017) 8061-8071.
[3] M. Gäßler, J. Stahl, M. Schowalter, S. Pokhrel, A. Rosenauer, L. Mädler, R. Güttel ChemCatChem 14 (2022) e202200286.
[4] D. Meyer, J. Friedland, J. Schumacher, M. Gäßler, R. Güttel Chem. Eng. Sci. 250 (2022) 117405.
[5] A. Raub, H. Karroum, M. Athariboroujeny, N. Kruse, Catal. Letters 151 (2021) 613-626
[6] R. Chacko, K. Keller, S. Tischer, A. B. Shirsath, P. Lott, S. Angeli, O. Deutschmann, J. Phys. Chem. C 127 (2023) 7628-7639.

Keywords
CO-hydrogenation, transient experimental methods, micro-kinetic modelling, metal-support interaction

Mon. 09/09 // 16:40-17:00

CK – III – 4

Mechanistic insights into r-WGS reaction on Rh and Pt via a combined experimental and structure-dependent microkinetic analysis

G. Spanò[1], L. Nardi[1], G. Contaldo[1], R. Cheula[1], C. Negri[1], and M. Maestri[1]*
[1]Laboratory of Catalysis and Catalytic Processes, Dipartimento di Energia, Politecnico di Milano, via la Masa 34, 20156, Milano (Italy)
**Matteo Maestri: matteo.maestri@polimi.it*

Highlights

- The oxygen affinity of the catalyst determines the Reverse Water-Gas Shift reaction mechanism.
- CO_2 is activated *via* a dissociation route on Rh and *via* a H-mediated pathway on Pt.
- Theoretical structure-dependent analysis is pivotal for a detailed description of reaction mechanisms.

Introduction

In the last few decades, there has been a significant increase in atmospheric CO_2 concentration, with carbon dioxide being the primarily responsible gas for the greenhouse effect. In this context, the upgrading of CO_2 produced by hard-to-replace processes into more valuable products is a compelling solution to cut the net CO_2 emissions. The Reverse Water-Gas Shift (r-WGS) reaction is an effective way to achieve this goal, producing CO, a fundamental block of the chemical industry. Despite its importance, there are still a lot of debates concerning the precise mechanism of this reaction, therefore a thorough mechanistic analysis is fundamental for the effective catalyst optimization [1,2]. As demonstrated by previous theoretical investigations from our group, the activation of CO_2 depends on the oxyphilic nature of the catalyst material [3]. In this study, we combine both theoretical and experimental methodologies to shed light on the r-WGS reaction's elementary steps. More in detail, we investigate how the reaction mechanism changes according to the specific oxygen-affinity of the surface, employing two different catalyst materials, 4wt.% Rh/α-Al_2O_3 and 4wt.% Pt/α-Al_2O_3. On one side, the experiments make it possible to identify the nature of the kinetically relevant transition state for the specific material. On the other side, the structure-dependent microkinetic analysis was pivotal to unveil the identity of the active site in terms of atomistic configuration, providing fundamental insights into the reaction mechanism.

Methods

Non-commercial 4wt.% Rh/α-Al_2O_3 and 4wt.% Pt/α-Al_2O_3 were prepared and tested in this work. The α-Al_2O_3 support was obtained from commercially available γ-Al_2O_3, through calcination at 1200°C. The preparation of the catalytic powder was made with the incipient wetness impregnation of the support, with $Rh(NO_3)_3$ and $Pt(NO_3)_4$ solutions. The catalytic tests were performed in powder and annular reactors (60mg of diluted (1:20) catalyst, to ensure an isothermal bed). PBE-D3 calculations were performed using QuantumEspresso. The morphology of heterogeneous catalyst nanoparticles as a function of the gas chemical potential is determined by means of *ab initio* thermodynamics and Wulff-Kaishew construction method. On the different Pt facets, the occurrence of 23 elementary steps is investigated to describe the r-WGS reaction mechanism. The climbing-image nudged elastic (CI-NEB) is adopted for the evaluation of the geometry of the transition states for each elementary step.

Results and discussion

We carried out a comprehensive experimental investigation of the kinetic mechanism governing the r-WGS reaction considering a wide range of operating conditions. The reaction rate of the r-WGS reaction measurements exhibited a direct proportionality on the concentrations of CO_2 for both catalysts. On the contrary, the dependence on H_2 concentration changed between Rh and Pt and was also affected by the specific operating conditions. On rhodium-based catalyst, the rate was found to depend on H_2 only at low concentrations, transitioning to a 0th-order dependence as H_2 concentration increased. Conversely, the reaction rate showed a dependency on H_2 on Pt in the entire range of operating conditions. In addition to that, CO caused a mild inhibition effect on both catalysts at 600°C. Pt and Rh possess differing affinities for oxygen (the binding energies are -4.5 and -5.3 eV respectively). As suggested in [3], oxophilic surfaces tend to activate CO_2 via dissociation into CO^* and O^*, while surfaces with a lower oxophilicity are more likely to facilitate a hydrogen-mediated pathway. This experimental evidence was therefore rationalized by proposing that on Rh-based catalyst, CO_2 is activated through dissociation into CO^* and O^* without direct involvement of H_2, while on Pt-based catalyst, CO_2 activation occurs *via* a hydrogen-mediated route with the formation of a $COOH^*$ intermediate. To elucidate this mechanistic interpretation, we conducted a structure-dependent microkinetic analysis on both materials based on DFT calculations [4]. We accounted for the presence of several facets that the catalyst nanoparticles can expose under reaction conditions, considering both their activity and abundance with respect to the total catalyst surface to compute reaction rates. This structure-dependency inclusion is essential for the identification of the dominant active site that determines the kinetics of the macroscopic reaction. As shown in Fig.1, CO_2 is found to be activated *via* dissociation into CO^* and O^* on Rh and *via* a hydrogen-mediated route on Pt, in agreement with experiments. In the case of rhodium, we found that Rh(100) is the dominant active site, since its relatively low abundance is counterbalanced by its high turnover frequency. In the case of platinum, Pt(111) is the prevalent active site, since it is the most abundant facet of Pt nanoparticles and exhibits the highest turnover frequency. The degree of rate control (DRC) analysis revealed that, on Rh, CO_2 dissociation is the most kinetically relevant step, while H_2O^* formation presents a small but not negligible DRC. The overall reaction rate is indeed proportional to the partial pressure of CO_2, while the mild positive order of H_2 is attributed to the direct proportionality of H_2O^* formation. In contrast, on Pt, the rate-determining step is the CO_2^* reaction with H^* to form t-$COOH^*$. The reaction rate is indeed proportional to the partial pressure of CO_2 and H_2. These findings led to apparent reaction orders which fully reconcile with experimental data.

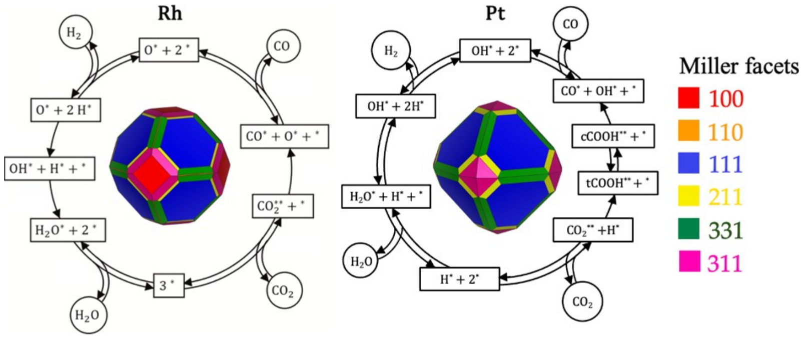

Figure 1. Reaction mechanisms for r-WGS on Rh (left) and Pt (right).

Conclusion

In this study we employed a combined theoretical and experimental approach to unveil the r-WGS reaction mechanism, crucial for reducing CO_2 emissions. Using 4wt.% Rh/α-Al_2O_3 and 4wt.% Pt/α-Al_2O_3 catalysts, we explored the impact of varying oxygen-affinity of the catalyst on the reaction mechanism. Rh catalyst activates CO_2 through dissociation into CO^* and O^*, while on Pt the reaction follows a hydrogen-mediated route forming a $COOH^*$ intermediate. The structure-dependent methodology adopted for the description of catalyst nanoparticles was essential for the interpretation of experimental measurements. Indeed, it allowed to identify the most kinetically relevant steps and the dominant active sites. These findings make it possible to derive fundamental rate equations for catalyst design and optimization. Project funded under PNRR-NextGenerationEU "Network 4 Energy Sustainable Transition – NEST".

References

[1] I. Alam, R. Cheula, G. Moroni, L. Nardi, M. Maestri, Catal. Sci. Technol., 2021, 11, 6601
[2] J.A. Martens et al., 2017, 10, 1039
[3] L. Dietz, S. Piccinin, M. Maestri, J. Phys. Chem. C 2015, 119, 4959
[4] R. Cheula and M. Maestri, Catalysis Today, 2022, 387, 159

Keywords
Active sites; multiscale modeling; density functional theory; reverse water-gas shift.

Mon. 09/09 // 17:00-17:20

CK – III – 5

Unravelling the liquid-phase oxidation of cyclohexane by computer-aided kinetic model development with 'ALKIMO'

Kevin De Ras[1,2], Gust Popelier[1], Lander Nelis[1], Connor Huntwork[2], Robin Vercauteren[1], Unni Kurumbail[3], Joris W. Thybaut[1], Ive Hermans[2,3], Kevin M. Van Geem[1,*]

1) Laboratory for Chemical Technology, Ghent University, Technologiepark-Zwijnaarde 125, Ghent 9052, Belgium; 2) Department of Chemistry, University of Wisconsin-Madison, 1101 University Avenue, Madison, Wisconsin 53706, United States; 3) Department of Chemical & Biological Engineering, University of Wisconsin-Madison, 1415 Engineering Drive, Madison, Wisconsin 53706, United States.

**Corresponding author: Kevin.VanGeem@UGent.be*

Highlights

- A tool has been developed for computer-aided kinetic model development of liquid-phase reactions
- The liquid-phase oxidation of cyclohexane was investigated as proof-of-concept
- Experimental data was obtained from a new continuous slug flow reactor unit
- The kinetic model can predict the experimental trends well without fitting adjustable parameters

1. Introduction

The design and optimal operation of industrial production processes requires a thorough understanding of the chemical process, from the molecular scale up to the scale of the entire process plant. An accurate kinetic model is thereby a powerful and valuable tool. Significant progress has been made in the development of kinetic models for various gas-phase processes. However, this is in stark contrast to liquid-phase processes governed by radical chemistry for which there is a lack of fundamental knowledge. Detailed kinetic models for radical reactions typically contain up to hundreds of species and several thousands of reactions. The manual development of a kinetic model would thereby be tedious, error-prone and often incomplete. To prevent this, automatic kinetic model generation tools have been developed for gas-phase reactions, such as the in-house developed tool 'Genesys' [1].

A new kinetic modeling tool has been developed, denoted as 'ALKIMO' (Automated Liquid-phase Kinetic Modeler), to transform gas-phase into liquid-phase models by considering the impact of the solvent. As proof-of-concept, the liquid-phase oxidation of cyclohexane has been investigated, which is the most important industrial process for synthesis of cyclohexanone and cyclohexanol, of which the molecular chemistry is still not fully understood [2]. New experimental data for this reaction has been acquired from a continuous slug flow reactor unit. A detailed kinetic model for the oxidation of cyclohexane has been developed with ALKIMO and reactor simulations have been performed with a slug flow reactor model to compare the model predictions and experimental observations.

2. Methods

To enable the construction of kinetic models for liquid-phase reactions, ALKIMO needs to assign accurate thermodynamic and kinetic parameters to species and reactions, respectively. Ideally, these parameters are obtained from experimental measurements or quantum chemical calculations. Since these methods are time-consuming, where possible, ALKIMO makes use of approximative methods such as equations of state (EoS), or group additivity theory to calculate the solvation energies. Quantum chemical calculations for the liquid phase were performed with the COSMO*therm* software [3]. The gas-phase thermodynamic parameters and reaction rate coefficients were adapted with a correction for the solvation energy to obtain the liquid-phase parameters. In addition, the reaction rate coefficients were adapted to include the effect of diffusion limitations by use of the Stokes-Einstein equation.

To validate the developed kinetic model, experiments were performed with a new continuous slug flow reactor unit at industrially relevant conditions, i.e., at a pressure of 1.0 MPa and temperatures between 150 and 180 °C. The experiments were carried out for varying residence times, which allows thorough validation of the primary and secondary chemistry in the kinetic model. Quantitative analysis of the liquid product stream is performed with an off-line 1-D gas chromatograph equipped with a flame ionization detector and liquid injection. The experiments were simulated in Cantera with a slug flow reactor model and the newly developed kinetic model.

3. Results and discussion

The normalized product distribution predicted by preliminary plug flow reactor simulations was compared with experimental measurements, see Figure 1. In general, the product distribution predicted by the simulation is in good agreement with the experimental data. However, at low residence times, pronounced deviations are observed for cyclohexanol and cyclohexyl hydroperoxide, which is expected to improve when considering a more complex slug flow reactor model that captures the mass transport limitations between the gas and liquid phase. In addition, the kinetic model will be updated to enable prediction of the yields of byproducts such as adipic acid, glutaric acid and 6-hydroxyhexanoic acid, which were experimentally observed but not yet included in the model. At higher residence times, the share of cyclohexyl hydroperoxide, cyclohexanol and cyclohexanone are well predicted as the impact of mass transport limitations is limited. It was found that a significant fraction of the reactions is diffusion limited and not kinetically limited.

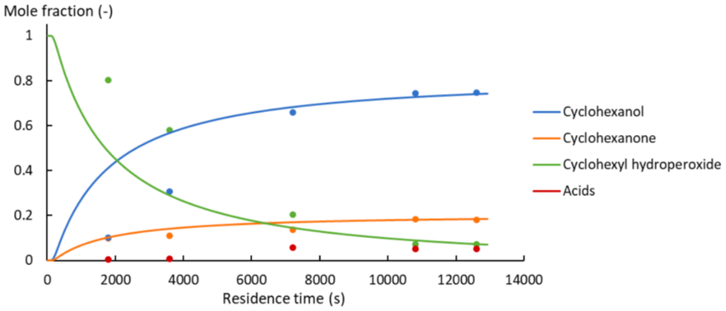

Figure 1. Normalized product distribution using mole fractions predicted by the liquid-phase kinetic model simulation (lines) and experimentally measured (symbols) at a temperature of 160 °C and pressure of 1.0 MPa.

4. Conclusions

A new kinetic modeling tool has been developed, denoted as ALKIMO, to transform a gas-phase kinetic model into a liquid-phase kinetic one. As a proof-of-concept, a kinetic model was generated for the liquid-phase oxidation of cyclohexane. Validation of the methodology was performed with a new experimental unit consisting of a continuous slug flow reactor, for a variety of industrially relevant reaction conditions. The experimental observations can be predicted by the kinetic model without fitting of parameters.

Acknowledgments

Kevin De Ras acknowledges financial support from the Fund for Scientific Research Flanders (FWO) via doctoral fellowship grant 3F018119 and long research stay abroad grant V402422N. The research leading to these results has also received funding from the European Research Council under the European Union's Horizon 2020 research and innovation program / ERC grant agreement n°818607.

References

[8] Vandewiele N., Van Geem K., Reyniers et al. (2012). Genesys: Kinetic Model Construction using Chemo-Informatics in Chemical Engineering Journal, 207, 526-538.

[9] Hermans I., Jacobs P. and Peeters J. (2007). The Formation of Byproducts in the Autoxidation of Cyclohexane in Chemistry: A European Journal, 13, 754-761.

[10] Klamt A. and Eckert F. (2004). Prediction of vapor liquid equilibria using COSMOtherm in Fluid Phase Equilibria, 217, 53-57.

Keywords

Automatic Kinetic Model Development; Cyclohexane Oxidation; Liquid-Phase Chemistry; Quantum Chemistry.

Wed. 11/09 // 10:40-11:00

CK – IV – 1
Impact of mild hydrothermal aging on NH_3, NO, CO, and SO_2 oxidation kinetics on a Cu/SSZ-13 catalyst

Tetyana Zheleznyak[1], Petr Kočí[1]*, William Epling[2]

1 University of Chemistry and Technology, Prague, Technická 5, Prague 16628, Czechia
2 University of Virginia, Charlottesville, 385 McCormick Rd, VA 22903, USA

**Corresponding author: petr.koci@vscht.cz*

Highlights
- Distinct rate coefficients for NH_3, NO, SO_2 and CO oxidation on ZCuOH and Z_2Cu.
- Cu sites transformation from ZCuOH to Z_2Cu described by a kinetic model.
- Analysis of TPR experiments suggests the activity is correlated to ZCuOH sites.
- Developed model predicts catalyst activity changes during mild hydrothermal aging.

1. Introduction

Selective catalytic reduction (SCR) using Cu/SSZ-13 catalysts is the prevailing method for reducing nitrogen oxides (NO_x) emissions from diesel engines. Different types of sites have been identified within the catalyst, including mono- and multinuclear framework copper sites and extra-framework CuO nanoparticles[1]. The distribution of copper sites depends on various factors such as Cu loading and Si/Al ratio. Within the literature, two primary framework sites are frequently discussed: ZCuOH and Z_2Cu. It has been reported that the more stable Z_2Cu sites are primarily formed at lower copper loadings, and the less stable ZCuOH sites are formed subsequently at higher Cu loadings. Elevated Si/Al ratios tend to favor ZCuOH sites, whereas lower Si/Al ratios lean towards a predominant Z_2Cu population[1].

The primary mechanisms responsible for Cu/SSZ-13 catalyst deactivation are hydrothermal aging (HTA) and sulfur poisoning. Mild HTA at temperatures below 750°C does not affect the zeolite structure but triggers the transformation of ZCuOH sites to Z_2Cu, thereby influencing catalyst activity[2]. In this work, we employ an integrated experimental and kinetic modeling strategy to study the impact of Cu site transformation during HTA on the rates of NH_3, NO, CO, and SO_2 oxidation. These reactions gain significance, particularly in the context of close-coupled SCR setups without an upstream oxidation catalyst, a configuration recently proposed to mitigate cold-start NO_x emissions and adhere to the upcoming stringent NO_x emission regulations.

2. Methods

The Cu/SSZ-13 catalyst used in this study was supplied by Cummins Inc. It was washcoated on a cordierite monolith structure with 300 cpsi. The Si:Al ratio in the SSZ-13 zeolite was 9.5 and the copper loading was 3.1 wt.%. All experiments were conducted in a tubular flow lab reactor. *In situ* experimental techniques such as diffuse reflectance infrared Fourier transform spectroscopy (DRIFTS), NH_3-TPD, H_2-TPR, and NH_3+NO titration, were used to quantify the active sites in the catalyst samples.

To describe transport and reactions in the studied catalyst samples, a heterogeneous 1D plug-flow mathematical model was employed, which consisted of mass and enthalpy balances in the gas and solid phases along the tubular reactor. The kinetics of NH_3, NO, CO, and SO_2 oxidation reactions were studied at steady state at temperatures ranging from 200 to 550 °C, comparing a degreened catalyst with the samples after 10 and 25 hours of hydrothermal aging at 600 °C.

3. Results and discussion

First, a kinetic model that describes the changes in ZCuOH and Z_2Cu site concentrations during hydrothermal aging was developed using the information from catalyst characterization. The model can predict the rate of Cu site transformation depending on temperature and actual site concentrations. Subsequently, the overall pre-exponential factors and activation energies of NH_3, NO, CO, and SO_2 oxidation were evaluated from reaction experiments on the degreened catalyst. The experimental data suggest no significant change in activation energies E_a with mild hydrothermal aging[3], hence the E_a parameters were fixed. Pre-exponential factors specific to ZCuOH and Z_2Cu sites were then evaluated from the experimental data including both degreened and aged catalysts, taking into account the changes in concentrations of the individual sites during the aging. The results suggest zero pre-exponential factors for all the oxidation reactions on Z_2Cu sites, thus the observed activity of NH_3, NO, CO, and SO_2 oxidation can be attributed to ZCuOH sites. The dependence on ZCuOH sites was further tested in two variants: (i) considering 1st order in ZCuOH site concentration (corresponding to a single Cu site involved in the reaction mechanism), and (ii) considering 2nd order in ZCuOH site concentration (corresponding to Cu dimers involved in the reaction mechanism)[3]. Figure 1 shows the results of the predictive 1st- and 2nd-order kinetic model coupled with ZCuOH and Z_2Cu site concentrations from HTA kinetics, compared to the best possible fit independent of the site concentrations. The developed predictive model provides reasonable estimates of the catalyst activity evolution during mild hydrothermal aging, depending on the actual distribution of active sites. The predictive model considering 1st order in ZCuOH site concentration matches the experimental data closely for NO and SO_2 oxidation. The measured data for NH_3 oxidation do not allow clear discrimination between the 1st and 2nd order. On the other hand, CO oxidation activity measured on the HTA samples is close to the predictions considering 2nd-order dependence on ZCuOH sites concentration.

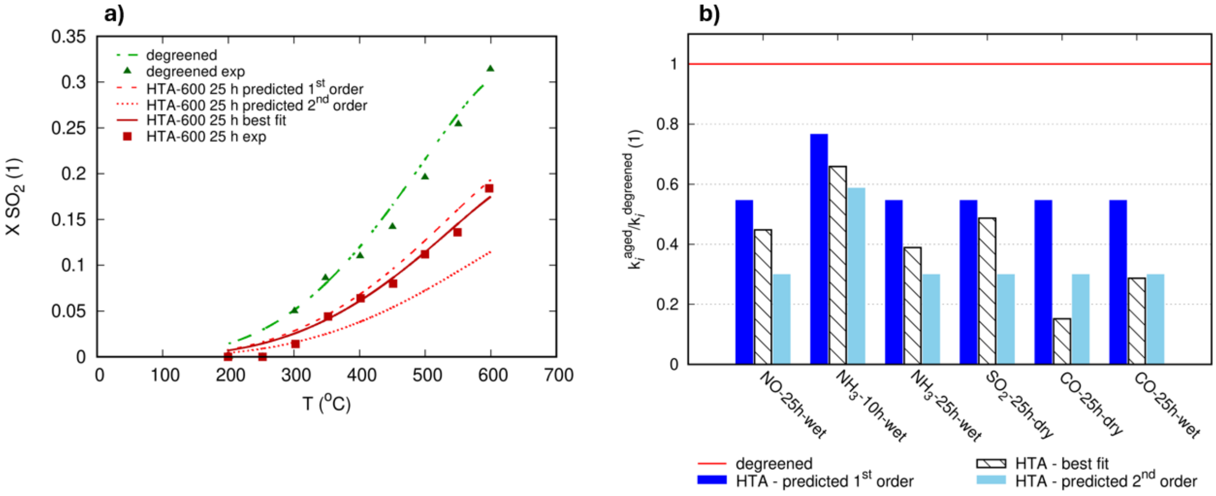

Figure 1. a) Temperature dependence of steady-state outlet conversions of SO_2 for degreened and hydrothermally aged (HTA) Cu/SSZ-13 catalyst; predictions based on actual ZCuOH site density vs. the best fit independent of site densities. b) Relative catalyst activity in individual reactions as predicted by the HTA model; dark blue – 1st order prediction, light blue – 2nd order prediction, dashed bars – fitted; red line = reference activity of the degreened sample.

4. Conclusions

The developed model can predict the evolution of active site densities during catalyst operation as well as the corresponding changes in catalytic activity for NH_3, NO, CO, and SO_2 oxidation. The experimental and modeling results suggest negligible rates of the studied reactions on Z_2Cu sites and a close correlation of the overall reaction rates to the concentration of ZCuOH sites.

The proposed coupling of Cu site transformation kinetics with the kinetics of oxidation reactions provides a powerful tool for predictive simulations of SCR catalyst performance in terms of changes with time and under realistic operating conditions. In particular, the changes in NH_3 oxidation rates are crucial for precise urea dosing and SO_2 oxidation represents a key step in the sulfur poisoning mechanism.

References

[1] C. Paolucci, A. A. Parekh, I. Khurana, J. R. Di Iorio, H. Li, J. D. Albarracin Caballero, A. J. Shih, T. Anggara, W. N. Delgass, J. T. Miller, F. H Ribeiro, R. Gounder, W. F. Schneider, J. Am. Chem. Soc. 2016, 138 (18), 6028-6048

[2] L. Wei, Y.-R. Chen, S. Marino, Y. Gu, W. S. Epling, Chem. Eng. J. 2023, 467, 143318

[3] T. Zheleznyak, P. Kočí, W. Epling, Chem. Eng. J. 2024, under review

Keywords
SCR; catalyst; aging; kinetics.

CK – IV – 2

Upscaling of a debenzylation reaction in pharmaceutical synthesis: the mass transfer paradox

Wout Callewaert[1], Jeroen Lauwaert[2], Mairtin McNamara[3], Joris W. Thybaut[1]*

1 Laboratory for Chemical Technology (LCT), Department of Materials, Textiles, and Chemical Engineering, Ghent University, Technologiepark 125, B-9052 Ghent, Belgium;

2 Industrial Catalysis and Adsorption Technology (INCAT), Department of Materials, Textiles, and Chemical Engineering, Ghent University, Valentin Vaerwyckweg 1, B-9000 Ghent, Belgium;

3 Pharmaceutical Research and Development, Division of Janssen Pharmaceutica, Johnson & Johnson, Turnhoutseweg 30, B-2340 Beerse, Belgium

**Corresponding author: joris.thybaut@ugent.be*

Highlights

- Up-scaling of a debenzylation reaction starting from lab scale data.
- Pilot scale can be simulated by incorporating a volumetric mass transfer coefficient.
- The overall kinetics are governed by an interplay between mass transfer and intrinsic kinetics.
- Direct industrial reactor simulation and optimization.

1. Introduction

Traditional process modeling approaches in pharmaceutical engineering, such as Design of Experiments (DoE), can be time-consuming and resource-intensive [1]. The present work explores an alternative strategy using readily available data gathered during the development phase and industrial production of the active pharmaceutical ingredient (API) for a more efficient model based optimization. The goal is to focus on those phenomena which are relevant, rather than covering every individual physical and chemical interaction in the utmost detail. The considered approach is reminiscent of the meso-scale modelling as proposed by J. Li et al [2].

In this work, a debenzylation reaction is upscaled, as it is performed in a pharmaceutical context. The reaction is catalyzed by a Pd/C catalyst, removing a benzyl group from an amine functionality. Debenzylation reactions are important in the pharmaceutical industry, as benzene is often used as a protection group to enable chemical stability of functional groups such as amines, alcohols, and acids, during the multi-step synthesis of APIs [3, 4].

2. Methods

The debenzylation reaction has been performed at three scales: lab, pilot, and industrial scale. The lab scale data was used to construct a kinetic model. Since the lab scale data was obtained during the development stage of the API, the experiments were carried out at conditions similar to the industrial ones, with temperatures ranging from 60 °C to 90 °C and total pressure varied between 2 and 4.5 bar absolute.

Preliminary assessments indicated that the reaction was partially mass transfer limited at the pilot and industrial scale. Consequently, the model equations incorporated a volumetric mass transfer coefficient (k_La), accounting for the hydrogen transfer from the gas phase to the solution. To determine this coefficient, the reactors were characterized by performing specific experiments in absence of reaction.

The conversion at the pilot scale was measured by both intermediate sampling and mid-infrared spectroscopy. Sampling was not feasible at the industrial scale, since the reaction was performed at temperatures above the atmospheric boiling point of the solution.

3. Results and discussion

A kinetic model was constructed for the debenzylation reaction based on lab scale data. The model exhibits a negative effect of increasing hydrogen pressure, suggesting that the catalyst surface is predominantly occupied by hydrogen.

$$r = \frac{k' \, c_{\mathrm{R_2N-Bn}} \sqrt{c_{\mathrm{H_2}}} \, c_{\mathrm{cat}}{}^2}{\left(1+\sqrt{K_{\mathrm{H_2}} c_{\mathrm{H_2}}}\right)^2}$$

Accounting for gas-liquid mass transfer, making use of a volumetric mass transfer coefficient, on top of the intrinsic chemical kinetics, the concentration profiles observed at the pilot scale can be successfully reproduced, see Figure 1. Furthermore, the simulated hydrogen concentration profiles indicate that the reaction is initially limited by the mass transfer from the gas phase to the liquid phase. As conversion increases and the intrinsic reaction rate decreases due to reactant depletion, the gas-liquid mass transfer is no longer rate limiting. As counter-intuitive as it may seem, the overall observed reaction rate at the pilot scale is higher than the intrinsic rate, because the mass transfer limitations induce a lower hydrogen concentration in the solution and, hence, a less pronounced inhibition of the debenzylation reaction.

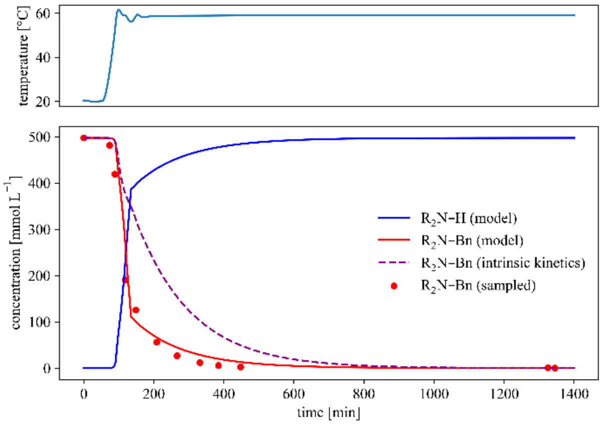

Figure 1. Concentration profiles of the reactant R_2N-Bn and the product R_2N-H during the debenzylation reaction for a batch conducted in the pilot-scale reactor. The temperature profile of the reactor is displayed above the concentration profiles. The reaction is limited by the mass transfer of hydrogen between 90 and 130 minutes. The concentration profile in absence of mass transfer limitations is also shown for the reactant R_2N-Bn.

Building upon the results from the pilot scale, the industrial scale can be simulated by incorporating the volumetric mass transfer coefficient of the specific reactor. This allows for the prediction of concentration profiles during the reaction, which could not be measured experimentally. As such, the model can be used to predict the reaction endpoint and optimize reaction times.

4. Conclusions

The developed model successfully simulates the debenzylation reaction at larger scales, where mass transfer limitations counterintuitively lead to a higher observed reaction rate due to a less pronounced hydrogen inhibition. In addition to these insights, the model can also simulate the behavior of the reactor at other operating conditions. For this specific reaction, the model can for instance support process optimization by identifying the optimal hydrogen pressure and stirring speed.

References

[1] Y. Dong, T. Yang, Y. Xing, J. Du, and Q. Meng, "Data-Driven Modeling Methods and Techniques for Pharmaceutical Processes," Processes, vol. 11, no. 7, p. 2096, 2023
[2] J. Li, W. G., W. Wang, N. Yang, X. Liu, et al. From Multiscale Modeling to Meso-Science: A Chemical Engineering Perspective; Springer-Verlag Berlin Heidelberg, 2013
[3] V. Pandarus, F. Béland, R. Ciriminna, and M. Pagliaro, "Selective Debenzylation of Benzyl Protected Groups with SiliaCat Pd(0) under Mild Conditions," ChemCatChem, vol. 3, no. 7, pp. 1146–1150, 2011
[4] Greene, Theodora W., and Peter G. M. Wuts. Protective Groups in Organic Synthesis. 1st ed., Wiley, 1999.

Keywords

kinetic modeling, multi-scale modeling, pharmaceutical industry

CK – IV – 3

Transient methods to overcome the thermodynamic limits of the levulinic acid esterification

Vincenzo Russo[1*], Francesco Taddeo[1], Riccardo Tesser[1], Martino Di Serio[1]

1 Department of Chemical Sciences, University of Naples Federico II, Via Cintia, IT-80126 Naples

**Corresponding author: v.russo@unina.it*

Highlights

- Amberlite IR-120 can promote the reaction and separate on stream the reactive mixture.
- Transient PBR allowed to reach full levulinic acid conversion.
- A dynamic PBR model was implemented and applied to describe the data.

1. Introduction

Levulinic acid (LA), 4-oxopentanoic acid, is considered an attractive building block with widespread applications in various fields, together with its derivatives. It can be used as lubricants, printing inks additive, corrosion inhibitors, products for the personal care and drug delivery [1]. In the present paper the attention was focused on the esterification of levulinic acid with ethanol promoted by a heterogeneous acid catalyst. The reaction is reversible, and water is formed as the unique byproduct. As the equilibrium constant is rather low (K_E=3 at 333K [1]) when the reaction is operated in packed bed reactors, the maximum conversion achievable is the equilibrium one. In order to overcome the thermodynamic limitations, an idea would be to use a peculiar heterogeneous catalysts acting both as reaction promoter and as stationary phase, leading to a in situ separation of the chemical components along the packed bed. For this reason, an ion-exchange resin, namely Amberlite IR120, was selected for this study. As the resin could accumulate water during the execution of the experiments, shifting the equilibrium through the reactant side, an interesting idea would be to change periodically the feed volumetric flowrate, i.e., applying transient methods. This approach led to very attractive outcomes when compared to the traditional fixed bed reactor, as water is removed continuously, and the equilibrium can be shifted obtaining full conversion [2]. In the present work, kinetic tests were made using a dynamic fixed bed reactor, packed with Amberlite IR-120, at different temperature varying the volumetric flowrate during the test. Nearly complete conversion of levulinic acid was achieved in experiments conducted at temperatures of T=313K, 323K, 343K, and 363K. Furthermore, high conversion, reaching 90%, was also attained at a lower temperature of 293 K. Data were described with reliable reactor model taking into consideration both fluid-solid adsorption and non-idealities in the flow pattern.

2. Methods

The transient experiments were conducted using an experimental setup consisting of a packed bed reactor (L=0.3m, ID=7.8·10^{-3}m) packed with the catalyst placed into a heating furnace connected to a thermoregulator to control the liquid temperature, measured using a thermocouple. Reactants were loaded in a tank and pumped into the reactor through an HPLC pump. To perform the fluid-dynamic characterization, an injector with a 20 μL loop was installed and a UV detector (Reach Devices, USA) was placed online at the outlet of the reactor. The system was pressurized at 2bar with nitrogen. Experiments were made at different temperatures (T=293K, 313K, 323K, 343K, 363K) with a volumetric flowrate varying between 2 and 4mL/min, fixing the composition of the feed solution at 6:1 ethanol in levulinic acid molar ratio. The flowrate ramp, together with sample withdrawal intervals, are reported in Figure 1A. To evaluate the concentration of acidic groups, and determine the conversion, samples were analyzed through acid-base titration. The collected data were interpreted with a dynamic axial dispersion packed bed reactor model (Eq. 1a), where the adsorbed phases are modeled separately taking into consideration that molecules are adsorbed (r_{ads}) on an active site prior reacting (r), and that must desorb (r_{ads}) after reaction (Eq. 1b).

$$a)\ \frac{\partial c_i}{\partial t} = -\frac{u}{L}\frac{\partial c_i}{\partial \chi} + \frac{D_z}{L^2}\frac{\partial^2 c_i}{\partial \chi^2} + \nu_i r_{ads}\rho_B \qquad \begin{cases} c_i|_{\chi=0} = c_{i,feed} \\ \left.\frac{\partial c_i}{\partial \chi}\right|_{\chi=1} = 0 \end{cases} ;\ b)\ \frac{\partial \theta_i}{\partial t} = (\nu_i r_{ads} + \upsilon_i r)\rho_B \quad (1)$$

3. Results and discussion

The effect of the temperature was evaluated by performing the experiments at different values by varying the volumetric flowrate. The test made at *T*=363K showed that the LA concentration increased in the time by increasing the volumetric flowrate. The reason of this behavior is due to a lower contact time between reactants and the catalyst. The experimental results of tests conducted at *T*=343K, 323K, and 313K show that the trend of levulinic acid concentration over time appears to be constant by increasing flow rates. This trend means a constant and almost complete conversion, reaching values of 99%. A comparison between the results reached in these tests and those derived from tests conducted in a conventional fixed bed reactor was made. The following figures showed a comparison in the cases of tests made at *T*=363K, 343K and 323K, in terms of LA conversion at different volumetric flowrates (see example in Figure 1B).

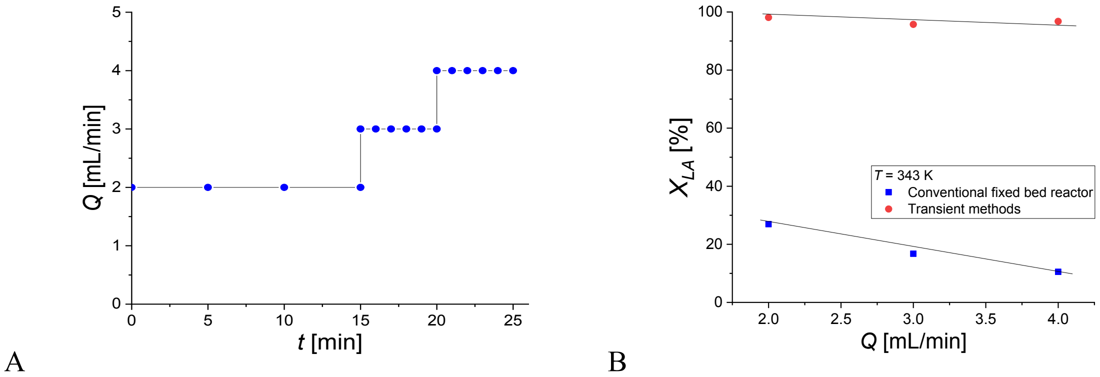

Figure 1. A. Volumetric flowrate program. B. Comparison between conventional fixed bed reactor and transient methods for levulinic acid conversion at different volumetric flowrate fixing *T* =343K.

The conversion obtained through a conventional fixed bed reactor was considerably lower than those achieved by applying transient methods.

4. Conclusions

The esterification of levulinic acid with ethanol was investigated in the presence of Amberlite IR120 as acid catalyst in a fixed bed reactor by applying transient methods. Kinetic tests were carried out by varying the volumetric flowrate during the experiment, method that led to unconventional conversions. An impressive result is the LA conversion next to 100% for a temperature range from 313 K to 343 K. Moreover, LA conversion equal to 90% were reached performing the esterification reaction at T = 293 K. At these operative conditions, low conversion degree can be reached with conventional fixed bed reactors. Therefore, the application of the transient methods, to influence the adsorption phenomena, have led to the optimization of the LA conversion, managing the achievement of excellent results even at low temperatures. The data were interpreted in a successful way with robust reactor model. In perspective, the developed tools could be used to scale-up the levulinic acid esterification process from batch to continuous operation.

References

[1] V. Russo, R. Tesser, C. Rossano, T. Cogliano, R. Vitiello, S. Leveneur, M. Di Serio, Chemical Engineering Journal 401 (2020) 126126.
[2] S. Haase, P. Tolvanen, V. Russo, Processes 10 (2022) 99.

Keywords

Dynamic operation; dynamic fixed bed reactor; levulinic acid esterification; ion-exchange resin.

Wed. 11/09 // 11:40-12:00

CK – IV – 4

Elucidating the Effect of Hydrocarbon Structure and Zeolite Topology on the β-Scission Activation Energy

Yannick Ureel[1], Konstantinos Alexopoulos[2], Maarten K. Sabbe[1], Kevin M. Van Geem[1,*]

[1]Laboratory for Chemical Technology, Ghent University, Technologiepark 125, 9052 Gent, Belgium

[2]Department of Chemical Engineering, Pennsylvania State University, University Park, Pennsylvania 16802-1503, United States

**Corresponding author: Kevin.VanGeem@UGent.be*

Highlights

- Clear effect of chain length, unsaturated bonds, and branches on the β-scission kinetics
- Four relevant different zeolite frameworks were investigated (FAU, MFI, MOR, TON)
- Proposed pore confinement descriptor correlates well with the activation energy
- Group additive-based model was developed for the prediction of activation energy

1. Introduction

Zeolites are indispensable for the current chemical industry both as adsorbent and highly-acidic catalyst. However, zeolites will also facilitate the development of a sustainable and climate-neutral industry. For example, zeolites can convert sustainable carbon sources like plastic waste and biomass via catalytic pyrolysis to valuable base chemicals such as light olefins and aromatics [1]. These processes require the design of improved zeolites and hence a proper understanding of the occurring reactions. The β-scission is the dominant elementary reaction within catalytic pyrolysis and hence requires a proper understanding to enable rational zeolite design. Various quantum chemical studies have been performed in the past on the zeolite-catalyzed β-scission, both static and dynamic. These studies predominantly focused on the effect of zeolite confinement, the distribution and location of acid sites, and order of the carbenium ion reactant on the kinetic properties [2]. In addition, it was found by Janda et al. that the chain length of small species influenced the activation enthalpy ($\leq C_6$) [3]. However, the effect of hydrocarbon type and zeolite framework on the intrinsic β-scission kinetics is unclear for hydrocarbons relevant in the cracking of plastic waste. In this work the effect of hydrocarbon chain length, unsaturated bonds, branching and zeolite topology on the β-scission activation enthalpy ($\Delta H^{\ddagger}$) was examined.

2. Methods

Periodic density functional theory (DFT) calculations were performed with the Vienna ab initio simulation package (VASP 6.2). Closed-shell calculations were executed with the Perdew-Burke-Ernzerhof functional and plane-wave energy cutoff was set at 600 eV. Zeolite structures were taken from the International Zeolite Association and optimized as empty cell. Geometry optimization and frequency calculations were performed for all reactants (23 hydrocarbons) in four different zeolites for a total of 92 reactions. Nudged elastic band and dimer calculations were performed to optimize the transition state geometry. In addition to qualitative results, a group additive-inspired predictive model was developed to facilitate the prediction of the relative activation enthalpy change in the four zeolite frameworks. For this, a so-called pore confinement descriptor was proposed which describes the change in distance of the hydrocarbon to the zeolite framework upon reaction. An easy-to-determine six-dimensional vector was proposed to describe every reaction and predict the activation enthalpy ($\Delta H^{\ddagger}$).

3. Results and discussion

A wide variety of 23 relevant hydrocarbons were studied in four relevant zeolites (FAU, MFI, MOR, TON). To demonstrate the importance of zeolite framework and hydrocarbon chain length, Figure 1 presents the variation of the activation enthalpy for seven linear carbenium ions with a total of 6-12 carbon atoms. The FAU framework is a large pore zeolite which does not fully stabilize the transition state resulting in increasing activation enthalpies for larger hydrocarbons. The MOR framework comprises of medium-sized channels which properly stabilize the linear transition state and reactant, resulting in a low dependency of chain length. The smaller channels in MFI, are not spacious enough and consequently destabilize the transition state slightly. Lastly, the small TON framework does not stabilize the more voluminous transition state resulting in a marked increase of activation enthalpy for larger hydrocarbons. This illustrates the influence of the hydrocarbon and zeolite on the kinetics.

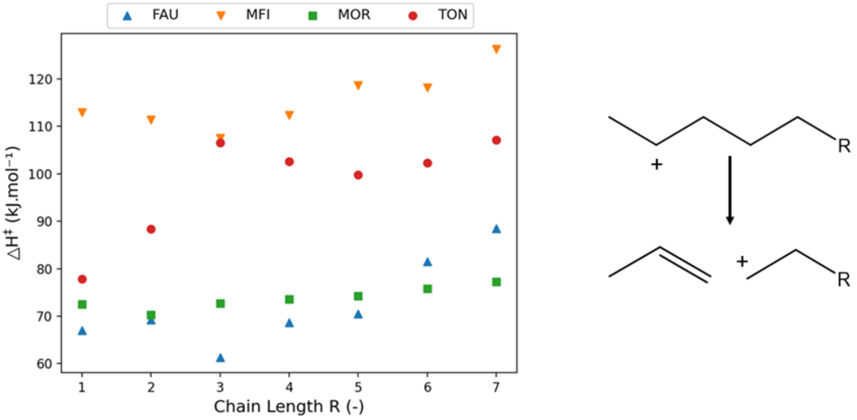

Figure 1. The variation of activation enthalpy ($\Delta H^{\ddagger}$) with increasing chain length of linear components (left) for the depicted reaction template (right).

In addition to a qualitative description of the effect of chain length, unsaturated bonds and branching, a predictive model was developed for usage in first-principle kinetic models. The group-additive inspired model achieves errors in line with the errors achieved by static DFT-calculations as illustrated in Table 1. Additionally, an internal consistency test was performed which demonstrated the validity of the developed model.

Table 1. Mean absolute error (MAE) on the prediction of the activation enthalpy ($\Delta H^{\ddagger}$).

MAE ($\Delta H^{\ddagger}$) [kJ.mol^{-1}]	
MFI	4.9
FAU	3.0
MOR	5.3
TON	6.4

4. Conclusions

Despite what is often assumed in kinetic models, a clear dependency of the activation enthalpy on the hydrocarbon reactant was found. Both the hydrocarbon chain length, branches and presence of double bonds influenced the intrinsic β-scission kinetics. In addition to the qualitative insights, a predictive model was developed which allows the prediction of the change in activation enthalpy depending on the hydrocarbon structure within the four zeolites. This predictive model can be incorporated in first-principle kinetic models to facilitate rational zeolite design.

References

[1] Abbas-Abadi MS, Ureel Y, Eschenbacher A, Vermeire FH, Varghese RJ, Oenema J, et al. Challenges and opportunities of light olefin production via thermal and catalytic pyrolysis of end-of-life polyolefins: Towards full recyclability. Progress in Energy and Combustion Science 2023;96:101046.

[2] Cnudde P, De Wispelaere K, Vanduyfhuys L, Demuynck R, Van der Mynsbrugge J, Waroquier M, Van Speybroeck V. How chain length and branching influence the alkene cracking reactivity on H-ZSM-5. ACS catalysis 2018;8(10):9579-95.

[3] Janda A, Vlaisavljevich B, Lin L-C, Mallikarjun Sharada S, Smit B, Head-Gordon M, Bell AT. Adsorption Thermodynamics and Intrinsic Activation Parameters for Monomolecular Cracking of n-Alkanes on Brønsted Acid Sites in Zeolites. The Journal of Physical Chemistry C 2015;119(19):10427-38.

Keywords

Catalytic Cracking; Activation Energy; DFT; Force Fields

RENEWABLE CHEMICALS

Mon. 09/09 // 10:20-10:40

RC – I – 1

Insights into the mild catalytic reductive depolymerization of Soda lignin: link between the catalytic properties of Pd and PdCu catalysts and the derived product pools

Boyana Atanasova[1*], T. De Saegher[1], J. Vercammen[1,2], A. Verberckmoes[1], J. De Clercq[1], J. Lauwaert[1]

[1] *Industrial Catalysis and Adsorption Technology (INCAT), Ghent University, Ghent, Belgium*
[2] *Interscience Expert Center (IS-X), Louvain-la-Neuve, Belgium*
**Corresponding author: boyana.atanasova@ugent.be*

Highlights

- Pd/activated carbon shows superior activity, attributed to unique catalytic properties
- Adding Cu to a Pd/oxide support catalyst alters the catalyst's selectivity
- C=C bond hydrogenation of functional side chains leads to favorable monomer yields
- Parallel solvolytic and catalytic depolymerization due to size-exclusion phenomena

1. Introduction

As much as 40% of all chemicals contain an aromatic moiety[1]. Currently, the main supplier of these compounds is the petrochemical industry, which is one of the main sources of environmental pollution[2]. With the worsening climate change crisis and the depletion of fossil feedstocks, finding alternative sources for aromatics becomes imperative. The indigestible aromatic biopolymer lignin is the most promising candidate as it is the largest renewable source of aromatic compounds in nature[2]. Furthermore, lignin allows the straightforward derivation of functionalized aromatics, which can be used directly for multiple industrial applications; e.g., polymers, resins, foams, and dyes, thereby also replacing toxic components such as bisphenol A and phenol[3]. Mild reductive depolymerization is a highly favored valorization strategy due to its sustainable nature and superior selectivity to functionalized aromatics; however, the efficiency of this method is hindered by slow depolymerization rates in addition to limited insights in the depolymerization mechanism[4]. To overcome the latter, highly performant redox catalysts are needed for the selective cleavage of lignin's beta-O-4 linkages [4]. By studying the complex product pool after reaction, the depolymerization mechanism can also be elucidated. This research extensively explores the impact of the support material (γ-Al_2O_3, SiO_2, and activated carbon (AC)) and Cu incorporation on the performance of Pd catalysts. All catalyzed reactions are also compared to the solvolysis reaction, i.e., depolymerization in the absence of a catalyst.

2. Methods

5 wt% Pd and 5 wt% PdCu (1:1 molar ratio) catalysts on γ-Al_2O_3, SiO_2, and AC were synthesized via incipient-wetness impregnation and calcined at 450°C for 4h. The depolymerization experiments are performed at 200°C and 10 bar H_2 in a 70/30 (vol%/vol%) ethanol-water mixture for 2, 3, 6, 20, and 30 hours. Both in-depth catalyst characterization (ICP, NH_3-TPD, TEM-EDX, N_2-sorption) and product pool analysis are performed (GPC, GC-MS, GPC-HPLC-UV/VIS, 2D-NMR, ^{31}P-NMR). The activity of the catalysts is expressed in function of time as the percentage reduction in molecular weight relative to the initial feedstock.

3. Results and discussion

The AC supported catalysts exhibit the highest activity, i.e., Mw reduction of 65% at 2h reaction time compared to 55% for the other catalysts. The higher activity of the Pd(Cu)/AC catalysts is attributed to several factors including the presence of larger nanoparticles and the higher oxophilicity of AC compared to the oxide supports. In terms of selectivity, Pd/AC exhibits higher hydrodeoxygenation rates compared to Pd/γ-Al_2O_3 and Pd/SiO_2. While Pd/AC mainly forms propyl functionalized monomers, Pd/γ-Al_2O_3 and Pd/SiO_2 mainly yield monomers with propanol side chains (Figure 1). The addition of Cu primarily impacts Pd's selectivity, with negligible effects on the overall activity. With subtle differences depending on the support, the main change in selectivity is the decreased hydrogenation of the obtain monomers, i.e., a significant increase of propenyl functionalized monomers is observed over the entire reaction time range. When the total monomer mass yields of the catalysts are compared, Pd(Cu)/γ-Al_2O_3 and Pd/SiO_2 exhibit the highest total mass yields. The maximum monomer mass yields of the above-mentioned catalysts range between 13 and 15 wt%. At longer reaction times Pd/AC also achieves a total monomer mass yield of 13 wt%. On the other hand, PdCu/SiO_2 and PdCu/AC, which mainly form propenyl functionalized monomers, are characterized by the lowest total monomer yields, i.e., respectively 7 and 9 wt%. The difference in total mass yields is hence related to the selectivity of the catalyst and the stability of the obtained monomers (Figure 1). Successful C=C bond hydrogenation in the side chains of the derived monomers is therefore important in order to obtain stable end products. In the absence of a catalyst, even lower total monomer yields (4 wt%) suggest increased condensation and/or repolymerization during solvolysis. Furthermore, the analysis of the entire product pools of both catalyzed and uncatalyzed reactions shows that while the use of a catalyst significantly increases the total monomer yield and steers the monomer functionalities, similar reactions occur in the high molecular weight fraction of the product pools. The latter suggests that due to size-exclusion phenomena the catalyst primarily stabilizes and modifies reaction intermediates after cleavage of the β-O-4 linkages while both solvolytic and catalytic processes occur in the larger molecular weight region.

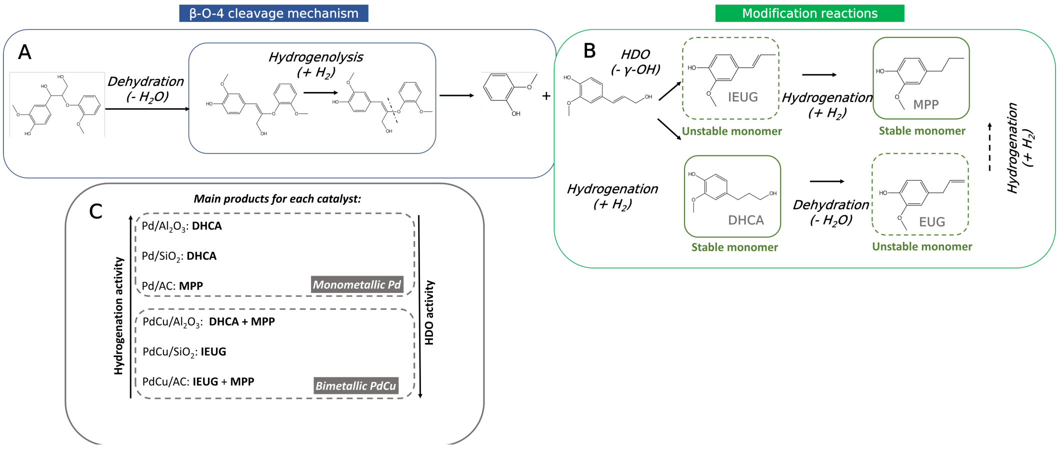

Figure 1. Cleavage mechanism of the β-O-4 linkage (A) including the possible consequent modification pathways (B). The main monomeric reaction products of each catalyst are also presented (C), including the catalysts' relative selectivity towards hydrogenation and hydrodeoxygenation reactions of the derived monomers

4. Conclusions

It can be concluded that the Pd(Cu) catalyst plays a crucial role in stabilizing reaction intermediates through multiple modification reactions, especially via hydrogenation of C=C bonds in the side chains of the reactive intermediates, resulting in a significant increase in the overall depolymerization degree and obtained monomeric mass yield. Moreover, a proper selection of the support material as well as incorporation of a promoting element (Cu) to the Pd catalyst can be used to steer the product pool towards specific components and/or functionalities. These insights are deemed pivotal for further advancing catalyst development.

References

[1] Biorizon, "Biobased aromatics: Europe leads the way," Mar. 07, 2020.

[2] Z. Sun, B. Fridrich, A. de Santi, S. Elangovan, and K. Barta, "Bright Side of Lignin Depolymerization: Toward New Platform Chemicals," Chemical Reviews, vol. 118, no. 2. American Chemical Society, pp. 614–678, Jan. 24, 2018. doi: 10.1021/acs.chemrev.7b00588.

[4] I. van Nieuwenhove, T. Renders, J. Lauwaert, T. de Roo, J. de Clercq, and A. Verberckmoes, "Biobased Resins Using Lignin and Glyoxal," ACS Sustainable Chemistry and Engineering, vol. 8, no. 51. 2020. doi: 10.1021/acssuschemeng.0c07227.

[5] W. Schutyser, T. Renders, S. van den Bosch, S. F. Koelewijn, G. T. Beckham, and B. F. Sels, "Chemicals from lignin: An interplay of lignocellulose fractionation, depolymerisation, and upgrading," Chemical Society Reviews, vol. 47, no. 3. Royal Society of Chemistry, pp. 852–908, Feb. 07, 2018. doi: 10.1039/c7cs00566k.

Keywords

Lignin depolymerization, biomass valorization, reaction mechanism, catalytic properties

RC – I – 2

Metal sulfates-catalyzed depolymerization of cellulose to alkyl levulinates

Viktória Flóra Csendes[1*], Karine Thomas[2], Sébastien Leveneur[1]

1 INSA Rouen Normandie, Univ Rouen Normandie, Normandie Univ, LSPC UR 4704, F-76000 Rouen, France;

2 Université de Caen Normandie, CNRS, ENSICAEN, Laboratoire LCS, 6 bd du Maréchal Juin, 14050 Caen, France

**Corresponding author: viktoria_flora.csendes@insa-rouen.fr*

Highlights

- A novel process for butyl levulinate production from cellulose is proposed
- Effect of reactor heat-up times on product and intermediate concentration profiles
- Effect of catalyst ratio in a dual-catalyst system
- Effect of an electrophilic co-solvent in a biphasic system

1. Introduction

Currently, intensive research activities focus on replacing fossil resources with renewable alternatives as their long-term availability and impact on the environment are questionable. Instead, one of the most promising carbon-rich feedstock to utilize is biomass. Although it is readily available worldwide, renewable, and cost-effective, it has not yet been utilized widely on an industry scale [1]. The valorization of lignocellulosic biomass to produce bio-renewable platform molecules is of great significance, supporting various fields in the chemical industry [2].

Cellulose has the largest share in the composition of lignocellulosic biomass and is a polymer-type molecule containing D-glucose monomers. Alkyl levulinates can be produced directly by alcoholysis from biomass-based sugars or through the esterification of levulinic acid [3]. In recent years, alkyl levulinates have built up great momentum; their advantages include low toxicity, high boiling point, stable flash point, excellent lubricity, and good low-temperature fluidity.

The synthesis of alkyl levulinates directly from biomass is a one-step alcoholysis−esterification reaction by adding alcohols, and catalysts simultaneously to a reactor that operates at high temperatures. This method is the simplest, with a short reaction route, and has the advantage of using a wide source of raw materials. The elevated temperatures cause the crystallinity of the cellulose to decrease as well as the degree of polymerization, but only when the operation temperature and reaction times are proper [4]. After producing sugars, the levulinate products can be obtained with the corresponding alcohol solvents. Above all, n-butanol as a solvent is less studied, but it is a promising green molecule that can be a product of fermentation and bio-ethanol production, further improving the sustainability of the process [5].

In this work, we investigated the depolymerization reaction of cellulose to butyl levulinate using a cheap and simple catalyst system of $Fe_2(SO_4)_3$ and $Al_2(SO_4)_3$, carried out in a co-solvent medium of butanol and γ-valerolactone.

2. Methods

Synthesis

The experiments were performed in a stainless-steel pressurized batch reactor, with a capacity of 300 ml. The vessel is equipped with a stirrer and an electric heating jacket, each experiment was carried out under isotherm and isobar conditions. Samples were withdrawn every hour of the reaction span.

Analytical methods

Quantitative analysis was performed on the time samples using gas chromatography (GC) coupled with a flame ionization detector (GC-FID), as well as HPLC equipped with evaporative light scattering detector (ELSD) and UV detection.

3. Results and discussion

First, we investigated the effect of the temperature ramp, the time that it takes to reach isotherm conditions in the reactor. The intermediate molecules showed great fluctuation in the concentration profiles even with slight changes to the ramp, but this did not affect the final product.

Increasing the catalyst amount leads to increasing production of the desired product in a shorter time, but as the reaction progresses, the strong acidic sites present with the high acidic loading can catalyze side reactions, such as decomposition of the product and condensation reaction of the alcohol solvent. The right ratio of Lewis acid sites of the $Al_2(SO_4)_3$ promotes the structural isomerization of monosaccharides, while Brønsted acid sites of the $Fe_2(SO_4)_3$ benefit the dehydration transformation of glucose to hydroxy-methyl-furfural.

With co-solvent systems, higher product yields can be achieved based on the solubility differences of the feedstock and the products. Co-solvent systems, meaning two or three water/alcohols/polar aprotic solvents, can increase the degradation and influence thermodynamic properties.

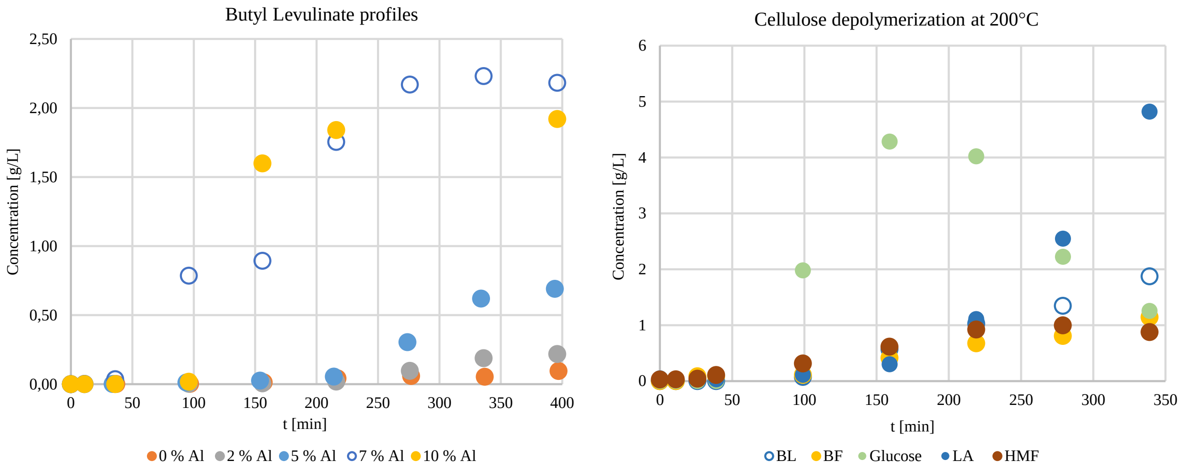

Figure 1. Effect of catalyst ratio on the product concentration profile (left). Concentration profiles of intermediates and products during the reaction (right).

4. Conclusions

We carried out various experiments to better understand the complex process of valorizing biomass-derived molecule cellulose to alkyl levulinates. We found that apart from temperature dependence, the concentration profiles of intermediate molecules are influenced greatly by the temperature ramp required to reach isothermal conditions. A co-solvent system was also studied, where the presence of γ-valerolactone beside butanol inhibited unwanted side reactions and helped obtain the product faster. A co-catalyst system was also introduced to fine-tune the acid-catalyzed depolymerization of cellulose. These findings are especially important to consider when developing the kinetic model for the overall reaction scheme.

References

[1] D. D. M. Di Bucchianico, M. Mignot, J. C. Buvat, V. C. Moreno, S. Leveneur, Chemical Engineering Journal 465 (2023) 142914
[2] V. F. Csendes, A. Egedy, S. Leveneur, A. Kummer, Processes 11(5) (2023) 1503
[3] X. Liu, W. Yang, Q. Zhang, C. Li, H. Wu, Frontiers in Chemistry, 8 (2020) 794
[4] N. Shi, Y. Zhu, B. Qin, T. Zhu, H. Huang, Y. Liu, ACS Sustainable Chemistry & Engineering, 10(32) (2022) 10444-10456
[5] J. Feng, T. Fan, C. Ma, Y. Xu, J. Jiang, H. Pan, Journal of Agricultural and Food Chemistry, 68(47) (2020) 13760 13769

Keywords

biomass valorization; cellulose; butyl levulinate; co-catalyst;

RC – I – 3

Magnetically heated Ru-catalyst for levulinic acid HDO in electrified slurry reactor

Miha Grilc[1], Darko Makovec[2], Blaž Likozar[1], Sašo Gyergyek[2]

[1]*Department of Catalysis and Chemical Engineering, National Institute of Chemistry, Hajdrihova 19, 1000 Ljubljana, Slovenia*
[2]*Department for Materials Synthesis, Jožef Stefan Institute, Jamova 60, 1000 Ljubljana, Slovenia*
**Corresponding author: miha.grilc@ki.si*

Highlights

- Ru-impregnated carbon-coated iron-oxide with ferrimagnetic and catalytic properties.
- Catalyst heated magnetically in alternating current (AC) field due to hysteresis losses.
- Direct catalyst heating in cold fluid advantageous for converting unstable biochemicals.
- Kinetic modelling allowed estimating the temperature of the catalyst grain.

1. Introduction

Electrification of the chemical and energy sector is a crucial step in the transition to a carbon neutral society. It offers possibilities that transcend traditional heating of catalytic processes, which unselectively heat the entire reaction vessels and reaction media. The heating of magnetic nanoparticles embedded within the catalyst can selectively heat the catalyst at the reaction site, overcoming the troublesome temperature gradients in the reactor, eventually favoring bulk-phase reactions or degradation of thermally unstable compounds (Figure 1c). Such rapid and selective heating enables a construction of adaptable and highly-responsive units, capable of flexible operation upon power availability as per the EU's new industrial paradigm. Hereby, the concept has been successfully applied in biomass valorisation by our research team.[1] Namely levulinic acid (LA) was hydro(deoxy)genated by molecular H_2 to γ-valerolactone (GVL) in a stirred slurry reactor, where magnetic nanoparticles (MN) coated by carbon and finely dispersed Ru clusters were heated directly by AC field. [2]

2. Methods

The synthetized MN-C-Ru catalyst contained three layers. Maghemite nanoparticles of 15 nm size (MN) exhibiting ferrimagnetic characteristic are confined within a carbon matrix (C) formed by hydrothermal carbonization of glucose, and finally Ru nanoparticles are deposited by solvothermal reduction of Ru^{3+} in iso-propanol (i-PR). MN-C-Ru heat up under AC fields due to hysteresis losses, termed "magnetic heating" unlike typical induction heating. For catalytic hydrotreatment experiment, MN-C-Ru, levulinic acid and i-PR were placed in a quartz reactor (to prevent inductive heating), pressurized with H_2 to 1 MPa, and subjected to vigorous stirring and an AC field (frequency of 273 kHz and amplitude of 46 mT). The latter heated the magnetic catalyst grains, which was the only heat source. The temperature of the liquid phase was monitored, samples were collected through dip tube and analyzed by GC-MS. Based on the intermediates and products detected, the reaction pathway was proposed, and kinetic model was formulated. Furthermore, the same catalyst was tested in a conventionally-heated stirred batch reactor of comparable geometry to determine crucial kinetic parameters which were also later used to estimate the surface temperature of magnetically heated catalyst surface.

3. Results and discussion

The nanocatalyst showcased its capability as both a heating agent and catalytically active material. Detailed examination and modeling of the hydrogenation and deoxygenation processes revealed that the nanocatalyst's surface attains a higher temperature (137 °C) compared to the bulk liquid phase (85 °C). This temperature differential led to enhanced conversion rates of isopropyl levulinate to γ-valerolactone, consequently boosting yields under mild conditions. Remarkably, MN-C-Ru maintained stability and retained its activity, achieving a consistent 100% yield of GVL even after four cycles.

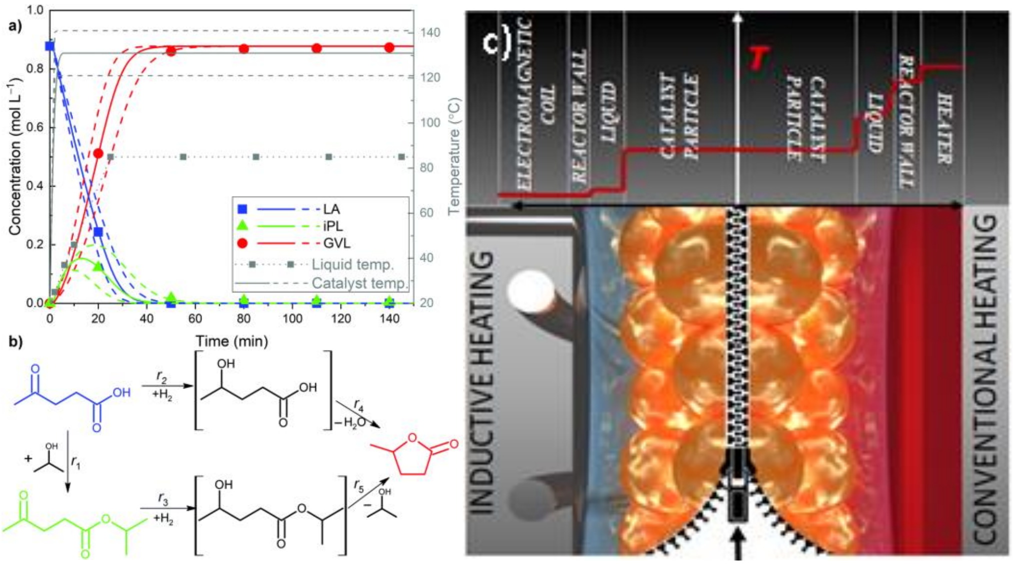

Figure 1. Reaction kinetics[a] (measured points, modelled lines) and mechanism[b] for HDO of LA to GVL in a slurry reactor with targeted magnetic heating of catalyst grains, resulting in beneficial temperature profiles[c] over conventional heating.[2]

The elevated surface temperature resulting from magnetic heating of the catalyst boosts the production of γ-valerolactone through direct hydrogenation (with an activation energy of 22 kJ mol^{-1}) and hydro(deoxy)genation of isopropyl levulinate (with an activation energy of 93 kJ mol^{-1}). The latter is inherently formed due to the low activation energy of esterification (32 kJ mol^{-1}).

4. Conclusions

We demonstrated the concept of magnetic heating to upgrade platform bio-based chemicals (LA) under mild conditions in a stirred slurry reactor (total pressure of 1 MPa maintained with H_2). Via reaction kinetics and predictive modelling we determined the catalyst surface temperature (137 °C) being significantly higher than the temperature of bulk liquid (85 °C).

5. Acknowledgments

The authors acknowledge the financial support from the Slovenian Research Agency (research core funding no. P2-0089, P2-0152, N2-0242).

References

[1] S. Gyergyek, D. Lisjak, M. Beković, M. Grilc, B. Likozar, M. Nečemer, D. Makovec, Magnetic Heating of Nanoparticles Applied in the Synthesis of a Magnetically Recyclable Hydrogenation Nanocatalyst, Nanomater. . 10 (2020). https://doi.org/10.3390/nano10061142.

[2] S. Gyergyek, M. Grilc, B. Likozar, D. Makovec, Electro-hydrogenation of biomass-derived levulinic acid to γ-valerolactone via the magnetic heating of a Ru nanocatalyst, Green Chem. 24 (2022) 2788–2794. https://doi.org/10.1039/D2GC00102K.

Keywords

Electrified biorefinery, magnetic heating, slurry reactor, bio-based chemicals.

RC – I – 4

Commercial polymeric waste mix characterization and pyrolysis in a lab-scale setup for gas and liquid fractions products valorization

Andrea Pastorino[1], Marcello Pagliero[1,2], Giancarlo Bruni[3], Renzo Di Felice[4], Antonio Comite[1,2]

1 Department of Chemistry and Industrial Chemistry, University of Genoa, Genoa, Italy; 2 National Interuniversity Consortium of Materials Science and Technology (INSTM), Florence, Italy; 3 Italiana Coke Srl, Cairo Montenotte (SV), Italy; 4 Department of Civil, Chemical and Environmental Engineering, University of Genoa, Genoa, Italy

* *andrea.pastorino998@gmail.com*

Highlights

- A commercial post-consumer plastic was analytically characterized.
- Discontinuous pyrolysis setups for liquid and gas products valorization.
- Influence of process parameters on yield and composition of products.
- Gas and liquid fraction analytical characterization.

1. Introduction

A huge portion of polymeric waste is still impossible to be recycled by any means. The only diffused alternative to landfill is their use as secondary solid fuel (SSF) for energy generation by combustion. Pyrolysis can be considered as an alternative route for ternary recycle, able to produce a wide variety of high value products while reducing CO_2 emissions. Although this technology is well-known its diffusion is still very limited due to the complexity of the processes occurring during pyrolysis, to the high variability of the polymeric waste composition and presence of other heterogenous materials (e.g. paper) that leads to results that are difficult to predict and generalize [1]. Furthermore, liquid products are composed of a wide spectrum of different compounds making valorization a serious challenge in view of practical applications. The main goal of this work was to study the pyrolysis process of a real polymeric waste mix, from its characterization and investigation of its decomposition kinetics through thermogravimetry, to tests in a discontinuous lab-scale plant, to both gain insight on the influence of several operative parameters (e.g. temperature, reactor setup) and determine product fractions yield and composition.

3. Methods

The study was conducted on a commercial waste polymeric mix designed as coke additive for steel industry, and on its main pure components. The identification of the main polymeric components was carried out by infrared spectroscopy (FT-IR) and differential scanning calorimetry (DSC); heterogenous impurities were identified by Field Emission Scanning Electron Microscopy (FE-SEM) coupled with EDX spectroscopy and Back Scattering detector. Thermogravimetric analysis (TGA) was conducted at different heating rates (5-30 °C/min) to assess the kinetic parameters (e.g. activation energy) of pyrolysis through the application of different model-free approaches [2].

Pyrolysis tests were carried out on two different setups, both consisting of three main sections: a first section for gas feeding during process, a batch reactor inside a programmable oven, and a final condensation zone to separate the liquid fraction from the gaseous products. In one case the reactor and oven were horizontally oriented to facilitate the removal of products from the thermal decomposition zone, while in the other the reactor was positioned vertically.

During the study different process parameters have been studied, varying heating rate (5-20 °C/min), maximum temperature reached (500-800 °C) and gas flowrate (50-200 mL/min) to evaluate their influence on products yield and composition.

Products were analyzed by means of gas chromatography (GC) equipped with a TCD for non-condensable species (e.g. CO_2, CO, H_2) and a FID for volatile organics. The condensed fraction was characterized with gas chromatography-mass spectrometry (GC-MS) and FT-IR spectroscopy. Measurements during tests and analysis carried out on products allowed for the evaluation of mass balances, calculating the yield of different fractions.

3. Results and discussion

Analysis on the feed mixture, allowed to gain insight on its main components and identify impurities. FT-IR showed the presence of intense signal (2922 cm^{-1} and 2852 cm^{-1}) in the region of C-H bond stretches, several other signals between 1700 and 1645 cm^{-1} in the C=O stretches zone and wider peaks in the 2650-3450 cm^{-1}, showing the presence of oxygen atoms in the mixture, linked to the presence of paper impurities and polyesters. These results confirmed the presence of polyolefin materials but also showed the presence of other heteroatomic components.

Thermal analysis gave additional information on the composition of the material: DSC helped identify phase transitions referable to polymeric components. TGA scans confirmed that water was not relevant validating FT-IR data. Between 200 °C and 400 °C a minor loss of weight is visible, while between 400 °C and 550°C the material undergoes a rapid and almost complete decomposition that leaves only around 5% of the sample weight as ashes. This behavior was correlated with the material composition Different thermal scanning speeds allowed to evaluate the apparent activation energy of the pyrolysis process, that seems in accordance with literature results and with the main polymeric composition.

Pyrolysis tests showed that changing process conditions can increase either liquid or gas products yield by 25 %, reaching values around 75%, and reducing solid residue to 5 %. This shows that setup used can convert almost completely the product reaching TGA results conversion with 500 times more sample mass. The two reactors showed differences in performance linked to different residence time of the vapors in the high temperature zone and to their condensation on the walls of the vertical reactors, that brought them back to the oven for further gasification. This was confirmed by a higher yield of gas products in the same conditions.

Main products were successfully identified in gas phase thanks to GC-TCD and GC-FID, that allowed to identify respectively H_2, CO, CO_2, and light hydrocarbons. FT-IR, together with GC-MS allowed to identify several of the main components of the wax like products condensed in the dedicated setup zone during the process showing, among others, the presence of heavy alcohols, carboxylic acids, and other oxygenated species.

4. Conclusions

The feed mixture was characterized with different techniques allowing to link pyrolysis behavior to its composition. Results obtained during pyrolysis tests proved to be in line with the literature on pure polymer components both regarding feed characterization and conversion. The effect of impurities during pyrolysis, if compared to pure materials, didn't decrease performance drastically while increased the amount of residue post-pyrolysis. Vertically arranging the reaction zone seems to have a positive influence on the gas yield and the complex liquid products fraction proved a challenge to thoroughly identify. Implementation of catalysts may further increase gas production, especially hydrogen.

References

[1] A. Antelava, N. Jablonska, A. Constantinou, G. Manos, S. A. Salaudeen, A. Dutta, S. M. Al-Salem, Energy Fuels, 35, 5 (2021), 3558–3571.

[2] U. Hujuri, A. K. Ghoshal, S. Gumma, Polymer Degradation and Stability, 93 (2008), 1832-1837

Keywords

Pyrolysis; polymeric waste; products characterization

Mon. 09/09 // 11:40-12:00

RC – I – 5
Catalytic Oxidation of Glucose: A Heterogeneous Pathway to Glucuronic Acid Production

ELHALLAL Maher[1]*, ORDOMSKI V. Vitaly[1], CAPRON Mickael[1]

[1] *UCCS-UMR CNRS 818, uni~~versité de Lille, 59655 Ville~~neuve d'Ascq cedex, France*
*maherhallal@univ-lille.fr

Highlights

- ***Optimal glucuronic acid yield reached 32% using $Au_{50}Pt_{50}$ bimetallic catalyst.***
- ***Reaction conditions: 120°C, 15 bars, 0.3 g catalyst, over 5 hours.***
- ***Au-based catalysts showed superior activity; Pt-based catalysts had higher selectivity.***

1. Introduction

The reliance on fossil fuels has led to environmental issues like carbon emissions, climate change, and resource depletion. Non-fossil alternatives are seen as a cleaner option. Glucose, an abundant renewable feedstock, offers potential for producing valuable chemicals through routes like fermentation and oxidation. Oxidizing glucose to glucuronic acid, a key precursor for biopolymers and pharmaceuticals, remains challenging due to the low reactivity of the C6 hydroxyl group compared to the anomeric carbon. Enzymatic production has issues with separation, low productivity, and wastewater treatment. This study aims to investigate heterogeneous metal catalysts for optimized glucuronic acid synthesis as a sustainable alternative to fossil-based chemicals.

2. Materials and methods

The catalyst used in the experiments was prepared using a microemulsion method[1]. This method involved reducing an aqueous phase containing metallic precursors ($HAuCl_4$ and/or $H_2PtCl_6{\cdot}6H_2O$) with an oil phase (cyclohexane) and an amphiphilic surfactant (AOT), along with the addition of TiO_2. The catalyst was denoted as $Au_xPt_{(100-x)}$, where x = 0, 25, 50, 75, or 100, with a total metal loading of 2.5 wt%. The catalytic reactions were carried out in a 300 mL stainless steel reactor with 200 mL of glucose aqueous solution, varying the catalyst mass (0-0,4 g), the time (5-9 hours), temperature (100-140 °C), and oxygen pressure (10-30 bars) without base addition. Samples were analyzed by HPLC with RI and UV detectors.

3. Results and discussion

In our study, we first optimized the reaction parameters, including reaction time, temperature, pressure, and catalyst mass. The reaction time was varied between 5 to 9 hours, revealing that the conversion plateaus at approximately 70% after 4 hours. Notably, the yield of glucuronic acid peaked at 300 minutes before declining due to its conversion into other products. We explored reaction temperatures ranging from 100 to 140 °C, determining that the optimal yield of glucuronic acid occurs at 120 °C. Temperatures exceeding 120 °C resulted in thermal degradation, while lower temperatures led to reduced activity. Additionally, we assessed oxygen pressure between 10 and 30 bars, identifying 15 bars as the optimal level; lower pressures slowed the reaction and decreased yield, while higher pressures did not provide significant benefits. Catalyst mass was varied from 0 to 0.4 g, with 0.3 g demonstrating optimal efficiency, yielding high conversion rates without the use of excess material. Control experiments confirmed the essential role of the catalyst in enhancing reaction performance.

Following this optimization, we investigated Au-Pt bimetallic catalysts under the established conditions of 5 hours, 120 °C, 15 bars, and 0.3 g of catalyst. Our findings indicated that Au-based catalysts exhibited superior catalytic activity (**figures 1,2** 71% conversion and 42% glucuronic acid selectivity) while Pt-based catalysts displayed the highest product selectivity (**figures 1,2** 29% conversion and 66% glucuronic acid selectivity). Remarkably, a 1:1 mass ratio of the Au-Pt bimetallic catalyst demonstrated a synergistic enhancement of overall catalytic performance (**figure 2** 32% glucuronic acid yield), underscoring the potential of bimetallic systems in optimizing reaction outcomes.

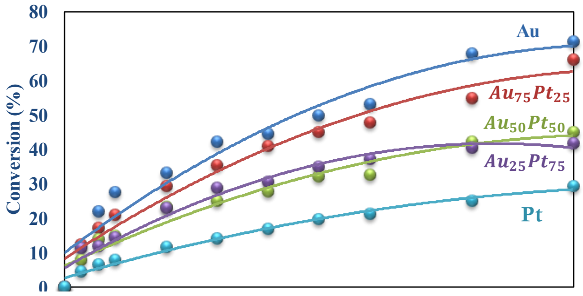

Figure 1. Kinetic analysis of glucose oxidation over Au-Pt bimetallic catalysts

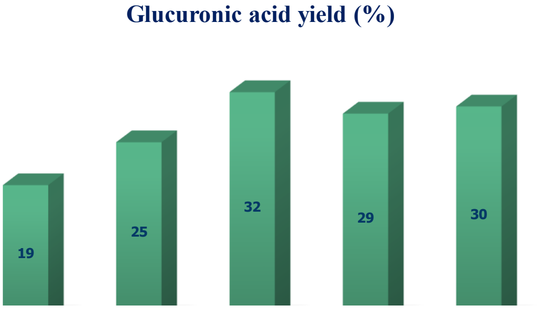

Figure 2. Yield of glucuronic acid after 5-Hour reaction with Au-Pt bimetallic catalysts

The investigation employed a range of catalyst characterization techniques, including Brunauer Emmett-Teller (BET) surface area analysis, Barrett-Joyner-Halenda (BJH) pore size distribution analysis, Inductively Coupled Plasma Atomic Emission Spectroscopy (ICP AES), X-ray Photoelectron Spectroscopy (XPS), X-ray Diffraction (XRD), Transmission Electron Microscopy (TEM), and Energy Dispersive X-ray (EDX) mapping. These methodologies were utilized to elucidate the catalytic activity and to analyze the selectivity distribution of the resultant products.

4. Conclusions

In this study, optimal glucose conversion was achieved at 120°C and 15 bar pressures, utilizing 0.3 grams of catalyst over a duration of five hours, resulting in a notable yield of 30% glucuronic acid. Among the various catalysts tested, the $Au_{50}Pt_{50}$ bimetallic catalyst, composed of 50% gold and 50% platinum, demonstrated the highest performance, achieving a yield of 32% under the optimized conditions. These findings highlight the effectiveness of the AuPt bimetallic catalyst in enhancing glucose conversion processes.

References

[1] R. Wojcieszak et al, “Selective oxidation of glucose to glucuronic acid by cesium-promoted gold nanoparticle catalyst”

Keywords
Glucose oxidation, glucuronic acid production, heterogeneous catalysts

Tue. 10/09 // 11:00-11:20

RC – II – 1

(Un)catalyzed depolymerization of hydrolysis lignin: experimental assessment and kinetic modelling

Lucas I. Garbarino[1], Matteo Deroma[2], Dhanjay Sharma[2], Jeriffa De Clercq[2], An Verberckmoes[2], Jeroen Lauwaert[2]* and Joris W. Thybaut[1]*

1 Ghent University, Laboratory for Chemical Technology, Technologiepark 125, Ghent, Belgium;

2 Ghent University, Industrial Catalysis and Adsorption Technology, Valentin Vaerwyckweg 1, Ghent, Belgium

**Jeroen.Lauwaert@UGent.be, Joris.Thybaut@ugent.be*

Highlights

- Experimental elucidations of (un)catalyzed depolymerization of hydrolysis lignin.
- Continuous lumping modelling for assessing lignin de(re)polymerization kinetics.
- Modelling perspectives for assessment on catalyst adequacy and performance.

Introduction

Aromatic chemicals represent more than 30 % of the building blocks produced in the chemical industry, 97 % of which are derived from fossil resources [1]. In this context, the largest source of renewable aromatics, i.e. lignin, is typically wasted in conventional biorefineries, particularly the so-called hydrolysis lignin (HL) obtained from bioethanol production. Although having a lower purity compared to their organosolv lignin counterparts, HLs represent a cheaper lignin source which is currently underutilized. The development of comprehensive kinetic models able to cope with the complexity and heterogeneity of the lignin structure is, therefore, key for reactor design and optimization. Correspondingly, a novel modelling strategy based on the continuum theory of lumping [2] is presented.

Experimental methods

The lignin stock solution was prepared by dissolving 0.5 g of dried HL (5.5 wt. % of carbohydrates) at room temperature in 10 mL of ethanol/water (70/30 vol. %) mixture, under vigorously stirring. The solution was then filtered to remove any remaining solids, and the lignin concentration was determined gravimetrically. Both solvolysis and catalytic depolymerization experiments were conducted in a stirred batch set-up consisting of 7 individual reactor vessels of 25 mL [3]. The catalytic depolymerization of HL was investigated over a commercial 5 wt. % Pd-Al_2O_3 catalyst. In a typical experiment, a reactor was loaded with 2.8 mL of lignin stock solution, 7.2 mL of the ethanol/water solvent mixture and 50 mg of catalyst, if applicable. Subsequently, the reactor vessel was pressurized up to 10 bar with H_2 and heated to the set temperature. Within this work, experiments were conducted at 200 °C in a reaction time span ranging from 0.5 to 6 h. The lignin oil samples were characterized through Gel Permeation Chromatography (GPC) equipped with a refractive index detector (RID), and targeted monomers identified *via* gas chromatography-mass spectrometry (GC-MS) analysis.

Model development

Modelling kinetics based on continuous lumping typically accounts for the reactivity of species (*k*- space) as a function of a single continuous characteristic, e.g., the molecular weight. Moreover, only reactions in the depolymerization direction are usually considered, which significantly simplifies the model formulation. In lignin depolymerization, however, repolymerization reactions should not be neglected, primarily for uncatalyzed depolymerization where intermediate species from solvolytic routes are not stabilized by, e.g., hydrogenation reactions. Naturally, since repolymerized species are typically less reactive towards depolymerization, the *k*-space should be affected accordingly. From the modelling perspective, two reactivity spaces are then proposed to describe the kinetics of depolymerization (*k*-space$_{de}$) and of repolymerization (*k*-space$_{re}$). The system is hereby characterized through pseudo-components, the reactivity of which is not only defined by their size, but also by the cumulative fraction of repolymerized species. To account for this effect, the *k*-space$_{de}$ is associated to a first-order decay function to describe the non-monotonic behavior of the *k*-space with respect to the molecular weight. Another important aspect of the model is the yield distribution function, which represents the stoichiometry of the system. A skewed-gaussian distribution is adopted since it can describe from middle-chain up to terminal-chain cracking, as well as condensation reactions from the monomeric region onwards. The proposed model comprises 5 kinetic parameters and 5 parameters to describe the stoichiometry, all of which are estimated *via* regression to the experimental data.

Results and discussion

Two groups of species in the monomer-to-dimer region of the molecular weight distribution were identified in the stock solution, see the grey dashed lines in Figure 1 A and 1 B. In the absence of the catalyst, the relative amount of species corresponding to the first group gradually decreases even from early stages of the reaction. This effect can be attributed to repolymerization of those species into heavier ones, which was further confirmed by GC-MS where, e.g., condensed benzofuran structures were identified. The catalytic depolymerization indicates, however, that the same group of species is stabilized. A higher depolymerization degree is also demonstrated by the weight-average (M_w) and number-average (M_n) molecular weight profiles, see Figure 1 C.

The model performance is depicted in Figure 1 A and 1 B for the uncatalyzed (i.e. solvolysis) and catalyzed HL depolymerization, respectively. As shown in Figure 1 A*, the model simulates the formation of condensed species primarily in the monomer-to-dimer region during solvolysis, which is consistent with the experimental findings, e.g., condensed monomers from alkylation reactions. On the contrary, a lower yield of such species is simulated for catalytic depolymerization in the bulk region, see Figure 1 B*. The latter can be attributed to the stabilization effect of the heterogenous catalyst being more pronounced for monomers and lighter oligomers. The model simulations are also consistent with the absence of condensed species in the monomeric region according to GC-MS analysis.

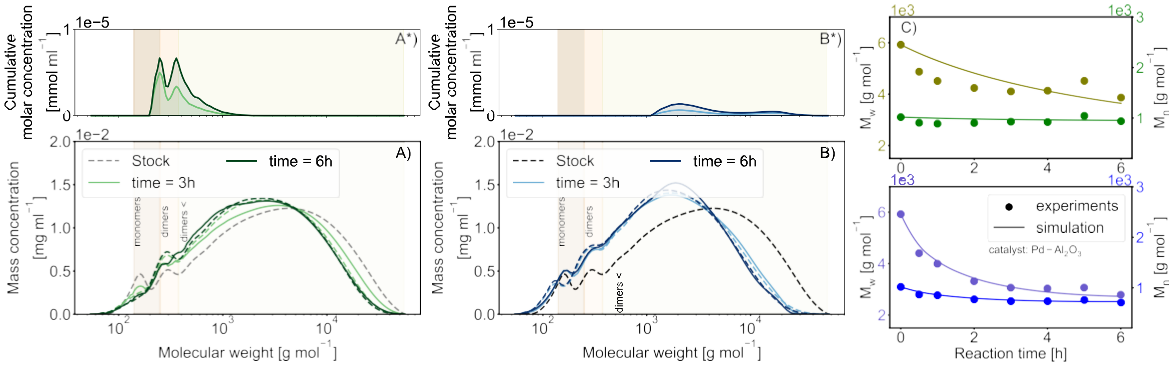

Figure 1. Molecular weight distributions at different reaction times (bottom subplots) and simulated profiles of repolymerized species (top subplots) for A) solvolysis and B) depolymerization under Pd-Al_2O_3 catalyst. C) M_w and M_n profiles. Dashed and solid lines depict experimental and simulation data, respectively.

4. Conclusions

A novel continuous lumping model has been developed to describe de(re)polymerization kinetics of HL, showing a good agreement between simulation results and experimentally observed trends. The model is able to simulate the formation of condensed species and corresponding differences between solvolysis and catalytic depolymerization, allowing for catalyst adequacy and performance assessment. Moreover, the *k*-spaces can ultimately be extended to key reaction families, e.g. β-O-4 moieties, providing additional chemical identities to the many species involved.

References

[1] F. Yang, H. Meerman, Z. Zhang, J. Jiang, and A. Faaij, Journal of Cleaner Production 372 (2022) 133727.
[2] C. S. Laxminarasimhan, R. P. Verma, and P. A. Ramachandran, AIChE Journal 42 (1996) 2645–2653.
[3] T. De Saegher, J. Lauwaert, J. Vercammen, K. M. Van Geem, J. De Clercq, and A. Verberckmoes, ChemistryOpen 10 (2021) 740–747.

Keywords
Hydrolysis lignin; catalytic depolymerization; continuum theory of lumping; kinetic modelling.

Tue. 10/09 // 11:20-11:40

RC – II – 2

Reaction kinetics prediction and modeling in the 5-HMF solvolysis to alkyl levulinate aided by structure reactivity relationships.

Erny Encarnacion Munoz[1*], Jean-Christophe Buvat[1], Sébastien Leveneur[1]

1 INSA Rouen Normandie, Univ Rouen Normandie, Normandie Univ, LSPC UR 4704, F-76000 Rouen, France;

** Corresponding author: erny.encarnacion_munoz@insa-rouen.fr*

Highlights

- Reaction medium effect.
- Kinetic modeling considering different solvents.
- Linear free energy and linear solvation relationships.
- Bayesian inference.

Introduction

The increasing energy demand makes the use of petroleum-based products a limited and unstable energy source which at the same time has led to critical environmental issues like greenhouse gases emissions. The use of biomass as feedstock seems a credible substitute source of organic compounds, that can be regarded as an ideal equivalent to petroleum for producing fuels and chemicals. Platform molecules such as 5- hydroxymethyl furfural (5-HMF), 5-alkoxymethyl furfural (RMF) and alkyl levulinate (Als) can be regarded as promising biofuels which can be produced through catalytic acid solvolysis from lignocellulosic biomass (LCB) and sugar monomers. Alkyl levulinates can be hydrogenated into γ-valerolactone (GVL), an essential intermediate for fuel production and solvent for biomass valorization for its dissolution properties[1].

In the case of Als and RMF production from the 5-HMF solvolysis, the alcohol plays a double role: as a solvent and reactant. The motivation of this study is to develop a kinetic model of this reaction considering the dual role of the alcohol reaction medium by combining linear free energy and linear solvation energy relationships via the Kamlet–Abboud–Taft (KAT) and Taft equations [2], such global kinetic model can help to accelerate the stages in lignocellulosic biomass process development and optimization.

Methods

Kinetic experiments were performed under controlled-temperature conditions in a 300 ml stainless steel batch reactor. The reaction was carried out using a fixed liquid volume with a ratio of 70/30 %wt. alcohol/GVL and Amberlite IR120 H+ as acid catalyst[3], it was pressurized with nitrogen at 20 bars to limit the boiling point of the liquid phase, the temperature was set between 80 and 110 °C with different initial HMF and catalyst loading. Samples were taken at ambient temperature then when the desired temperature was reached, every hour up to 7 hours and analyzed by FID gas chromatography. The kinetic modeling and regression methods were carried out using the commercial software Athena Visual Studio to estimate the kinetic model parameters and Bayesian inference was used to estimate their corresponding credible interval.

Results and discussion

The solvolysis of 5-HMF to alkyl levulinates was performed in (H_2O, MeOH, EtOH, PrOH, BuOH, PeOH, HeOH) reaction medium, Figure 1 shows the reaction medium effect by comparing kinetic experiments under the same operating conditions.

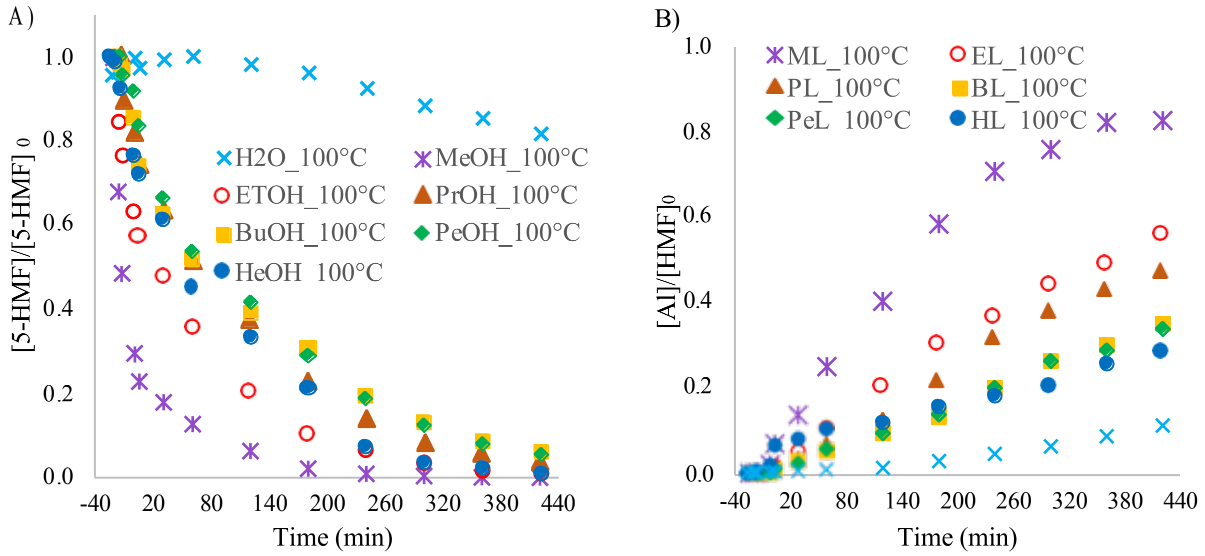

Figure 1 Reaction medium effect on the solvolysis of 5-HMF at 100°C, A) HMF solvolysis, B) alkyl levulinates

Figure 1A shows that the consumption rate of 5-HMF with short carbon chain alcohols is the most rapid, notably for methanol and ethanol. Nevertheless, there is no explicit relationship between the number of carbon and the consumption rate; for instance, the 5-HMF generation rate is slightly faster for hexanol than propanol. In contrast Figure 1B shows higher rates in Als production for short carbon alcohols, it is also observed that the LA production is quite slow compared to the others alkyl levulinates.

Conclusions

Preliminary experiments showed that the transformation of 5-HMF to levulinic acid (LA) in water reaction medium was the slowest transformation compared to the other alcohol reaction medium. These experiments show that the production LA from HMF is negligible in an alcohol reaction medium. Experimentally, it was found that the rates of Als production follow the order: $r_{ML}^{Methanol} > r_{EL}^{Ethanol} > r_{PL}^{Propanol} > r_{BL}^{Butanol} > r_{PeL}^{Penthanol} > r_{HeL}^{Hexanol} > r_{LA}^{Water}$. In order to build robust kinetic models, it is needed to consider the solvent and substituent effect to provide a better understanding of the kinetics which could be helpful to predict the production of a specific alkyl levulinate in the solvolysis of 5-HMF in alcohol medium.

References

[1] T. Raj, K. Chandrasekhar, R. Banu, J.-J. Yoon, G. Kumar, S.-H. Kim, Fuel 303 (2021) 121333.
[2] Y. Wang, M. Cipolletta, L. Vernières-Hassimi, V. Casson-Moreno, S. Leveneur, Chem. Eng. J. 374 (2019) 822–831.
[3] D. Di Menno Di Bucchianico, J.-C. Buvat, M. Mignot, V. Casson Moreno, S. Leveneur, Fuel 318 (2022) 123703.

Keywords
Taft equation; KAT; Kinetic modeling; Alkyl levulinates; Renewable chemicals.

Tue. 10/09 // 11:40-12:00

RC – II – 3

Exploring Selective Glucose Oxidation: Monometallic versus Bimetallic Catalysts

Žan Lavrič[1 5], Janvit Teržan [1 2*], Ana Kroflič [1], Janez Zavašnik [3], Matej Huš [1 4 5], Miha Grilc [1 5], Blaž Likozar [1 6]

1 Department of Catalysis and Chemical Reaction Engineering, National Institute of Chemistry, Hajdrihova 19, SI-1000 Ljubljana, Slovenia

2 Department of Synthesis of Materials, Jožef Stefan Institute, Jamova Cesta 39, 1000 Ljubljana, Slovenia

3 Gaseous Electronics, Jožef Stefan Institute, Jamova Cesta 39, 1000 Ljubljana, Slovenia

4 Institute for the Protection of Cultural Heritage of Slovenia (ZVKDS), Poljanska cesta 40, SI-1000 Ljubljana, Slovenia

5 University of Nova Gorica, Vipavska 13, SI-5000 Nova Gorica, Slovenia

6 Faculty of Polymer Technology, Ozare 19, SI-2380 Slovenj Gradec, Slovenia

**Janvit Teržan: Janvit.terzan@ki.si*

Highlights

- Oxygen adsorption was enhanced with the use of bimetallic catalysts
- The catalyst composition predicted by DFT was decisive for the balance of oxygen activation
- Kinetics from regression analysis *vs*. DFT kinetics
- The bimetallic AuPt/ZrO_2 catalyst showed the highest glucaric acid yield (32 %)

Introduction

The advancement of our society, coupled with the finite nature of fossile fuels and the environmental repercussions of current industrial practices, has spurred research into bio-based and renewable chemical resources. Over the past two decades, biomass conversion has garnered increasing attention due to the vast array of materials it offers [1,2]. Among these, glucaric acid (GA) stands out as a promising compound derived from biomass [3], traditionally obtained through nitric acid oxidation on an industrial scale. However, this method lacks ecological sustainability, prompting exploration of alternative technologies. One particular promising approach in recent years involves heterogeneous oxidation utilizing Au-supported metallic catalysts under base-free conditions [4]. Nevertheless, the literature focusing on the initial step towards GA remains insufficient, largely focusing on the initial step towards gluconic acid. In this study, our focus was on investigating heterogeneous monometallic Au, as well as bimetallic AuPt and AuCu catalysts supported on ZrO_2. Our primary objectives were to discern differences in activity for selectively oxidizing glucose to GA using mono- and bimetallic catalysts. Furthermore, this research marks the first comprehensive description of the entire pathway from glucose to GA. Each reaction step was meticulously examined, with additional insights gained through DFT calculations for comparison with experimental data [5].

Methods

The catalysts underwent preparation via the deposition-precipitation method, employing hydrazine hydrate as a reducing agent. Subsequently, the synthesized catalysts underwent analysis through transmission electron microscopy (TEM), oxygen pulse chemisorption (OPS), X-ray diffraction (XRD), and X-ray photoelectron spectroscopy (XPS) to ascertain their surface properties. Following this, batch experiments were conducted at varying temperatures and oxygen partial pressures. The resulting experimental data were utilized to construct a microkinetic model endowed with predictive capabilities. Bridging the gap between experimental observations and kinetic investigations, DFT calculations were executed.

Results and discussion

Analysis of the catalysts using X-ray photoelectron spectroscopy (XPS), transmission electron microscopy (TEM), and X-ray diffraction (XRD) confirmed the formation of alloys in bimetallic catalysts, revealing the presence of nano-sized Au crystallites in both mixed AuPt and AuCu samples. DFT calculations revealed enhanced oxygen adsorption on Cu and Pt surfaces, correlating with improved catalytic activity. The investigation identified key factors influencing the oxidation of glucose to gluconic acid (GU) and glucuronic acid (GLU), emphasizing the significance of surface coverage and charge transfer. Bimetallic catalysts exhibited enhanced GU production, and recyclability tests affirmed their stability over three cycles. Notably, compared to existing literature findings, the bimetallic AuPt/ZrO2 catalyst demonstrated the highest GA yield under optimized conditions, highlighting its efficacy in the oxidation reaction.

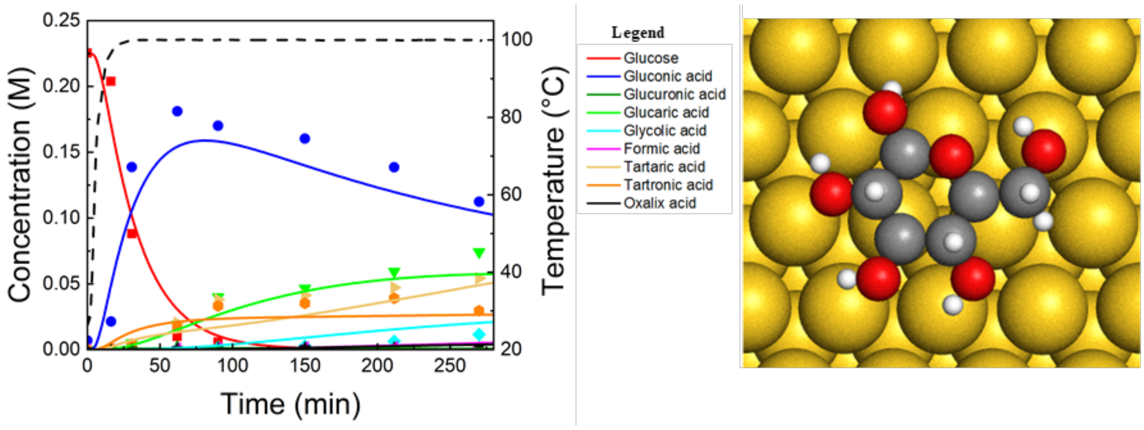

Figure 1. Oxidation experiment at 100 °C and 30 bar_g O_2 on AuPt/ZrO_2 catalyst (left). Top-down view of glucose ring on gold nanoparticle (right).

Conclusions

DFT calculations have corroborated that the varying performance of Au, AuPt, and AuCu catalysts can be attributed to differences in oxophilicity. The dynamics of the reaction heavily rely on the availability of oxygen species (O2* and O*) provided by Pt and Cu, which in turn influence reaction rates and selectivity. Microkinetic investigations are consistent with DFT findings, revealing the limitations in glucose oxidation by pure Au and the improved selectivity of bimetallic AuPt. This comprehensive study, which integrates catalyst synthesis, characterization, DFT analysis, and microkinetic modeling, lays the groundwork for future research endeavors in biomass valorization and applications within the circular economy.

References

[28] Z. Zhang, J. Song, B. Han, Chem. Rev. 117 (2017) 6834–6880
[29] B.M. Upton, A.M. Kasko, Chem. Rev. 116 (2016) 2275–2306
[30] R. G´erardy, D.P. Debecker, J. Estager, P. Luis, J.-C.M. Monbaliu, Chem. Rev. 120 (2020) 7219–7347
[31] J. Teržan, A. Sedminek, Ž. Lavrič, M. Grilc, B. Likozar, Green Chem., 25 (2023), 2220-2240
[32] Ž. Lavrič, J. Teržan, A. Kroflič, J. Zavašnik, J.E. Olszowka, Š. Vajda, M. Grilc, B. Likozar, Appl. Catal. B, 343 (2024), 123455

Keywords

Glucaric acid; Glucose oxidation; Catalyst characterization; DFT; Microkinetic modelling

Acknowledgments

This work was funded by the Slovenian Research Agency (ARRS) under core funding P2-0152 and project number N2-0242.

Wed. 11/09 // 10:40-11:00

RC – III – 1

Novel superbases as organocatalysts in low temperature depolymerization of polyethylene terephthalate (PET)

Ali Harlin*, Henri Olander, Erno Karjalainen

VTT Technical Research Centre of Finland Ltd, Tietotie 4E, PO Box 1000, Espoo 02044, Finland

**Corresponding author: Ali.Harlin@vtt.fi*

Highlights

- High catalytic activity of superbases at low temperatures in glycolytic depolymerization of PET
- Separation and purification of the reaction product simply via recrystallization from water
- Highly pure reaction product, bis(2-hydroxyethyl) terephthalate (BHET) in short reaction times

1. Introduction

Chemical recycling is a prospective solution for tackling the vast amount of polyester waste generated. Polyethylene terephthalate (PET), often referred as polyester, is a synthetic polymer which is widely employed in various industrial fields, such as textile and packaging industry. Nowadays, polyester is the most produced synthetic fiber for textile use with more than 60 million tons produced in 2021 [1].

The depolymerization of PET via glycol alcoholysis often takes 6-8 hours and is conducted at reaction temperatures of 180-250°C and pressure of 0.1-0.6 MPa [2]. Commercially available guanidine superbase, 1,5,7-triaza-bicyclo-[4,4,0]dec-5-ene, which is commonly abbreviated as TBD, has been previously investigated as organocatalyst in transesterification reaction aiming towards complete depolymerization of PET into its monomer bis(2-hydroxyethyl) terephthalate (BHET) [3]. In the study conducted by Fukushima et al., (2011) [3] the catalytic efficiency of TBD was comparable to metal acetates commonly applied at elevated reaction temperature of 190°C.

In this work, low temperature depolymerization of polyethylene terephthalate was investigated by utilizing glycolysis as a chemical recycling method for both virgin and post-consumer PET. Novel superbases were used as reaction catalysts, and their efficiency was compared to conventionally applied zinc acetate ($Zn(OAc)_2$). Two of the studied superbases have not been reported for recycling of PET. The focus of the research was to find the lowest potential depolymerization temperature in glycolysis reaction, while maintaining the reaction time in feasible limits. In an industrial scale the decrease in reaction temperature will generate beneficial impact in both capital expenditures (CapEx) and operating expenses (OpEx).

2. Methods

In this work, glycolytic depolymerization of PET was conducted in excess ethylene glycol (EG) and in presence of an organocatalyst. The effect of temperature on reaction efficiency was studied for each catalyst. The investigated temperature range was from 80°C to 180°C, which is lower than is typical for glycolytic depolymerization of PET. The decrease of temperature was made possible by the very high activity of the catalysts, and this will lead significant savings in industrial scale.

The unreacted PET and water insoluble fraction were separated by filtration after addition of water into the reaction mixture. Separation and purification of the desired reaction product, bis(2-hydroxyethyl) terephthalate (BHET), was conducted via straightforward recrystallization from water.

The purity of BHET, was determined by nuclear magnetic resonance (NMR) and differential scanning calorimetry (DSC). The results obtained from analyses on reaction product BHET were compared to its commercial analogue recrystallized in similar manner. It was found out that the product achieved very high purity with only one simple purification step.

3. Results and discussion

The novel superbases investigated demonstrated increased efficiency at significantly lower reaction temperatures compared to conventionally applied metal acetate catalyst. As depicted in Figure 1, conversions of over 90 % were achieved in just two hours of reaction time at temperatures as low as 120°C, where conventional zinc acetate catalyst is not active anymore.

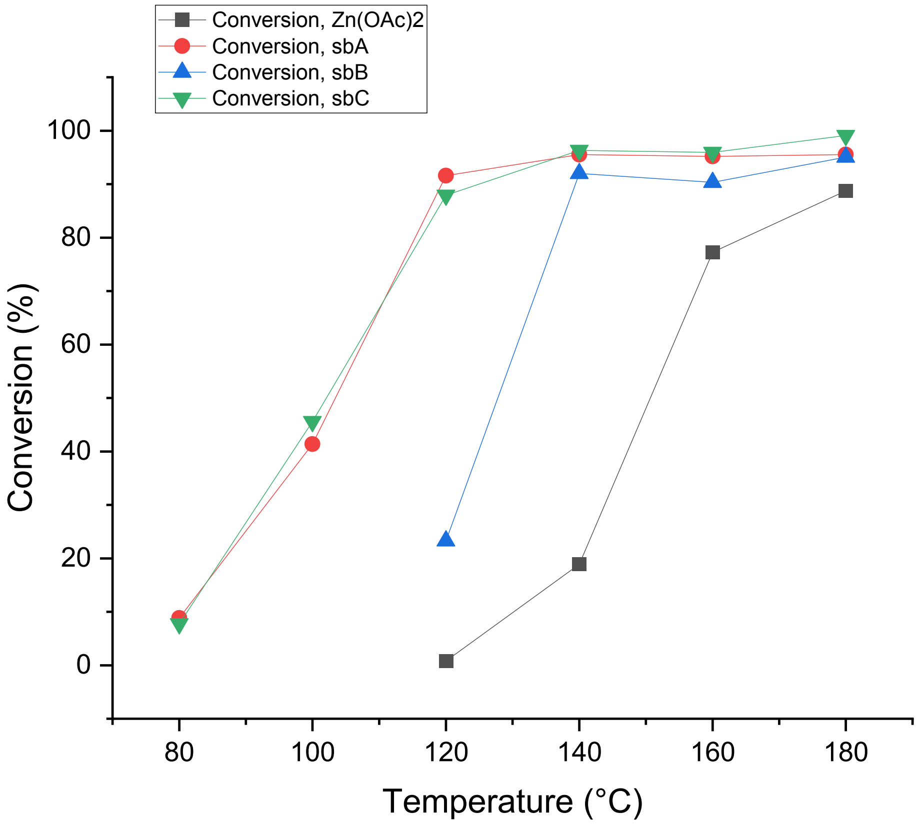

Figure 1. Overview of the conversion of polyethylene terephthalate (PET) with investigated catalysts after two hours of reaction time at different temperatures.

4. Conclusions

All of the investigated superbase catalysts show greater efficiency as compared to zinc acetate by reaching high PET conversion rates at low temperatures, where conventionally used catalyst is not active anymore. Additionally, novel superbases are promising for the implementation into industrial scale as they would provide beneficial impact in both capital expenditures (CapEx) and operating expenses (OpEx).

References

[1] Textile Exchange. Preferred Fiber and Materials Market Report 2022. https://textileexchange.org/knowledge-center/reports/materials-market-report-2022/

[2] Cao, F., Wang, L., Zheng, R., Guo, L., Chen, Y., &Qian, X. (2022). Research and progress of chemical depolymerization of waste PET and high-value application of its depolymerization products. RSC Advances, 12(49), 31564-31576. https://doi.org/10.1039/d2ra06499e

[3] Fukushima, K., Coulembier, O., Lecuyer, J. M., Almegren, H. A., Alabdulrahman, M. M., Alsewailem, F. D., McNeil, M. A., Dubois, P., Waymouth, R. M., Horn, H. W., Rice, J. E., & Hedrick, J. L. (2011). Organocatalytic depolymerization of poly(ethylene terephthalate). *Journal of Polymer Science Part A: Polymer Chemistry*, 49(5), 1273-1281. https://doi.org/10.1002/pola.24551

Keywords

Superbase, polyester, glycolysis, depolymerization

RC – III – 2

Evaluation of Piston reactor to produce hydrogen from methane via gas-phase SMR and ATR routes

Aya Abousrafa[1], Mary Anna Katebah[1], Patrick Linke[1], Ma'moun Al-Rawashdeh[1]*
1. Department of Chemical Engineering, Texas A&M University at Qatar, Doha, Qatar

**Corresponding author: mamoun.al-rawashdeh@qatar.tamu.edu*

Highlights

- Piston reactors offer flexible electro-mechanical conversion for chemical processes.
- Autothermal reforming of methane in the piston reactor is an attractive and economical approach for hydrogen generation.
- The piston reactor provides energy savings and lower CO_2 emissions compared to conventional processes.

1. Introduction

Hydrogen is recognized as a crucial energy carrier pivotal for low-carbon and net-zero economies. Presently, the predominant source of hydrogen stems from hydrocarbon feedstocks, particularly methane and natural gas. There are presently three established commercial pathways for hydrogen generation from natural gas: partial oxidation of methane (POM), autothermal reforming (ATR), and steam reforming (SMR) [1]. While all three methods are commercially mature, they also exhibit significant CO_2 emissions. The adoption of electrified and compact reformers has emerged as a strategic approach to enhance hydrogen production and mitigate carbon emissions. This approach could facilitate hydrogen production installations in regions with limited gas reserves, utilize biomethane sourced from various decentralized locations, and harness stranded gas that would otherwise be flared [2]. Furthermore, the importance of electrification lies in its ability to integrated store intermittent renewable energy sources into the hydrogen production process. The piston reactor technology is a novel potential concept in achieving this purpose by enabling the conversion of electrical and mechanical power into chemical products and operating uniquely under rapid adiabatic compression-expansion cycles. The rapid gas expansion leads to quenching of the reacting mixture which hinders secondary reactions of metastable species toward undesired by-products. This study aimed to assess the feasibility of gas-phase SMR and ATR as potential routes for hydrogen production in the piston reactor.

2. Methods

A zero-dimensional single-zone thermodynamic model is developed for a four-stroke single-cylinder piston reactor, accounting for changes in cylinder volume, pressure, temperature, and species concentrations over time. The model incorporates the POLIMI gas phase detailed mechanism.

3. Results and discussion

A base case scenario of a 400 cc (16.4 compression ratio) piston reactor operating under SMR conditions is shown in Figure 1 (a). In this case, an intake pressure of 1 bar and an H_2O/CH_4 ratio of 3.56 was implemented. A minimum intake temperature of 1100 K was required to trigger the SMR reaction leading to only 12% CH4 conversion. The introduction of argon into the feed mixture was analyzed to increase the in-cylinder temperature by reducing the heat capacity of the mixture. However, it was found that at least an 80 mol% argon dilution is required to achieve high conversions exceeding 80%. Hence, the highly endothermic nature of the SMR reaction was found to be impractical under a wide range of conditions, leading to its exclusion from further assessments and investigations. On the other hand, ATR emerged as an attractive option for hydrogen production as shown in Figure 1(b). An H_2O/CH_4 ratio of 1.25 and an O_2/CH_4 ratio of 0.6 were implemented. In comparison to a simulated industrial catalytic ATR reformer reactor operating under conventional conditions, the piston reactor achieved a similar methane conversion of 89%, operating in the gas phase without the need for a heterogeneous catalyst, with a lower intake temperature of 673K and pressure of 1 bar compared to the conventional reactor conditions. To understand the economics and emissions associated with hydrogen production using piston reactor, a process flowsheet is designed embedding the piston reactor for ATR hydrogen production The developed ATR process design, demonstrated favorable economics even at a small production capacity of 25 tons/day of hydrogen, with comparable CO_2 emissions to those of large-scale industrial ATR processes. The piston reactor introduced a novel approach to energy integration utilizing mechanical power and heat, which proved beneficial for the carbon capture and compression process, leading to the production of low CO_2 hydrogen.

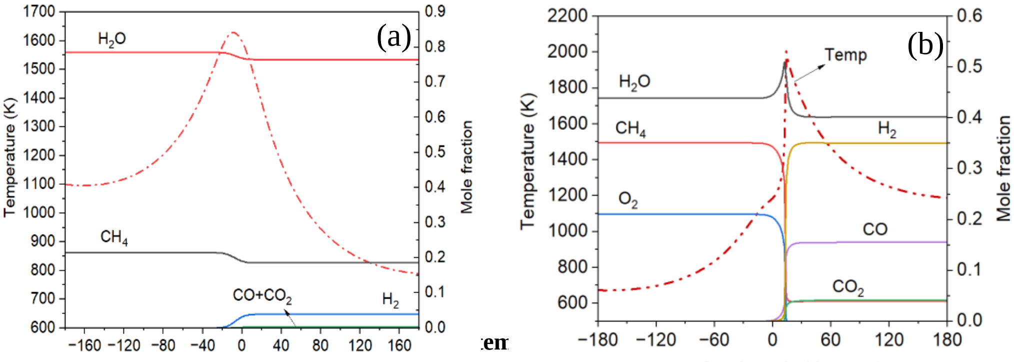

(A) case of SMR at N = 3000 RPM, T_intake = 1100 K, P_intake = 1 bar, H_2O/CH_4 = 3.561,

(B) case of ATR at N = 3000 RPM, T_intake = 673 K, P_intake = 1 bar, H_2O/CH_4 = 0.75, O_2/CH_4 = 0.6

4. Conclusions

The ATR route is an attractive pathway for hydrogen generation within the piston reactor. In comparison to a simulated industrial packed-bed ATR reactor, the piston reactor achieves a comparable methane conversion rate ranging from 89% to 97% while operating in the gas phase without relying on any heterogeneous catalysts, as typically employed in industrial conventional processes. Moreover, the piston reactor operates at significantly lower intake feed temperatures, with differences reaching up to 300 K. Additionally, the piston reactor demonstrates a higher hydrogen production rate per reactor volume, reaching 3545 kgH_2/m^3.hr, whereas the industrial reformer operates at a lower rate of only 1702 kgH_2/m^3.hr. These results are highly attractive, showcasing the unique features of the piston reactor, including its fast and dynamic operation capabilities and modularization potential. The piston reactor offers a pathway to achieve process intensification by reducing energy requirements, lowering CO_2 emissions, eliminating the need for a catalyst, improving reactor volume utilization, and enabling the co-generation of power and excess heat, which are valuable for energy integration at the process level.

References

1. El-Emam, R.S. and H. Özcan, *Comprehensive review on the techno-economics of sustainable large-scale clean hydrogen production.* Journal of Cleaner Production, 2019. **220**: p. 593-609.
2. Anderson, D.M., et al., *Sorption-Enhanced Variable-Volume Batch–Membrane Steam Methane Reforming at Low Temperature: Experimental Demonstration and Kinetic Modeling.* Industrial & Engineering Chemistry Research, 2015. **54**(34): p. 8422-8436.

Keywords

E-reactor, Sustainability, Electrification, Hydrogen.

Acknowledgment

This work was made possible by funding from the Qatar National Research Fund (QNRF) project number NPRP12S-0304-190222 and co-funding by Shell Global Solutions International B.V.

Wed. 11/09 // 11:20-11:40

RC – III – 3

Kinetic modelling and packed bed reactor technology in the catalytic oxidation of furfural to valuable products

Enrico Marchi[1], Wander Perez Sena[1], Kari Eränen[1], Johan Wärnå[1], Dmitry Murzin[1], Tapio Salmi[1]*

1 Laboratory of industrial Chemistry and Reaction Engineering (TKR), Åbo Akademi, FI-20500 Turku/Åbo

**Corresponding author: tapio.salmi@abo.fi*

Highlights

- Furfural oxidation to valuable products was investigated in a packed bed reactor
- An improved reaction network was proposed for the complex reaction system
- The kinetic parameters of the system were successfully estimated by non-linear regression analysis using a dynamic axial dispersion model
- The recycled packed bed reactor system is a working concept for oxidation processes

Introduction

Catalytic oxidation of furfural is an important reaction among environmentally friendly biomass-based technologies to provide precursors for chemical industry. Bio-based furfural is obtained from the hydrolysis of hemicelluloses to monomeric sugar molecules, and their subsequent dehydration. Hemicelluloses can be obtained from lignocellulosic biomass by extraction, after which they can be hydrolyzed to monomeric sugars at moderate temperatures (<100°C). In this way, arabinose, galactose, glucose, mannose and xylose can be obtained from arabinogalactan, galactoglucomannan and arabinoglucuronoxylan. Valorization of furfural via liquid-phase oxidation with hydrogen peroxide as the green oxidant yields primarily succinic and maleic acids, both molecules of significant interest for polymer industry [1]. Conventional technology is based on the use of mixed batch reactors, but the application of tubular reactors either in continuous or semibatch mode is an attractive alternative, because it would enable flexible reaction conditions for commercially available and inexpensive solid catalysts. An improved reaction network compared to existing literature was developed, with additional pathways explaining the routes for the succinic acid formation. The system was modelled using the transient axial dispersion model for the packed bed and parameter estimation was carried to fit the model to the experimental data and to obtain both pre-exponential factors and activation energies of the model.

Methods

Oxidation of furfural with hydrogen peroxide was investigated on the strongly acidic Amberlyst-15 catalyst. Experiments at different operating conditions in an aqueous environment were conducted in a packed bed loop reactor operated in upflow mode. The effect of various operation conditions such as temperature, reagent concentrations, volumetric flow rates and catalyst loadings were investigated. The experiments were performed in a glass packed bed reactor, the outlet of which was connected to a mixing tank. The outlet of the mixing vessel was connected to the inlet of the reactor (diameter 3 cm, height 50 cm), achieving a closed loop configuration. The flow pattern in the loop reactor was determined by tracer experiments. The effect of various operation conditions such as temperature (60-80°C), reagent concentrations (the hydrogen peroxide-to-furfural molar ratio 4-7), and volumetric flow rates (28-110 ml/min) were investigated. The reaction time was varied between 7 and 24 h. The first three experiments were conducted at the same operating conditions to ensure a good repeatability of the procedure. Samples were withdrawn at regular intervals from the mixing tank and the packed bed reactor outlet and analyzed by high-performance liquid chromatography (HPLC, Agilent 1100) instrument equipped with an RI detector and an Aminex HPX-87H column. The packed bed reactor was described with a dynamic axial dispersion model. The spatial derivatives in the model were discretized with finite differences and the created set of ordinary differential equations were solved numerically during the estimation of the kinetic parameters in in the complex reaction network. The results of the parameter estimation were analyzed with statistical tools. Matlab was used as the programming tool in the work.

Results and discussion

The main oxidation products were formic acid, 2(5H)furanone and succinic acid. The modelling results displayed in Figure 1, confirm that the reaction network is very representative for the reactions appearing in the furfural oxidation with H_2O_2 on Amberlyst-15. Specifically, 2(3H)-furanone, the key intermediate responsible of the formation of succinic acid, was well described in the experiments. The model prediction applied to the formulated reaction network gave an estimate of the concentration profiles for the intermediate molecules, which were not detected in the chromatograms. In Figure 2, two plots of the intermediates are shown. It can be concluded that the concentrations of the intermediates were very low compared to the main components. Statistical analysis confirmed the reliability of the parameters.

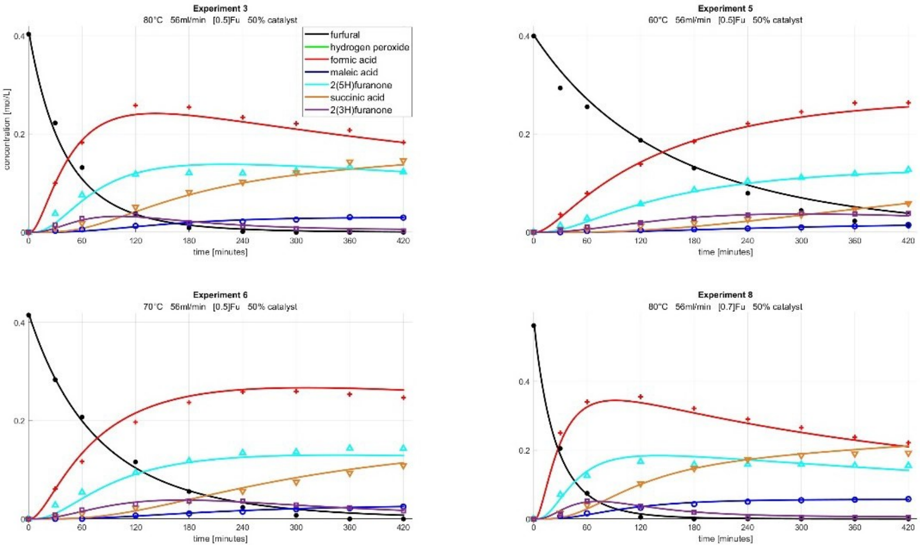

Figure 1. Experimental and predicted concentration profiles of the main components.

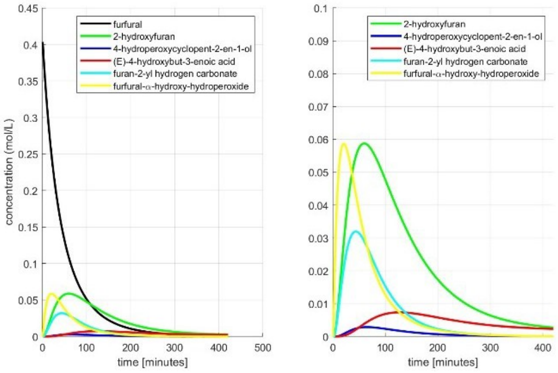

Figure 2. Predicted concentration profiles of the reaction intermediates.

Conclusions

The recycled loop reactor was a successful concept for furfural oxidation to high-value products. Advanced mathematical modelling enabled a reliable estimation of kinetic parameters in this very complex reaction system. The approach can be applied to other molecules originating from biomass.

References

[1] F. Saleem, P. Müller, K. Eränen, J. Wärnå, D. Yu Murzin, T. Salmi, Kinetics and modelling of furfural oxidation with hydrogen peroxide over a fibrous heterogeneous catalyst: effect of reaction parameters on yields of succinic acid, Journal of Chemical Technology & Biotechnology 92 (2017) 2206–2220

Keywords

Biomass conversion, furfural oxidation, complex reaction network, packed bed reactor in recycle mode

Wed. 11/09 // 11:40-12:00

RC – III – 4
Levulinate esters valorization: the production of γ-valerolactone and ethyl pentenoates through an innovative gas-phase continuous flow process

Luca Visentin[1], Pietro Zappalorti[1], Stefania Albonetti[1], Nikolaos Dimitratos[1],
Leandro Ardemani[2], Nicola Scotti[2], Tommaso Tabanelli[1]*, Fabrizio Cavani[1]

[1]Department of Industrial Chemistry "Toso Montanari" and Center for Chemical Catalysis-C3,
University of Bologna, Viale del Risorgimento 4, 40136 Bologna, Italy;
[2]CNR Istituto di Scienze e Tecnologie Chimiche "Giulio Natta", via Golgi 19, 20133 Milano, Italy;

**Corresponding author: tommaso.tabanelli@unibo.it*

Highlights

- Alternative hydrogenation using EtOH as H-donor and cheap catalyst based on zirconia
- A fine tuning of the acid/base properties can extend significatively the catalyst lifetime
- The deactivation is reversible and the catalyst can be regenerated *in situ*
- Catalyst's water tolerance makes possible the utilization of cost-effective diluted EtOH

1. Introduction

Obtaining chemicals and fuels from biomass is a key step for a sustainable development. From this prospective, cellulose is a potential source for a vast array of bioderived platform molecules, such as ethanol, levulinic acid (LA) and its esters (LE). In this context, the PRIN2020 LEVANTE project deals with the valorization of these biobased molecules through different strategies. A promising route consist of the reduction and cyclization of LE to produce γ-valerolactone (GVL), an important platform molecule that find several applications in the chemical industry as green solvent, additive for fuels and intermediate for organic synthesis (figure 1)[1]. Usually, this reduction is carried out in the liquid-phase and batch conditions involving the utilization of hydrogen at high-pressure (5-100 bar), in the presence of expensive noble-metal-based catalysts[2]. In this regard, a more suitable approach consisting in the catalytic transfer hydrogenation (CTH) mediated by secondary alcohols as H-donor has recently shown interesting results using zirconia based catalyst[1,2]. More recently, our group has proved the possibility to achieve high LE conversion and good GVL selectivity using a bio-based primary alcohol, namely ethanol, under continuous flow, gas-phase conditions at relative mild conditions (250°C, 1 bar)[3].

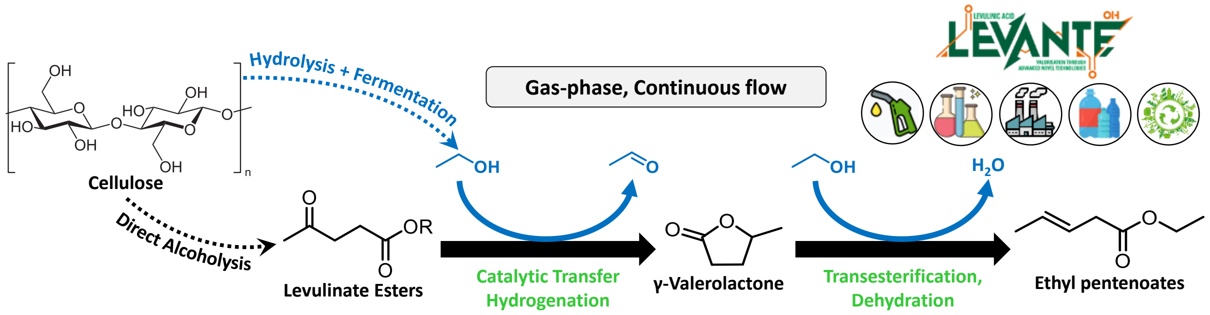

Figure 1. LE reduction to GVL and other reduction products using EtOH as H-donor.

2. Methods

The catalytic tests were carried out on a fixed-bed reactor operating in the gas-phase and continuous flow. LE and EtOH were vaporized under a nitrogen stream and subsequently forced to pass through the catalytic bed where the reaction takes place. Then, the reaction products were condensed in a liquid trap, which is analyzed through GC-MS/FID every 60 minutes in order to monitor the reactivity during the time-on-stream process. *t*-ZrO_2 and high SSA zirconia were synthesized by precipitation, *m*-ZrO_2 via hydrothermal synthesis, while ZrSiOx mixed oxides were synthesized through sol-gel method. Whereas, the sulfated catalysts were prepared by stirring the starting material in a diluted solution of H_2SO_4. Finally, catalysts were characterized by means of BET, XRD, TGA, FT-IR, NH_3- and CO_2-TPD.

3. Results and discussion

ZrO_2 showed remarkable performance in the CTH process, giving a GVL yield of 65%. On the other hand, it is subjected to deactivation due to the deposition of heavy carbonaceous species on the surface of the catalyst. However, the *in situ* regeneration of the catalyst by feeding air at 400 °C permitted an almost complete recovery of the initial catalytic behavior, showing that the deactivation is reversible. Interestingly, *m*-ZrO_2, which has a higher basic sites density than *t*-ZrO_2, was much more sensitive to deactivation [4]. Actually, it was found basic sites can promote the formation of angelica lactones (ALS), resulting from a rapid intramolecular cyclization of LE, and ALS consecutive oligomerisation seems the main responsible for the catalyst deactivation. For this reason, the acid/base properties of the catalytic system were further optimized. Surprisingly, introducing the Bronsted acidity, the basic sites density, as well as the local concentration of ALS, was reduced, and consequently the catalyst lifetime was strongly extended (Figure 2). Moreover, the Bronsted acid sites can catalyze consecutive reactions to produce ethyl pentenoates (EP), which are high value-added compounds, that find several applications in chemical industry due to their dual functionality (figure 1). Additionally, depending on the operating conditions applied, the selectivity can be moved towards GVL or ethyl pentenoates, providing in both cases a quite stable yield close to 70%.

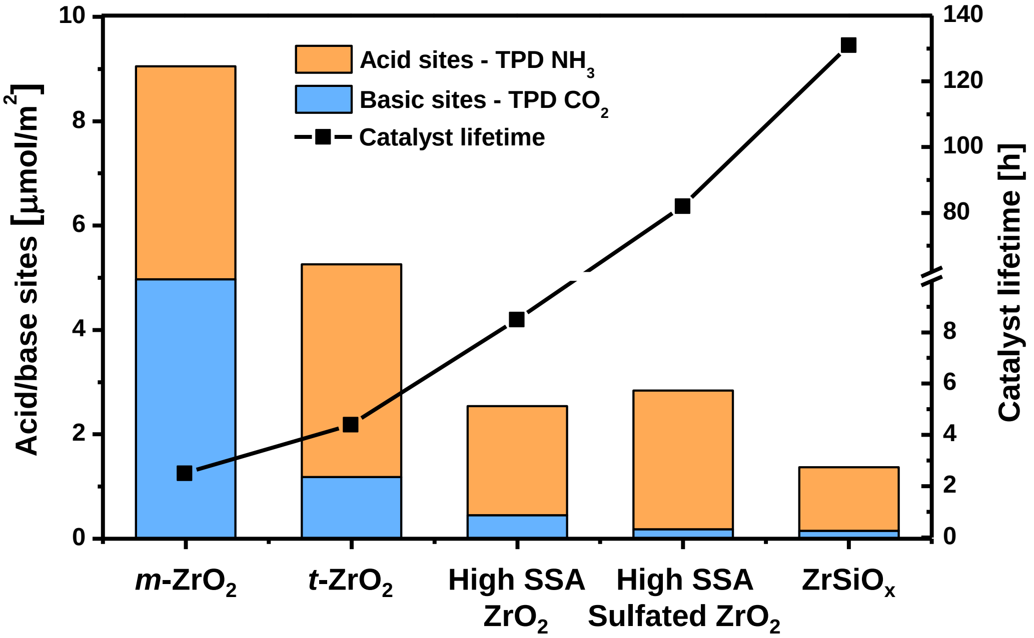

Figure 2. Correlation between catalyst lifetime and acid/base properties of *m*-ZrO_2 (120m^2/g), *t*-ZrO_2 (120m^2/g), high SSA ZrO_2 (210m^2/g), high SSA Sulfated ZrO_2 (190m^2/g) and ZrSiOx (290m^2/g).

4. Conclusions

CTH using ethanol as H-donor and cheap catalyst based on zirconia represents a sustainable alternative for the production of GVL and ethyl pentenoates compared to the conventional route involving hydrogenation over noble metal catalysts. A fine tuning of the acid/base properties can extend significatively the catalyst lifetime and once deactivated, it can be regenerated *in situ*. Moreover, water tolerance of the catalyst makes possible the utilization of cost-effective diluted ethanol.

MUR is acknowledged for the financial support provided through the LEVANTE project “LEvulinic acid Valorization through Advanced Novel TEchnologies”, PRIN-Bando 2020, Prot. 2020CZCJN7.

References

[1] D. Alonso et al., Green Chem., 2013, 15, 584–595
[2] T. Tabanelli et al., ACS Sustainable Chem. Eng., 2019, 7, 9937−9947
[3] P. Vásquez et al., ACS Sustainable Chem. Eng., 2019, 7, 8317−8330
[4] R. Bacchiocchi et al., J. Catal., 2023, 428, 115177

Keywords

Catalytic transfer hydrogenation; Catalyst lifetime; Acid/base properties; Biomass derivatives.

PROCESS INTENSIFICATION

Mon. 09/09 // 14:20-14:40

PI – I – 1

Sorption-Enhancement with in-situ water removal for an Intensified Methanol Production from CO_2

Enrico Antonuccio[1], David Edouard[1], Pascal Fongarland[1] *

[1]CP2M, Université Claude Bernard Lyon 1, CNRS, CPE, 3 Rue Victor Grignard, 69100, Villeurbanne (France)

**Corresponding author: enrico.antonuccio@univ-lyon1.fr*

Highlights

- Process intensification to produce e-fuels coupling reaction and adsorption
- Generalized reaction adsorption model and simulation
- CO_2 capture and conversion to MeOH

Introduction

The necessity to find an alternative route from fossil carbon for the synthesis of valuable fuels imposes the use of CO_2-rich syngas. Methanol is an excellent candidate for this: being liquid at ambient temperature and pressure, it shows a better exergy than hydrogen or hydrocarbons of similar molecular weight. Furthermore, it is a versatile building block in chemical industry: it can be either oxidized to formaldehyde or dehydrated to di-methyl-ether. Anyhow, the yield of the conventional methanol synthesis process is threatened on the one hand by the thermodynamic equilibrium of the exothermic reaction (1), and on the other by a parallel reaction, RWGS (2). High temperature is required for the breakage of the stable CO_2 bonds, but the latter would boost the parasitic reduction of carbon dioxide to CO, thus decreasing selectivity.

$$CO_2 + 3H_2 \underset{-Q}{\Leftrightarrow} CH_4O + H_2O \qquad 1$$

$$CO_2 + H_2 \underset{+Q}{\Leftrightarrow} CO + H_2O \qquad 2$$

$$CO + 2H_2 \underset{-Q}{\Leftrightarrow} CH_4O \qquad 3$$

To improve the yield of methanol without exceeding the 250 °C threshold, one strategy lies in the use of a sorbent (zeolites or MOF) that can selectively adsorb water in situ. The solution consists in exploiting Le Chatelier's principle to favorably displace the chemical equilibrium of reaction 1 rightward. This is made possible by temperature induced reaction/adsorption and regeneration/desorption cycles via controlled temperature or pressure swings, thus approaching the 'SERP' (Sorption Enhanced Reaction Process) technology. The aim of our project is to acquire a better understanding of the interaction between the various contributions (material transfer, heat, catalytic reaction and sorption), to efficiently design the process (duration and nature of cycles, integration of operations, scale-up…).

Methods

For the first part, we have simulated the process according to the data available in the literature. A dynamic, heterogeneous, non-ideal plug flow reactor model has been designed for this purpose. Mass balance equations (I,II,III) are discretized in space by a finite element approximation, using Matlab software for time integration. First, a grid of 50 points is defined in the spatial domain. Two additional points had to be added upstream and downstream of the reactor due to the second-order space-centric scheme used. At these two points, the variables (C, v, T) are assumed to be equal to the feed gas values, whereas the adsorbent load is set to zero. The total number of grid points used is therefore 52. This number provides a good trade off, as neither increasing the number of grid points leads to a more accurate solution, nor CPU shows hurdles in calculation. The resulting set of ordinary and algebraic differential equations was integrated with respect to time using Matlab's ode15s software, specifically capable of solving stiff differential equation systems.

$$\varepsilon_b \frac{\partial C_{dyn_i}}{\partial t} = -\frac{\partial\left(v * C_{dyn_i}\right)}{\partial z} + D_{ax_i}\frac{\partial^2\left(C_{dyn_i}\right)}{\partial z^2} + a_{v_{ads}} k_{m_{ads_i}}\left(C_{sta_i} - C_{dyn_i}\right) + a_{v_{cat}} k_{m_{cat_i}}\left(C_{cat_i} - C_{dyn_i}\right) \qquad \text{I}$$

$$(1-\varepsilon_b)\xi_{ads}\varepsilon_{p_{ads}} \frac{\partial C_{sta_i}}{\partial t} = a_{v_{ads}} k_{m_{ads_i}}\left(C_{dyn_i} - C_{sta_i}\right) - (1-\varepsilon_b)\xi_{ads}\rho_{ads} * \frac{dq_i}{dt} \qquad \text{II}$$

$$(1-\varepsilon_b)\xi_{cat}\varepsilon_{p_{cat}} \frac{\partial C_{cat\,i}}{\partial t} = a_{v_{cat}} k_{m_{cat_i}}\left(C_{dyn_i} - C_{cat_i}\right) + (1-\varepsilon_b)\xi_{cat}\rho_{cat} * R_i \qquad \text{III}$$

Results and discussion

Figure 1 presents an example of a typical ‘TSA’ (temperature swing adsorption) cycle. After a retention time that depends on the mutual affinity between the targeted molecule and the sieve, as well as its abundance along the packed bed, we see methanol exiting the reactor. Its main feature is the overshoot in concentration before its gradual plateauing at the equilibrium. The peak shows the gain in the yield due to the water sorption. Its duration and its height depend on the amount of adsorbing beads measured via the mass ratio Catalyst/Adsorbent. Water loading of the 3A zeolites homogeneously mixed with the Cu/ZnO/Al_2O_3 catalyst explains the behavior of these profiles. When the adsorbent is new, the water capture is possible, allowing to boost and exceeding thermodynamic equilibrium. As it reaches saturation, the tendency is gradually reversed and a desorption/regeneration stage at higher temperature is needed to repeat the process.

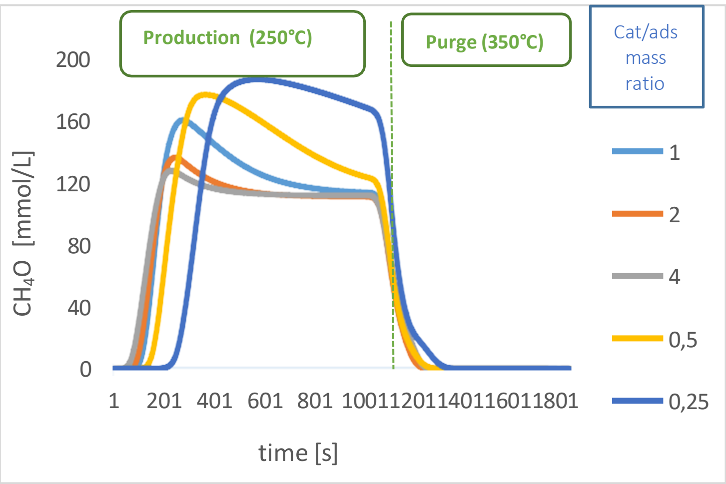

Figure 1. Methanol breakthrough. Dotted line marks the switch from the reaction stage to desorption (350°C)

Conclusions and perspectives

We have found that the coupling of reaction and sorption entails a raise of the average methanol yield over the cycle up to 50%. Moreover, the downstream flux has a higher purity, since H_2O passage is limited by the molecular sieve, thus preventing the catalyst from potential deactivation due to water induced sintering. Meanwhile, at a lab scale, an experimental packed bed reactor has been developed for implementing methanol synthesis from syngas. The pilot can undergo pressure swings, and eventually temperature ones, using Ohmic heating technology, based on the Joule effect of an electric current passing through it. The results obtained will be used to validate the modeling previously presented and to experimentally evaluate the optimized strategies identified.

References

[1] Terreni, J.; Trottmann, M.; Franken, T.; Heel, A.; Borgschulte, A. *Sorption-Enhanced Methanol Synthesis*. Energy Technology 2019, 7 (4).

[2] Dobladez, J. A. D.; Maté, V. I. Á.; Torrellas, S. Á.; Larriba, M.; Pascual Muñoz, G.; Alberola Sánchez, R. *Comparative Simulation Study of Methanol Production by CO2 Hydrogenation with 3A, 4A and 5A Zeolites as Adsorbents in a PSA Reactor*. Sep. Purif. Technol. **2021**, 262 (December 2020).

[3] Guffanti, S.; Visconti, C. G.; Groppi, G. *Model Analysis of the Role of Kinetics, Adsorption Capacity, and Heat and Mass Transfer Effects in Sorption Enhanced Dimethyl Ether Synthesis*. Ind. Eng. Chem. Res. 2021, 60 (18), 6767–6783

Keywords Zeolites; Methanol; Reactive separation; Low carbon fuel

Mon. 09/09 // 14:40-15:00

PI – I – 2

Development of semi-batch process for the synthesis of Methyl Pentenone

Nitin Sharma[1], Sumit Kamal[2]*

Department of Chemical Engineering, IIT Jodhpur, Rajasthan, India-342030

Highlights

- The overall process is optimized with a selectivity of 92 % and 95 % conversion.
- The energy requirement for distillation has been reduced by 16 %.
- Simulation model is validated with experimental data and shows robustness in model.
- The technique used for optimization can be generalized for similar aldol reactions.

1. Introduction

Fine chemicals such as pharmaceuticals, agrochemicals, flavors and fragrances (F&F), and intermediates are important aspects of the chemical industry. 3-Methylpent-3-en-2-one (MPO) is one such intermediate which is extensively used in the F&F industry to manufacture Iso-E-Super (a precursor for the synthesis of sandalwood fragrance)[1], filbertone[2]. Conventionally, MPO is produced through the aldol condensation of methyl ethyl ketone (MEK) and acetaldehyde (AcH) using H_2SO_4 as catalyst.[3] However, homogeneous catalysts lead to lesser yield, expensive material of construction (MOC), and neutralization after every batch which poses hazards to the environment. The use of heterogeneous catalyst such as Amberlyst-15 is reported as a better catalyst than the others to develop the green technology for MPO synthesis mainly because of higher MPO yield and better catalyst life.[4] MPO being a specialty chemical with low consumption, the commercial production of MPO is performed using batch operations. The objective of this research is to develop a production strategy to utilize the existing equipment such as batch reactors, distillation and purification units of any typical industry to produce MPO using heterogeneous catalyst. As per the reaction kinetics (Table 1), the emphasis is to optimize the MPO yield by the semi-batch addition of acetaldehyde in the batch reactor filled with MEK and catalyst. The use of excess MEK favors the higher selectivity for MPO, however, the unreacted MEK forms an azeotrope with water. Hence, the overall energy consumption for breaking the MEK-water azeotrope *vs.* effect of recycling azeotrope in the reactor over MPO yield and catalyst activities needs to be compared. Commercially available simulation tool ASPEN PLUS (Aspen Technology, V12) was used for developing the process of 4 TPD MPO production.

2. Methods

The list of different products considered in the simulation is shown in Table 1. Since, the binary interaction parameters for the components viz. Oligomers, Methyl Pentenone are not available in the data bank of ASPEN, it was estimated using UNIFAC method. BatchOp model of ASPEN PLUS was used for the optimization of semi-batch reactor and BatchSep was used to optimize the distillation and purification process. The LHHW based reaction kinetics as shown in Table 1 was used and the simulation results were compared with the experimental values reported in literature as shown in Figure 1. Also, the result of batch reaction *vs.* semi-batch reaction by the side injection of acetaldehyde was compared with an objective to get the maximum MPO yield. BatchSep was used for the separation of reaction mixture consisting more than 5 representative side products. A substantial quantity of unreacted MEK remains in the reactor due to higher ratio of AcH:MEK (1:3.5) in inlet feed. Also, the energy consumption for the separation of MEK-Water azeotrope *vs.* recycling of MEK-water azeotrope to the reactor and its effect over reaction performance was compared. It is required to recycle the unreacted MEK in the next batch cycle. There exist two distinct methodologies for accomplishing the task of recycling unreacted MEK as shown in Figure-2. The effect of recycling azeotrope over the catalytic activity of Amberlyst-15 was evident mainly because of high affinity of water for resin catalyst. The semi-batch operation of the reactor was optimized to maintain the consistent higher yield of MPO (more than 92 %).

3. Results and discussion

The conversion of limiting reactant acetaldehyde obtained from the simulation were compared with the experimental result and as evident in Figure 1, the values obtained from the simulation are in line with the experiment which validate the robustness of our model. Further, the simulation for the effect of semi-batch addition time of acetaldehyde over MPO selectivity were compared. As anticipated, the MPO selectivity increase from 71 % to 92% when addition time was increased from 0 min (pure batch) to 240 min. This increment in MPO selectivity has not only decreased the acetaldehyde consumption by 23%, but also significantly reduces the rate of catalyst deactivation because of less generation of coke and other oligomers. As discussed, the energy required for the distillation schemes shown in Figure 2, is 16% less than the approach 1, which leads to an important conclusion to recycle the MEK-water azeotrope (approach 2) rather than its separation followed by recycling. However, due to the strong affinity of water w.r.t resins, the rate of reaction decreases and in order to compensate its effect, the catalyst amount was increased from 4%(w/w) to 9% (w/w). With significant increase in selectivity and energy efficient purification process, the process development of MPO synthesis shows better results as compared to conventional process.

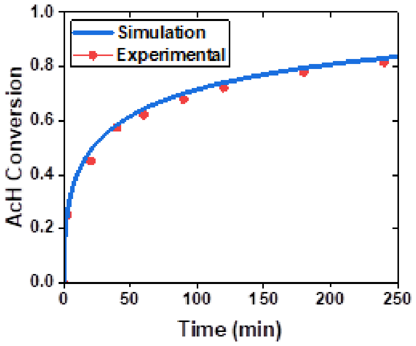

Figure 1: Simulation vs. Experimental results for Batch Reactor, AcH conversion vs. Time (min). Mole ratio 1:3 (AcH: MEK), Temperature: 363 K, 6% (w/w) catalyst loading

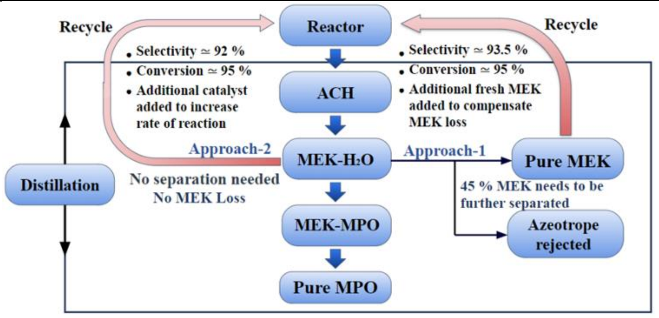

Figure 2. Operating strategy of distillation column and approaches for recycling of unreacted MEK

Table 1. Reaction scheme and reaction kinetics for MPO synthesis using Amberlyst 15 catalyst (A: Acetaldehyde, B: Methyl ethyl ketone, D: Crotonaldehyde, X: 7,9,11,13,15-Pentahydroxy Hexadec-2,4-dienal, Y: 3-Methylhepta-3,5-dien-2-one)

Reaction scheme	Reaction kinetics
$AcH + MEK \rightarrow MPO + H_2O\,(W)$	$r_1 = \frac{k_1 C_A C_B}{(1 + K_A C_A + K_W C_W)^2}$
$2AcH \rightarrow Cr - Al + H_2O$	$r_2 = \frac{k_2 C_A^2}{(1+K_A C_A+K_W C_W)^2}$
$8AcH \rightarrow X + 2H_2O$	$r_3 = \frac{k_3 C_A^2}{(1 + K_A C_A + K_W C_W)^2}$
$MEK + Cr - Al \rightarrow Y + 2H_2$	$r_4 = \frac{k_4 C_B C_D}{(1 + K_A C_A + K_W C_W)^2}$

4. Conclusions

The model validation against experimental data demonstrates sufficient reliability for its use in plant scale applications. The discussion regarding the approach of MEK recycling have been effectively incorporated into the process development, resulting in optimization of the process without breaking the azeotrope. The optimized operating conditions are 4 hrs addition time, 9% w/w catalyst loading with an overall reaction time of 10 hrs. Under these operating conditions, conversion of 95% and increased selectivity of 92 % is achieved in the semi-batch operation. The recycling approach of unreacted reactants can be generalized to similar aldol reactions in which numerous side products are formed via self and cross aldol condensation reactions. This project represents a significant advancement in the development of MPO production methods.

References

[1] Wang, Z.; Jia, W.; Cheng, C. Process for Preparation of Iso-E Super. CN Patent No 101081f808, 2007.
[2] Cheng, C. The synthetic method for Filbertone. CN Patent No101597223, 2009
[3] Yoshida, T.; Hall, J. B. Process for Preparing Ketones Using Zinc Acetate condensation Catalysts, Products Produced Thereby and Organoleptic Uses of Same. U.S. Patent 4169109, 1979
[4] Kamal, S.; Mahajani, A Greener Alternative for the Synthesis of Methyl Pentenone Using Reusable Cation Exchange Resin. Industrial & Engineering Chemistry Research 2020 59 (49), 21312-21321.

Keywords

Methyl Pentenone, Green technology, Amberlyst-15, 98% recovery

PI – I – 3

STUDY OF HETEROGENEOUS ENZYMATIC REACTIVE DISTILLATION: FROM EXPERIMENT TO COMPREHENSIVE MODELING

Nicolas Chaussard[1]*, Clémence Nikitine[1], David Rouzineau[2], Michel Meyer[2] and Pascal Fongarland[1]

[1] CP2M, UMR 5128, Université Claude-Bernard Lyon 1, CNRS, CPE Lyon, Villeurbanne, France;

2 LGC, UMR 5503 Université de Toulouse, CNRS, INPT, UPS, Toulouse, France

**Corresponding author: nch@lgcp.cpe.fr*

Highlights

- Novel distillation packings functionalized with a xerogel containing the CALB lipase
- Enzymatic reactive distillations achieved 13-22.5% of conversion
- Complete EQ and NEQ models of the setup successfully developed

1. Introduction

Heterogeneous reactive distillation (RD) offers the possibility to eliminate by-products from the reactive section, such a feat giving the opportunity to exceed thermodynamics and inhibitions limitations imposed by reversible reactions. Numerous “chemical” reactive distillation setups were studied in the literature and are applied industrially as of now, whereas heterogeneous enzymatic catalyzed reactive distillation (ERD) systems are only marginally studied because of the large amount of constraints coming from the enzyme deposit homogeneity and stability.

As such, the objective of this project is to better understand the coupling of various phenomena during enzymatic reaction-distillation and their interactions. A vacuum ERD setup with an internal diameter of 3.2 cm and packed bed length of 72 cm was designed to establish solid foundations for the development of multifunctional enzymatic processes. Extensive modeling were as well developed to evaluate the impact of experimental parameters, and the influence of internal/external mass transfers and scale-up. Enantioselective transesterification of 2-pentanol (2-PeOH) with ethylbutyrate (EtBu) forming ethanol (EtOH) and 2-pentylbutyrate (2-PeBu) has been selected as model reaction in line with earlier work. [1][2]

2. Methods

The kinetics of the enantioselective transesterification were determined in a Spinchem® rotating bed reactor (150 mL) using Novozym®435, a Candida Antartica Lipase B (CALB) supported on acrylic resin beads. The intraparticle concentration gradient was computed employing an orthogonal collocation method in Matlab®. All reaction kinetics were followed using gas chromatography with a Chirasil CB-Dex column, allowing for quantification of all components including the 2-pentanol and formed 2-pentylbutyrate enantiomers. The reaction kinetics were studied in a flask reactor (25 mL) with a catalytic xerogel composed of a lipozyme CALB L solution, methyltrimethoxysilane and tetramethyl orthosilicate.[1][2]

Enzymatic xerogel coatings were applied by sol-gel dip-coating on novel distillation packings such as 3D printed *Tetra Splines* developed by our partner LGC, and 10, 20 pores per inches (ppi) aluminum foams produced by investment casting. Mechanical and chemical stabilities of the xerogel on packings surface were enhanced by preliminary application of an adhesion promoter or “primer” containing (3-glycidyloxypropyl) trimethoxysilane. Losses in coated xerogels were assessed in both the Spinchem® reactor and the reactive distillation setup for 20 ppi foams. The xerogel distribution, appearance and pore distributions were assessed by scanning electron microscopy and X-ray tomography.

The separation efficiencies of all packings were determined in the distillation setup using an ethanol-isopropanol mixture. Continuous enzymatic reactive distillations were conducted by filling the bottom half of the column with the functionalized foams or *Tetra Splines*. The ERD system was entirely modelled using equilibrium (EQ) and non-equilibrium (NEQ) approaches under Matlab®, with product properties extracted from Prosim®; experimental data from the separation efficiencies measurements and ERDs will allow for adjustment of necessary hydrodynamic correlations and determination of the catalyst portion in contact with the liquid.

3. Results and discussion

The reaction was found to be athermic with an experimental reaction enthalpy of 4.66 kJ/mol, its equilibrium conversions ranging between 56.6% and 58.2% for temperatures of 30 to 60°C. The studied enantioselective transesterification kinetics were best modeled by a Michaelis-Menten ping-pong model coupled to the Arrhenius law. All 9 parameters of the model were optimized and yielded a Mean Average Percentage Errors (MAPE) of 3.7% for Novozym$^{®}$435 (774 data points), and 4.1% for the xerogel (480 data points, tests still undergoing). Only the produced ethanol exhibited a strong inhibition behavior, highlighting the necessity of its elimination from the reaction medium by ERD. Novozym$^{®}$435 presented an effectiveness factor varying from 0.37 to 1 depending on experimental conditions while the xerogel showed no intraparticle resistance for the studied particle size (90-710 µm). This absence of diffusional limitations is partially caused by the xerogel lower activity and its macroporosity. Xerogel coated on packings presented identical activity to that of the crushed xerogel. After one run of 6h at 60°C and 200 rpm in the reaction medium, a functionalized 20 ppi foam lost respectively 27.2% and 30.7% in mass and overall activity, increased to 36.4% and 42.3% after 4 runs.

Height equivalent to a theoretical plate (HETP) were evaluated at 0.196, 0.171 and 0.294 meters for 10, 20 ppi foams and *Tetra Splines*. As coatings clog the packing pores and create preferential pathways that may reduce separation efficiencies, these HETP are also to be evaluated with the catalytic packings,. A non-reactive distillation of ethylbutyrate and 2-pentanol was conducted to validate the EQ model and adjust the NEQ correlations with 20 ppi foams, leading to MAPEs inferior to 5% for both models.

A first ERD with 4.57 g of xerogel on 20 ppi foams allowed for a conversion of 13% when stationary state was reached (17 hours), and another with 6.08 g of xerogel on 10 ppi foams yielded a conversion of 22.5%. Such low conversions are mainly due to the maximum amount of xerogel and enzyme that can be deposited on the packings, which could be overcomed with enzymes of greater catalytic activity.

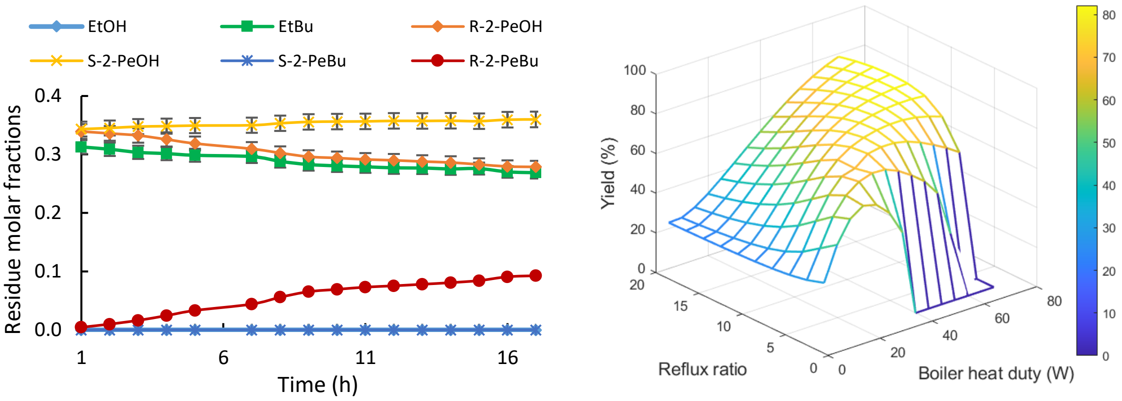

Figure 1. Experimental evolution of residue compositions during ERD with 4.57 g of xerogel on 10 ppi foams (left) and simulation of yields depending on operating conditions with enzymes of enhanced catalytic activity (right)

4. Conclusions

The kinetics of an enantioselective transesterification catalyzed by Novozym$^{®}$435 and a CALB xerogel were successfully established, with accountability of internal mass transfers. Novel distillation packings were functionalized with the biocatalytic coating and applied to continuous heterogeneous ERD with final conversions ranging from 13 to 22.5%. An EQ and NEQ model were developed to simulate the setup, their correlations being adjusted with the performed ERDs. These models will allow simulation of similar experiments with enhanced enzymes, scaled-up setups and internal/external mass transfer limitations to better grasp the impact of these parameters on the stationary state.

References

[1] Heils R. et al, Chem. Ing. Tech. 54 (2015) 9458-9467
[2] Blatkiewicz M., Mißfeldt F. & Smirnova I., Ind. Eng. Chem. Res. 58 (2019) 222820-22834

Keywords

Reactive distillation ; Enzymatic catalysis ; Xerogel coatings ; Process modeling; Process intensification

Mon. 09/09 // 16:20-16:40

PI – II – 1

Intensification of mass-transfer limited catalytic applications through POCS structured supports with optimized cell and streamlined strut shape

Claudio Ferroni[1], Mauro Bracconi[1], Matteo Ambrosetti[1], Matteo Maestri[1], Gianpiero Groppi[1] and Enrico Tronconi[1]*

1 Laboratory of Catalysis and Catalytic Processes, Department of Energy, Politecnico di Milano, Via La Masa 34, 20156 Milano, Italy

**enrico.tronconi@polimi.it*

Highlights

- Orientation and shape of POCS struts are adjusted to boost the fluid-solid interaction
- POCS are optimized to enhance the trade-off between mass transfer and pressure drop
- Optimized POCS offer superior mass transfer coefficients than honeycomb supports at same pressure drop

Introduction

Periodic Open Cellular Structures (POCS – Figure 1) are innovative structured catalytic supports which look attractive Process Intensification, as they provide enhanced heat and mass transfer rates within catalytic reactive systems [1-3]. POCS are typically produced with additive manufacturing, allowing for a high degree of freedom in design, allowing to optimize their geometry to meet specific process requirements. For instance, POCS can be tailored to enhance flow distribution within chemical reactors [1,2], making them a versatile option for various applications.

Herein, POCS are envisioned as alternative structured supports for processes affected by a trade-off between gas-solid mass transfer and pressure drop, e.g., aftertreatment applications. In this context, the honeycomb monolith is typically employed due to the low pressure drop. While conventional POCS shapes (Figure 1 (a)) exhibited inferior overall performance compared to state-of-the-art support, our previous research [3] has demonstrated the possibility to overcome this limitation. In particular, the orientation of struts within the unit cell was modified to align them with the flow direction (Figure 1 (b)), leading to lower pressure drop than conventional POCS shapes without significantly compromising mass transport properties, ultimately outperforming honeycomb monoliths. Starting from these findings, this study proposes an evolution of POCS with streamlined elliptical struts lined up with the flow direction (Figure 1 (c)), aiming to further enhance their performances.

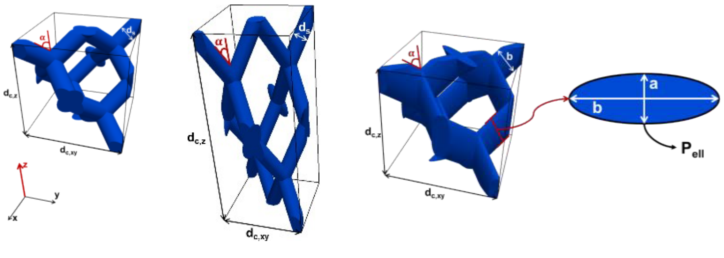

(a) (b) (c)

Figure 1. Illustration of different configurations of Periodic Open Cellular Structures (POCS): (a) Regular diamond lattice with circular struts, (b) Modified design with circular struts [3], and (c) Modified design with elliptical struts.

Methods

We employ a numerical approach based on reactive Computational Fluid Dynamics (CFD) simulations conducted to fundamentally investigate the transport properties and pressure drop of POCS. The methodology is reported in detail in [3] and is hereby briefly summarized. Computational domains constituted by a single unit cell, identified as the Representative Elementary Volume [3] of the POCS, are generated. Periodic boundary conditions are then implemented at the domain side boundary, ensuring asymptotic fluid flow and concentration profiles are achieved within the system. These conditions are typically obtained as the size of the equipment is order of magnitude higher than the unit cell (i.e., 10^0 m vs. 10^{-3} m).

Results and discussion

The original Diamond unit cell (Figure 1 (a)) was previously modified by adjusting the angle α between the struts and the fluid flow direction z, resulting in a stretched unit cell along z (Figure 1 (b)) [3]. We refined the geometry by introducing elliptical struts aligned with the flow direction (illustrated in Figure 1 (c)). The new geometry offers increased specific surface area, leading to larger volumetric mass transport coefficients. Additionally, the streamlined struts offer lower drag, leading to lower pressure drop. The combined beneficial effect of these two features is demonstrated in Figure 2 (a), where the performances are reported as a dimensionless trade-off index balancing mass transfer and pressure drop - Merit Index (M.I.) [3]. The optimized cell with elliptical struts is compared against the other shapes of POCS (Figure 1 (a) – (b)), and a reference honeycomb (HC) monolith (900/2.5). Despite owning the same porosity ($\varepsilon = 0.85$) with the HC, the original Diamond cell consistently exhibited inferior performance. Conversely, the modified cell achieved up to a 1.5-fold higher M.I.. A further enhancement of the M.I. is obtained due to streamlined struts, allowing also to extend the range of Re where the new structure outperforms state-of-the-art supports. This is a crucial aspect for potential applications in automotive systems, where significant load variations are obtained during driving cycles. Supports are then compared by considering CO oxidation at 300°C as a mass transfer-limited reaction realistically occurring in an abatement system (Figure 2 (b)). POCS with a strut size of approximately 340 µm were designed, corresponding to $Re \cdot (L_{char} Sv)^{-1} = 250$. The simple Diamond cell offers up to a 20% higher mass transfer-limited CO conversion (X_{CO}) than the HC. However, it provides a 5-fold higher pressure drop, limiting its practical application. In contrast, the modified cell achieved the same pressure drop as the HC, along with a 10% higher X_{CO}. Finally, the structure with elliptical struts demonstrates the same conversion as the standard shape (i.e., 20% higher X_{CO} than HC), with the same pressure drop as the HC, resulting in a significant enhancement of abatement efficiency without any additional penalty.

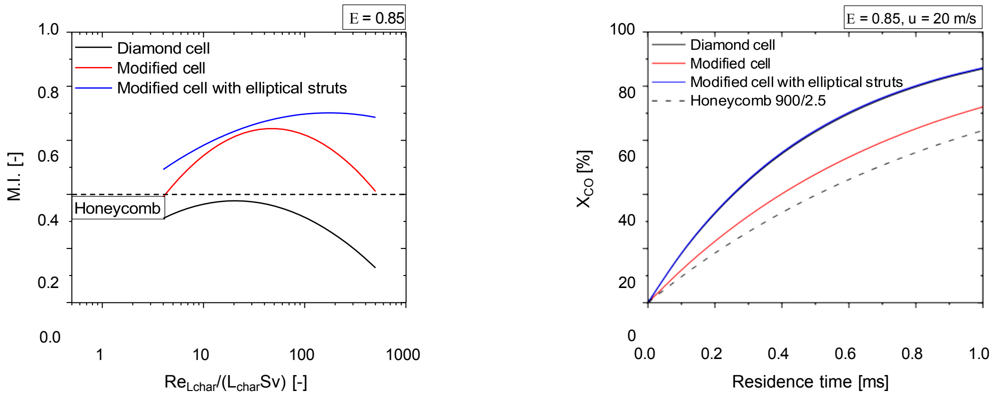

(a) (b)

Figure 2 (a) Trade-off index between mass transfer and pressure drop, evaluated using the Merit Index (M.I.). (b) mass transfer limited CO conversion (X_{CO}) versus residence time.

Conclusions

This study demonstrates that optimized POCS with finely-tuned geometrical features, hold significant promise as intensified structured supports, opening a new era of catalytic reactors.

References

[1] Do G. et al., Chem. Eng. Process 148 (2020) 107786
[2] Lämmermann M. et al., Chem. Eng. Process. 126 (2018) 178-189
[3] Ferroni C. et al. Chem. Eng. Process. 195 (2024) 10961
[4] Giani L. et al., Ind. Eng. Chem. Res. 44 (2005) 4993-5002

Keywords
Process Intensification, Structured Catalytic Supports, Heat and Mass Transfer, Lattice Materials

Mon. 09/09 // 16:40-17:00

PI – II – 2

Model Development of Gas-Liquid Vortex Reactor for Process Intensification of CO_2 Capture

Afroditi Kourou[1], Gozde Gecim[2], Siyuan Chen[1], Geraldine J. Heynderickx[1], Yi Ouyang[1]*, Kevin M. Van Geem[1]

1 Laboratory for Chemical Technology, Ghent University, Technologiepark-Zwijnaarde 125, B-9052, Zwijnaarde, Belgium; 2 Department of Chemical Engineering, Faculty of Engineering and Natural Sciences, Bursa Technical University, 16310, Bursa, Turkey

**Corresponding author: yi.ouyang@ugent.be*

Highlights

- A 1D representation of the gas-liquid vortex reactor is developed using two simulation techniques.
- Correlations based on experimental and CFD data are created.
- A process simulation will be constructed for CO_2 capture using liquid solvents.
- A techno-economic analysis will predict the cost-effectiveness of GLVR for intensifying CO_2 capture.

Introduction

In 2021, the energy sector experienced a record increase in emissions [1]. The transition to a net-zero, circular economy is an ongoing, yet challenging process, especially for sectors facing significant hurdles in decarbonizing. Therefore, developing Carbon Capture (CC) technologies to **efficiently capture CO_2 from point-source gases** is imperative. Among various CC technologies, chemical absorption is a mature, commonly used technique on an industrial scale. However, various barriers associated with the high capital expenditure (CAPEX) linked to large columns used and high operational expenditure (OPEX) due to the elevated energy required for solvent regeneration are yet to be overcome. Process intensification can be a key factor in achieving energy and mass transfer efficiency, resulting in a substantial cost reduction. Additionally, the development of a one-dimensional (1D) model allows thorough techno-economic analysis and optimization at process level, highlighting its pivotal role in addressing these challenges.

The Gas-Liquid Vortex Reactor (GLVR) is an intensified reactor developed at the Laboratory for Chemical Technology (LCT, UGent) for gas-liquid applications. The reactor consists of a static, cylindrical, fluidization chamber where gas is injected tangentially creating a high slip velocity and gravity field. Experimental studies have confirmed that the intensification of the momentum transfer inside the reactor results in favorable hydrodynamics and micromixing efficiency [2]. Computational Fluid Dynamics (CFD) simulations have been performed in parallel for the GLVR targeting to optimize the design and performance of the reactor [3]. The next step is the development of a 1D, process model of the GLVR, capable of integrating the reactor in a complete design of CO_2 capture process simulation. As GLVR is an intensified, recently developed reactor, it doesn't exists in existing libraries and therefore developing a custom model is necessary. A process model offers a time-saving advantage, while embedding GLVR in a process simulator allows for the complete design and scale-up of the process.

Methods

Two distinct methods were developed for modeling the GLVR based on relevant methodology proposed for rotating packed bed (RPB) reactors [4, 5]. The first method involves linking a conventional process simulation software such as Aspen Plus with Fortran. In this case, GLVR was discretized into distinct annular sections, each one corresponding to a conventional packed bed column. This way, Fortran subroutines were used to embed the hydraulics correlations of each GLVR ring. The columns were connected in series to represent the GLVR as a unit. The second method includes the development of a model using empirical correlations. For this purpose, Aspen Custom Modeler (ACM) was employed, as it provides the environment to create a customized model that can be later integrated in Aspen Plus. In both approaches, the reactor's characteristics such as the specific interfacial area, mass transfer coefficient, and liquid hold-up were derived from experimental and CFD data. Currently, a comprehensive process simulation for CO_2 absorption and desorption based on the GLVR model is being developed, so that a techno-economic analysis can follow. Smart process design and advanced heat integration configurations will be employed to determine the final cost of capturing CO_2 (\$/tonCO_2), aligning with the existing literature.

Results and discussion

Figure 1 (left) shows preliminary results from the GLVR model using the Aspen Plus/Fortran method. The absorbed CO_2 in the liquid phase (C_{CO3-2}) is presented at various liquid flowrates (Q_L) at a gas flow rate of $G=25\ m^3/h$ for a CO_2/NaOH system. Experimental data from previous studies [2] are used to validate the model. Different numbers of columns in series were investigated, showing that ten columns approach the experimental data. For comparison, five conventional packed bed columns in series are included, showing a substantial lower absorption performance, and therefore indicating the capability of the GLVR for process intensification. Figure 1 (right) shows the recently developed model using the ACM method, where a gas and a liquid are introduced to the reactor where the absorption takes place.

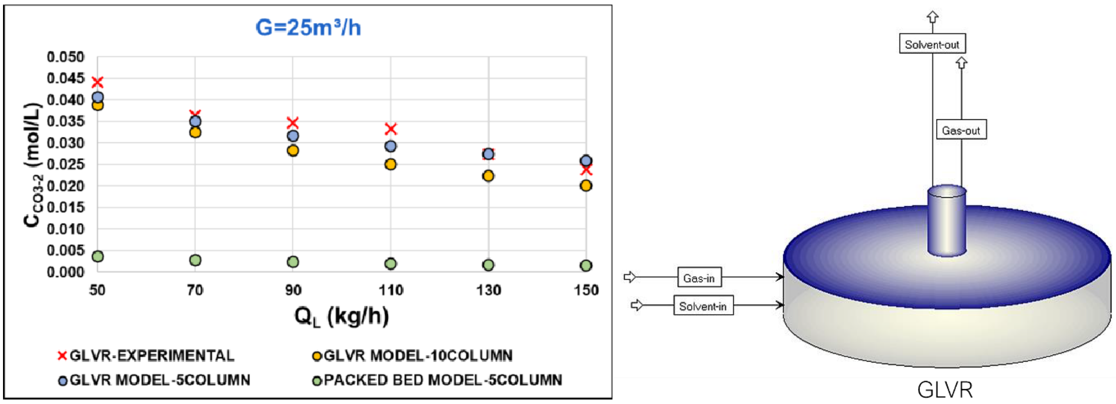

Figure 1. Preliminary results of the Aspen Plus/ Fortran method (left) and recently developed ACM model (right).

Conclusions

A customized process model of the GLVR has been developed and validated using two different computational techniques: coupling Aspen Plus with Fortran subroutines and employing Aspen Custom Modeler. Correlations based on experimental and CFD data are created to efficiently develop the model. The development of the complete process simulation of the CO_2 capture process based on the customized GLVR model will take place. The ultimate goal is to perform a comprehensive techno-economic analysis and optimization at process level to evaluate the cost-effectiveness of integrating the GLVR in a CO_2 capture process design.

References

[1] IEA, World energy outlook 2022, IEA Paris, France, 2022.

[2] Y. Ouyang, M. Nunez Manzano, S. Chen, R. Wetzels, T. Verspeelt, K.M. Van Geem, G.J. Heynderickx, Chemisorption of CO2 in a gas–liquid vortex reactor: An interphase mass transfer efficiency assessment, AIChE Journal 68(5) (2022) e17608.

[3] S. Chen, P. Malego, K.M. Van Geem, Y. Ouyang, G.J. Heynderickx, Design and Optimization of Gas–Liquid Vortex Unit Using Computational Fluid Dynamics (CFD) Simulation, Industrial & Engineering Chemistry Research 62(42) (2023) 17068-17083. https://doi.org/10.1021/acs.iecr.3c02380.

[4] C.-H. Yu, Y.-J. Lin, D.S.-H. Wong, C.-C. Chen, Process Modeling of CO2 Absorption with Monoethanolamine Aqueous Solutions Using Rotating Packed Beds, Industrial & Engineering Chemistry Research 61(33) (2022) 12142-12152. https://doi.org/10.1021/acs.iecr.1c04323.

[5] M. Pahlavan, A. Shahsavand, M. Panahi, Design and simulation of rotating packed beds for an industrial acid gas enrichment process, Fuel 361 (2024) 130696. https://doi.org/https://doi.org/10.1016/j.fuel.2023.130696.

Keywords

Model development, gas-liquid vortex reactor, process intensification, carbon capture

Mon. 09/09 // 17:00-17:20

PI – II – 3

Photodegradation of phenol in rotating disk reactor and 3D modelling

Ewan Westgate[1], Dom Johnson [1] and Farid Aiouache[3]*

[1] Lancaster University e.westgate@lancaster.ac.uk; *[2] Lancaster University* d.m.johnson1@lancaster.ac.uk; *[3] Lancaster University* f.aiouache@lancaster.ac.uk
**Corresponding author:* f.aiouache@lancaster.ac.uk

Highlights

- Photochemical degradation of phenol was intensified efficiently by a rotating disk reactor.
- Thickness of liquid film and phenol conversion were assessed by parametric study.
- Modelling was carried out by volume of fluid, moving mesh discretization and particle tracing.

1. Introduction

Phenol is a chemical that is associated with the regulations in place that control the release of contaminants to the water environment. The photocatalytic degradation as advanced oxidation process is seen among the promising routes for reduction of a wide range of organic pollutants. This work investigates the degradation of phenol in a rotating disc reactor (RDR) as process intensification approach and highlights the role of the process parameters and relevant impacts on both mass transfer effectiveness and reaction rate performance over the essential role of oxygen penetration in the liquid film, the surface reaction catalyzed by the intermediate hydroxyl radicals and the UV light activation. Ensuring a sufficient supply to the catalyst surface is achieved by the thin film subject to the dynamic operations of the rotating disk and the deep light penetration across the bulk liquid film. This work aims to assess via a laboratory work the impact of hydrodynamics generated by the rotational speed and flow dynamics on the degradation rate and 3D computer fluid dynamics (CFD) modeling validation. Thorough reactor design, photocatalysis and flow dynamics are applied as a sustainable treatment method for phenol in water.

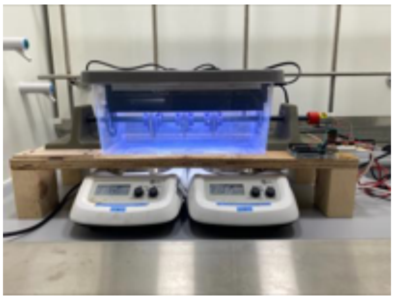

Figure 2. Water velocity in bulk RDR

2 Methods

2.1. Experimental.

The manufacture of the reactor design included three distinct activities; (i) the chemical one for the immobilization of TiO_2 onto stainless steel disk through dispersion and dip-coating procedures of a suspension of TiO_2, calcination, and coating thickness and surface adherence assessments by 3D microscopy imaging and shear flow tests, (ii) mechanical one: design by additive manufacturing for production of 3D polymer parts as well as mechanical machinery for the manufacture a wooden base; and (iii) electrical one for the control of the rotation speed of the electrical motor controlled by an Arduino board and the UV light intensity. This design consists of three discs (90 mm diameter), an axle (500 mm length), couplers (46.8 mm diameter, 20 mm height, 12.7 mm diameter of the hole and a vessel (315 mm length, 85 mm height, 100 mm width) and UV-lights of a broad spectrum in the UV range. Phenol degradation was monitored by use UV-Vis spectrophotometry.

2.2. Modelling by 3D CFD modelling.

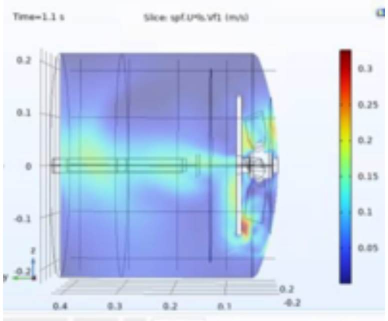

Figure 2. Water velocity in bulk RDR

The opportunity to apply computational fluid dynamics (CFD) as a tool to model the flow distribution has enabled visualization of the wetting efficiency from the water-catalytic disk interactions. The volume of fluid (VOF) approach was conducted in combination with the Eulerian-Eulerian model, which was discretized by the moving mesh method, allowing capture of the interphase of surfaces between the liquid and the rotating disk. The spatial resolution of these methods helped link the geometrical configuration of the disk and operational parameters to the patterns of the flow and thus assessed interactions of air, water and solid disk of multiphase systems . The VOF captured the diffuse interface between water and air and used the mixing and the storage energies at the interface by decomposition of the Cahn-Hilliard second-order partial differential equations. The time-dependent study iteratively solved several non-linear equations for every time step using Newton's approach. The simulation started by discretizing the fluid domain into many cells and the governing equations were then integrated for each cell. The differential equations were computed using an iterative solver.

Results and discussion

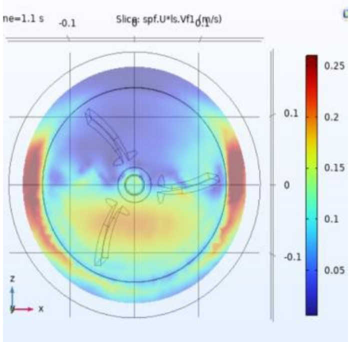

Figure 3. Water velocity over

The first parameter influencing the conversion of phenol that was investigated was the rotation speed of the disk. Increasing the rotation speed up to 200 rpm was found positive on the conversion was associated with a decrease in the film thickness. The generated drag forces from disk rotation promoted the entrainment of the surface liquid via surface adherence and wettability off hydrophilic nature. Increasing the rotational speed caused part of the liquid to be removed off the disk surface instead of flowing along the disk, accelerated by insufficient adhesive forces balancing the drag ones, forming irregular think layers and droplets above the disk surface. The droplets imposed a shielding effect, which was derived from scattering and reduced the availability of UV light for photochemical reaction. The CFD results illustrated the trends of water velocity in bulk water phase as shown in **Figure 2** where pronounced flow at the free air-water interphase is illustrated, which is the reference rotation angle of the disk but with reduced mixing in bulk water phase of the RDR. The distribution of average velocity along disk surface is shown in **Figure 3**. The light-exposure was simulated by trajectory of the particle, using the particle tracing module of Comsol, in the RDR and visualise the attenuation effect of UV light intensity in the RDR along with the fluctuations of streamlines in the irradiation direction. The particles traveled mainly along a horizontal direction but interconnected at the surface of the disk reactor, promoting exchange between the fluid and the light-irradiation. Photon absorption rate (not shown) was highly affected by fluid flows throughout the reactor as shown in **Figure 4** since the irradiation could be sufficiently utilized in the turbulent zone in the photoreactor. The variation of concentration of phenol in different disk zones was derived from the alteration of turbulent kinetic energy.

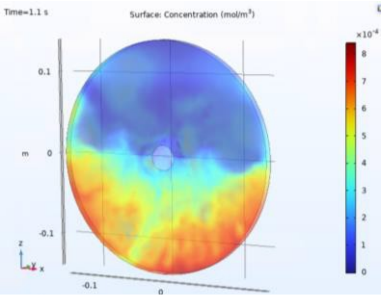

Figure 2. Concentration of phenol over the disk surface

Conclusion

In this work, the rotating disk reactor performance was assessed by different disk configurations and operations conditions. CFD simulations were used to assess the laboratories, including impact of disk rotation speed, light intensity, surface configuration. The results of conversion trends validated those available in literature. The CFD model methodology is novel since the rotation of the disk was simulated but the moving mesh method instead of mathematical model. The light penetration was carried out by particle tracing method. In future work this combination was added to the ray tracing module of the CFD package, leading representation of RDR as close as possible to industrial operations.

References

[1] D. D. Dionysiou, et al. “Rotating disk photocatalytic reactor: development, characterization, and evaluation for the destruction of organic pollutants in water,” *Water Research,* vol. 34, no. 11, pp. 2927-2940, 2000

[2] C. Montalvo-Romero, C. Aguilar-Ucán, R. Alcocer-Dela Hoz, M. Ramirez-Elias and V. Cordova-Quiroz, “A Semi-Pilot Photocatalytic Rotating Reactor (RFR) with Supported TiO2/Ag Catalysts for Water Treatment,” *Molecules,* vol. 23, no. 1, 2018

Keywords

Photocatalysis; rotating disk reactor; CFD modelling; Volume of fluid method

REACTOR DESIGN

RD – I – 1

InterPOCS for in operando adjustment of fluid flow and mass transport characteristics in heterogeneous catalysis

Lisa Eckendörfer*, Hannsjörg Freund

TU Dortmund University, Institute of Reaction Engineering and Catalysis, Dortmund, Germany

**Corresponding author: lisa.eckendoerfer@tu-dortmund.de*

Highlights

- Interpenetrating periodic open cellular structures (interPOCS) as flexible catalyst support.
- CFD investigations on the hydrodynamic fluid-structure-interaction influencing a reaction network.
- Potential of interPOCS for the in operando adjustment of the CO_2 methanation.

Introduction

Periodic open cellular structures (POCS) are additively manufactured lattice-like catalyst support structures. The unit cell, formed by characteristically arranged solid struts, builds the basis of POCS. The POCS' three-dimensional solid lattice is formed by periodically repeating the unit cell in all spatial directions. Despite the unit cell configuration itself, the dimensions of the unit cell and the struts can be customized. This design flexibility inherent to additive manufacturing allows for the precise tailoring of the structures to meet specific reactor requirements of a chemical process. However, the flexibility is restricted to the design process, the direct modification of POCS during the application in a chemical process is usually limited.

Interpenetrating periodic open cellular structures (interPOCS), a subset of POCS, overcome this limitation with the ability of in operando adjustment of the structure. In interPOCS, two POCS lattices (commonly diamond unit cell based) are interwoven in such a way that a relative displacement of the two interwoven but independently movable structures is possible. The relative shift respectively the offset is visualized in Figure 1. It changes the local morphology of the structure, while the global characteristics as porosity and specific surface area remain constant. Previous work showed that the relative shift of the two lattice structures enables a change of the hydrodynamic behavior within the interPOCS [1, 2]. The local flow path changes systematically with the offset: an increasing proportion of the available volume is shielded when the distance between the two moveable parts becomes smaller and the effective overflown solid surface is reduced [1]. As hydrodynamics and mass transport are directly linked, chemical reactions can be influenced by the shift.

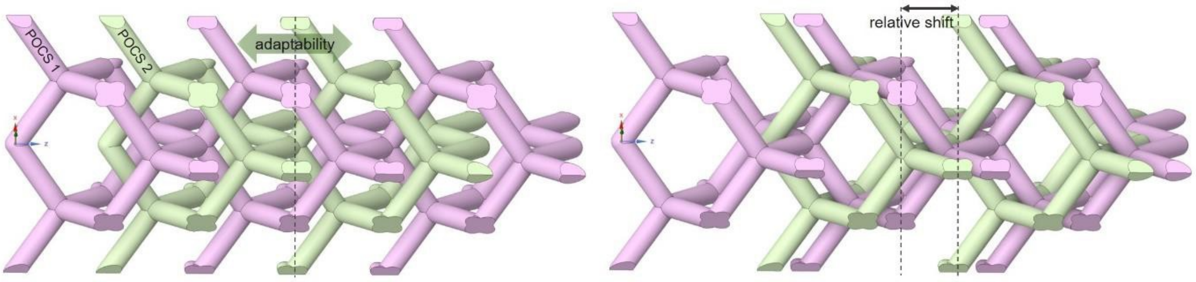

Figure 1. Visualization of the interPOCS principle. The interPOCS consists of two interwoven moveable POCS lattice parts. On the left side the distance between the two independent diamond unit cell based POCS is equal, on the right side the second POCS lattice is shifted in axial direction towards the first.

Methods

The interplay between hydrodynamics and chemistry in interPOCS was investigated numerically using

CO and CO_2 methanation as an example reaction network in the context of power-to-X processes. For the setup of the computational fluid dynamics (CFD) simulations, the periodic character of the interPOCS was exploited to reduce the simulation domain. Periodic boundary conditions were applied perpendicular to the main flow direction. In the main flow direction, a representative structure length was used to resolve representative changes in the composition of the reaction mixture along the structure. The methanation reaction is included by a microkinetic reaction mechanism [3]. To systematically study the interplay between the hydrodynamic behavior and the reaction process, the offset of the interPOCS was gradually varied. Since the flow regime strongly influences the degree of change between the individual offsets [1], a wide range of gas velocities was covered within the investigations. In a first approximation an isothermal process was considered, which is reasonable due to the solid matrix of POCS, which exhibits very good heat conduction and thus low temperature gradients. Despite the lower computational effort, another advantage of the constant temperature assumption is that all observed differences can be attributed solely to the hydrodynamic effects.

Results and discussion

For the methanation, the in operando shift of the interPOCS affects the conversion of carbon dioxide as well as the selectivity towards the desired product methane. In the reactive simulations, there is a clear difference in concentration and surface reaction rate between the shielded areas identified in the hydrodynamic studies and the remaining free flow volume. On the one hand, the interaction of the fluid with the solid surface is reduced in the shielded areas, which can lead to a limited mass transport to the catalytically active surface and a lower effective reaction rate. On the other hand, the local residence time in these areas is increased, which can promote slow consecutive reactions. Which of the described phenomena is dominating and therefore which offset is preferable depends on the applied process conditions. In addition, the prevailing flow regime influences the intensity of the offset effect on the hydrodynamics and the reaction progress.

Conclusions

The simulation results highlight the complex interplay between the hydrodynamic behavior and the reaction process in interPOCS. The identified characteristic behavior of the flow paths for the different offsets of interPOCS clearly influences the methanation reaction. Differences in the conversion and the selectivity can be identified, although the global parameters such as porosity and specific surface area remain constant for the in operando shift of interPOCS. A preferred offset cannot be determined in general, as it depends on the process conditions. The demonstrated approach allows for investigating the interaction between hydrodynamics and reaction for different process scenarios and reaction systems and for indentification of advantageous configurations of catalyst support structure geometries. It is conceivable that dynamic reactor operations in context of modern power-to-X processes can benefit from the flexible in operando adaptability of interPOCS.

References

[1] S. Trunk, H. Freund, Chem. Eng. Process. 195 (2024) 109617

[2] G. Do, M. Geißelbrecht, W. Schwieger, H. Freund, Chem. Eng. Process. Process Intensif. 148 (2020) 107786

[3] D. Schmider, L. Maier, O. Deutschmann, Ind. Eng. Chem. Res. 60(16) (2021) 5792–5805

Keywords

Structured catalysts; interPOCS; in operando adaptability; CO_2 methanation.

Tue. 10/09 // 11:20-11:40

RD – I – 2

Measurement of Bubble Property Distributions for Better Description of Mass Transfer Limitations in Chemical Reactors

Philipp Riechmann[1], Lukas Schlagenhauf[1], Evert C. Wagner[2], J. Ruud van Ommen[2], Tilman Schildhauer[1]*

[1]*Paul Scherrer Institut, Energy and Environment Division, CH-5232 Villigen PSI, Switzerland*

[2]*Delft University of Technology, Department of Chemical Engineering, Van der Maasweg 9, HZ Delft, 2629, Netherlands*

**Corresponding author: tilman.schildhauer@psi.ch*

Highlights

- Bubble properties in fluidized bed reactors were derived from X-ray tomography.
- Properties are broadly distributed; shape and rise velocity are correlated.
- Data can be used for validation of CFD models.

Introduction

In gas-solid bubbling fluidized bed reactors, the knowledge of the size and rise velocity of the particle free voids, usually referred to as bubbles, is of importance for the understanding and correct prediction of mass transfer between the gas and the solid particles. Correlations from literature often rely on one average bubble size as a function of the fluidization number and measurement height.

Methods

In this contribution, X-ray tomography data, measured in collaboration with TU Delft in the Netherlands [1], were evaluated at Paul Scherrer Institut in detail by pseudo three-dimensional reconstruction of individual bubbles in a freely bubbling fluidized bed.

Results and discussion

The X-ray tomography measurements showed that the bubble properties are broadly distributed for a given location within the investigated BFBs, see figure 1. It was found that several aspects of the applied methodology significantly influenced the results: i) the consideration of the individual rise velocities of the bubbles for the calculation of the vertical dimension of each bubble, ii) the determination of the surface area and shape of each bubble which turned out to be correlated with the rise velocity, as well as iii) a new adaptive threshold method for the binarization of the reconstructed void fractions, ensuring that the measured void fraction is maintained throughout the reconstruction procedure.

The individual bubble property distributions can be described with generalized extreme value distribution (GEV) functions and their correlations can be accounted for with t-copula functions. Data sampled by these distribution functions can be used for the verification of CFD models or as a foundation for the development of semi-empirical correlations.

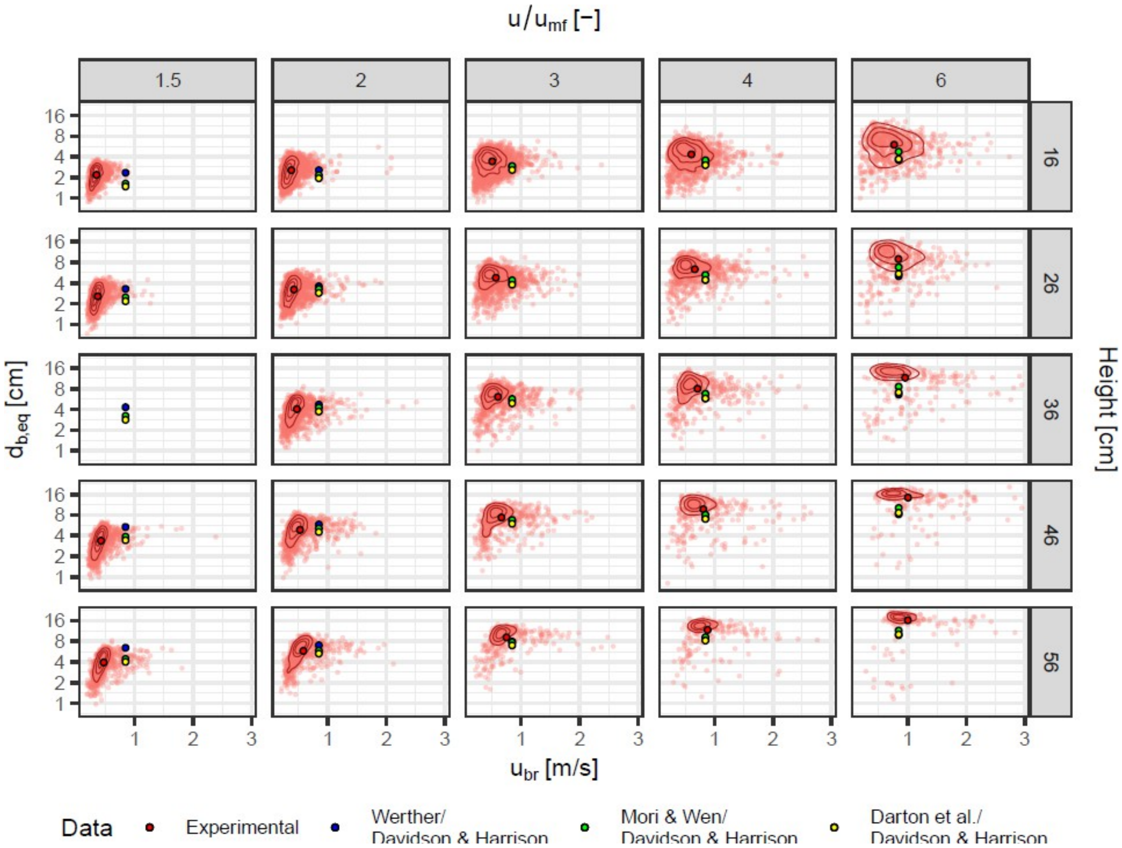

Figure 1. Scatter plots including density contour lines of the equivalent bubble diameter $d_{b,eq}$ over the bubble rise velocity u_{br} in comparison to mean values predicted by a combination chosen literature correlations for a selection of experimental settings

Conclusions

The X-ray tomography measurements showed that the bubble properties in bubbling fluidized bed reactors are broadly distributed for a given location within the investigated BFBs. This indicates that the description of the hydrodynamics in BFB merely by mean values of the bubble properties might not be sufficient. This is especially relevant for the prediction of critical reactor characteristics such as mass transfer limitations which could be caused by bubbles that are faster and larger than the corresponding mean values suggest.

Another important finding is the strong correlations between the size, the rise velocity and the shape of the bubbles. These correlations are particularly important in the context of measurements with optical probes or similar methods.

References

[1] Philipp Riechmann, Cross-verified independent measurements of correlated bubble property distributions as part of the scale-up of a catalytic bubbling fluidized bed reactor, Thèse EPF Lausanne n° 9873, 2022

Keywords
Bubbling fluidized bed; bubble properties; X-ray tomography

Tue. 10/09 // 11:40-12:00

RD – I – 3

Validity of the Generalized Film-Model Criteria for Instantaneous Gas-Liquid Reactions in Higbie's Penetration Model

Pieter Janssens[1], Jeroen Poissonnier[1], René Bos[1,2], Joris W. Thybaut[1]*

1 Laboratory for Chemical Technology, Ghent University, Technologiepark 125, 9052 Ghent, Belgium;

2 Shell Global Solutions International B.V., P.O. Box 38000, 1030 BN Amsterdam, The Netherlands

**Corresponding author: joris.thybaut@ugent.be*

Highlights

- Fast reaction regime allows to introduce the film-concept in liquid elements
- Film-model criteria predict the penetration breakthrough within 2%
- Validity of the infinite enhancement factor for interphase flux calculation

Introduction

Mass transfer accompanied by a chemical reaction in gas-liquid reactions has been extensively investigated during the last century and has resulted in several convection-reaction models such as the stagnant-(two-)film or penetration models. While the former assumes a stationary film along the gas-liquid interface, the latter puts forward a (distribution of) contact time(s) which dictates when these interface elements are renewed with bulk elements [1,2]. For a single gas-liquid reaction in the instantaneous reaction regime, the limitations of the classic film-model criteria, particularly with respect to breakthrough of a gas component towards the bulk of the liquid phase, were recently demonstrated, and improved criteria were derived, validated and generalized to systems of N-parallel reactions [3].

The instantaneous regime implies that the infinite enhancement factor $(E_!)$ can be used to calculate the flux across the gas-liquid interface, and that the breakthrough of the gas-phase reactant into the bulk liquid is negligible. The latter is not straightforward for penetration models, as unreacted species inside an interface element are transferred to the liquid bulk upon renewal. In this work, an extensive parameter screening was performed to investigate both aspects for Higbie's penetration model, in which it is assumed that each liquid element has an identical residence time at the gas-liquid interface.

Methods

The instantaneous gas-liquid mass transfer ($A_{''} \rightarrow A_{\#}$) and a single irreversible liquid-phase reaction $A + B \rightarrow C$ with $r_{\$,\&} = k\, c_{\&}\, c_{'}$ are described by the following mass balances:

$$\frac{\Omega_!}{(^*} = \mathcal{D}_+ \frac{(^{''})_!}{\overline{\mathcal{C}''}} - k_- \, c_+ \, c_- \tag{1}$$

$$\frac{\Omega_\#}{(^*} = \mathcal{D}_- \frac{(^{''})_\#}{\overline{\mathcal{C}''}} - k_- \, c_+ \, c_- \tag{2}$$

The set of partial differential equations was numerically solved using MATLAB's built-in pdepe function. All simulations were performed with an absolute and relative tolerance of 10^{-6}. The solution of these equations allows to calculate the time-dependent flux across the gas-liquid interface:

$$J_{+,/}(t) = -\mathcal{D}_+ 3\frac{\Omega_!}{\mathcal{C}}4_{*,,01} \tag{3}$$

The breakthrough of A into the bulk liquid was calculated by dividing the amount of A in the liquid element at $t = \tau$ by the total amount of A that crossed the gas-liquid interface during the contact time:

$$\text{Breakthrough of A} = \frac{\int_{\&}^{\$\%})_!(4,,)6,}{\int_{\&}^{)} 7_{!,}(^*)6^*} \tag{4}$$

Results and discussion

For $k\tau > 2$, stationary concentration profiles are obtained in the penetration model as the interface flux is balanced by the reaction within the liquid element. This allows to introduce a hypothetical stagnant film as shown in Figure 1. However, due to the mathematical framework of Higbie's penetration model, the concentration of liquid-phase reactant B at $x = \delta_8$ is not equal to its bulk-liquid concentration $c_{.,9}$. Also, the breakthrough of A into the bulk liquid cannot be calculated through a ratio of the bulk flux over the interface flux.

As discussed in reference [3], key concepts within the film model are the Hatta number (Ha) and the infinite enhancement factor. Their numerical threshold was adjusted in view of the imposed film, to ensure that $c_+(\delta_8) = 0$ as well as that the location of the reaction zone is sufficiently close to the gas-liquid interface (i.e., $\overline{E}_{+,!}$>2α with α=$8/\sqrt{\pi}$, grey area, Figure 1). This effectively limits the amount of unreacted A in the element at $t = \tau$ The amount of breakthrough of A into the bulk liquid could be limited to approximately 2% for a wide range of rate coefficients and reactant concentrations (Figure 2) using two film-model derived criteria:

$$Ha_+ > 2\sqrt{\alpha}\text{and } \boldsymbol{\varphi}_{.,!} = \frac{:;\#}{<_{\#,*}=-} - \boldsymbol{E}_{.,!} > 10 \qquad (5)$$

To conclude, *in silico* experiments confirmed that, for equal diffusivities, the infinite enhancement factor as defined within the film-model, accounts for the mass-transfer enhancement of the gas-phase reactant when the so-called "classic" film-model criterion for the instantaneous regime is met: $Ha_+/(E_{+,!} - 1) > 10$. This result is identical to the one obtained for the film model [1].

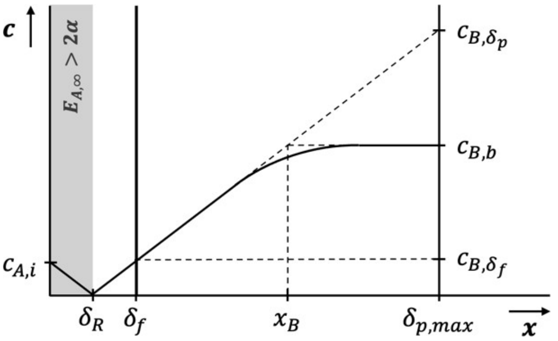

Figure 1. Stagnant film within the liquid element at contact time τ for Higbie's penetration model. The maximum penetration depth, $\delta_{.,/01}$, is obtained at $t = \tau$ in the absence of a chemical reaction. The position of the film-boundary is calculated by $\delta_2 = \overline{k_3} 1\mathcal{D}_-$

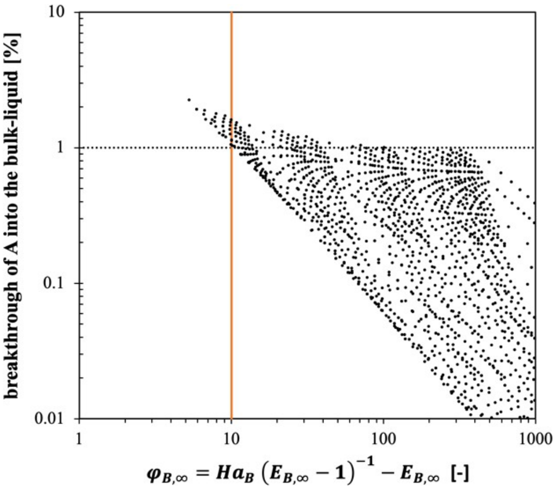

Figure 2. Transfer of reactant A to the bulk liquid, quantified as "breakthrough", as a function of $\varphi_{+,\_}$. For $E_{-,\_}$>2α and $Ha_- > 2\sqrt{\alpha}$, the film-model criterion $\varphi_{+,\_} > 10$ limits the breakthrough to 2%.

Conclusions

Within the penetration model, the instantaneous reaction regime yields stationary concentration profiles which allows to introduce a modified film concept in Higbie's penetration model. By adjusting the numeric thresholds for Ha_+ and $\boldsymbol{\varphi}_{.,!}$, the transfer of A to the bulk liquid was limited to 2%. With respect to the validity of the infinite enhancement factor to calculate the interface flux, it was found the classic criterion for the instantaneous regime accurately describes the mass-transfer enhancement for the Higbie model under identical conditions as obtained for the film model.

References

[1] K.R. Westerterp, W.P.M. van Swaaij, A.A.C.M. Beenackers, H. Kramers, Chemical reactor design and operation, Wiley, 1991.

[2] G.F. Froment, K.B. Bischoff, J. De Wilde, Chemical reactor analysis and design. 3rd Edition, John Wiley and Sons, Inc., 2011.

[3] P. Janssens, J. Poissonnier, J.W. Thybaut, W.P.M. van Swaaij, R. Bos, Improved and generalized criteria for the instantaneous regime for multiple parallel Gas-Liquid reactions, Chem. Eng. J. 465 (2023) 142744. https://doi.org/10.1016/J.CEJ.2023.142744.

Keywords

Gas-Liquid mass transfer; instantaneous reaction; penetration model; enhancement factor

Tue. 10/09 // 14:20-14:40

RD – II – 1
LOGIC 2.0: Characterisation of a natural convection driven methanol reactor

Tim van Schagen[1]*, Wim Brilman[1]

1 Sustainable Process Technology, Faculty of Science and Technology, University of Twente, PO Box 217,
7500AE Enschede, The Netherlands

**Corresponding author: t.n.vanschagen@utwente.nl*

Highlights

- A highly integrated CO_2-to-methanol reactor was successfully demonstrated
- Space-time yield of 600 $kg_{MeOH}/m^3_{cat.}/day$ under natural convection circulation
- Potential for operating with an intermittent feed supply

1. Introduction

Methanol is a promising intermediate in the transition towards carbon-neutral chemicals and fuels, as it is selectively made from CO_2 and green hydrogen. Methanol can be stored and transported easily as it is a liquid at ambient conditions. A major challenge in directly converting CO_2 and hydrogen to methanol is the limited equilibrium conversion (below 25% per pass under typical operating conditions), leading to a large gas recycle in a thermochemical process. Furthermore, when using green hydrogen, intermittency in the feed supply gives rise to the need for a flexible process. The Liquid-Out Gas-In Concept (LOGIC 2.0) condensing methanol reactor has been developed to overcome these challenges and is now demonstrated at small pilot scale (10 kg_{MeOH}/day). The highly integrated reactor system combines the catalyst bed, heat integration, product separation by condensation and free convection-driven gas recycle within a single pressure vessel, without recompression of the recycle. The present work reports on the first experimental results obtained with this new lab pilot.

2. Methods

Figure 1 schematically shows the operation of the LOGIC 2.0 reactor. CO_2 and H_2 are mixed with mass flow controllers in a 1:3 molar ratio, compressed and fed to the bottom of the reactor. Inside the reactor, tubes are placed in a vertical 'shell-and-tube' configuration. The tubes contain a section with a catalyst bed (commercial $Cu/ZnO/Al_2O_3$ catalyst) where the reaction takes place. The product gas flows upwards through the tubes to the top of the reactor. Here the temperature is lowered using cooling water to condense the methanol and water produced. These liquid products are removed and unconverted gases are recycled to the shell side. In the central section heat integration between the upwards flowing product gas and downwards flowing recycle gas streams takes place. The PLC system registers continuously temperatures, pressures and flows. The liquid- and gas composition (inside the reactor) are periodically sampled and analysed with GC analysis. Total liquid produced is collected and weighed.

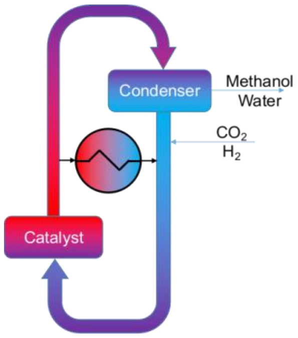

Figure 1. Schematic view of the LOGIC 2.0 reactor

Figure 2. Picture of the LOGIC 2.0 set-up.

3. Results and discussion

Experiments were performed at varying pressure (40-90 bar) and catalyst bed inlet temperature (210-250 °C). Figure 3 shows the space-time yield during these experiments. It is clear that the system productivity increases with pressure, which is expected since the thermodynamic equilibrium, reaction kinetics and natural convection flow are more favourable at higher pressures. There are two outliers from this trend: the point at 50 bar and 235 °C (lying well above the trend) and the point at 70 bar and 220 °C. During the former experiment the gas composition was different due to an issue with the gas sampling and control system, whereas during the latter experiment severe oscillations in the temperature trends in the reactor were observed, leading to a lower productivity. The effect of the bed inlet temperature in Figure 3 is not immediately clear. One might have expected that there is an optimal inlet temperature (as trade-off between kinetics and equilibrium), but this was not observed yet. Despite the use of natural convection, the measured space-time yields (up to 600 $\text{kg}_{\text{MeOH}}/\text{m}^3_{\text{cat.}}/\text{hr}$) are similar to those from comparable processes in literature [1-2].

Figure 4 highlights the favourable dynamic behaviour of the set-up. Start-up is fast, limited mostly by the feed flow rate (since the productivity curve has the same shape as the pressure curve). At 17:00 the reactor feed turned off, but the temperature levels maintained and during the night the remaining gas inside the set-up is almost fully converted into products. This shows the favourable dynamics of the set-up which can easily deal with fluctuations in the feed supply.

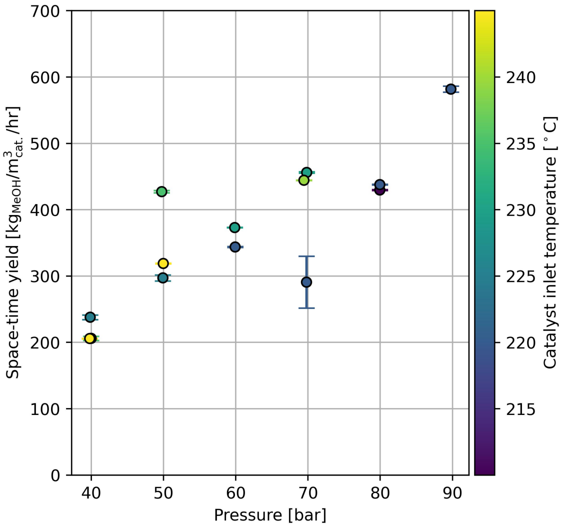

Figure 3. Space-time yield as function of pressure and catalyst bed inlet temperature.

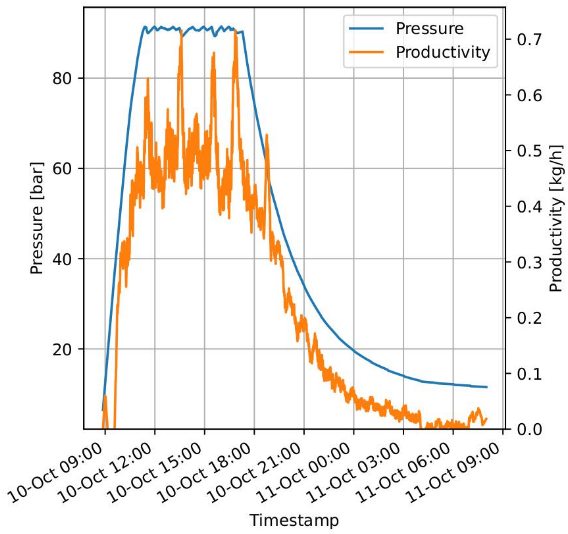

Figure 4. Pressure and productivity over time during the experiment at 90 bar and 220 °C

4. Conclusions

The LOGIC 2.0 reactor for selective CO_2 hydrogenation to methanol has successfully been demonstrated with a near-100% yield of methanol over the reactor. A productivity of just under 10 $\text{kg}_{\text{MeOH}}/\text{d}$ is achieved at a space time yield of 600 $\text{kg}_{\text{MeOH}}/\text{m}^3_{\text{cat.}}/\text{hr}$, comparable to other CO_2 to methanol processes. Further optimisation of the operating conditions and prevention of heat losses to the environment are expected to increase the productivity even further. Stable operation was achieved and the response time to fluctuations in operating conditions is fast, highlighting the potential of the system to operate with an intermittently available feed.

References

[1] O. S. Joo, K. D. Jung, I. Moon, A. Ya. Rozovskii, G. I. Lin, S. H. Han, and S. J. Uhm. *Carbon dioxide hydrogenation to form methanol via a reverse-water-gas- shift reaction (the CAMERE process)*. Ind. Eng. Chem. Res., 38(5):1808–1812, 1999.

[2] M. Bertau, H. Offermanns, L. Plass, F. Schmidt, and H. Wernicke, editors. *Methanol: The Basic Chemical and Energy Feedstock of the Future*. Springer Berlin Heidelberg, 2014

Keywords

CO_2 utilisation, methanol, reactor design, intermittent operation

RD – II – 2
Development of an improved one-dimensional fixed-bed catalytic reactor model through CFD simulations

Liantsoa Randriambololona[1], Arnaud Cockx[1], Philippe Schmitz[1], Marie-José Huguet[2], Olivier Peruch[3]

1 Toulouse Biotechnology Institute, Université de Toulouse, CNRS, INRAE, INSA, Toulouse France ;
2 LAAS-CNRS, Université de Toulouse, CNRS, INSA, Toulouse France ;
3 Adisseo France SAS

**lliantsoa.randriambololona@insa-toulouse.fr*

Highlights

- A pseudo-periodic 3D comprehensive model of a fixed bed reactor is developed
- Heat transfer in catalytic reactors is impacted by an inlet effect
- A 1D model enhanced with results from a 3D model is developed

1. Introduction

Catalytic fixed bed reactors are widely used in the chemical and process industries. From an industrial and academic point of view, the modelling of fixed bed reactors is important for a better understanding of the coupling between the flow, the heat transfer and the reactions. The present study aims to propose an improved one-dimensional (1D) comprehensive model of a monotube fixed bed reactor composed of spherical particles. The 1D model is solved with the software gProms Process, but it is enriched with the results of a three-dimensional (3D) model developed with the software Comsol Multiphysics for a finer description. First, the coupling between the laminar flow and heat transfer in the fixed bed reactor is studied and compared with literature. Then the inlet effect and the heat exchange process are studied. Finally, a reaction in the fluid phase is added and a comparison is made between the 1D and the 3D models.

2. Methods

Reduced models and especially 1D models are interesting because they require less computation time and are easy to handle[1]. However, the correlations used in these models are based on the literature and do not necessarily describe the system to be modelled with sufficient accuracy. Therefore, 3D simulations of fixed bed reactors with Computational Fluid Dynamics (CFD) models coupling flow and heat transfer [2] and sometimes chemical reactions [3] are becoming increasingly useful. The aim of the present work is to develop a 3D model whose simulation results are used to enrich a 1D axial model.

- Geometrical domain

The ratio of the monotube internal diameter over the particle diameter is $\mathrm{N} = \mathrm{d_{cyl}}/\mathrm{d_p} = 5$. The total height of the studied tube is $\mathrm{H_{cyl}} = 54\mathrm{d_p}$. This height corresponds to 10 times the height of the geometric domain, but pseudo-periodic conditions are used in order to simulate the entire monotube. This method allows the simulation of larger geometries, such as industrial configurations, without any loss of quality in the meshing and simulation results[4].

- Multiphysics modeling: coupling laminar flow, heat transfer and chemical reaction

Uniform velocity and temperature are set at the inlet. The wall temperature is kept constant. First, the flow and heat transfer are studied, with heat transfer coming only from the wall side (in a two-way coupling manner, as the fluid properties are temperature dependent). Once this first step is validated, a simple oxidation reaction from species A to B is added: $A + \mathrm{O_2} \rightarrow B + \mathrm{H_2O}$. The boundary conditions are the same as before, but the wall temperature acts as a cooling system because the volumetric reaction is now exothermic. The reaction then affects the heat transfer and therefore also the flow in the reactor (in a three-way coupling).

3. Results and discussion

A preliminary study of mesh independence was carried out and a mesh size of 2.5 million elements for a 15 $\mathrm{cm^3}$ fixed bed tube was selected for the 3D periodic model which contains 109 particles generated by Discrete Element Method (DEM). Flow and heat transfer simulations were first conducted. The inlet temperature is set to $T_0 = 200°C$ and the wall temperature is $T_w = 300°C$. Different values of the Reynolds number were studied, but only Re_{inlet}=138 (with a flowrate of 1.79m^3/h), corresponding to an inertial dominated flow, is presented here.

The evolution of the pressure drop in the reactor is in good agreement with the correlation of Ergun(1952)[5], so the latter is used in the 1D model to describe the flow. The temperature field from the 3D simulation is similar to previous 3D models in the literature[4][2]. Furthermore, global heat transfer correlations in the literature such as Leva's[6] are in accordance with our results. However, an axial heat transfer correlation that more accurately accounts for the inlet effect is proposed and implemented in the 1D model as shown in Figure 1(a):

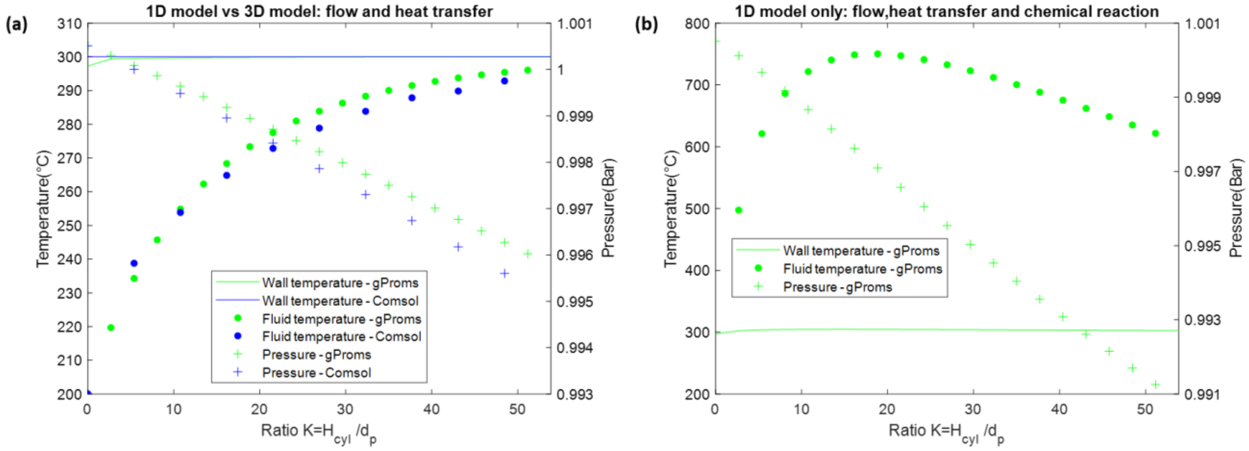

Figure 1. Comparison of average temperature and pressure from 1D and 3D model results: (a) Coupling of flow and heat transfer, (b) coupling of flow, heat transfer and chemical reaction for 1D model

The pressure and temperature profiles from the simulations of the 1D and 3D models are in good agreement with each other. Figure 1 (b) shows the evolution of the axial temperature in the presence of a chemical reaction, with a significant increase in temperature due to the exothermicity of the reaction, followed by a progressive decrease due the cooling by the wall. 3D CFD Multiphysics simulations involving chemical reactions in a three-way coupling are still in progress for comparison with 1D results.

4. Conclusions

A first study was performed considering only the flow and heat transfer in the fixed bed and the results are in agreement with the literature. Simulation results of the 3D model highlight the inlet effect and led to the formulation of a heat transfer correlation, which was then implemented in the 1D model. Results from both models show excellent agreement between them, confirming that the proposed enriched 1D model is a simplified model of the 3D one, at least for flow and heat transfer. The comparison with the exothermic reaction, which drastically changes the results, will be investigated in the near future.

References

[1] G.W. Koning, A.E. Kronberg, W.P.M. van Swaaij, Improved one-dimensional model of a tubular packed bed reactor, Chemical Engineering Science 61 (2006) 3167–3175.

[2] S. Das, N.G. Deen, J.A.M. Kuipers, A DNS study of flow and heat transfer through slender fixed-bed reactors randomly packed with spherical particles, Chemical Engineering Science 160 (2017) 1–19.

[3] X. Zhou, Y. Duan, X. Huai, X. Li, 3D CFD modeling of acetone hydrogenation in fixed bed reactor with spherical particles, Particuology 11 (2013) 715–722.

[4] M. Nijemeisland, A.G. Dixon, CFD study of fluid flow and wall heat transfer in a fixed bed of spheres, AIChE Journal 50 (2004) 906–921.

[5] S. Ergun, Fluid flow through packed columns, Chemical Engineering Progress 48 (1952) 89–94.

[6] M. Leva, Heat Transfer to Gases through Packed Tubes, Ind. Eng. Chem. 39 (1947) 857–862.

Keywords

Reactive Fixed bed, CFD, Heat transfer, 1D modeling

Tue. 10/09 // 15:00-15:20

RD – II – 3
Pilot scale methanation and PtG of (simulated) wood gasification gas

Tilman Schildhauer*, Chiara Berretta, Lukas Schlagenhauf, Tanja Wieseler, Martin Künstle, Julian Indlekofer, Robert Janz, Daniel Erne

Paul Scherrer Istitut, CH-5232 Villigen PSI, Switzerland

**Corresponding author: tilman.schildhauer@psi.ch*

Highlights

- Pilot scale experiments conducted for methanation of CO_2 and simulated wood gasification gas
- Hydrogen addition to the wood gasification gas to simulate Power-to-Gas
- Wide range of part load operation (20%-100%)
- Concentration and temperature profiles measured

1. Introduction

Catalytic fluidized bed methanation has proven its ability to convert different sources of carbon oxides into methane rich gas streams (renewable or synthetic natural gas; RNG or SNG), allowing for nearly isothermal conditions despite the strongly exothermic character of methanation. This has been shown during long duration tests both, for biogas methanation within PtX-applications [1] and for the conversion of gasification derived producer gas [2]. It could be demonstrated that the movement of the catalyst particles in the up-flow of reactive gas between zones with carbon depositing and less coking conditions enables a carbon management on the catalyst surface [2]. Due to this resilience of the fluidized bed reactor against coke formation, fluidized bed methanation was therefore chosen as second main production step for a planned demonstration plant in Tondela/ Portugal within the European Union project *HyFuelUp*. To broaden the technology basis with respect to part-load operation and to obtain performance data of the up-scaling of the methanation reactor, the pilot-scale methanation plant at PSI (200 kW) was operated with gas composition according to methanation of CO_2 and producer gas from biomass gasification.

2. Methods

The reactor diameter (22 cm) and the bed height (up to 2 m) of the pilot reactor are chosen such that the results (up to 11 bar) can be considered representative for larger reactors. The plant is thus able to conduct experiments on the technical readiness level (TRL) 6. From top, an axially movable sampling tube is introduced allowing to measure temperatures and to take gas samples. Nearly continuous profiles of temperature and concentrations can be obtained for the lower half of the bed, while in the upper half of the bed, the device comprises additional four sampling points.

The different sampling points in the plant were connected by 16 stainless steel capillaries with micro gas chromatographs (mGC) as analytical device. In the analytical room, the flow of each individual sampling line can be controlled before the gas flows are distributed via a system of valves to the different mGCs. The micro gas chromatographs are regularly calibrated and can quantify the expectable species H_2, CO, CO_2, CH_4, and N_2, and also He, O_2, ethane, propane and certain sulphur species if present.

3. Results and discussion

A wide range of operation conditions could be tested starting from 37 kW methane output representing low part load (15-20%). 200 kW methane output was reached without issues. The concentration profile of the 131 kW CO_2 methanation experiment as example in Figure 1 shows that significant reactor volume is needed to convert the hydrogen and to form methane. The reaction progress of this volume contracting reaction system can also be followed by the concentration of the nitrogen (leaking in from a non-tight valve). Taking out the N_2 concentration (assuming a situation with a tight valve), one can see that very high methane concentration close to 90% can be easily reached due to the low stoichiometric excess of hydrogen (H_2/CO_2 = 4.07). According to the recent changes in injection specification Switzerland, this gas would be close to fit the specification for unlimited injection without any further upgrading (besides drying). This is even more the case when instead of pure CO_2, biogas (60% methane, 40% CO_2 is converted). Then, more than 95% methane would be reached which is sufficient in many European countries for unlimited injection. Methanation of gasification derived producer gas leads to high CO_2-contents which necessitates a CO_2 separation in the upgrading section. Alternatively, or as flexible Power-to-Gas option, hydrogen can be added to obtain more methane and lower CO_2 content in the raw RNG/SNG.

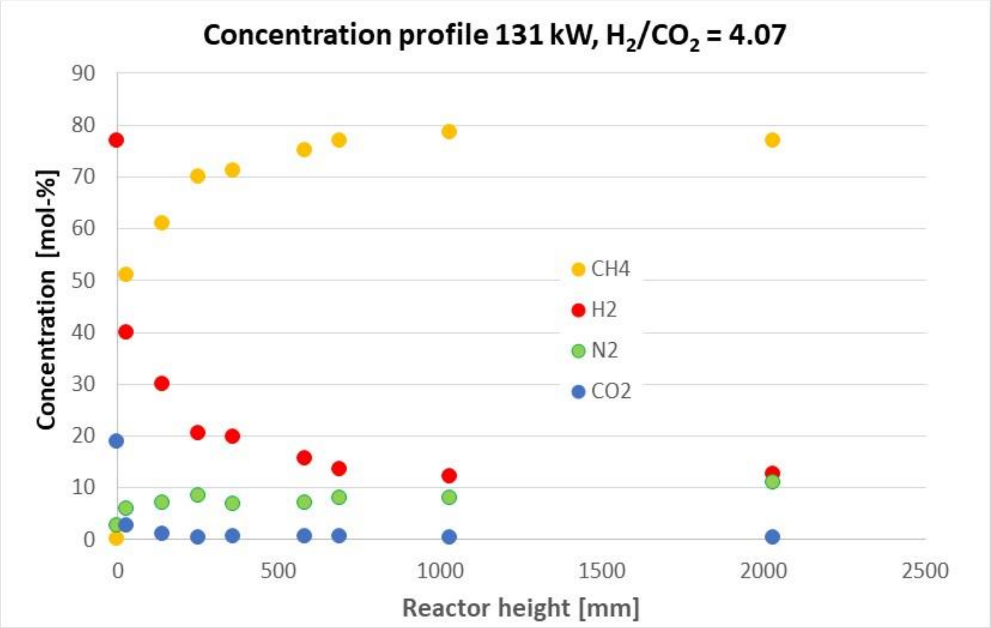

Figure 1. Concentration profile measured in PSI's pilot scale methanation reactor.

4. Conclusions

Performance data of the methanation reactor with the standard operation and state-of-the-art feedstock were obtained. For this, the pilot-scale methanation plant at PSI (200 kW) was operated with gas composition according to CO_2 and of wood gas methanation. The gas was taken from bottles in case of $CO/CH_4/CO_2$ and from a PEM-electrolyser in case of hydrogen. Proper sampling of the gas at several heights of the reactor as well as many thermocouples inside allowed obtaining axial temperature and concentration profiles. These data allow a detailed understanding of the reactor performance and validation of reactor models in ongoing work to support scale-up. A wide range of operation conditions could be tested. Further, it was possible to investigate flexibility of the system with respect to turn-down ratio, start-up and load change procedures.

References

[1] J. Witte, A.S. Calbry-Muzyka, T. Wieseler, P. Hottinger, S.M.A. Biollaz, T.J. Schildhauer, Demonstrating Direct Methanation of Real Biogas in a Fluidised Bed Reactor, Applied Energy Applied Energy 240, 359-371 (2019)

[2] T.J. Schildhauer, Methanation for SNG production – Chemical reaction engineering aspects, in Synthetic Natural Gas from Coal, Dry Biomass, and Power-to-Gas Applications, T.J. Schildhauer, S.M.A. Biollaz (Eds.), Wiley & Sons, New York, 77-159 (2016)

Keywords

Methanation; Bubbling fluidized bed; Pilot plant; Concentration profiles

PLASTIC RECYCLING

Tue. 10/09 // 13:40-14:00

PRC – 1

A combined experimental and modeling study of a 3D printed gyroidal copper structure for post-plasma chemical process intensification in non-reactive conditions

Victor Rosa[1], Fabio Cameli[1], Kevin M. Van Geem[1,*], Georgios Stefanidis[1,2*]

1 Laboratory of Chemical Technology (LCT), Ghent University; 2 Department of Process Analysis and Plant Design, National Technical University of Athens.

**Corresponding author: Kevin.VanGeem@UGent.be*
Georgios.Stefanidis@ntua.gr

Highlights

- **Methane-to-ethylene plasma route**
- **Additive manufacturing of copper periodic open-cellular structure (POCS)**
- **CFD-experiment spatial POCS temperature profile matching**

Introduction

Given the European Union's 2050 carbon neutrality target, the chemical industry is experiencing significant transformation. Process electrification is pivotal in developing sustainable reactor technologies powered by renewable energy sources. Electrified hydrocarbon conversion pathways, such as the Non-Oxidative Coupling of Methane (NOCM) to Ethylene, are instrumental in this endeavor. In a two-step reactor configuration, methane conversion to acetylene occurs through a non-thermal plasma (NTP) step followed by catalytic hydrogenation to ethylene in a post-plasma catalysis (PPC) setup. Adopting a warm NTP approach, such as Nanosecond-pulsed discharges (NPD), can achieve up to 47% single pass conversion of methane to acetylene in the plasma section, subsequently enhancing the olefin yield wt% via PPC. Notably, a heat-integrated 3D printed periodic open-cellular structure (POCS), coated with a Pd/Al2O3 layer, has demonstrated the highest energy efficiency in a plasma-mediated methane-to-ethylene pathway recorded to date. (1200kJ/mol$_{C2H4}$, 28% C_2H_4 yield [1]) . However, the effect of catalyst support geometry on heat integration efficiency has never been studied to the best of our knowledge. The present study aims to provide initial insights into the matter by a hybrid modeling and experimental approach in non-reactive conditions.

Methods

The experimental setup from Cameli et al. [1] was adopted to gather validation data for the computational model. The setup uses a nanosecond pulsed power supply (nPS) (Megaimpulse Ltd. NPG-18/3500 for ≤3 kHz and NPG-18/100 k for > 3 kHz applied pulse frequencies), triggered by a waveform generator (WFG) (33220A, Keysight Technology) within a frequency range 1–100 kHz. A novel (Cu) POCS geometry was placed downstream of the plasma section to characterize its heat transfer features during plasma operation as a possible post-plasma catalyst support candidate. The geometry was manufactured by AddToShape with an EOS 3D printer following a design procedure aimed at optimal porosity and external surface area within the nTopology software. Space and time-resolved monitoring of POCS temperature was achieved through a multipoint fiber optic instrument, whose sensor placing was specifically designed for the purpose. The present study focused on non-reactive post-plasma simulation of a POCS reactor, whose inlet matches the plasma outlet composition shown in Table 1 with a 200sccm flow. The model enclosed a fully-resolved 3D steady-state simulation via computational fluid dynamics (CFD), accounting for thermophysical properties of the gas mixture and heat losses through the reactor walls (-110W/m2 applied), together with heat exchange between gas and POCS via conjugate heat transfer (cht). Both a POCS post-plasma reactor and an empty post-plasma reactor were simulated for comparative purposes, with same heat loss through the wall.

Table 1 Composition of plasma outlet stream entering the POCS simulated in a CFD environment.

Species	C_2H_2	C_2H_4	CH_4	H_2
Molar fraction [-]	0.1	0.05	0.25	0.6

Results and discussion

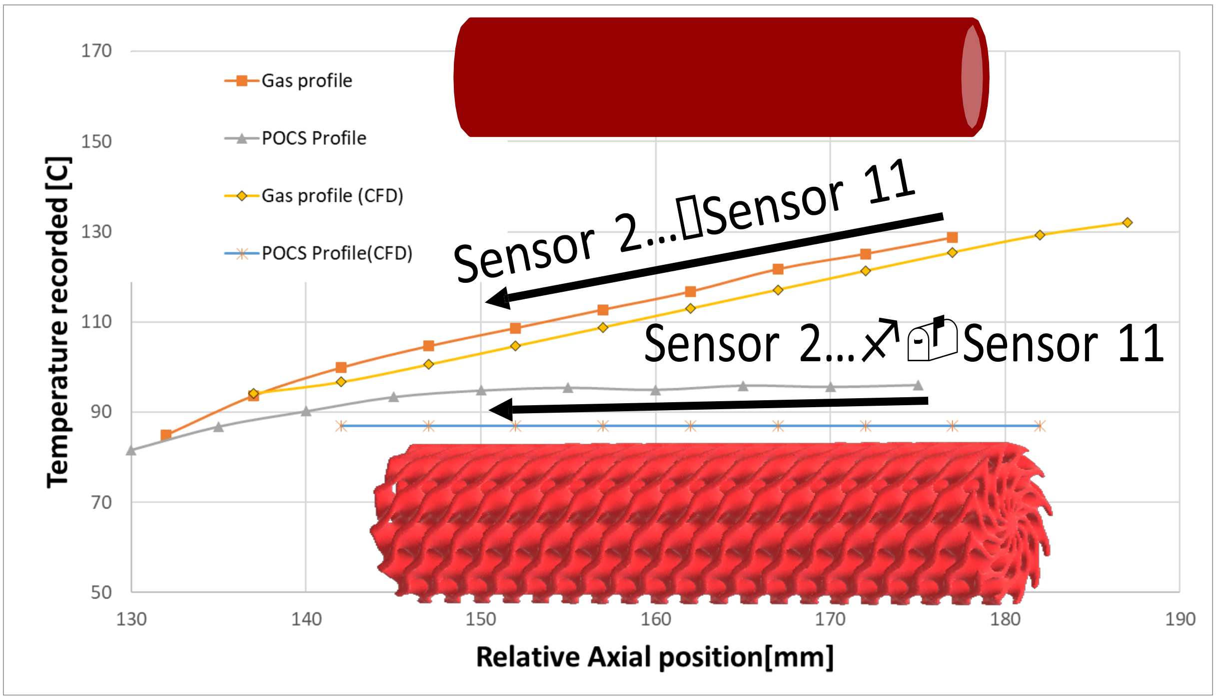

Figure 2. Temperature measurements along reactor axis in steady-state conditions, validated against CFD simulations for an empty plasma-downstream reactor section and a POCS-integrated plasma downstream reactor section.

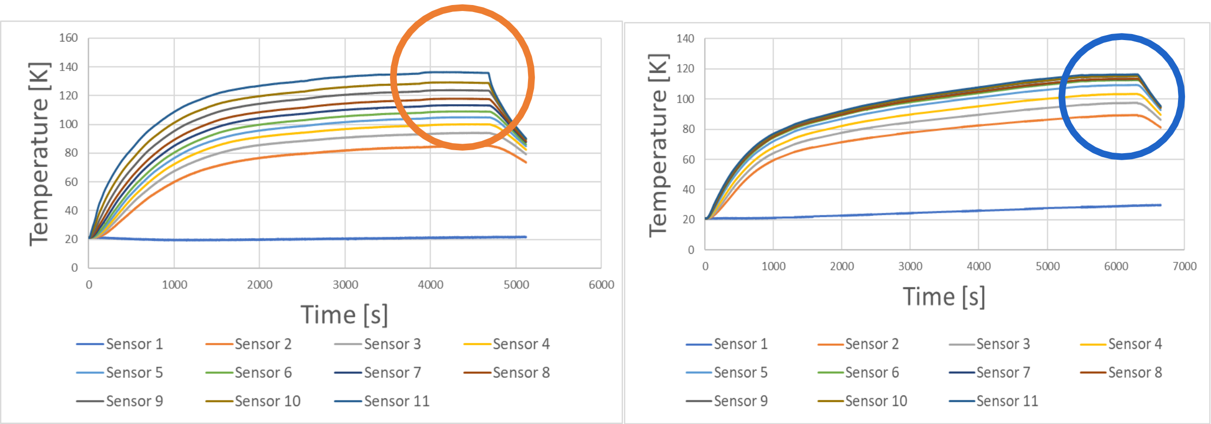

Figure 2. Time-resolved temperature profiles recorded by multiple sensors placed along the reactor axis. **a.** Empty reactor. **b.** POCS inserted in reactor.

The results in Figure 1 show excellent agreement of the CFD and experimental trend, both in the empty reactor case (orange and yellow line) and the POCS case (blue and grey line), suggesting that reality is closely reproduced by the model. Steady-state validity of the temperature measurements performed is confirmed by analysis of time-resolved trends obtained with the multipoint fiber optic inserted in the plasma downstream reactor (Figure 2 a. and b.). The plateau reached in both cases suggests that the reactor is near achievement of the steady state.

Conclusions

The consistent temperature profile noted and quantified within the solid copper POCS indicates its heightened thermal conductivity, potentially reducing temperature differentials within the 3D printed structure. This attribute is advantageous for its application as a washcoat catalyst support. Additional experimental and modeling investigations are necessary to ascertain whether the structure can proficiently mitigate gradients in a reactive environment, thereby optimizing reactive heat integration with the upstream plasma section.

References

[1] F. Cameli *et al.*, "Intensification of plasma-catalytic processes via additive manufacturing. Application to non-oxidative methane coupling to ethylene," *Chemical Engineering Journal,* p. 148720, 2024/01/14/ 2024, doi: https://doi.org/10.1016/j.cej.2024.148720.

Tue. 10/09 // 14:00-14:20

PRC – 2

Maximizing Olefin Yields for Steam Cracking of Plastic Waste Pyrolysis Oils: An Experimental and Modeling Study

Tamás Buzogány[1], Ismaël Amghizar[2], Marvin Kusenberg[1], Lin Chen[2], David J. Brown[2], Guy B. Marin[2], Geraldine J. Heynderickx[1], Kevin M. Van Geem[1]*

1: Ghent University, Ghent, Belgium; 2: AVGI, Ghent,

**Corresponding author: kevin.vangeem@ugent.be*

Highlights

- Plastic-waste pyrolysis oils
- Simulation model COILSIM1D
- Single-event microkinetic model CRACKSIM
- Maximizing olefin yields

1. Introduction

The mismanagement of end-of-life plastics is no secret as the main part is being incinerated, discarded into the environment, exported, or landfilled [1, 2]. This leads to a linear economy for a large stream of products, which is not only unsustainable but also leads to the loss of a potentially valuable carbon source. To reduce society's dependence on fossil fuels and its burden on the environment, improved recycling of mixed plastic waste streams is necessary, both mechanically and chemically. Within chemical, or advanced recycling, thermal pyrolysis of plastic waste followed by the steam cracking of the produced oils is one of the most promising technologies. It is expected to grow exponentially in the coming years. This method is more robust compared to mechanical recycling in terms of the allowable degree of plastic waste mixing, since mechanical recycling typically requires pure waste polymer streams to close the material loop. However, chemical recycling also faces challenges related to impurities present in plastic-waste-derived feeds, particularly halogenated- and hetero-atom-containing components, and the high concentration of olefinic components [3-5]. As their effect on steam cracking in terms of yields and operating conditions is unknown, olefin producers are hesitant to feed the new feedstock into their existing steam crackers.

To shed more light on the effect of plastic waste pyrolysis oils on the steam cracking performance, a kinetic model, CRACKSIM, is developed for the steam cracking of plastic waste-derived feeds, enabling fast and reliable simulation of product yields using COILSIM1D [6]. Specifically, next to olefinic components, this model will also incorporate hetero-atom-containing components in the future. In this work, the method to develop kinetic schemes for the steam cracking of (hetero-atom-containing) hydrocarbons is presented. This framework allows capturing the essential chemistry for components commonly found in plastic-waste-derived feedstocks. Comparing the results of this methodology with pilot plant data gives valuable insights into pyrolysis oils' behavior during steam cracking.

2. Methods

In this work, we are investigating the decomposition of important components present in plastic waste pyrolysis oils to develop a simulation model that can predict both yields and optimal operating conditions. CRACKSIM considers all elementary reaction steps, including all important reaction families, under the considered operating conditions. The corresponding kinetic and thermodynamic parameters are derived from CBS-QB3 level ab initio calculations [7-11], leading to a consistent set of Arrhenius parameters.

To understand the effect of plastic-waste derived oils on steam cracker operation, yields, and run-length, detailed feedstock analysis is performed using state-of-the-art analytical equipment at the Laboratory for Chemical Technology (LCT) at Ghent University, including GC×GC/MS coupled with specific detectors (NCD, SCD, AED, etc.). This allows extending the microkinetic model by incorporating additional details for the olefinic components, particularly related to their branching structure and additional reaction families. This has a large effect on the final yields and on the overall reactions these species can undergo.

The abovementioned approach has been tested by performing analysis and cracking on three feedstocks: a reference naphtha, a PE-derived oil, and a mixed plastic olefins-derived oil. Both plastic-waste derived feedstocks were blended with the reference naphtha in a 3:1 ratio to ensure plant integrity. Finally the effluents from the reactor are analyzed and compared to the model predictions.

3. Results and discussion

The effluents from the pilot plant steam cracker compared to the model predictions are presented in Figure 1. Clearly, the model predicts the most important components well, even without fitting. The model predictions can be further improved by providing additional details concerning the intermediate radical species, which have not been elaborated upon in this work.

Overall, this work demonstrates that COILSIM1D is a promising tool to aid in implementing plastic-waste derived feeds in olefin production. Additionally, thanks to its capabilities for run-length simulations and sensitivity analysis, olefin production can be optimized using renewable feedstocks.

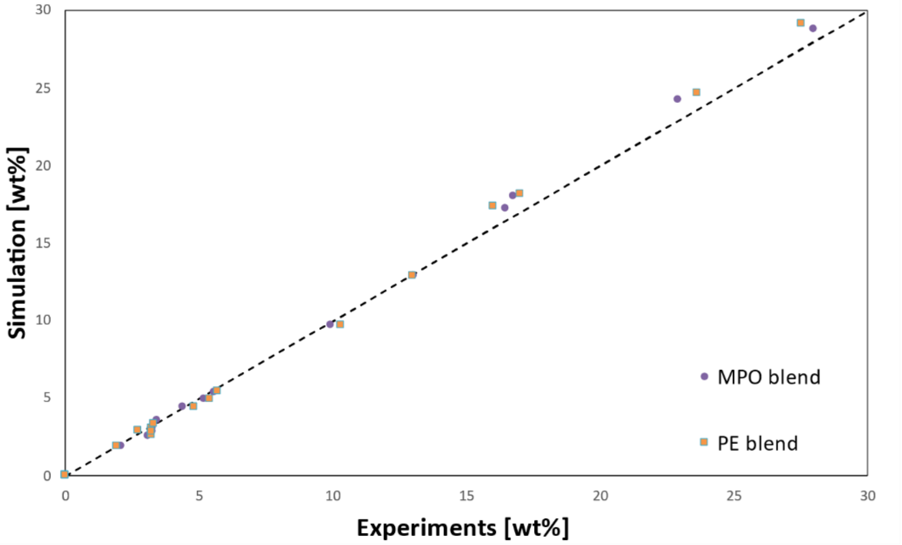

Figure 1. Results of modeling the steam cracking of a blend of plastic-waste derived feeds with a reference naphtha. Experimental results are plotted against the model-derived results.

4. Conclusions

A single-event microkinetic network known as CRACKSIM is currently under development for the decomposition of feedstocks derived from plastic waste pyrolysis. In this work, the details concerning olefinic species have been refined, which are abundantly present in plastic-waste derived feedstocks. Subsequently, the model has been compared to experimental results performed with an in-house steam cracker. The findings demonstrated good agreement between experimental and model predictions. Overall, COILSIM1D exhibits promising results in predicting steam cracking yields for novel feedstocks. By incorporating comprehensive details of olefinic species, branching structure, and halogenated species, COILSIM1D has the potential to play a fundamental role for plant operators in transitioning and enhancing chemical recycling efforts.

References

[1] SYSTEMIQ, " ReShaping Plastics: Pathways to a Circular, Climate Neutral Plastics System in Europe.," 2022. [Online]. Available: https://plasticseurope.org/reshaping-plastics/

[2] D. Damayanti *et al.*, "Current Prospects for Plastic Waste Treatment," *Polymers (Basel)*, vol. 14, no. 15, Jul 31 2022, doi: 10.3390/polym14153133.

[3] M. Kusenberg *et al.*, "Towards high-quality petrochemical feedstocks from mixed plastic packaging waste via advanced recycling: The past, present and future," (in English), *Fuel Process Technol,* vol. 238, Dec 15 2022, doi: ARTN 107474
10.1016/j.fuproc.2022.107474.

[4] M. Kusenberg *et al.*, "Opportunities and challenges for the application of post-consumer plastic waste pyrolysis oils as steam cracker feedstocks: To decontaminate or not to decontaminate?," *Waste Manag,* vol. 138, pp. 83-115, Feb 1 2022, doi: 10.1016/j.wasman.2021.11.009.

[5] M. Kusenberg *et al.*, "Assessing the feasibility of chemical recycling via steam cracking of untreated plastic waste pyrolysis oils: Feedstock impurities, product yields and coke formation," *Waste Manag,* vol. 141, pp. 104-114, Mar 15 2022, doi: 10.1016/j.wasman.2022.01.033.

[6] K. Van Geem, "Single event microkinetic model for steam cracking of hydrocarbons," 2006., 2006. [Online]. Available: http://lib.ugent.be/catalog/rug01:000974532

[7] M. K. Sabbe, M. F. Reyniers, V. Van Speybroeck, M. Waroquier, and G. B. Marin, "Carbon-centered radical addition and beta-scission reactions: modeling of activation energies and pre-exponential factors," *Chemphyschem,* vol. 9, no. 1, pp. 124-40, Jan 11 2008, doi: 10.1002/cphc.200700469.

[8] M. K. Sabbe, F. De Vleeschouwer, M. F. Reyniers, M. Waroquier, and G. B. Marin, "First principles based group additive values for the gas phase standard entropy and heat capacity of hydrocarbons and hydrocarbon radicals," (in eng), *J Phys Chem A,* vol. 112, no. 47, pp. 12235-51, Nov 27 2008, doi: 10.1021/jp807526n.

[9] M. K. Sabbe, M. Saeys, M. F. Reyniers, G. B. Marin, V. Van Speybroeck, and M. Waroquier, "Group additive values for the gas phase standard enthalpy of formation of hydrocarbons and hydrocarbon radicals," *J Phys Chem A,* vol. 109, no. 33, pp. 7466-80, Aug 25 2005, doi: 10.1021/jp050484r.

[10] M. K. Sabbe, M. F. Reyniers, M. Waroquier, and G. B. Marin, "Hydrogen radical additions to unsaturated hydrocarbons and the reverse beta-scission reactions: modeling of activation energies and pre-exponential factors," (in eng), *Chemphyschem,* vol. 11, no. 1, pp. 195-210, Jan 18 2010, doi: 10.1002/cphc.200900509.

[11] C. A. R. Pappijn, F. H. Vermeire, R. Van de Vijver, M. F. Reyniers, G. B. Marin, and K. M. Van Geem, "Bond additivity corrections for CBS-QB3 calculated standard enthalpies of formation of H, C, O, N, and S containing species," (in English), *International Journal of Chemical Kinetics,* vol. 53, no. 3, pp. 345-355, Mar 2020, doi: 10.1002/kin.21447.

Keywords
Steam cracking; micro-kinetic model; plastic waste; olefins

PRC – 3

Unlocking Radical Insights: Integrating Detailed Kinetic Modeling and Method of Moments for Pyrolysis of Polystyrene

Daniël Withoeck[1], Florence Vermeire[2], Oguzhan Akin[1], Robin John Varghese[1] Kevin Van Geem[1], Steven De Meester[3], Paul Van Steenberge[1,*]

1 Laboratory for Chemical Technology; Ghent University; Technologiepark-Zwijnaarde 125, 9052 Zwijnaarde
2 Chemical and Biochemical Reactor Engineering and Safety (CREaS); Celestijnenlaan 200F, 3001 Leuven
3 Laboratory for Circular Process Engineering; Sint-Martens-Latemlaan 2b, 8500 Kortrijk, Belgium

**Corresponding author: Paul.VanSteenberge@UGent.be*

Highlights

- Application of a Method of moments based model for polystyrene pyrolysis
- Detailed analysis of impact of reaction families and starting materials on PS pyrolysis
- Quantification of chain-length dependencies on PS pyrolysis product yields and mean residence time

Introduction

Plastics are amongst the world's most abundant commodity materials. The omnipresence of plastics is due to their excellent material properties. However, the large use of plastics, also in short life applications, has resulted in the production of large volumes of solid plastic waste (SPW). Blatant mismanagement has resulted in huge amounts of SPW being accumulated in the environment, producing one of the world's most significant environmental crises. Developing efficient recycling processes is crucial to tackle this crisis. Polystyrene (PS) is an important constituent of SPW, either as a polymer stream or contaminant [1]. In the past, mechanical recycling has been investigated for this purpose. However, it merely downcycles the PS, implying that other recycling processes are required, based on chemical recycling.

Pyrolysis is a versatile chemical recycling process. It treats SPW at high temperatures (typically 450 – 600 °C), decomposing the polymers into their monomers or other light molecules. In the case of PS, the polymer is mainly degraded into styrene, its monomer [2]. Therefore, the pyrolysis of PS will play an important role in the transition towards a circular chemical industry. Implementing this process in industry requires process optimization. This is only possible if the pyrolysis process is fully understood.

Pyrolysis is governed by a complex set of kinetics and transport phenomena. Understanding their complex interactions requires the construction of detailed (kinetic) models. This work applies a detailed kinetic model for PS pyrolysis and a detailed sensitivity analysis to provide fundamental insights into the complex underlying radical reaction mechanism, deepening our understanding of the fundamental mechanism and paving the way for the construction of better tools to determine kinetic parameters.

Methods

This work uses a detailed kinetic model for PS pyrolysis to obtain unprecedented insights into the underlying free radical chemistry. This model combines accurate, but computationally demanding, detailed radical chemistry simulations with the well- known simulation speed of the Method of Moments (MoM). The model thus combines two sets of equations, as illustrated in Figure 1. It adopts the rate coefficients from [3] and was validated using three PS standards with tabulated molar masses of 2000, 4000, and 100000 g/mol. The sensitivity analysis is performed by running simulations with different sets of Arrhenius parameters. These parameter sets are obtained from

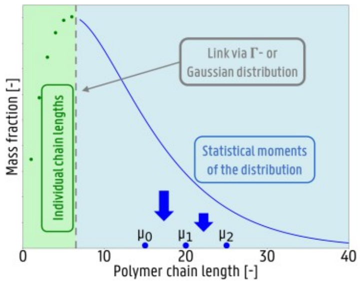

Figure 1: modelling methodology as used by the applied detailed kinetic model. The model's two sets of equations and their interconnection are shown.

the initial set, as published in [3], by multiplying one pre-exponential factor by 0.25, 0.5, 2, and 4 in separate simulations. From these, a correlation matrix can be constructed to quantitatively describe the impact of individual rate coefficients on the main product yields and mean residence time. A separate correlation matrix can be constructed for each material.

Results and discussion

The detailed sensitivity analysis produces three correlation matrices: one for the 2000 g/mol PS reference, one for the 4000 g/mol, and one for the 100 000 g/mol PS standard. **Figure 2** shows the correlation matrix for the 2000 g/mol PS reference.

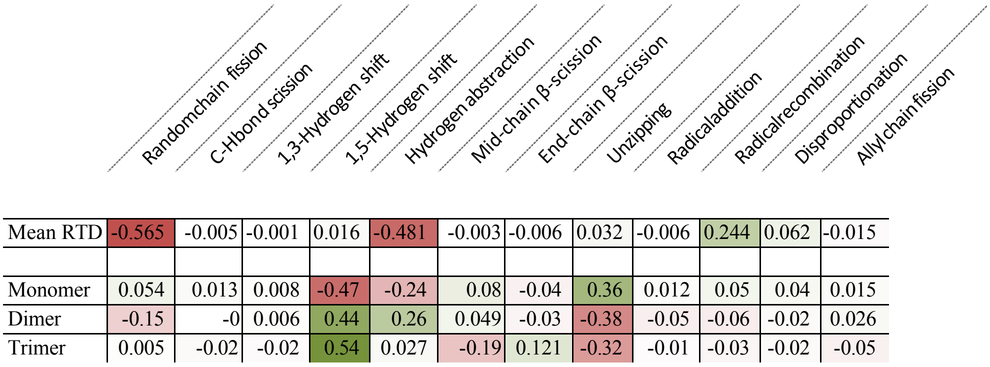

	Randomchain fission	C-Hbond scission	1,3-Hydrogen shift	1,5-Hydrogen shift	Hydrogen abstraction	Mid-chain β-scission	End-chain β-scission	Unzipping	Radicaladdition	Radicalrecombination	Disproportionation	Allyl chainfission
Mean RTD	-0.565	-0.005	-0.001	0.016	-0.481	-0.003	-0.006	0.032	-0.006	0.244	0.062	-0.015
Monomer	0.054	0.013	0.008	-0.47	-0.24	0.08	-0.04	0.36	0.012	0.05	0.04	0.015
Dimer	-0.15	-0	0.006	0.44	0.26	0.049	-0.03	-0.38	-0.05	-0.06	-0.02	0.026
Trimer	0.005	-0.02	-0.02	0.54	0.027	-0.19	0.121	-0.32	-0.01	-0.03	-0.02	-0.05

Figure 2: Correlation matrix, showing the correlation between the main product yields of the 2000 g/mol PS reference material and at 550°C and the rate coefficients of the involved reaction families. Strongly negative correlations are highlighted in red, positive correlations in green.

The results show that our model can be used to successfully provide detailed insights into the mechanism of PS pyrolysis. The detailed sensitivity analysis identifies the most dominant reaction families and their impact on the product yields and mean residence time. Our analysis is the first to provide this insight for the wide range of initial molar mass distributions, spanned by the set of three reference materials. Our work is thus the first to quantify the impact of chain-length dependent phenomena on the pyrolysis process. These chain-length dependent phenomena contain for example the number of propagation reactions undergone by any produced radical prior to its termination. Furthermore, we successfully quantify the contribution of reaction families with a chain-length dependent rate (like hydrogen abstractions and random chain fission reactions) and how they compete with other reactions, like unzipping.

Next to the presented sensitivity analysis, which merely provides a global overview of the process, a detailed reaction path analysis is used to confirm the results of the sensitivity analysis. In addition, the reaction path analysis allows to link the results of the latter to the actual reaction mechanism and explain the observed trends mechanistically.

Conclusions

A hybrid kinetic model for the pyrolysis of polystyrene is developed and tested to enhance our fundamental understanding of PS pyrolysis. Through a sensitivity analysis, backed up by more detailed reaction path analysis, detailed insights into the factors impacting PS pyrolysis are obtained. Our model successfully describes the factors impacting the process, its product spectrum and the residence time of the plastics in the reactor. Whereas other works in the literature limit themselves to a single material, our work shows its versatility and successfully describes the impact of the most crucial model parameters for a wide range of initial molar mass distributions.

References

[1] Roosen M, Mys N, Kleinhans K, Lase IS, Huysveld S, Brouwer M, et al. Expanding the collection portfolio of plastic packaging: Impact on quantity and quality of sorted plastic waste fractions. Resources, Conservation and Recycling 2022;178:106025.

[2] Locaspi A, Pelucchi M, Faravelli T. Towards a lumped approach for solid plastic waste gasification: Polystyrene pyrolysis. Journal of Analytical and Applied Pyrolysis 2023;171:105960.

[3] Levine SE, Broadbelt LJ. Reaction pathways to dimer in polystyrene pyrolysis: A mechanistic modeling study. Polymer Degradation and Stability 2008;93(5):941-51.

Keywords: Polystyrene; detailed kinetic modeling; chemical recycling; pyrolysis

Tue. 10/09 // 14:40-15:00

PRC – 4

Characterization and Pyrolysis Analysis of PVC Waste: Insights into Composition, Degradation Products, and HCl Emissions

Mohammadhossein Havaei[1], Robin John Varghese[1], Florent Minette[2], Eric Romers[2], Kevin Van Geem[1]*

1 Laboratory for Chemical Technology (LCT), Department of Materials, Textiles and Chemical Engineering, Ghent University, Technologiepark-Zwijnaarde 125, B-9052 Zwijnaarde, Belgium; 2 Research, Technology & Engineering (RTE), INEOS Inovyn, Rue Solvay 39, B-5190 Jemeppe-sur-Sambre, Belgium

**Corresponding author:Kevin.VanGeem@UGent.be*

Highlights

- Five PVC waste samples were characterized by various techniques and pyrolyzed in two stages.
- Characterization of PVC Waste indicates complex formulation with high metal content.
- Window profile and window frame pyrolysis results in the highest HCl production.
- Flexible applications produce higher amounts of organic products despite lower HCl yield.

Introduction

Poly(vinyl chloride) (PVC) is an indispensable plastic in several sectors such as construction, medical, and packaging thanks to its versatility and a combination of characteristics [1]. This versatility, however, is mainly achievable by highly complex formulations of PVC products [2]. This, as well as the inherent instability of PVC, has led to a challenging recycling scene in PVC waste management [3, 4]. Although 27% of PVC waste in Europe is recycled, mechanical recycling is responsible for almost all of the recycling and the potential of chemical processes is yet to be realized [5]. Thermal degradation of PVC follows a two-step process in which HCl is the main product of the first step and the hydrocarbon structure breaks down in the second [6]. The complex nature of PVC waste streams has a significant impact on the pyrolysis products and the decomposition mechanism [7]. Therefore, a comprehensive characterization of the pyrolysis of different PVC waste streams was performed using the micropyrolyzer unit and two-dimensional gas chromatography offering advanced identification and quantification.

Methods

Five waste samples of segregated PVC articles were received from INEOS Inovyn: window profile (WPW), cable (CW), tarpaulins (TW), flooring (FW), and window frame (WFW). The samples were characterized for their ash content and elemental composition.

Pyrolysis was carried out in a micropyrolyzer described previously [8] at two stages of 350 and 550 °C for 5 min each. After each pyrolysis stage, the reactor was quenched and the products were analyzed using a GC×GC program. Quantification of organic products was done using a flame ionization detector and the estimation of HCl and the identification of the products was done using a time-of-flight mass spectrometer.

To assess the effects of larger scale in the pyrolysis, the pyrolysis was performed on ~100 g of each sample in a stainless steel reactor placed inside a muffle furnace at the same two stages with 10 $°C.min^{-1}$ temperature ramp.

Results and discussion

HCl is the main compound of interest in PVC pyrolysis since it is a building block for vinyl chloride monomer. Although window profile and window frame samples yielded relatively higher HCl productions (i.e., 50.4 and 23.7 wt.%, respectively), the yield for other samples was below 15 wt.% in the large-scale experiments, mainly due to lower PVC content in those articles. **Error! Reference**

source not found. shows the HCl production of different samples obtained by ion chromatography on the scrubber solutions.

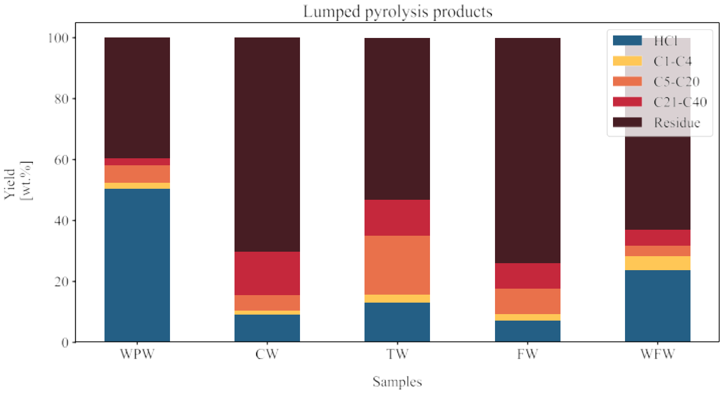

Figure 1. Lumped yields of products combined after two stages of pyrolysis at 350 and 550 °C.

The organic products of the PVC waste pyrolysis were mainly produced in the first stage of the pyrolysis (i.e., 350 °C) and the second stage had much less contribution to the total organic products. WPW showed the highest total organic yield at the second stage. Figure 1 represents the combined yields of each fraction of compounds after two stages of pyrolysis in the micropyrolyzer unit. Heavier (C21+) compounds resulted from PVC resin's high char propensity and additives in PVC compounds were the largest fraction of the organic products quantified at the end of the two-stage pyrolysis. Flexible applications of PVC resulted in higher yields of organic products while manifesting lower HCl yields.

Conclusions

Conventional pyrolysis processes encounter challenges when dealing with PVC due to the generation of corrosive HCl and the formation of high levels of char. Consequently, much research has focused on understanding the pyrolysis chemistry and resultant products of PVC. However, the PVC waste composition presents an additional layer of complexity, as it contains a diverse array of additives and fillers. Despite the extensive literature on PVC pyrolysis, studies specifically addressing real PVC waste and its decomposition products are scarce. Our findings highlight the significant contribution of PVC article formulation to the pyrolysis products of PVC waste. Considering the complex composition of PVC waste, understanding its pyrolysis products is crucial for evaluation the feasibility of thermal recycling methods. Achieving this goal necessitates a thorough characterization of PVC waste pyrolysis products, thereby providing insights essential for developing effective.

References

[1] V. Najafi, H. Abdollahi, Internally plasticized PVC by four different green plasticizer compounds, European Polymer Journal 128 (2020) 109620.
[2] G. Akovali, 2 - Plastic materials: polyvinyl chloride (PVC), in: F. Pacheco-Torgal, S. Jalali, A. Fucic (Eds.), Toxicity of Building Materials, Woodhead Publishing2012, pp. 23-53.
[3] M. Sadat-Shojai, G.-R. Bakhshandeh, Recycling of PVC wastes, Polymer Degradation and Stability 96(4) (2011) 404-415.
[4] Plastics – the fast Facts 2023, Plastics Europe, 2023.
[5] Progress Report 2023, VinylPlus, 2023.
[6] J. Zhou, G. Liu, S. Wang, H. Zhang, F. Xu, TG-FTIR and Py-GC/MS study of the pyrolysis mechanism and composition of volatiles from flash pyrolysis of PVC, Journal of the Energy Institute 93(6) (2020) 2362-2370.
[7] T. Karayildirim, J. Yanik, M. Yuksel, M. Saglam, C. Vasile, H. Bockhorn, The effect of some fillers on PVC degradation, Journal of Analytical and Applied Pyrolysis 75(2) (2006) 112-119.
[8] O. Akin, R.J. Varghese, A. Eschenbacher, J. Oenema, M.S. Abbas-Abadi, G.D. Stefanidis, K.M. Van Geem, Chemical recycling of plastic waste to monomers: Effect of catalyst contact time, acidity and pore size on olefin recovery in ex-situ catalytic pyrolysis of polyolefin waste, Journal of Analytical and Applied Pyrolysis 172 (2023) 106036.

Keywords
Poly(vinyl chloride), two-stage pyrolysis, plastic waste

Tue. 10/09 // 15:00-15:20

PRC – 5

Sustainable Waste Polypropylene Recycling: Enhancing Catalyst Stability and Selectivity in Light Olefin Production

Oğuzhan Akin [1], Qing He, Parviz Yazdani, Robin John Varghese, Kevin Van Geem*

Laboratory for Chemical Technology (LCT), Department of Materials, Textiles and Chemical Engineering, Faculty of Engineering & Architecture, Ghent University, Technologiepark 125, 9052 Zwijnaarde, Belgium

**Corresponding author: kevin.vangeem@ugent.be*

Highlights

- Polypropylene is converted to light olefins with ~80 wt.% selectivity.
- The presence of PVC in pyrolysis feed resulted in the poisoning of HZSM-5.
- The stability of HZSM-5 was enhanced through phosphorus impregnation.

Introduction

Recycling polyolefins is imperative for realizing sustainability objectives within the chemical industry and advancing towards a circular economy. In recent years, considerable attention has been directed towards chemical recycling techniques, notably pyrolysis, for their capacity to thermally convert plastic waste into valuable products. Among these methods, catalytic pyrolysis has emerged as a promising recycling route. It not only reduces energy requirement for conventional pyrolytic cracking but also enhances selectivity for valuable products, such as light olefins (C2-C4 olefins), which serve as platform chemicals for plastic products. However, the presence of hazardous contaminants, such as polyvinyl chloride (PVC), in plastic waste poses a substantial challenge to catalytic pyrolysis. PVC pyrolysis generates highly corrosive and toxic HCl gas, leading to severe and irreversible catalyst deactivation through dealumination and framework rupture. Polypropylene (PP), extensively utilized in packaging, construction materials, and medical equipment, yields PP waste with varying compositions and levels of PVC contamination, thereby constraining its recycling rate. Effective catalytic pyrolysis of PP waste necessitates a robust catalyst capable of selectively converting different polyolefins into light olefins while maintaining its performance. Addressing these challenges, this study examines the impact of phosphorus impregnation and mesopore introduction on catalyst stability and light olefin selectivity. Therefore, the catalytic upgrading of PP pyrolysis vapors containing PVC (5 wt.%) was explored using a micro-pyrolyzer facility coupled with comprehensive two-dimensional gas chromatography (GCxGC-FID/TOF-MS). This analytical approach facilitates precise quantification and identification of complex pyrograms, offering insights into the processes of pyrolysis and catalytic cracking [1].

Methods

Catalysts characterization were done by temperature-programmed desorption of NH_3, N_2-physisorption, and X-ray photoelectron spectroscopy (XPS). Operating temperatures for pyrolysis and catalytic reactors were maintained at 550 °C and 600 °C, respectively. The catalyst-to-plastic (C/P) ratio was kept at 80 (wt./wt.) for the modified catalysts, whereas, it was kept at 20 (wt./wt.) for the parent HZSM-5, due to its higher acidity.

Results and discussion

HZSM-5, P-HZSM-5, and P-mesoHZSM-5 demonstrated acidity levels of 0.65, 0.1, and 0.09 mmol NH3/g, respectively. This reduction in acidity, attributed to steaming and catalyst modifications, led to a slight decrease in light olefin yields when fresh catalysts were employed with pure PP as the pyrolysis feedstock. However, it notably enhanced stability against coke deposition. For instance, HZSM-5 exhibited a light olefin selectivity of 79 wt.% in the initial experimental run, modified catalysts yielded only 75 wt.% light olefins. However, throughout 150 consecutive experiments, the parent HZSM-5 experienced the most pronounced activity loss, with light olefin selectivity decreasing to 43 wt.%. In contrast, P-HZSM-5 and P-mesoHZSM-5 sustained their activity to a greater extent, yielding 57 and 63 wt.% light olefins, respectively. Importantly, deactivation was found to be reversible, as all catalysts exhibited performance similar to their initial states after regeneration through coke combustion with air at 700 °C. When PP was intentionally contaminated with 5 wt.% of PVC, activity loss occurred more rapidly compared to catalytic pyrolysis utilizing pure PP as feedstock, with light olefin selectivity decreasing below 65 wt.% within 50 runs (see **Figure 1**) . The catalyst regeneration process revealed intriguing findings. While modified catalysts were effectively regenerated, HZSM-5 suffered permanent activity loss, yielding only 60 wt.% light olefins even after regeneration. This was attributed to dealumination induced by HCl, which severely compromised the catalyst framework and reduced the number active sites. Conversely, the interaction between phosphorus and partially displaced framework alumina can enhance the stability of the zeolite framework by forming localized framework silico-aluminosphosphate (SAPO) interfaces [2]. These interfaces secure Si-O-Al bonds within the zeolite lattice, thereby preserving the Si/Al ratio and pore structure. This elucidates the heightened stability of P-modified catalysts against dealumination, a phenomenon potentially induced by the release of HCl-containing vapors during PVC-containing PP pyrolysis, ultimately leading to successful catalyst regeneration.

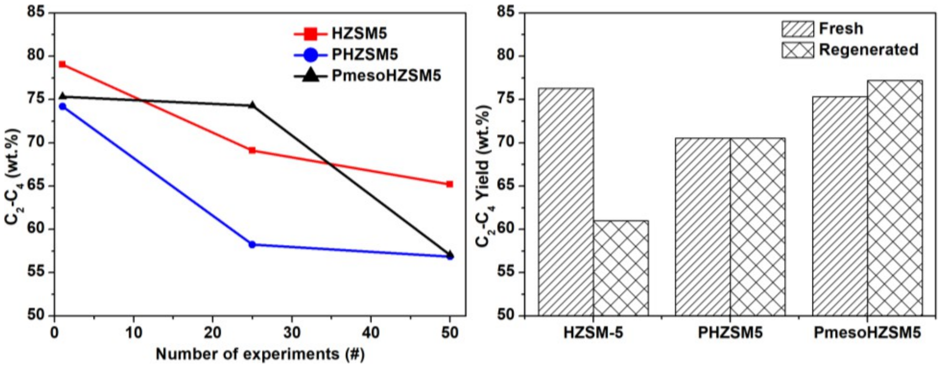

Figure 1. Light olefin yields obtained along the consecutive 50 run using HZSM-5, PHZSM5 and P-meoHZSM5 catalysts during PVC containing PP pyrolysis (Left), light olefin yield comparison of fresh and regenerated catalysts (Right).

Conclusions

Polypropylene was effectively converted into light olefins with high selectivity using both parent and modified forms of HZSM-5. The incorporation of phosphorus and mesopores notably improved light olefin selectivity and resistance to coke formation during polypropylene pyrolysis. Despite experiencing reversible deactivation due to coke formation over 150 runs of pure polypropylene pyrolysis, all catalysts demonstrated successful regeneration. However, when PVC-contaminated polypropylene was pyrolyzed, catalyst deactivation occurred more rapidly, leading to light olefin selectivity dropping below ~65 wt.% after only 50 runs. Notably, P-modified catalysts showed effective regeneration, while the parent HZSM-5 suffered permanent activity loss. This difference may be attributed to phosphorus modification preventing dislodged alumina from leaving the zeolite framework by interacting with silicon and leached aluminum to form SAPO species, thus preserving the framework and acidity. Nevertheless, further investigation of spent catalysts is necessary to fully elucidate the mechanism by which phosphorus influences catalyst stability. Given the considerable impact of 5 wt.% PVC contamination in the feed, the development of robust catalysts is inevitable for scaling up the proposed plastic waste recycling method, with phosphorus impregnation showing promising potential.

References

[1] O. Akin, R.J. Varghese, A. Eschenbacher, J. Oenema, M.S. Abbas-Abadi, G.D. Stefanidis, K.M. Van Geem, Chemical recycling of plastic waste to monomers: Effect of catalyst contact time, acidity and pore size on olefin recovery in ex-situ catalytic pyrolysis of polyolefin waste, Journal of Analytical and Applied Pyrolysis, 172 (2023).
[2] M. Ibanez, M. Gamero, J. Ruiz-Martinez, B.M. Weckhuysen, A.T. Aguayo, J. Bilbao, P. Castano, Simultaneous coking and dealumination of zeolite H-ZSM-5 during the transformation of chloromethane into olefins, Catalysis Science & Technology, 6 (2016) 296-306.

Keywords
Polypropylene, Pyrolysis, Zeolite, Polyvinyl Chloride

LOW CARBON TECHNOLOGY

Tue. 10/09 // 16:20-16:40

LCT – I – 1

Evaluation of the relevant mass and heat transfer phenomena in a packed bed membrane reactor for the direct conversion of CO2 to dimethyl ether

Serena Poto, Huub van den Bogaard, Fausto Gallucci, Fernanda Neira D'Angelo*

Eindhoven University of Technology

**Corresponding author: m.f.neira.dangelo@tue.nl*

Highlights

- Intraparticle mass transfer limitations and concentration polarization affect the direct conversion of CO2 to dimethyl ether (DME)
- Developed easy-to-use correlations from rigorous 2D heterogeneous models.

Introduction

The direct conversion of CO_2 to dimethyl ether (DME) is an attractive CO_2 recycling solution [1]. Besides, this technology presents advantages over the traditional DME synthesis (i.e., conversion of syngas to methanol and subsequent dehydration in two steps) by reducing the processing steps and increasing the overall yields. The one-step DME synthesis requires a bifunctional catalyst combining a hydrogenation metal and an acid catalysts (e.g., physical mixtures of Cu/ZnO/Al2O3 and HZSM-5 catalysts) and optimized operation conditions (ca. 200-300 ^{0}C and ca. 30-50 bar) to balance the kinetics and thermodynamic requirements. Both the methanol and DME production are exothermic and thermodynamically limited reactions, thus favored by higher pressures and low temperatures. Besides, all the reactions lead to significant water formation, which poses even stronger thermodynamic limitations and contributes to catalyst deactivation during long-term operation [2]. Thus, effective thermal management strategies as well as in situ removal of water are key to achieve high DME yields and catalyst stability [4]. In our recent works, we propose the use of a packed bed membrane reactor to combine reaction and separation (i.e. in this case product removal) to overcome the thermodynamic limitations (Le Chatelier principle) and meet cooling requirements [6,7]. In this work, we dive into the heat and mass transfer effects at different reactor scales via the implementation of 2D heterogeneous particle and reactor models in Matlab. These limitations are often neglected given the complexity of this reaction system. Thus, in this work, once a particular transport phenomenon is identified as significant using the rigorous modeling approach, these results are used to develop simplified easy-to-use correlations that can be used by a wider audience (e.g., for process design in industry).

Methods

First, a particle model is developed by solving mass and heat balances in the two catalyst particles (i.e., Cu/ZnO/Al2O3 HZSM-5) to assess the extent of intra-particle mass and heat transfer limitations under relevant reaction conditions, as well as their impact on the performance of the packed bed reactor, with and without the membrane (i.e., PBR and PBMR, respectively). Then, using a rigorous modeling approach, we propose and develop a Thiele modulus-efficiency correlation for the calculation of the effective reaction rate via a short-cut method, which does not require to couple reactor and particle model. Thereafter, we investigate the particle-fluid interphase to assess the relevance of external mass or heat transfer limitation, and we further analyze deviations from the ideal plug flow behavior via the implementation of the axial dispersion model, using the axial dispersion coefficient approach. Finally, the introduction of the membrane in the packed bed reactor adds more complexity to the transport phenomena as concentration gradients can develop in the radial direction giving rise to a phenomenon of concentration polarization (CP). Further, we develop a 2D packed bed membrane reactor model to evaluate the relevance of the radial concentration gradients generated by the presence of the membrane. From the simulations results of the 2D model, we developed a Sherwood-type correlation to account for the CP phenomena via a simplified approach.

Results and discussion

Intra-particle diffusion limitations were found relevant for particle larger than 1 mm and temperature above 220 ºC, such that the catalyst efficiency drops down to 50% and 5% for the Cu/ZnO/Al2O3 and the HZSM-5, respectively, in the most critical conditions (i.e., 270 ºC and Dp of 10 mm). A component-specific Thiele modulus-efficiency correlation was developed based on the results of the rigorous particle model to account for pore-diffusion limitations without having to solve a complex heterogeneous reactor model. This correlation shows the typical behavior reported in literature for power law kinetics and accurately predicts the reaction performance with deviation of less than 5% for values of the Thiele modulus lower than 2. In the packed bed membrane reactor (PBMR), the concentration polarization (CP) also showed to affect the reactor performance. The concentration of water at the surface of the membrane selective layer was found to be up to 64% lower than the concentration in the bulk phase, hindering the effectiveness of the membrane separation. To account for this phenomenon via a simplified approach, a Sherwood-type correlation was developed to determine a CP mass transfer coefficient, based on the results obtained via the rigorous 2D PBMR model. Such correlation showed to predict with high accuracy (i.e., errors lower than 5%) the effect of the CP on the PBMR performance. Differently from the pore diffusion and CP phenomena, the intra-particle heat transfer, the particle-fluid mass and heat transfer as well as the axial dispersion were found to have a negligible effect on the reactor behavior. Finally, given the relevant mass/heat transfer phenomena, this study proposes some examples on further reactor optimization strategies, such as the reduction of the zeolite loading in the bifunctional catalyst bed of by ca. 90% with respect to what is reported in literature.

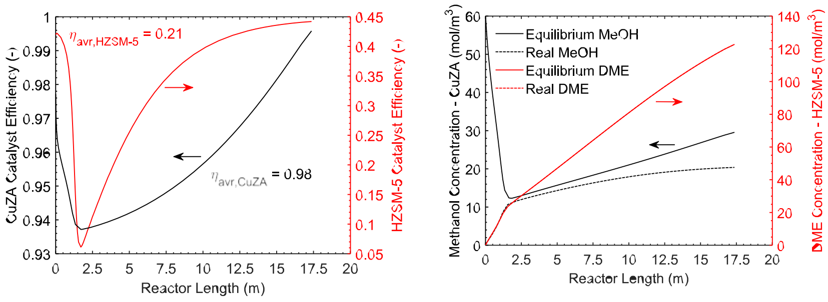

Figure 1. Catalyst efficiency (a) and methanol real (i.e., in the reactor) and equilibrium concentration (b) for both the CuZA (left axis) and HZSM-5 (right axis) as a function of the reactor length.

Conclusions

This study demonstrates that intra-particle diffusion and concentration polarization are both phenomena that affect the packed bed (membrane) reactor performance for the CO2 hydrogenation to DME, especially at conditions which are relevant to large scale operation. Thanks to the findings of this work, the PBMR and PBR could be further optimized, in view of the relevant mass/heat transfer phenomena. As an example, due to the fast methanol dehydration reaction, a considerably large fraction (i.e., up to 90%) of the zeolite in the catalytic bed could be removed with no effect on the final DME yield. Finally, to reduce the effects of the CP phenomenon, the geometry of the membrane can be optimized.

References

[1] J. Ma et al., "A short review of catalysis for CO2 conversion," Catal. Today, 148, 3–4, 221–231, 2009

[2] S. Hosseininejad, A. Afacan, and R. E. Hayes, "Catalytic and kinetic study of methanol dehydration to dimethyl ether," Chem. Eng. Res. Des., vol. 90, no. 6, pp. 825–833, 2012,

[3] K. W. Jun, H. S. Lee, H. S. Roh, and S. E. Park, "Catalytic dehydration of methanol to dimethyl ether (DME) over solid-acid catalysts," Bull. Korean Chem. Soc., vol. 23, no. 6, pp. 803–806, 2002,

[4] S. Poto, F. Gallucci, and M. F. Neira, "Direct conversion of CO 2 to dimethyl ether in a fixed bed membrane reactor : Influence of membrane properties and process conditions," *Fuel*, vol. 302, no. February, p. 121080, 2021,

[5] S. Poto, T. Vink, P. Oliver, F. Gallucci, and M. F. Neira D'Angelo, "Techno-Economic Assessment of the One-Step Co2 Conversion to Dimethyl Ether in a Membrane-Assisted Process," *SSRN Electron. J.*, vol. 69, no. December 2022, p. 102419, 2022,

Keywords

"Membrane reactor modeling"; "Intra-particle diffusion limitations"; "Concentration polarization"; "CO_2 hydrogenation, DME synthesis".

This project has received funding from the European Union's Horizon 2020 research and innovation programme under grant agreement No 838014 (C2Fuel project).

Tue. 10/09 // 16:40-17:00

LCT – I – 2

Design and construction of a large-scale GDE-based electrolyzer for sustainable formate production using CO_2 as feedstock

Jose Antonio Abarca[1], Axel Arruti[2], Esther Santos[2], Guillermo Díaz-Sainz[1], Angel Irabien[1]

[1]Departamento de Ingenierías Química y Biomolecular, Universidad de Cantabria, Avenida de los Castros s/n, 39005 Santander, Spain.
[2]APRIA Systems S.L, Parque Empresarial de Morero, 39611 Guarnizo, Spain

**joseantonio.abarca@unican.es*

Highlights

- Successful development and construction of a 100 cm^2 CO_2 electrolyzer prototype.
- Preliminary results show formate production of 96 g L^{-1} at 30 mA cm^{-2}, with an impressive 83 % of Faradaic Efficiency.
- Findings indicate scalability of the technology to large-scale applications.

1. Introduction

The electrochemical conversion and valorization of CO_2 into value-added products offer a highly efficient and promising alternative to reduce CO_2 emissions from industrial sources. This process involves utilizing CO_2 as feedstock for chemical production, with a focus on closing industrial carbon loops and transforming CO_2 into useful products such as formic acid or formate, methanol, or ethylene. The technology employs an electrochemical reactor where CO_2 is supplied to the cathode and undergoes transformation over a catalyst surface, while an oxidation reaction occurs at the counter-electrode. Typically, the compartments are separated by an ion exchange membrane, which aids in separating reaction products and enhancing overall system efficiency [1].

Although CO_2 electroreduction has been extensively researched in laboratories, efforts are still underway to develop efficient reactor configurations, selective electrocatalysts, various electrode configurations, and to evaluate different operating conditions [1]. However, the current Technological Readiness Level of the process is between 3 and 5, indicating a significant gap from industrial scale-up. Therefore, consolidating prior knowledge is crucial to efficiently design and construct a CO_2 electrolyzer capable of successful technology scaling.

This work aims to design and construct an industrial demonstrator of a CO_2 electrolyzer as a first step towards implementing CO_2 electroreduction to formate on an industrial scale. The prototype's design and testing have been collaboratively undertaken by the DePRO research group, actively involved in advancing CO_2 conversion technology in recent years [1-3], and APRIA Systems, a technology supplier company responsible for constructing the CO_2 electrolyzer.

2. Methods

The electrolyzer comprises several components: i) outer closure plates made of stainless steel, ii) an external reactor structure constructed from polypropylene, iii) internal spacers composed of Viton, and iv) titanium current collectors. In the anode compartment, an iridium mixed oxide plate acts as the counter electrode for the water oxidation reaction. As for the cathode, a Gas Diffusion Electrode (GDE), with an active geometric area of 100 cm^2 is employed. This electrode was fabricated using an automated spray pyrolysis process that had been previously optimized. [2]. The catalytic ink consists of commercial Bi_2O_3 catalyst and Vulcan, with a mass ratio of 50:50, suspended in ethanol as a solvent and Sustainion XA-9 as a binder. This ink is applied over a Teflon-coated (50 %) carbon paper. Finally, a Nafion cation exchange membrane (CEM) separates the cathode and anode compartments.

The electrochemical reactor can operate in two configurations: Liquid-Liquid (L-L) and Liquid-Gas (L-G). In the L-L configuration, two aqueous electrolytes are introduced into the reactor. Aqueous 1M KOH is supplied to the anode, while a CO_2-saturated 0.5 M KCl + 0.45 M $KHCO_3$ is provided to the cathode. Both are fed to the reactor at a flowrate of 0.57 mL min^{-1} cm^{-2}. For the L-G configuration, a humidified CO_2 pure stream is fed into the cathode compartment at a flow rate of 10 mL min^{-1} cm^{-2}. In preliminary tests, a current density of 30 mA cm^{-2} was supplied to the system.

3. Results and discussion

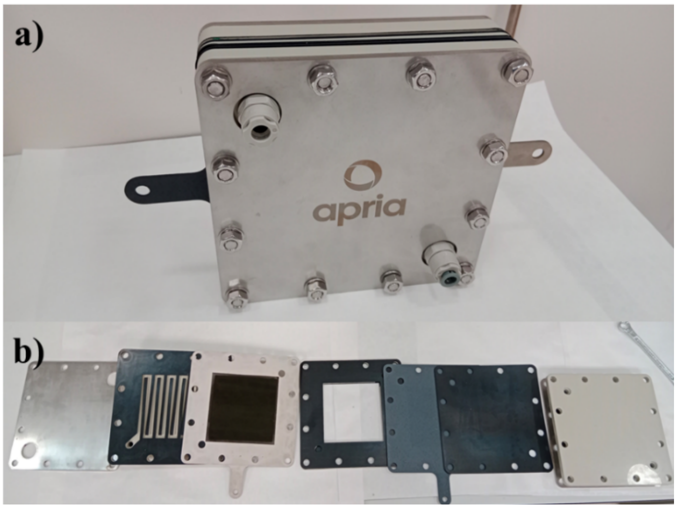

Figure 1. CO_2 electrolyzer prototype, a) L-G assembly, and b) L-G internal configuration

The final prototype, constructed by APRIA Systems (Figure 1), measures 180x180 mm in total dimensions and can be operated in both L-L and L-G configurations by adjusting the internal system configuration. The system has some limitations regarding its operating conditions. Firstly, the temperature should not exceed 40 ºC, and secondly, the pressure drop must not exceed 1.5 bar. However, these specifications do not affect the CO_2 electroreduction process since it is conducted at ambient temperature and pressure. After construction, the prototype underwent testing to evaluate its performance. In this regard, the system operated continuously for 2 hours with a single pass of CO_2 and electrolyte through the system. The applied current density was 30 mA cm^{-2}, resulting in a cell voltage of 4 V. This led to a formate concentration of 96 g/L, with a Faradic Efficiency of 82.59 %, and an energy consumption of 259 kWh $kmol^{-1}$. These outcomes align with prior findings within the research group [3], demonstrating the system's scalability.

Nevertheless, ongoing efforts are necessary to improve the stability and efficiency of the system, alongside increasing the current density of operation up to 200 mA cm^{-2}, which is the targeted level for industrial implementation. This will mainly focus on the configuration and stability of GDE, as it is crucial to achieve hundreds of hours of continuous operation at high current densities to attain the technical and practical feasibility of large-scale CO_2 electroreduction to formate.

4. Conclusions

A functional prototype of a CO_2 electrolyzer industrial demonstrator has been successfully designed and constructed, displaying promising results in initial tests. The scalability of CO_2 electroreduction technology was demonstrated through the efforts invested in this project. To ensure the long-term viability of the system, future work should focus on maximizing the stability and efficiency of the GDE employed in the system.

Acknowledgments

The authors of this communication fully acknowledge the financial support from the Spanish Research Agency (AEI) through the projects PID2022-138491OB-C31(MCIN/AEI /10.13039/501100011033 / FEDER, UE), PLEC2022-009398 (MCIN/AEI/10.13039/501100011033 and UE Next GenerationEU/PRTR), and TED2021-129810B-C21 (MCIN/ AEI /10.13039/501100011033 and UE NextGenerationEU/PRTR). Jose Antonio Abarca gratefully acknowledges the predoctoral research grant (FPI) PRE2021-097200 conceded by the Spanish Ministry of Science through the AEI.

References

[1] K. Fernandez-Caso, G. Diaz-Sainz, M. Alvarez-Guerra, A. Irabien, Electroreduction of CO_2: Advances in the Continuous Production of Formic Acid and Formate, ACS Energy Lett. 8 (2023) 1992-2024

[2] J.A. Abarca, G. Diaz-Sainz, I. Merino-Garcia, G. Beobide, J. Albo, A. Irabien, Optimized manufacturing of gas diffusion electrodes for CO_2 electroreduction with automatic spray pyrolysis, J. Environ. Chem. Eng. 11 (2023) 109724.

[3] G. Diaz-Sainz, M. Alvarez-Guerra, B. Avila-Bolivar, J. Solla-Gullon, V. Montiel, A. Irabien, Improving trade-offs in the figures of merit of gas-phase single-pass continuous CO_2 electrocatalytic reduction to formate, Chem. Eng. J. 405 (2021) 126965.

Keywords: CO_2 electrolyzer, industrial demonstrator, reactor design, formate.

Tue. 10/09 // 17:00-17:20

LCT – I – 3
Alternative to Claus process through COS as intermediate: CO_2 and H_2S competitive adsorption and reaction on sodium zeolites

Marco Fabbiani[1], Syeda Rabia Batool[1], Ludovic Pinard[1]*, Alexey Novikov[2], Helene Retot[2], Igor Shlyapnikov[3], Valentin Valtchev[1]*

1 LCS, CNRS-ENSICaen-UniCaen, 14000 Caen, France. 2 Saint Gobain Research Provence and NORPRO, Cavaillon, France. 3 Center of Ekscelence for Low Carbon Technologies, Hajdrihova ulica 19, 1000 Ljubljana, Slovenia.

**Corresponding author: ludovic.pinard@ensicaen.fr; *valentin.valtchev@ensicaen.fr*

Highlights

- The project e-CODUCT provides a new technology for two-step acid gas valorization via the conversion of CO_2 and H_2S into COS and the subsequent conversion of COS into CO and S_X.
- The project aims to develop electrothermal fluidized bed technology for process intensification.
- The reaction between H_2S and CO_2 is carried out on different catalysts.
- The results allow identifying the fraction of chemisorbed H_2S involved in the reactivity.

1. Introduction

According to recent data, the largest share of carbon emissions per sector in 2021 came from producing electricity and heat, accounting for 40% of global CO_2 emissions, reaching a historic high of 14.6 Gt [1]. In industrial-scale applications, fossil fuel combustion is commonly used to generate the heat required for chemical reactions. It is estimated that approximately half of the CO_2 emissions in the chemical industry are attributed to fuel combustion for heat supply purposes, where refineries and petrochemical industries are responsible for 1.24 Pty of CO_2 emissions. At the same time, this sector handles more than 3.6 Mt/y of H_2S, which in admixture with CO_2 is called acid gas and is handled not only in refining but also in exploration and production (as components of natural gas reservoirs), in biogas treatment (as natural components of the gas mixture from a digester), etc. The existing acid gas treatment approach relies on the Claus process to recover sulfur from gas streams rich in H_2S and demands additional use of fuel gas for lean H_2S sources (<55%). Moreover, to this date, no existing technologies allow simultaneous reduction of CO_2 and H_2S.

To address the transition to a low-carbon economy, the chemical industry needs to reduce its fossil fuel consumption by decarbonizing its processes, particularly through electrification. The project e-CODUCT provides a new technology for two-step acid gas valorization via i) conversion of CO_2 and H2S into COS in a fixed bed reactor, following the reaction:

$$H_2S(g) + CO_2(g) \rightleftharpoons COS(g) + H_2O \qquad (l)$$

and ii) COS conversion into CO and S_x using an electrothermal fluidized bed (ETFB) reactor. In this work, we address the first step (i) by studying the role of FAU- and LTA-type basic zeolites on the competitive dsorption and reaction of CO_2 and H_2S.

2. Methods

Adsorption and reaction of CO_2 and H_2S were performed at atmospheric pressure in a fixed-bed quartz reactor (9 mm diameter) at 45°C. The reactor was fed with a mixture of H_2S (Linde, purity: 95%v in N_2) and CO_2 at different dilutions (3-12%v) using a constant flow of 4.8 L/h (STP). Before testing, catalysts (commercial and lab-made nanosized 13X and 4A zeolites, SAR=1.5 and 1.2, respectively) were compacted under 5 tons, crushed, and sieved to obtain homogenous particles (0.2-0.5 mm), then 4 g were loaded in the reactor. All samples were pre-treated at 350°C under nitrogen flow 1.8 L/h (STP) for 8-10 h before being fed with the acid gas mixture with different flow sequences.

3. Results and discussion

Because of the low temperature, physisorption and chemisorption are discriminated through the saturation of the zeolite followed by a thermal desorption procedure. For both molecules, H_2S and CO_2 adsorbed separately on 13X, the amount is less than 10%, corresponding to an extremely low ratio with respect to the sodium cation (0.6 mol/g for 13X). Moreover, the adsorption strength of H_2S is higher than CO_2, as witnessed by a higher desorption temperature (T_{des}>350°C), typically attributed to a dissociative adsorption mechanism on the sodium cation [2,3]. A series of experiments, using alternated, mixed and pulsed flows, allows to separate components adsorption and reaction. Chemisorbed H_2S^* is completely converted upon reaction with CO_2.

$$H_2S(g) \rightleftharpoons H_2S^* \qquad (2)$$

$$H_2S^* + CO_2(g) \rightleftharpoons H_2O(ads.) + COS(g) \qquad (3)$$

The reaction proceeds towards a slow deactivation of the catalyst, possibly by polluting Na ions with strongly adsorbed water. The same experiments are carried out with the reverse order of reagents, leading to low reactivity. A series of experimental sequences allow to study the effects of temperature, pressure and water presence on the COS production. Moreover, a reagent conversion of about 10% is obtained at pseudo-steady state. The co-adsorption and reactivity of H_2S and CO_2 are further characterized by operando infrared spectroscopy. The reaction is then tested on different zeolites.

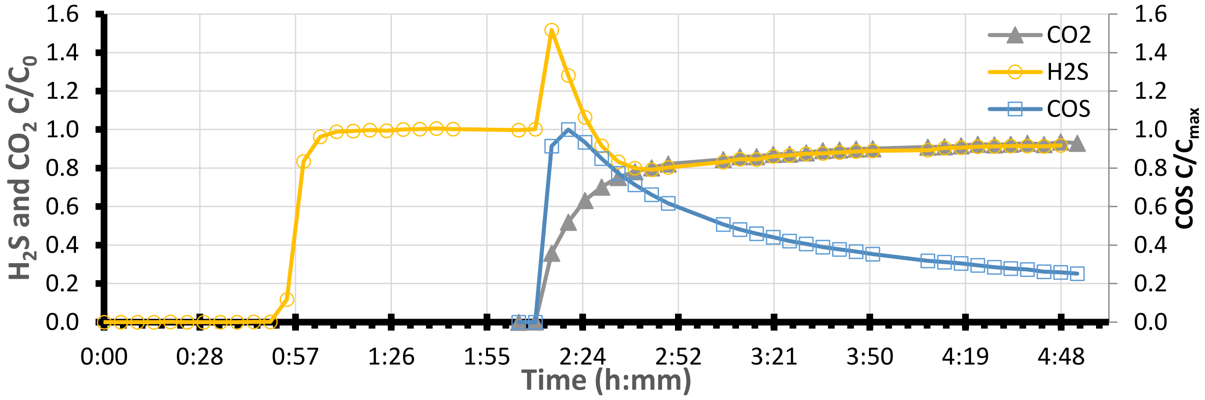

Figure 1. H_2S, CO_2, and COS relative concentrations on 13X.

4. Conclusions

The reactivity of H_2S and CO_2 is studied on 13X, showing a slow deactivation of the catalyst. The contribution of chemisorbed H2S is evidenced by its complete conversion.

References

[1] The Paris Agreement UNFCCC, (May 2023), unfccc.int/process-and-meetings/the-paris- agreement
[2] T. Yu, Z. Chen, Z. Liu, J. Xu, Y. Wang, Separations. 9 (2022) 229
[3] M. Khabazipour, M. Anbia, Ind. Eng. Chem. Res. 58 (2019) 22133−22164

Keywords

Electrothermal fluidized bed technology; Zeolites; Acid gas valorization: Low-carbon technology.

Wed. 11/09 // 08:40-09:00

LCT – II – 1

Intensifying the catalytic process via the conservative perturbed equilibrium (CPE): methane tri-reforming as an example

Mykhailo O. Vilboi[1*], Vitaly R. Trishch[1], Gregory S.Yablonsky[2]

1 National Technical University of Ukraine, Kyiv, Ukraine; 2 Washington University in St. Louis, St. Louis, USA

**Corresponding author: mvilboy@gmail.com*

- Conservatively Perturbed Equilibrium is demonstrated using tri-reforming as an example process.
- CPE allows for increase in yield of up to 36.8% compared to equilibrium values.
- Increased yield is achieved on much shorter reactor length than full equilibrium.

1. Introduction

Intensification of catalytic processes caused by their thermodynamic and kinetic peculiarities is a special crossroad of chemical thermodynamics, kinetics, and engineering. This paper is devoted to the possible application of the Conservatively Perturbed Equilibrium (CPE)-phenomenon for intensifying the methane reforming. The CPE is a new phenomenon in chemical kinetics and engineering first distinguished by Yablonsky et al [1]. The CPE is described as dynamic behavior of complex chemical reactions in closed or some open systems at the fixed temperature and given amounts of any chemical element and at some initial/inlet concentration(s) which are equal to the equilibrium one(s). In catalytic regimes, the CPE- results in unavoidable passing of a reacting system from the initial or inlet concentration(s), some of which are equal to the equilibrium concentration, to the complete chemical equilibrium, and this transition is occurred through a point of the concentration extremum/extrema of initially 'equilibrated' components. Model examples of cyclic and acyclic mechanisms representing the CPE-effect are presented in papers [2,3]. Experimentally, this phenomenon was justified by Peng et al [4].

2. Methods

In this work, the CPE-phenomenon will be used for intensifying the catalytic process taken the complex tri-reforming process as an example. This process is still in infancy, but its potential industrial importance is obvious. The reversible 'block' of reactions is chosen as the subject of studying, i.e., dry reforming of methane (1) and steam reforming of methane (2):

$$\mathrm{CH4 + CO2 \leftrightarrow 2CO + 2H2} \qquad (1)$$

$$\mathrm{CH4 + H2O \leftrightarrow CO + 3H2} \qquad (2)$$

Kinetic models of these reactions are formulated by Wei and Iglesia [5].For achieving the CPE effect, it is necessary first to calculate the equilibrium composition for a given set of conditions, such as the temperature, pressure, and initial element amounts. This was done within the temperature range from 973 to 1123 K with intervals of 50 K. Based on these calculations, it is possible to conduct the CPE-experiment itself. To do this, it is necessary to set one (or multiple) of initial molar flow rates to the equilibrium value, say flow rates of products, CO, or hydrogen, and set other ones to not be equal to the equilibrium values, but do this in such a way to not change overall amount of each chemical element in the mixture. Temperature and pressure must be held the same as well.

3. Results and discussion

Figure 1 depicts one of possible scenarios in which CO molar flow rate was set equal to its equilibrium value, and other ones were not. This reactor can be a second stage of the two-stage process. In the first stage, complete equilibrium can be achieved. In the second stage, the equilibrium is perturbed using the CPE-procedure.

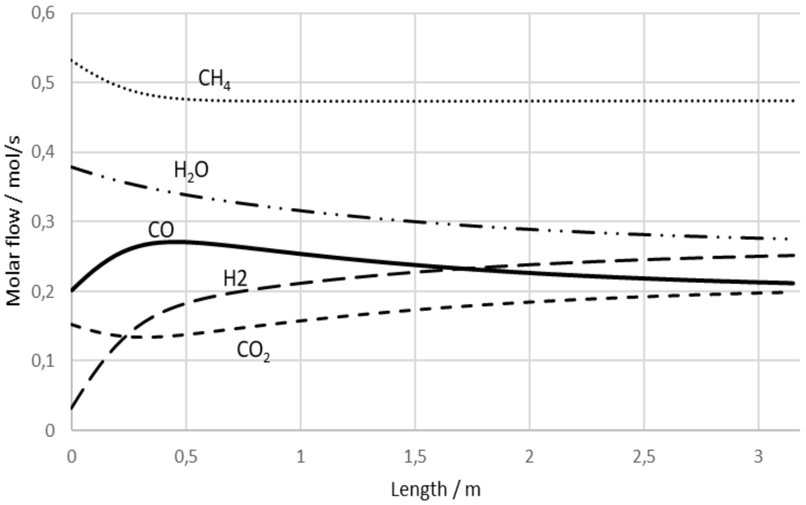

Figure 1. Molar flow rate profile, T = 973 K, P = 10 bar. CO initial = CO equilibrium.

In our calculations of CPE-regimes, the typical CO molar flow rate profile experienced a maximum at 0.4 m of the reactor length, which is a much shorter length that is needed to reach equilibrium. The value of CO flow rate at this maximum is, obviously, greater that equilibrium one. It is possible to evaluate the degree of the over-equilibrium. In this case, it is 36.8 %.

4. Conclusions

Application of the CPE-phenomenon to the complex catalytic tri-reforming process demonstrates two improvements: 1. Achieving the over-equilibrium product molar flow rate. 2. This value is achieved at the reactor length that is much shorter than the length corresponding to the vicinity of the complete equilibrium.

References

[1] G.S. Yablonsky, P.D. Branco, G.B. Marin, and D. Constales. Chem. Eng. Sci. Vol. 196. pp. 384-390. 2019.
[2] V.R. Trishch, Y.O. Beznosyk, D. Constales, and G.S. Yablonsky. Journal of Non-Equilibrium Thermodynamics. Vol. 47. pp. 103-110. 2022.
[3] V.R. Trishch, Y.O. Beznosyk, G.S. Yablonsky, and D. Constales. Bulletin of NTUU "KPI". Chem. Eng. Ecology and Resource Conservation. Vol. 3. pp. 39-55. 2021.
[4] B. Peng, X. Zhu, D. Constales, and G. S. Yablonsky. Chem. Eng. Sci. Vol.229. 2021.
[5] J. Wei, and E. Iglesia (2004). Journal of Catalysis. Vol. 224. Issue 2. 370-383.

Keywords
Conservatively Perturbed Equilibrium, Tri-reforming, Over-equilibrium.

Wed. 11/09 // 09:00-09:20

LCT – II – 2

CFD design of photocatalytic mesostructured reactors for green ammonia production

Isabel S.O. Barbosa[1,2], M. Teresa Oliveira[1,2], Margarida S.C.A. Brito[1,2], Cláudia G. Silva[1,2],
Ricardo J. Santos[1,2]*

1Laboratory of Separation and Reaction Engineering – Laboratory of Catalysis and Materials (LSRE-LCM), Faculty of Engineering, University of Porto, Rua Dr. Roberto Frias, 4200-465 Porto, Portugal. 2ALiCE – Associate Laboratory in Chemical Engineering, Faculty of Engineering, University of Porto, Rua Dr. Roberto Frias, 4200-465 Porto, Portugal.

**Corresponding author: rsantos@fe.up.pt*

Highlights

- A new mesostructured photocatalytic reactor was developed for ammonia production.
- The unitary cell (DeanCell) of the reactor was designed based on CFD simulations.
- DeanCell proves effective as an elementary unit in mesostructured photoreactors.

Introduction

Ammonia (NH_3) holds significant importance as a widely produced chemical, primarily used in fertilizer production and as a potential hydrogen carrier for energy storage [1]. Traditional ammonia synthesis via the Haber-Bosch process relies on methane and is energy-intensive, contributing to greenhouse gas emissions [1]. To mitigate this, photo-assisted ammonia production using renewable resources is gaining traction. However, to fully realize its potential, advancements in reactor design are crucial.

Micro and mesostructured reactors offer promising advantages in chemical engineering due to their enhanced mixing and reaction rates, scalability, and safety [2]. These reactors, characterized by high surface-to-volume ratios, facilitate uniform light and flow distribution, crucial for efficient photocatalytic reactions [3]. Scaling up is achieved by replicating unit elements while maintaining surface/volume ratios to preserve mass and heat transfer performance.

The design of a photocatalytic mesostructured reactor for ammonia production involves the use of Computational Fluid Dynamics (CFD) to optimize reactor performance. CFD simulations enable the analysis of fluid flow patterns, mass transfer, and reaction kinetics, aiding in exploring reactor configurations, assessing mixing efficiency, and optimizing operating conditions.

This study proposes an innovative prismatic unit cell (DeanCell) arrangement for mesostructured photocatalytic reactors, evaluated through CFD simulations focusing on vorticity and velocity profiles. Simulations for geometric optimization and mixing efficiency assessment provided insights into fluid phase flow paths and dynamic structures like Dean vortices for Reynolds numbers in a range from 1 to 1000.

Methods

The initial design of the DeanCell, the fundamental unit of the structured reactor, was crafted to promote secondary flow in the shape of Dean vortices, aiming to increase fluid mixing within the reactor. Illustrated in Figure 1, this prismatic geometry features an inlet channel and a main body where the catalyst immobilization will take place. The primary inlet channel was set with characteristic meso scale dimensions of 1x1 mm² (*d* and *w*) for the cross-sectional area and a length of 6 mm (l_{in}) to foster a developed flow at the entrance.

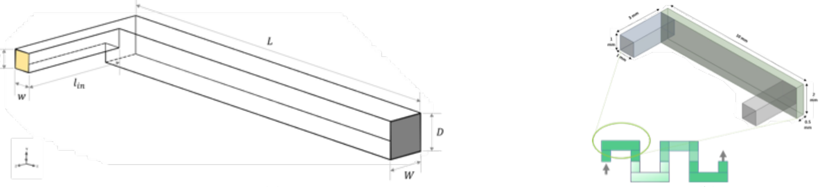

(a) (b)

Figure 1. (a) Base case geometry of the unit-cell of the mesostructured reactor and (b) Final DeanCell configuration and schematic representation of the suggested structured network.

A parametric study was conducted using ANSYS Fluent 2020 R2 to evaluate the geometry and dimensions of the optimal unitary element configuration. Simulations were performed under laminar flow conditions with a Reynolds number (Re) of 100. The dimensions of the main channel (*D*, *W*, and *L*) were analyzed, with vorticity and velocity maps used as optimization targets. Mesh independence was assessed for the most promising geometry (D2W0.5) to ensure sufficient resolution for accurate representation of hydrodynamic phenomena. Subsequently, Reynolds numbers ranging from 1 to 1000 were tested to examine the effect of inlet velocity on Dean vortices generation. Additionally, dynamic simulations of tracer injection were conducted for further hydrodynamic analysis. Water was chosen as the working fluid, with default physical properties retained: density (ɟ) of 998.2 kgIm^{-3} and viscosity (ε) of 1 x 10^{-3} PaIs.

Results and discussion

Vorticity profiles along the cell's length indicate increased mixing due to the structural step, with higher vorticity observed for channel heights of 2mm or more. Figure 2a summarizes the results from testing several cases at a Reynolds number (Re) of 100, identifying the optimal geometry as a 10mm length (*L*), 2mm diameter (*D*), and 0.5mm width (*W*) configuration. After determining the optimal DeanCell shape, Reynolds numbers ranging from 1 to 1000 were evaluated at a fixed 10mm length. Vortices were only detected for Re higher than 125. Figure 2b illustrates the vortices formed along the main channel through velocity contours for a Re of 250. Tracer contours in Figure 2c indicate stagnant zones at the corners of the main body, with less efficient fluid mixing observed at the bottom and top of the reactor, particularly at a dimensionless time *d*=5.

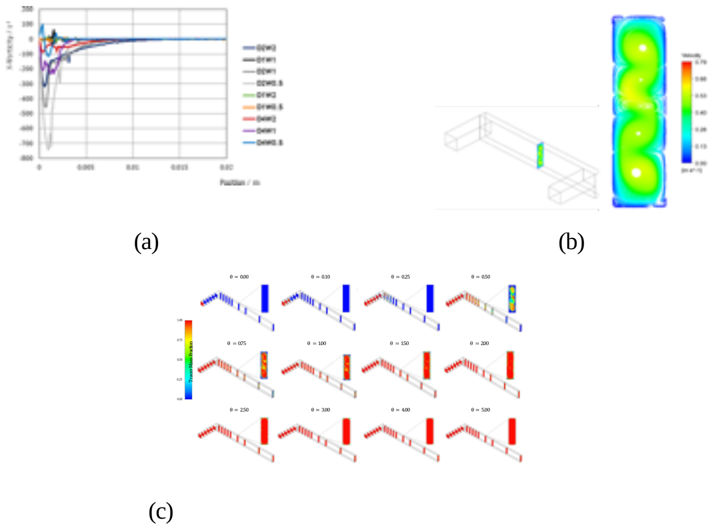

(a) (b)

(c)

Figure 2. (a) Vorticity profiles in the main body along flow x-direction, (b) Velocity contour of the flow field for a Re of 250, and (c) Evolution of tracer concentration over dimensionless time, at *x* = 10 mm, for Re of 250.

The final design of the DeanCell is presented in Figure 1b. This unitary element will be repeated to generate a structured network, as shown.

Conclusions

Based on the simulations performed, the DeanCell appears effective for use as an elementary cell of a mesostructured photocatalytic reactor. Analysis of flow dynamics reveals that the prismatic shape and expanded inlet channel increase system dynamics. Even at low Reynolds numbers, rotational flow enhances contact between fluid elements, facilitating mass dispersion. Effective fluid homogenization in small-scale reactors can improve photocatalytic reaction efficiency.

References

[1] Q. Han, H. Jiao, L. Xiong, J. Tang, Mater. Adv. 2 (2021) 564ï 581

[2] I.S.O. Barbosa, R.J. Santos, C.G. Silva, M.S.C.A Brito, Chem. Eng. Process. Process Intensif. 46 (2021) 1241-1250

[3] E. Kayahan, M. Jacobs, L. Braeken, L.C.J. Thomassen, S. Kuhn, T. Gerven, M.E. Leblebici, Beilstein J. Org. Chem. 16 (2020) 2484-2504

Keywords: Computational Fluid Dynamics, Mesostructured reactors, Photocatalysis, Dean vortices

Acknowledgements This work was supported by national funds through FCT/MCTES (PIDDAC): LSRE-LCM, UIDB/50020/2020 (DOI: 10.54499/UIDB/50020/2020) and UIDP/50020/2020 (DOI: 10.54499/UIDP/50020/2020); ALiCE, LA/P/0045/2020 (DOI:10.54499/LA/P/0045/2020); and the project SuN2Fuel 2022.04682.PTDC (DOI:10.54499/2022.04682.PTDC). I.S.O. Barbosa acknowledges her FCT grant UI/BD/151092/2021.

Wed. 11/09 // 09:20-09:40

LCT – II – 3

Spatially resolved measurements and reactive CFD modelling of the selective catalytic reduction of nitrogen oxides in the context of future hydrogen engines

Lisa Nordhausen, Marie Richter, Marion Börnhorst*

Technische Universität Dortmund, Lehrstuhl Reaction Engineering and Catalysis
44227 Dortmund, Germany

**Corresponding author: marion.boernhorst@tu-dortmund.de*

Highlights

- Intracatalytic capillary sampling under real application conditions
- Implementation of NO_x SCR and HNCO hydrolysis reaction kinetics in a CFD model
- Influence of hydrogen on the catalytic reaction system

1. Introduction

The reduction of nitrogen oxides (NO_x) has become increasingly important worldwide over the last decades, particularly for the after treatment of lean-burn engine exhaust gases. In particular in the context of future hydrogen engines, where NO_x are the only emissions of concern, the selective catalytic reduction (SCR) of NO_x is expected to maintain its relevance. By SCR NO_x is reduced to N_2 and H_2O by NH_3 over state-of-the-art Cu-zeolites or vanadia catalysts (VWT). For safety reasons, the reducing agent NH_3 is not supplied as gas but in form of a urea water solution (UWS). The water evaporates and the urea reacts to HNCO and NH_3 by thermolysis. The produced HNCO is then hydrolyzed to NH_3 and CO_2. Due to inhomogeneous spray distribution and urea side reactions undesired solid deposits such as biuret, triuret and cyanuric acid can be formed which lead to a decrease of SCR efficiency. In order to enable detailed kinetic investigations on the chemical interactions of UWS with the SCR reaction system, spatially resolved temperature and concentration measurements are carried out in the monolith channels. [1-2]

2. Methods

The invasive capillary sampling technique has been used in various studies and models were developed to predict the hydrodynamics modified by the capillary within the channel [3]. In this work, a setup for capillary sampling was adapted to an existing model gas test rig including an SCR monolith. Sampling is carried out through a thin capillary, which can be moved through a monolith channel by a motorized stage. FTIR and H_2-MS analytics are installed downstream the capillary to determine the gas phase concentrations of NH_3, NO, NO_2, H_2, HNCO, H_2O and CO_2. Since the sampling flow rate extracted from the monolith channel by the capillary is by two orders of magnitude smaller than the required sample flow rate for the FTIR, a coil setup is designed for sample accumulation. The effect of sample residence time and dispersion within the coil on the measured concentration is analyzed. Additional measurements were performed without the capillary and the coil setup in order to quantify the influence of the sampling technique. The quantitative influence of the analytical setup and measurement procedure on the resulting spatially resolved concentration data is evaluated in detail.

Ansys Fluent is used to simulate the hydrodynamics inside the monolithic channel and implement an extended reaction kinetic model. The 3D model is then validated against the experimental data.

3. Results and discussion

Reaction kinetic studies were carried out after detailed calibration of the measurement technique in order to improve the understanding of the interactions between urea decomposition and the SCR reactions. Both measurements with gaseous NH_3 dosing and with liquid UWS dosing were carried out. Furthermore, the influence of hydrogen on the multiphase reaction system was examined.

In addition, a CFD model was developed to investigate the interaction of hydrodynamics and chemical reaction kinetics in the monolith channel. A literature reaction kinetic model of the NH_3-SCR was implemented and complemented by HNCO hydrolysis kinetics based on the experimental data. The simulations were then validated against experimental data. A comparison of both simulated and experimentally determined concentration profile is shown in Figure 1. The coil setup can lead to an underestimation of the measured concentrations. Due to the hydrodynamic influence of the capillary, the residence time increases, which leads to a decreasing of the underestimation of concentration along the channel. The equimolar decrease of the NO and NH_3 concentrations is reproduced well by the simulation.

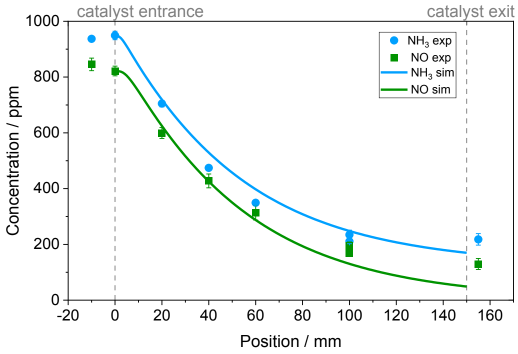

Figure 1: Comparison of experimental and simulated results of the SCR of NO_x in a monolith channel. T = 578 K, $\dot{V}_{gas} = 1065\ \mathrm{L\ min}^{-1}$, $c_{NH3} = 911$ ppm, $c_{NO} = 911$ ppm

4. Conclusions

Based on the presented experiments and the developed model, the influence of the analytical setup downstream the capillary on the measured concentrations was quantified in detail. A method is developed to predict deviations in measured concentrations originating from the analytical setup and correction procedures are proposed. The determined deviations add up on the frequently investigated hydrodynamic influence induced by the invasive character of the capillary sampling technique.

Furthermore, the knowledge of the influence of hydrogen on the multiphase reaction system is crucial for the implementation of NH_3-SCR technology in future hydrogen engines. Based on the results of this work a potential combination of H_2- and NH_3-SCR can be evaluated.

References

[1] M. Börnhorst, O. Deutschmann, Progress in Energy and Combustion Science 2021, 87, 100949. DOI: https://doi.org/10.1016/j.pecs.2021.100949

[2] M. Börnhorst, C. Kuntz, S. Tischer, O. Deutschmann, Chemical Engineering Science 2020, 211, 115319. DOI: https://doi.org/10.1016/j.ces.2019.115319

[3] M. Hettel, C. Antinori, O. Deutschmann, Emiss. Control Sci. Technol. 2016, 2 (4), 188 – 203. DOI: https://doi.org/10.1007/s40825-016-0043-1

Keywords

Selective catalytic reduction; Reaction kinetics, Capillary sampling technique, Reactive CFD

Wed. 11/09 // 09:40-10:00

LCT – II – 4

Ni-decorated $BiVO_4/WO_3$ photoanodes for an enhanced photoelectrochemical response under solar light

Ivan Merino-Garcia*, Sara Crespo, Jose Antonio Abarca, Jonathan Albo

Departamento de Ingenierías Química y Biomolecular, Universidad de Cantabria, Avenida de los Castros s/n, 39005 Santander, Spain.

**Corresponding author: merinoi@unican.es*

Highlights

- Ni-doped $BiVO_4/WO_3$ photoanodes have been developed for an improved OER.
- Higher $BiVO_4$ loadings lead to improved current densities at the cathode.
- The photoanode design is optimized with different configurations and supports.
- The influence of Ni loading on energy efficiency is investigated.

1. Introduction

Integrating photoactive materials in the anodic compartment of electrochemical reactors has the potential to decrease the overall energy consumption of electrochemical systems by generating an extra flow of electrons for an enhanced photoelectrochemical (PEC) response [1]. In this sense, different semiconductors such as $BiVO_4$ and WO_3 can enhance light absorption and electron extraction, leading to an improved harvest of solar irradiation by enhancing light absorption and reducing electron-hole recombination [2]. Moreover, considering the high energy consumed by the Oxygen Evolution Reaction (OER) (around 90%) [3], the use Ni-doping strategies may help reducing the required overpotential and inhibiting charges recombination, which can result in improved kinetics for water oxidation [4].

Thus, this work aims to develop nanoparticulated Ni-decorated $BiVO_4/WO_3$ photoanodes with different Ni loadings and electrode configurations for an enhanced PEC response under solar light, that can be coupled to interesting reactions such as solar water splitting and eventually photo-assisted CO_2 reduction.

2. Methods

Surfaces preparation is carried out using an automated spray pyrolysis technique (ND-SP Mini Ultrasonic Spray Coater, Nadetech Innovations), previously optimized for depositing materials in different layers [5]. The ink contains the catalysts, isopropanol as the solvent (97 %), and Nafion as the binder. The different catalysts are coated onto Fluorine Doped Tin Oxide (FTO) or carbonaceous substrates with different $BiVO_4/WO_3$ mass ratios. The decoration of the photoanodes is carried out with different Ni loadings (1-3 mg/cm^2) for an enhanced PEC performance. Different electrode configurations are proposed, including the manufacturing through independent layer-by-layer deposition or physical mixing between $BiVO_4$ and Ni as the top layer, with WO_3 as the bottom layer for an enhanced extraction of electrons.

The different photoactive surfaces are photoelectrochemically characterized by continuous chronoamperometries at a constant voltage of -1.8 V vs. Ag/AgCl with and without visible light irradiation to evaluate on-off PEC activity, as well as electrochemical impedance spectroscopy (EIS) measurements across a range of frequencies from 10 kHz to 50 Hz to study charge transfer resistance and charges recombination. The performance is studied in a photoanode-driven divided filter-press reactor in continuous mode under visible light irradiation (100 mW cm^{-2}), with a platinized titanium plate as the dark cathode and an aqueous solution of 0.5 M $KHCO_3$ as the electrolyte. Additional experiments under simulated sunlight (100 mW/cm^2; LSH-7320 LED Solar Simulator, Newport) and a solar concentrator (> 1 sun; Photo Emission Tech, Inc.) are conducted to improve the overall energy efficiency of the water splitting process.

3. Results and discussion

The results on evaluating the $BiVO_4/WO_3$ mass ratio, with WO_3 as the bottom layer for an enhanced extraction of electrons, shows that higher $BiVO_4$ loadings (80:20) exhibit the most favorable results in terms of photogenerated current density and H_2 production (155.7 µmol m^{-2} s^{-1}) in the cathode, denoting an efficient electron-hole separation and electrons transfer, which is confirmed by the lower charge transfer resistance achieved in EIS measurements, in comparison with alternative $BiVO_4/WO_3$ ratios (50:50 and 20:80).

The next step covers the decoration of the $BiVO_4/WO_3$ photoanodes with Ni nanoparticles. First, we explore different electrode configurations such as three independent layers or the combination of Ni and $BiVO_4$ in the same matrix (physical mixture) as the top layer, where WO_3 is the bottom electron collector layer. Second, we evaluate the effect of different supports (transparent FTO for back illumination or porous carbon papers under front-illumination conditions) on process performance, paying special attention to the generated photocurrent density in the cathode. Finally, the behavior of the photoanode is optimized by controlling Ni loading. The work also includes light concentration strategies for an enhanced electron flow to identify the optimal conditions for potential scaling up.

4. Conclusions

Although promising results have been achieved with multi-layered $BiVO_4/WO_3$ photoanodes, research efforts on design and optimization of photoanodes for water oxidation are still needed to increase light harvesting and catalytic activity and, thus, reduce the energy consumption. Thus, this communication investigates the effect of decorating $BiVO_4/WO_3$ multi-layered photoanodes with Ni nanoparticles, with special emphasis on electrode configuration, effect of catalyst support, and Ni loading. Overall, this work advances towards the design and optimization of photoanodes with special emphasis of reducing the energy requirements of the OER, which is crucial to enable the scaling up and practical application of PEC systems with solar energy at a larger scale.

Acknowledgements

The authors gratefully acknowledge the financial support from Ministerio de Ciencia e Innovación, Agencia Estatal de Investigación (MCIN/AEI/10.13039/501100011033/) and European Union (NextGenerationEU/PRTR) through the project TED2021-129810B-C21. The project PID2022-138491OB-C31 (MCIN/AEI /10.13039/501100011033 / FEDER, UE) is also acknowledged.

References

[33] S. Castro, J. Albo, A. Irabien, ACS Sustain. Chem. Eng. 6 (2018) 15877–15894.
[34] I. Merino-Garcia, S. Crespo, M. Perfecto-Irigaray, G. Beobide, A. Irabien, J. Albo, Catal. Today (2024) 114581. Article in press.
[35] S. Verma, S. Lu, P.J.A. Kenis, Nat. Energy 4 (2019) 466-474.
[36] H. Bai, X. Li, Y. Zhao, W. Fan, Y. Liu, Y. Gao, D. Xu, J. Ding, W. Shi, Appl. Surf. Sci. 538 (2021) 148150.
[37] J.A. Abarca, G. Díaz-Sainz, I. Merino-Garcia, G. Beobide, J. Albo, A. Irabien, J. Environ. Chem. Eng. 11 (2023) 109724.

Keywords

Photoanode design, Ni-decorated $BiVO_4/WO_3$, energy efficiency, water splitting.

Wed. 11/09 // 10:00-10:20

LCT – II – 5

Catalyst coatings for hydrogen generation by ammonia decomposition at high temperatures and elevated pressure

Gunther Kolb[1]*, Tobias Weissenberger[1], Ralf Zapf[1], Helmut Pennemann[1]

1 Fraunhofer Institute for Microengineering and Microsystems IMM, Carl-Zeiss-Straße 18-20, 55129 Mainz, Germany

**Gunther.Kolb@imm.fraunhofer.de*

Highlights

- Nickel catalysts are well suited for ammonia decomposition at high temperature.
- Barium doped nickel catalysts surpass ruthenium in activity at high temperatures.
- Nickel catalysts are stable at high reaction temperatures.

1. Introduction

Hydrogen is expected to play a significant role as a carbon-neutral energy vector in the future. However, its low energy density poses a significant challenge for the transportation and storage of hydrogen [1]. Ammonia can be used as a hydrogen carrier to address this issue. Ammonia is carbon free, has a high gravimetric hydrogen density of 17.7wt.% and a high energy density. Additionally, it can be liquified at a moderate pressure of 0.86 MPa at 20.0°C. Today about 150 million tons ammonia are produced annually and the technologies for the production, storage, and transport (by e.g., ship, train and truck) of ammonia are already well-established. [2]

The decomposition of ammonia to hydrogen and nitrogen is a crucial step for the use of ammonia as a hydrogen and energy vector. We will introduce ammonia decomposition catalysts developed for the use in micro-structured heat-exchanger reactors [3] under elevated pressure and high temperatures for decentralized and mobile applications. Nickel-based catalysts were applied and tested as coatings in microreactors, and the studies were focusing on long-term catalyst stability.

2. Methods

Catalysts were prepared by impregnation of the support with a metal precursor, calcined and wash coated into the channels of microstructured reactors. Two catalyst-coated microstructured plates were then assembled to a microreactor by laser welding.[4] The prepared catalyst powders were characterized using by XRF, TEM, EDX, N_2-physisorption, XPS and H2 chemisorption measurements. The catalytic performance was investigated using a test rig equipped with electrical heating, back pressure regulator and gas dosing via mass flow controllers. The product gas was analyzed online using a µGC and an online FTIR spectrometer. Reaction conditions were WHSV=200 $L/g_{cat}h$ and reactor pressure of 5 barg. Feed composition: 90% ammonia and 10% argon as internal standard.

3. Results and discussion

Alumina, silica and ceria were studied as support and the effect of the nickel loading and different promotors on the catalytic performance were investigated. The effect of the catalyst support on the catalytic activity at a pressure of 5barg is displayed in Figure 1 a).

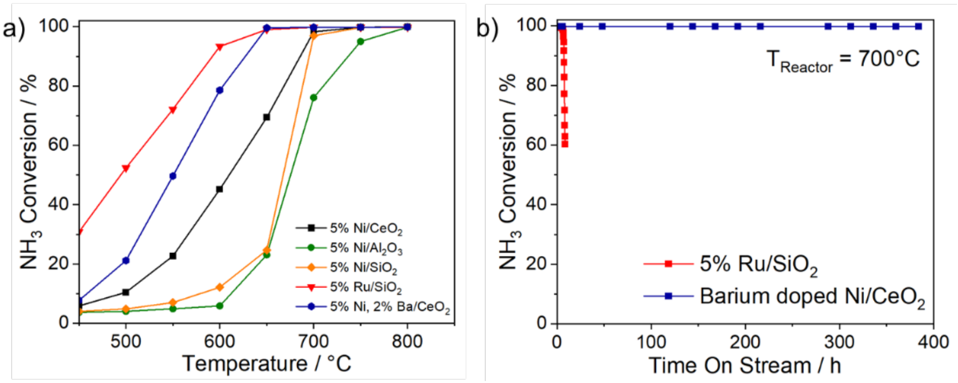

Figure 1. a) NH_3 conversion over temperature for different catalysts, b) ammonia conversion over time on stream at 700°C. (WHSV=200 L/gh, 5bar, 10% Ar).

Compared to the ruthenium catalyst the nickel catalysts are less active at lower temperatures. At higher temperatures all catalysts reach the equilibrium conversion. The highest activities among the tested nickel catalyst on different supports can be observed for ceria followed by silica and alumina. The activity of Ni/CeO_2 catalysts can be further enhanced by addition of different additives as dopants. Among the studied dopants bariums showed the best performance and surpasses the performance of the ruthenium catalyst at temperatures of 650 °C and higher. A major advantage of the nickel catalyst is the long-term stability at high reaction temperatures as shown in Figure 1b). The ruthenium-based reference catalyst shows a fast decline in activity after only 5 hours of reaction at 700°C. The nickel-based catalyst is much more stable, and no sign of deactivation was visible even after 380 hours time on stream.

Figure 2. Microstructured ammonia decomposition processor for 21 kg/h ammonia feed

4. Conclusions

Nickel catalysts are less active at lower temperatures compared to ruthenium but perform very well at higher temperatures. Of the studied support materials, nickel-based catalysts supported on ceria showed the best performance and addition of barium enhanced the activity further. In contrast to the ruthenium-based catalysts the nickel-based catalyst also displayed a very promising long-term stability. Currently a micro-structured heat-exchanger reactor has been built and is tested for an ammonia feed flow of 21 kg/h applying the novel catalyst coating technology and integrated off-gas of a pressure swing adsorption (PSA) unit (see Fig.2).

References

[38] G.Kolb, Fuel Processing for Fuel Cells, Wiley (2008)
[39] J K. Lamb, M. Dolan, D. Kennedy, Int. J. Hydrog. Energy, 44(7) (2019) 3580
[40] G.Kolb, Chem. Eng. Proc. 3 (2013) 1
[41] T. Weissenberger, R. Zapf, H. Pennemann, G. Kolb, Catalysts 14.2 (2024) 104.

Keywords
Ammonia; Hydrogen; decomposition; cracking

PROCESS DEVELOPMENT

PD – 1

Electrothermal Fluidized Bed Reactor model for high temperature endothermic reactions: The case of COS decomposition

Klaus Jacobs[1], Soroush Zareghorbaei[1], Jeroen Lauwaert[2], Igor Shlyapnikov[3], Miha Grilc[3,4], Gleb Veryasov[5], Joris Thybaut[1]*

1 Laboratory for Chemical Technology (LCT), Ghent University, Ghent, Belgium; 2 Industrial Catalysis and Adsorption Technology (INCAT), Ghent University, Ghent, Belgium; 3 Center of Excellence for Low Carbon Technology (CONOT), Ljubljana, Slovenia, 4 National Institute of Chemistry (NIC), Ljubljana, Slovenia ; 5 Total Energies Feluy, Belgium.

**Joris Thybaut: Joris.Thybaut@UGent.be*

Highlights

- A 1D heat balance model of an ETFBR has been developed.
- COS decomposition is a promising reaction for ETFBR.
- Electrode configuration and dimensions determines the temperature profile.

1. Introduction

One of the strategies for the defossilization of energy-intensive industries is the electrification of high-temperature chemical reactors. A specific type of reactor which uses Ohmic/Joule heating as thermal energy supply source appears as a good candidate to be scaled-up: the Electrothermal Fluidized Bed Reactor (ETFBR). ETFBR is the combination of two already proven technologies (fluidization and resistive heating). While there are models that separately attempt to describe fluidized beds, bed resistance and bed resistivity [1], [2], there is to our knowledge, no current model that can describe the temperature profile of an ETFBR over the length of the bed. Fluidized beds are particularly useful for these type of reactions due to their improved heat transfer. The COS thermal decomposition reaction to valuable CO and S is a highly endothermic reaction of about 300 kJ mol^{-1}.

2. Methods

The mass balances of a fluidized bed are described and kinetics are inspired from elsewhere [3],[4]. The heat balance of an adiabatic ETFBR with reaction in the gas phase, isothermicity between low and high density phases, no radial profiles and steady state can be described by Eq.1.The model further assumes constant parameters (Dispersion and conductivity coefficients, current, etc.), thermodynamic properties and superficial velocity, calculated at average reactor temperature, i.e. constant phase allocation (Phase volume fraction, flow fraction, etc.), negligible contact resistance with the electrodes. A close circuit voltage is given as input and an average reactor temperature is assumed to calculate the previously mentioned parameters and properties. The system of second order ODEs is solved using available IVP and BVP solvers from the SciPy library in python and iterating until the assumed and calculated average temperature converge. The feed is assumed to be 50 w/w% COS in N_2 in order to avoid thermodynamic limitations, preheated to 600°C, flow of 15 NL min^{-1}. The reactor is assumed to be filled with 1.5kg (100mm static bed height) of spherical graphite particles of 100μm in diameter. Flow velocity lies in the bubbling regime. The targeted COS conversion was set to 90%.

$$u\rho_g Cp_g \frac{dT}{dz} - k_e \frac{d^2T}{dz^2} - \varepsilon \sum_{j}^{N_j} \left(-\Delta H_{rxn,j} R_{v,j}\right) - dQ_{JH} = 0 \tag{1}$$

3. Results and discussion

The assumed scheme of the ETFBR is shown in Figure 1. Under this scheme, two different configurations can be used. Coaxial configuration; without the lower electrode, treats the differential resistance as resistances in parallel while the End-to-End configuration; without a side electrode, treats the differential resistance as resistances in series (See Figure 1). A combination of the two configurations is also possible. The joule heating terms (dQ_{JH}) for coaxial and End-to-End configurations are shown in Figure 1. Since the energy needed to reach 90% conversion (≈0.95 kW) is the same for the three cases, the difference in performance lies in how the geometry of the ETFBR affects the electrical resistance distribution along the bed and how the electrically conductive zones are defined.

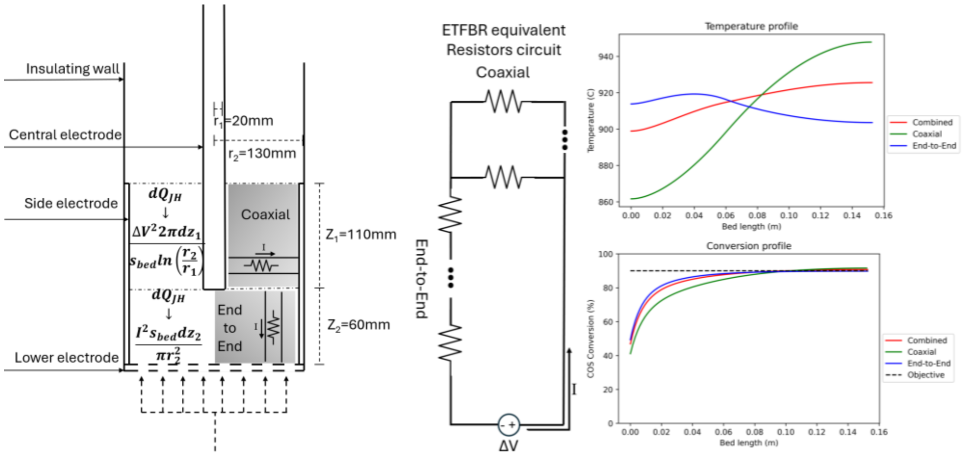

Figure 1. ETFBR scheme, resistor configuration and its respective temperature and conversion profiles.

In the coaxial configuration, it is assumed that there is no Joule heating under the tip of the central electrode. The temperature at the bottom of the ETFBR is the lowest but has the highest ΔT at 86 ºC. In the end-to-end configuration, it is assumed that Joule heating occurs below the tip of the central electrode. It is possible to observe the effect of the endothermic reaction as it has a ΔT of –11ºC. The combined configuration generates heat in the two zones and as a result it behaves somewhere in between the two configurations with a ΔT of 27 ºC. The total resistance is the sum of the resistances of the sections, it has the highest resistance at 3.3 Ω_{combined}, meaning it needs the highest applied voltage at 57 V. The coaxial configuration has the lowest resistance (1.4 Ω_{Coaxial} vs 1.9 $\Omega_{\text{End-to-End}}$) as the current flows from central electrode to wall which is through the shortest path. The applied voltages for the coaxial and end-to-end configuration are 38 V and 46 V, respectively.

4. Conclusions

A heat balance model for an ETFBR has been developed using combined electronic circuits of resistances in series and resistances in parallel as analogies for the resistive heating. Furthermore, the model takes into consideration the electrode configuration and reactor geometry and produces reasonable results for ETFBR parameters such as applied voltage, current and resistance. Electrode configuration has a significant effect on the temperature profile which can affect the selectivity and even operational security of the process. ETFBR is a promising technology for high-temperature endothermic reactions.

[1] S. Fedorov *et al.*, “Ultrahigh Temperature Continuous Reactors Based on Electrothermal Fluidized Bed Concept J Fluids Eng April 2016.” Apr. 29, 2016.
[2] T. Knowlton, “Components of interelectrode resistance in an electrofluid bed reactor,” Jan. 1971, Accessed: Feb. 08, 2023. [Online]. Available: https://www.academia.edu/68884089/Components_of_interelectrode_resistance_in_an_electrofluid_bed_reactor
[3] I. Abba, J. Grace, H. Bi, and M. Thompson, “Spanning the flow regimes: Generic fluidized-bed reactor model,” *AIChE J.*, vol. 49, pp. 1838–1848, Jul. 2003, doi: 10.1002/aic.690490720.
[4] K. Karan, A. Mehrotra, and L. Behie, “Thermal Decomposition Of Carbonyl Sulfide At Temperatures Encountered In The Front End Of Modified Claus Plants,” *Chem. Eng. Commun. - CHEM ENG COMMUN*, vol. 192, Jan. 2005, doi: 10.1080/00986440590477764.

Keywords

Electrothermal fluidized bed reactor; Joule heating; Electrical resistance; COS decomposition

Acknowledgements

This research is being supported by the project e-CODUCT under Horizon Europe Agreement No. 1012058100.

PD – 2

Techno-economic analyses of NETmix-based facilities for the production of CO_2 hydrates

Isabel S. Fernandes[1,2], Mariana G. Domingos[3] , Marcelo F. Costa[3], Ricardo J. Santos[1,2] , José C. B. Lopes[1,2]*

1 LSRE-LCM - Laboratory of Separation and Reaction Engineering – Laboratory of Catalysis and Materials, Faculty of Engineering, University of Porto, Rua Dr. Roberto Frias, 4200-465 Porto, Portugal Affiliation and address; 2 ALiCE - Associate Laboratory in Chemical Engineering, Faculty of Engineering, University of Porto, Rua Dr. Roberto Frias, 4200-465 Porto, Portugal; 3 CoLAB NET4CO2, Rua Júlio de Matos, 828-882, 4200-355 Porto, Portugal

**Corresponding author: lopes@fe.up.pt*

Highlights

- NETmix surpasses most state-of-the-art technology for mass and heat transfer.
- Hydrate formation occurs in low-temperature and high-pressure environments.
- Heat integration was considered to reduce the energy requirement of the processes.
- NETmix-based facilities have the potential to contribute to solve critical societal challenges.

1. Introduction

The formation of CO_2 hydrates (clathrates) requires mixing two phases: CO_2 and water within temperatures ranging from 0 to 10 ºC and pressures ranging from 10 to 60 bar. These hydrates are solid water cages where CO_2 is trapped and are stable in deep ocean conditions; therefore, they are a great technology for CO_2 storage. Applications for CO_2 hydrates include Carbon Capture and Storage (CCS) and seawater desalination. Hence, hydrate-based technologies can address two societal challenges: global warming and drinking water scarcity.

Hydrate formation is a strong exothermic process. The enclathration of CO_2 releases around 1.5 $\text{GJ}\cdot\text{tonne CO}_2^{-1}$ [1]. This is quite critical for hydrate production, where low temperatures are needed. Besides, it is necessary to ensure that a considerable amount of guest compound is enclatherated in water cavities for hydrate stability. NETmix is a mesosized mixer introduced and patented in 2005 at the University of Porto NETmix [2], consisting of a network of mixing chambers interconnected by channels. Due to its outstanding mass and heat transfer capabilities, NETmix has been the core technology of the Collaborative Laboratory NET4CO2 for the continuous production of CO_2 hydrates and synthetic fuels [3]. This work intended to develop process simulators in Aspen Plus that integrate NETmix technology for the production of CO_2 hydrates for three applications: CO_2 transportation via pipeline, seawater desalination and CO_2 capture from a post-combustion technology. The objective is to optimise the flowsheet design to minimise energy requirements, introducing efficient technologies.

2. Methods

Aspen Plus does not include built-in property methods capable of predicting hydrate formation. Thus, an in-depth analysis of available properties methods was done to ensure that realistic models were used to predict the properties of the components and mixtures. The formation of hydrates requires a supersaturated environment; therefore, an accurate prediction of CO_2 solubility is crucial. The performance of different thermodynamic models in estimating the CO_2 solubility in water, seawater and in the presence of N_2 was evaluated. Another key step was the implementation of the unit process where the formation of hydrates occurs. The mass and energy balances and the reactor's experimental operational data were implemented using a User-block function. After building the processes in Aspen Plus, the heat sources and sinks were identified to enhance energy integration and reduce operating costs. The operating and capital costs were estimated and compared with conventional solutions.

3. Results and discussion

CO_2 preparation for pipeline transportation

The process flow diagram of the industrial facility modelled for the preparation of 100 tonne $CO_2 \cdot h^{-1}$ for continuous production of a hydrate slurry for pipeline transportation is shown in Figure 1.

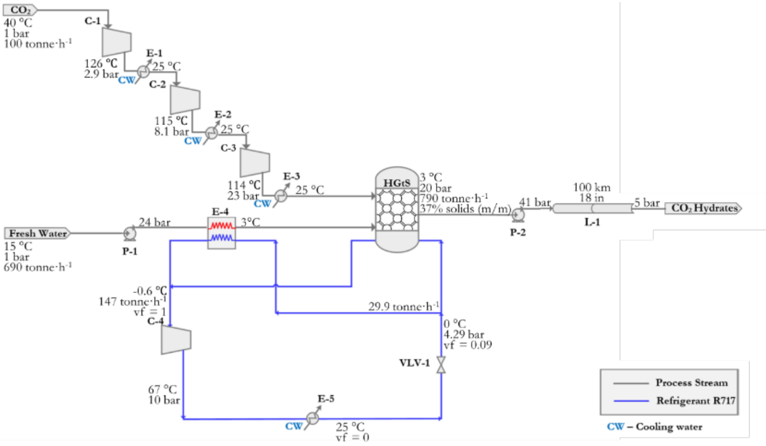

Figure 1. Process flow diagram of CO_2 hydrates production and pipeline transportation.

The CO_2 preparation for pipeline transportation is an attractive option in terms of safety as it requires smaller operation pressure than the conventional method (CO_2 transportation in supercritical conditions). However, the estimated cost is about 55 % higher for the hydrates scenario due to the low-temperature environment required for CO_2 hydrate formation.

Seawater desalination

Hydrate-based desalination modelling showed that using the regasification heat of Liquefied Natural Gas (LNG) as cold utility, replacing the refrigeration units, permits producing drinking water with a specific energy consumption of ~3.8 $kWh \cdot m^{-3}$, which is in the same range as reverse osmosis (3-4 $kWh \cdot m^{-3}$), the current leading desalination process.

CO_2 capture

The cost analysis of the hydrate-based CO_2 separation process from a post-combustion flue gas stream showed that this method can be economically competitive compared to the conventional amine-based capture process. The electricity needed to operate an electric boiler to provide the required heat in the reboiler for amine regeneration is in the same range as the values obtained for operating all hydrate-based CO_2 separation process.

4. Conclusions

Process simulators were successfully developed in Aspen Plus to model the production of CO_2 hydrates using NETmix technology. The techno-economic analyses enabled to conclude that hydrate-based technologies have a large potential to contribute to solutions to solve global problems. Still, it is necessary to pursue studies to deepen the knowledge of the technology, mainly at an experimental level, to validate the numerical data. The use of thermodynamic promoters that moderate hydrate formation conditions, which increase the hydrate formation equilibrium temperature and reduce the operating pressure, should be evaluated principally for CO_2 preparation for pipeline transportation and CO_2 capture.

References

[1] G.K. Anderson, Enthalpy of dissociation and hydration number of carbon dioxide hydrate from the Clapeyron equation, J. Chem. Thermodyn. 35(7) (2003) 1171-1183.

[2] J.C. B. Lopes, P.E. M. S. C. Laranjeira, M. M. G. Q. Dias, A.A.A. Martins, Network mixer and related mixing process, US 8434933 (2013).

[3] M.F. Costa, C.M. Teixeira, A.M. Lopes, J.P. Araújo, M.M. Dias, R.J. Santos, J.C.B. Lopes, Carbon Capture and Storage Toward Industrialization: A Novel Continuous Process for the Production of Carbon Dioxide Clathrates, Energy Technol. (2022).

Keywords

CO_2 hydrates; process integration; NETmix; economic evaluation

POSTER SESSION

Poster 1: Process intensification for ammonia synthesis – Analyzing the potential of in situ product removal for high single-pass conversion

Theresa Kunz[1], Johannes Geri, Robert Güttel[1]*

1 Institute of Chemical Engineering, Ulm University, 89081 Ulm, Germany

**Corresponding author: robert.guettel@uni-ulm.de*

Highlights

- Steady-state and dynamic reactor models for sorption-enhanced ammonia synthesis are developed
- Simulations show that virtually full single-pass conversion is reachable under relevant conditions
- Full single-pass conversion supersedes reactant recycling and purging losses

1. Introductionntroduction

Conventional ammonia synthesis usually suffers from low single-pass conversion due to thermodynamic limitations that arise from high temperatures used to achieve relevant reaction rates [1, 2]. The low conversion results in extensive recycling of reactants and considerable purging losses, which significantly decreases the overall efficiency of the process [2, 3]. Strategies to overcome those boundaries and enhance the single-pass conversion include process intensification approaches like the integration of ammonia synthesis and separation by absorption into one vessel, i.e. sorption- enhancement [1, 3]. As sorbent materials, mainly metal halides like $MgCl_2$ or $MnCl_2$ are discussed in literature, as they show relevant ammonia sorption capacity even at high temperatures of > 300 °C [1]. In this work, we aim at identifying process conditions under which significantly increased or even full single-pass conversion is thermodynamically possible, but also achievable kinetically using Fe- or Ru- based catalysts. To determine the simultaneous equilibrium of ammonia synthesis and absorption in metal chlorides, a novel equilibrium model based on Gibbs energy minimization is developed. Kinetic simulations are performed additionally to evaluate to what extent the thermodynamic potential of sorption-enhanced ammonia synthesis can be exploited under realistic process conditions. For this purpose, steady-state and dynamic reactor models are developed.

2. Methods Equilibrium calculations are performed using Gibbs energy minimization. To include the sorption equilibrium, Gibbs energies of formation of the loaded sorbents are obtained by data fitting, as – to the best of our knowledge – this data is not available in literature. For kinetic modeling of the sorption- enhanced ammonia synthesis, both dynamic and steady-state reactor models are developed. In steady- state, an isothermal 1D1D heterogeneous gas-flowing solids-fixed bed reactor (GFSFBR) is considered, where the solid sorbent flows co-currently with the gas phase through the reactor containing the fixed catalyst bed [4]. The polytropic 1D dynamic reactor model considers both the catalyst and the solid sorbent to be fixed inside a tubular reactor. In both reactor models, kinetics for Fe- and Ru-based ammonia synthesis catalysts as well as ammonia sorption kinetics are implemented.

3. Results and discussion Results of both the equilibrium and the steady-state reactor model are shown in Figure 1. The nitrogen conversion achieved in a GFSFBR at stoichiometric reactant ratio is compared to the equilibrium conversion calculated with the equilibrium model at different temperatures, for both the Ru- and the Fe- based catalyst with and without sorbent present in the reactor. Regarding the equilibrium conversion, we observe that it significantly increases in the sorption-enhanced ($\lambda = 1$) case as compared to the conventional ($\lambda = 0$) case, reaching virtually full N_2 conversion over the featured temperature range.

At 50 bar (Figure 1 (a)), equilibrium N_2 conversion is reached in the conventional case without sorbent ($\lambda = 0$) only with the Ru catalyst at almost 400 °C, while equilibrium is not quite reached using the Fe catalyst. In the sorption-enhanced case ($\lambda = 1$), the conversion significantly increases for both catalysts over the entire temperature range, but equilibrium is reached with neither catalyst. It can be observed that the Ru catalyst is much more influenced by both the temperature and the sorbent, as at low temperatures (< 340 °C for $\lambda = 0$ and < 360 °C for $\lambda = 1$), the N_2 conversion is always higher using the Fe catalyst while at higher temperatures, the Ru catalyst becomes more active. Similar behavior is observed by Smith and Torrente-Murciano for the conventional case without sorbent [2]. Here, however, we observe an additional temperature-dependent effect of the sorbent addition on the Ru catalyst, as the N_2 conversion increase due to sorption-enhancement is much stronger at high temperatures, whereas it only slightly increases with temperature for the Fe catalyst. At low temperatures, the addition of the sorbent and thus the removal of ammonia has only a slight effect on the Ru catalyst, while the activity of the Fe catalyst is significantly enhanced. Since N_2 conversion is far from reaching equilibrium at low temperatures, this hints at a kinetic effect. Similar trends can be observed at 100 bar (Figure 1(b)): In the conventional case, the Ru catalyst becomes more active at higher temperatures (> 360 °C) and equilibrium N_2 conversion is reached at 400 °C, while the same is not true for the Fe catalyst. In the sorption-enhanced case, however, equilibrium N_2 conversion, i.e. virtually full conversion, is reached at > 375 °C for both catalysts.

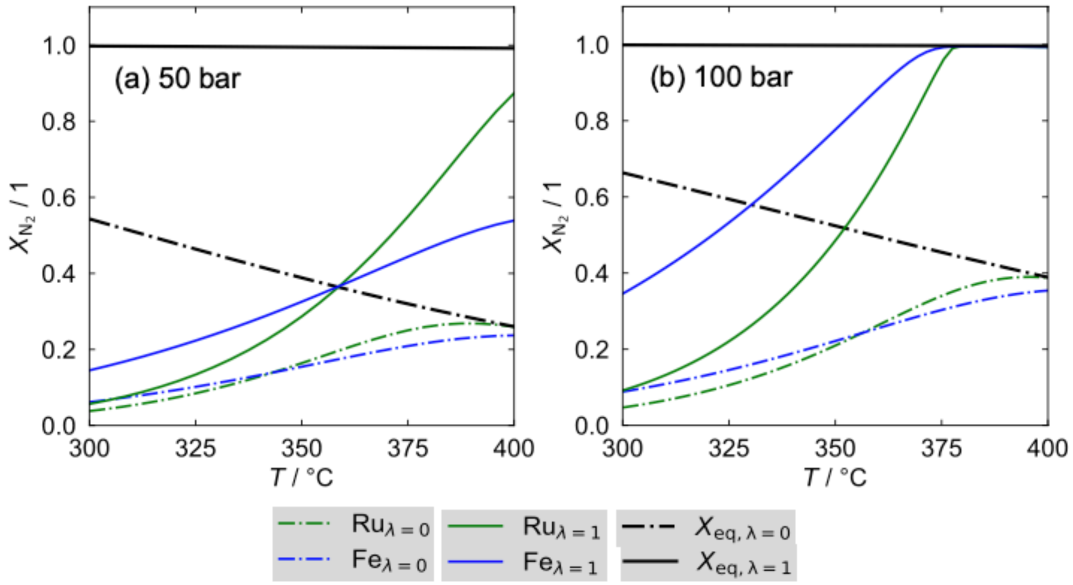

Figure 1. Nitrogen conversion over temperature at (a) 50 bar and (b) 100 bar, on (green) Ru and (blue) Fe-based catalysts without ($\lambda = 0$) and with ($\lambda = 1$) sorbent $MgCl_2$ at $H_2/N_2 = 3$ and 2500 h^{-1}, $\lambda = \frac{n_{MgCl_2}}{n_{NH_3,X_{N_2}=1}}$.

4. Conclusions By including the ammonia sorption equilibrium into an equilibrium model, we can show that virtually full conversion is thermodynamically possible under a wide range of relevant conditions. The potential of sorption-enhanced ammonia synthesis is further substantiated by kinetic modeling considering both steady-state and dynamic reactors. Herewith, we show that conversions much higher than under conventional conditions are reachable not just in equilibrium but using relevant process parameters and realistic residence times. Additionally, ammonia formation especially on Fe-based catalysts is significantly enhanced at low temperatures and conversions well below equilibrium.

References

[1] C. Smith, L. Torrente-Murciano, Adv. Energy Mater. 11 (2021), 2003845
[2] C. Smith, L. Torrente-Murciano, Johnson Matthey Technol. Rev. 66, 4 (2022), 435-442
[3] T. Cholewa, M. Semmel, F. Mantei, R. Güttel, O. Salem, ChemEngineering 6, 13 (2022)
[4] N. Nikačević, M. Jovanović, M. Petkovska, Chem. Eng. Res. Des. 89 (2011), 398-404

Keywords
ammonia synthesis, sorption-enhancement, equilibrium modeling, kinetic modeling

Poster 2: Equations of state: The critical component of supercritical water-hydrocarbon mixtures

Gust Popelier[1], Maarten Sabbe[1], Florence Vermeire[2], Kevin M. Van Geem[1,*]

1) Laboratory for Chemical Technology, Ghent University, Technologiepark-Zwijnaarde 125, Ghent 9052, Belgium; 2) Department of Chemical Engineering, KU Leuven, Celestijnenlaan 200F, 3001 Leuven, Belgium

**Corresponding author: Kevin.VanGeem@UGent.be*

Highlights

- Development of a programming framework for the modelling of phase behaviour
- Development of a variant Equation of State to model the behaviour of supercritical water-hydrocarbon mixtures

1. Introductionntroduction

The goal of recycling 50% of all plastic waste by 2025, set by the European Union, has caused a recent increase in interest in chemical recycling techniques for plastic waste. Chemical recycling is a so-called omnivorous technique, this means that it can take in a mixed plastic waste stream to produce feedstocks that can be used for the production of new plastic materials. This in contrast to mechanical recycling, which requires extensively sorted polymer streams, cannot handle all types of polymers and often produces material that is used in lower-value applications. Pyrolysis is one technique for chemical recycling, here the plastic waste is degraded at high temperatures to form a liquid oil that can be sent to the refinery/cracker to produce new base chemicals. However plastic waste comes with many contaminants that need to be removed before the oil can be further processed, this is often done through expensive post treatments such as hydrotreatment, making the overall process uneconomical.

A new form of pyrolysis makes use of supercritical water (SCW), i.e., water at high pressures and temperatures. Under these conditions water is able to dissolve relatively long hydrocarbon chains, up to C26 or higher, which results in a two-phase system of a polymer melt diluted with water and an aqueous phase with dissolved hydrocarbon chains. The polymer melt is diluted compared to classical pyrolysis, suppressing bimolecular reactions that result in coke formation. While the aqueous phase is more dense than the gas phase in classical pyrolysis, enhancing bimolecular reactions resulting in less gas formation and a higher liquid yield. These effects combined with the ability of water to remove heteroatomic organic contaminants results in a much cleaner oil with higher liquid yields and a lighter cut compared to classical pyrolysis. Since these effects are heavily dominated by the phase separation of the polymer melt and the aqueous phase, it is important to fundamentally understand the behaviour of water-hydrocarbon mixtures at these conditions. A thermodynamic model is developed to predict this phase behaviour along with the numeric methods required for its verification.

2. Methods

The basis of phase behaviour prediction is often an Equation of State (EoS), this is an equation that is able to describe a mixture's behaviour at varying temperatures, pressures and composition. From this relation properties such as the chemical potential can be derived which allow the determination of the mixtures phase behaviour. Very few Equations of State have been designed to predict the behaviour of supercritical mixtures. Additionally, mixtures of strongly associating compounds and non-associating compounds such as water-hydrocarbon mixtures are notoriously difficult to model [1]. One attempt has been made to model water-hydrocarbon mixtures with a focus on the supercritical domain through the use of the PPR78 EoS[2]. This EoS uses a temperature dependent binary interaction parameter (BIP) obtained via a group contribution scheme to characterise the interactions between water and the hydrocarbons. This EoS is relatively successful in predicting the phase behaviour of water-hydrocarbon systems at supercritical conditions, yet the authors mention that some form of composition dependence of the BIP is required for a more complete description of the behaviour.

The composition dependence of the BIP of water-hydrocarbon mixtures is likely related to the associating behaviour of water. Analogously to the Cubic plus Association EoS a SAFT-like associating term is combined with the PPR78 to result in a model that is capable of describing the complex hydrogen bonding interaction of water [3]. The constructed thermodynamic model is validated against experimental data, with a focus on predicting critical points and behaviour at supercritical conditions.

3. Results and discussion and discussion

Using the programming framework developed in this work the PPR78 Equation of State was reproduced and used for the prediction of phase separation, three-phase equilibria and critical points. Specifically for finding three-phase equilibria and critical points several new algorithms had to be developed to obtain stable convergence. The PT-projection of the binary phase diagram of water-octane and water-benzene as predicted by the Equation of State are shown in Figure 1. The critical lines predicted by the Equation of State, correspond roughly with the critical points detected experimentally. Specifically, the minima detected in the critical lines of benzene clearly show its better interaction with SCW compared to a linear alkane such as n-octane. Currently, obtaining an improved fit of one critical line has a detrimental effect on the fit of the other critical line, but this is expected to improve when the associating character of water is incorporated into the Equation of State.

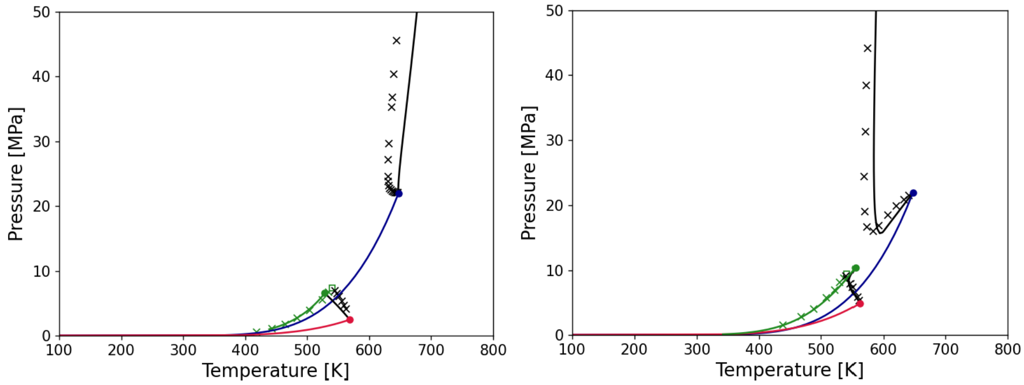

Figure 1.. PT-projection of the phase diagram of water-octane (left) and water-benzene (right). Showing the three-phase line (green), water vapor-liquid line (blue), hydrocarbon vapor-liquid line (red) and critical lines (black)

4. Conclusions A programming framework was developed to predict properties of fluids and fluid mixture based on equations of state. This include predicting phase separation, three-phase equilibria and the presence and location of critical points.

Acknowledgments Gust Popelier acknowledges the Fund for Scientific Research Flanders (FWO) for financial support via doctoral fellowship grant 1S58323N.

References

1. Piña-Martinez, A., Privat, R., Nikolaidis, I. K., et al. “What Is the Optimal Activity Coefficient Model To Be Combined with the translated–consistent Peng–Robinson Equation of State through Advanced Mixing Rules? Cross-Comparison and Grading of the Wilson, UNIQUAC, and NRTL aE Models against a Benchmark Database Involving 200 Binary Systems,” *Industrial & Engineering Chemistry Research*, V. 60, No. 47, 2021, pp. 17228–47.
2. Qian, J.-W., Privat, R., and Jaubert, J.-N. “Predicting the Phase Equilibria, Critical Phenomena, and Mixing Enthalpies of Binary Aqueous Systems Containing Alkanes, Cycloalkanes, Aromatics, Alkenes, and Gases (N2, CO2, H2S, H2) with the PPR78 Equation of State,” *Industrial & Engineering Chemistry Research*, V. 52, No. 46, 2013, pp. 16457–90.
3. Kontogeorgis, G. M., Voutsas, E. C., Yakoumis, I. V., et al. “An Equation of State for Associating Fluids,” *Industrial & Engineering Chemistry Research*, V. 35, No. 11, 1996, pp. 4310–8.

Keywords

Keywords

Equations of State, Supercritical water, Phase behaviour

Poster 3: Modeling of Baker's Yeast and Ethanol Production by Saccharomyces Cerevisiaeiae

Elio Santacesaria[1]*, Riccardo Tesser[2], Martino Di Serio[2]

1 Eurochem Engineering Ltd, Via Codogno 5 (20139) Milano, Italy; 2 NICL - Department of Chemical Sciences, University of Naples Federico II, 80126 Naples, Italy

**Corresponding author: elio.santacesaria@eurochemengineering.com*

Highlights

- Modelling aerobic Saccharomyces Cerevisiae growth to obtain Bakers'yeast.
- Modelling anaerobic Saccharomyces Cerevisiae growth to obtain Ethanol.
- Review of the most performant kinetic model.

1. Introduction

Several million tons of fresh baker's yeast cells are produced yearly in the world for human food use. Bioethanol is known as the most widely used biofuel with a today production of more than 100 billion liters. Saccharomyces Cerevisiae is fundamental for both the mentioned industrial productions. Saccharomyces Cerevisiae is a facultative microorganism that grows in both anaerobic and aerobic conditions. The first condition is normally adopted for producing, in a satisfactory yield, ethanol, while the second one is adopted in the production of bakers' yeast. In both cases, the growth rate and the nutrient consumption are affected by the type of available strain and by the composition of the nutrient mixture. Therefore, any kinetic model (related to gas-liquid-solid multiphasic system) before the use for predictive simulation or overall process optimization needs to be tested in a preliminary experimental batch run at the scope of determining the kinetic parameters that are characteristic of the used couple "cells strain-substrate". Then, these parameters can be used for simulating other types of reactors, such as fed-batch or continuous reactors, and for the scale-up provided that the same cell strain and substrate composition are used. Many kinetic models have been proposed in the literature describing the behavior of Saccharomyces Cerevisiae in the bakers' yeast or for ethanol production in laboratory bioreactors, but few have been tested for the description of industrial-size bioreactors. A review of the most recent progress in this field would be one of the scopes of this work. One of the proposed models defined Cybernetic Model, first proposed by Kompala and Ramkrishna [1] improved and successfully applied by Di Serio et al. [2] has given very satisfactory results in simulating baker's yeast production in bioreactors of different sizes from the laboratory to the industrial scale reactors and we start from this model as a reference point for the review. Moreover, in the present work, the use of the Cybernetic model will be extended also to the simulation of bioethanol production.

2. Methods Modeling the growth behavior of Saccharomyces Cerevisiae requires a detailed knowledge of the intracellular control mechanisms. The metabolism of Saccharomyces Cerevisiae is characterized by 3 metabolic pathways, that are:

(1) Sugar fermentation $\text{Sugar} \longrightarrow \text{Ethanol} + CO_2$
(2) Sugar oxidation $\text{Sugar} + O_2 \longrightarrow CO_2 + H_2O$
(3) Ethanol oxidation $\text{Ethanol} + O_2 \longrightarrow CO_2 + H_2O$

A simplification of this problem can be achieved, for example, by using a cybernetic viewpoint. The cybernetic modeling framework is based on the hypothesis that microorganisms optimize the utilization of available substrates/nutrients to maximize their growth rate. The detailed regulatory processes of the cells are replaced by two cybernetic variables u_i and v_i representing, respectively, the optimal strategies for enzyme synthesis and activity. According to Kompala and Ramkrishna [1] the value of u_i can be assessed assuming that cell resources will be allocated in such a way as to obtain the maximum biomass growth rate The variable controlling the inhibition/activation mechanism of the "key" enzyme i-th (v_i) is determined considering a null inhibition effect when the microorganism grows on the substrate which accelerates the biomass growth rate to the utmost, whereas the inhibition effect progressively increases at decreasing growth rate [3]. Therefore:

$$u_i = \frac{r_i}{\Sigma r_j} \qquad v_i = \frac{r_i}{max_J(r_J)}$$

The specific growth rates for the different metabolic pathways are modeled according to a modified Monod rate equation, where the modification consists in the fact that each growth rate r_i has been assumed proportional to $e_i/e_{i,max}$, the relative intracellular "key" enzyme concentrations :

$$r_1 = \mu_{1,\max} \frac{e_1}{e_{1,\max}} \frac{Z}{K_1 V_L + Z} \qquad r_2 = \mu_{2,\max} \frac{e_2}{e_{2,\max}} \frac{E}{K_2 V_L + E} \frac{Ox}{K_{ox} + Ox} \qquad r_3 = \mu_{3,\max} \frac{e_3}{e_{3,\max}} \frac{Z}{K_3 V_L + Z} \frac{Ox}{K_{ox} + Ox}$$

Z and E are respectively the quantity of sugars ethanol that can be metabolized in the bioreactor; Ox is the concentration of dissolved oxygen, V_L is the volume of the liquid in the bioreactor. $\mu_{i,max,}$ and K_i represent the maximal specific growth rate and the saturation constants for the substrate of each metabolic pathway i. K_{ox} is the saturation constant for the dissolved oxygen which is independent of any single oxidative metabolic pathway. With these growth rate equations, the balance equations for batch ($F_{in} = 0$) and fed-batch ($F_{in} \neq 0$) bioreactors can be written as an ODEs system of 8 differential equations considering the balances of respectively: biomass, sugar, ethanol, liquid volume, the concentration of oxygen in the liquid phase and the relative concentrations of the enzymes promoting the three different metabolic pathways.

3. Results and discussion

An example of obtained simulations [3] in a batch bioreactor, by using optimized model parameters, can be appreciated in Figure 1. As can be seen, the cybernetic model can reproduce correctly both the lag-phase and the diauxic growth of the microorganism, the last occurring when the energy source becomes ethanol instead of sugar. Many experimental runs have been simulated demonstrating the predictive ability of this model and the obtained results will be compared with the ones of other models more recently proposed in the literature.

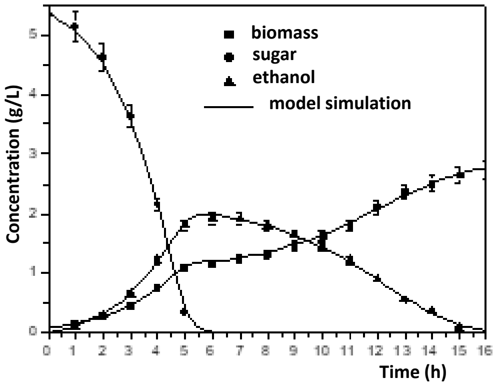

Figure 1.. An example of batch run simulated by the Cybernetic Model [3]. Points are experimental data.

4. Conclusionss

As seen, the described cybernetic model works well in predicting the Saccharomyces Cerevisiae behavior for the production of baker's yeast in any type of bioreactor. As a first element of novelty, the use of this model will be extended to the optimization of ethanol production. A second element of novelty will be a critical review of the kinetic models, more recently proposed in the literature, with a useful comparison of their performances.

Referenceseferences

[1] D.S. Kompala, D. Ramakrishna, N.B. Jansen, G. T. Tsao, Biotechnol- Bioeng. 28 (**1986**) 1044-1055

[2] M. Di Serio, R. Tesser, E. Santacesaria, *Chem. Eng. J.*, 82 (**2001**) 347-354.

[3] M. Di Serio, P. Aramo, E. De Alteriis, R. Tesser, E. Santacesaria,Ind. Eng. Chem. Res. 42 (**2003**) 5109-5116

Keywords

"Bakers' yeast"; "Ethanol"; "Saccharomyces Cerevisiae"; "Modelling".

Poster 4: Intelligent Catalyst Carrier Concept with Reversible Wall Contact in Tubular Reactors for an Improved Wall Heat Transferat Transfer

Dominik Rudolf*, Hannsjörg Freund

TU Dortmund University, Institute of Reaction Engineering and Catalysis,

Emil-Figge-Str. 66, 44227 Dortmund, Germany

**Corresponding author: dominik.rudolf@tu-dortmund.de*

Highlights

- Novel concept of periodic open cellular structures is realized for a reversible tube wall contact.
- The structures combine the design of auxetic behavior with the shape memory effect of NiTi alloy.
- Estimation of the effective wall contact and analysis of heat transfer based on a 2D model.

1. Introductionntroduction

Periodic open cellular structures (POCS) are additively manufactured, grid-like structures that are used as novel catalyst support structures. POCS are built up from a unit cell that is repeated in all three spatial directions. Metallic structures exhibit high thermal conductivity due to the continuous solid matrix [1]. However, previous work has identified solid contact between the structure and the reactor tube wall as an essential factor for heat transfer [2].

In order to intensify the heat transfer, but also take into account the deactivation of heterogeneous catalysts and thus the necessity of an exchange of the POCS, the aim is to realize a reversible wall contact of POCS in tubular reactors. In this work, we propose to exploit an auxetic behavior of POCS as a promising option for this purpose. Auxetic structures exhibit a negative Poisson's number under mechanical load [3]. The principle involves designing an auxetic POCS with radial oversize, catalytic coating, compression and insertion of the POCS into the tubular reactor. If the structure is manufactured from a shape memory alloy, the POCS regains its original shape by a temperature increase, and thus a wall contact is established by an interference fit. In this regard, the high flexibility of additive manufacturing is utilized in the design and manufacturing of such POCS as intelligent catalyst carrier concept.

2. Methods

There are many ways to design POCS in order to provide for an auxetic behavior. In this work, we focus on highly anisotropic structures where the auxetic effect is based on the reentrant mechanism [3]. Further, a hexagonal cell design in the tube's cross section ensures a good radial fit in general. Figure 1 shows a reentrant hexagonal POCS, as-built from the shape memory alloy NiTi (Nitinol) via powder bed fusion electron beam melting, along with the planar projection of the POCS mounted in a tube as a sketch. In order to characterize the heat transport properties of these POCS, experiments are conducted using a double tube heat exchanger. In this inert system, cold air flows through the inner tube, where the POCS is installed. Operated with thermal oil, the outer jacket serves as heat source and the resulting temperature profiles in the inner tube are recorded at steady state.

The total scope of investigation comprises eight auxetic POCS made of Nitinol, differing in the three characteristic geometrical parameters cell size, strut diameter and amplitude of the curved struts (cf. Figure 1). The latter describes an eigenmode of the hexagonal cellular x-y-plane with oscillation in z-direction that is responsible for the auxetic effect [3]. Moreover, specific reference measurements are conducted:

i. Identical auxetic POCS made of Nitinol are tested with a loose fit, i.e., the usual POCS application.
ii. Auxetic POCS were manufactured along with the inner tube in the same process, using Ti-6Al-4V. These setups with a predefined, complete solid wall contact provide comprehensive

reference measurements.

The experimental data are analyzed based on a 1D model. For varying flow rates of air, the derived overall heat transport coefficient serves as a quantity for comparison.

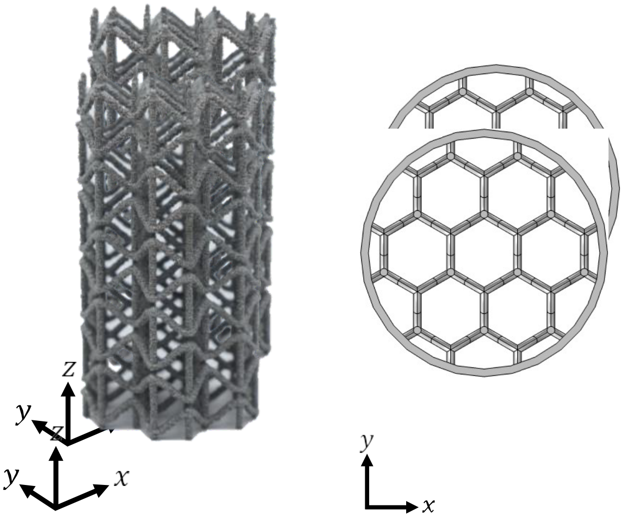

FigFigure 1.. Reentrant hexagonal POCS, additively manufactured from Nitinol via powder bed fusion electron beam melting (left), planar projection of the tube's cross section (right).

3. Results and discussion The reference measurements provide proof of concept and we are able to estimate the effective wall contact as a quantitative parameter. Subsequently, this parameter can be implemented in a 2D heat transfer model. Here, dependencies of the heat transport parameters on geometrical parameters are identified and correlated. Especially the extent of the amplitude exhibits a high influence on the fluid dynamics, and hence on the convective heat transport.

4. Conclusions The initially proposed concept of using the design freedom of additive manufacturing to combine structural properties with a unique material property was realized in the form of auxetic, reentrant hexagonal POCS, manufactured from the shape memory alloy Nitinol. In this work, it is demonstrated that heat transfer in tubular reactors can be intensified via a reversible contact of POCS and the tube wall. Moreover, it will be possible to easily exchange the catalyst carrier structure in case of catalyst deactivation. Furthermore, the influences of the geometrical parameters on the heat transport are revealed by an analysis applying a 2D heat transport model.

Referencesferences

[1] E. Bianchi, W. Schwieger, H. Freund, Adv. Eng. Mater. 18(4) (2016) 608-614
[2] C. Busse, H. Freund, W. Schwieger, Chem. Eng. Process. Process Intensif. 124 (2018) 199-214

[3] C. Körner, Y. Liebold-Ribeiro, Smart Mater. Struct. 24(2) (2015) 025013

Keywords

Keywords

Structured catalyst supports; additive manufacturing; process intensification.

Poster 5: Epoxidation of tall oil in the presence of metal doped SBA15 heterogeneous catalysts

Tommaso Cogliano[1], Angie Desgouliere[2], Wander Perez Sena[1], Kari Eränen[1], Vincenzo Russo[1,3], Laurence Pirault-Roy[2], Tapio Salmi[1]*

1 Laboratory of Industrial Chemistry and Reaction Engineering (TKR, Åbo Akademi, FI-20500 Turku/Åbo;

2 Institute of Environmental and Materials Chemistry (IC2MP, Université de Poitiers, F-86073 Poitiers;

3 Department of Chemical Sciences, Università di Napoli "Federico II", IT-80126 Napoli

**Corresponding author: tapio.salmi@abo.fi*

Highlights

- Tall oil as raw material to produce value-added compounds.
- Screening of metal-doped SBA-15 catalysts.
- Catalysts synthesis, characterization and catalytic experiments.
- Activity performances of the different catalysts proposed.

1. Introductionntroduction

Epoxidized vegetable oils (EVOs), thanks to the highly reactive epoxy group are excellent molecular platforms. EVOs have already been used to obtain polyols, carbonates and plasticizers [1]. In industrial scale, epoxidation of vegetable oils is carried out in semi-continuous mode via the Prilezhaev process, where an added carboxylic acid (formic or acetic acid) acts as the reaction carrier. The carboxylic acid reacts with the oxidant, hydrogen peroxide giving the corresponding a percarboxylic acid, which acts as the oxidant agent by shuttling an oxygen atom from the polar aqueous medium to the organic apolar one [2]. Despite its wide application, the process suffers from several drawbacks due to the use of homogeneous mineral acids to catalyze the formation of the percarboxylic acid, as well as a low selectivity toward the target product, demanding separation steps and corrosion of the reaction and separation equipment. To overcome these problems, alternative reaction pathways are explored. The most studied reaction routes include the presence of peroxides, namely hydrogen peroxide, and heterogeneous catalysts, i.e., either metal-based catalysts or enzymes [3,4]. The advantages in using heterogeneous catalysts are mainly related to the easier separation step and the absence of corrosion problems. In the epoxidation via peroxides, the oxidant takes directly part in the epoxidation reaction, promoted by the heterogeneous catalyst, and does not donate the oxygen to a carrier. Thus, differently from the Prilezhaev method, the perhydrolysis reaction step is avoided which produces a hazardous chemical and, according to the literature, is the rate-determining step in the epoxidation via the Prilezhaev concept [3]. In the present project, we have focused our attention on the epoxidation of tall oil, a non-edible Scandinavian raw material originating as a high-value by-product from Kraft pulping process. Tall oil is rich in unsaturated fatty acids, such as oleic, linoleic and linolenic acids. Hydrogen peroxide was used as the oxidizing agent in the presence of heterogeneous catalysts. The catalysts were all SBA15 doped with different metals. The aim was to analyze the main and side products of the reaction and to find the best catalyst in terms of activity and selectivity.

2. Methods

The solid catalysts were synthetized with a nominal Si/M ratio equal to 5, following the procedure reported by Zhao et al. [5], where the deposition of the metal was done in-situ along the synthesis of the support, namely SBA15. The steps consisted of dissolution of the triblock copolymer (Pluronic 123) in a HCl solution under vigorous stirring at 40°C; addition of the metal precursor and tetraethyl orthosilicate (TEOS). The solution was kept under vigorous stirring at 40°C for 24 h, transferred in a PP bottle and aged in an oven for 24 h at 100°C. After filtration under vacuum, the solid material was dried in an oven at 100°C for 24 h and calcination up to 550°C. The catalytic experiments were carried out in a semi-batch experimental apparatus. In a typical experiment, the semi-batch reactor was at first filled with a certain amount of tall oil and the solvent, acetonitrile (ACN). Next, by mixing the reaction media, the system was brought to the operating temperature. At the desired temperature, the catalyst was carefully added to the reactor. Finally, hydrogen peroxide was fed into the reaction system with the aid of a syringe pump. Samples were periodically withdrawn from the reaction system and analyzed with ^{1}H-NMR (double bonds, epoxy groups, ring-opening products) and the Greenspan and Mackellar method (hydrogen peroxide) [6,7]. The set of catalysts was characterized through different techniques, such as SEM, XRD, XPS and nitrogen physisorption to understand and correlate the behavior of the different catalysts in the catalytic experiments. Finally, after selecting the best catalyst among the screened ones, a set of experiments was devoted to find the best operating conditions.

3. Results and discussionts and discussion

All the screened catalysts had according to the SEM analysis the typical fiber-like structure of SBA-15. Thus, the deposition of the metal did not affect the structure, which was also confirmed by XRD analysis. Furthermore, from nitrogen physisorption results it was possible to appreciate that all the catalysts presented the typical mesoporous distribution. Among the different catalysts screened, Mo-, Ti- and V-SBA-15 showed a good degree of activity. However, all these catalysts were not selective at all but preferred the consecutive reaction, namely ring-opening of the epoxide. Mn-SBA-15 showed a decent activity and a good selectivity to the target product even after 24 h reaction time.

4. Conclusions

An investigation on the activity and selectivity of a set of metal-doped SBA-15 catalysts was performed in the epoxidation of vegetable oil. Among the catalysts, Nb- and Co-SBA-15 mainly promoted the H_2O_2 decomposition, being useless for the present purpose, whereas Mo-, Ti- and V-SBA-15 gave a good double bond conversion both after 8 and 24 h of reaction. However, the epoxide selectivity was very low preferring side reactions, i.e., ring-opening processes. Finally, Mn-SBA-15 showed a discrete degree of conversion and selectivity at 8 h of reaction. Further experiments were conducted using this catalyst and varying the operating conditions to identify the best ones to maximize the selectivity. In order to understand the reason behind these results, extensive catalyst characterization was performed.

Referencesferences

[1] B.R.Moser, S.C. Cermak, K. M. Doll, J. A. Kenar, B. K. Sharma, A review of fatty epoxide ring opening reactions: Chemistry, recent advances, and applications, Journal of the American Oil Chemists' Society 99(10) (2022) 801-842

[2] E. Santacesaria, R. Tesser, M. Di Serio, R. Turco, V. Russo, D. Verde, A biphasic model describing soybean oil epoxidation with H_2O_2 in a fed-batch reactor, Chemical Engineering Journal, 173(1) (2011) 198-209

[3] W. Yan, Z. Wang, C. Luo, X. Xia, Z. Liu, Y. Zhao, F. Du, X. Jin, Opportunities and Emerging Challenges of the Heterogeneous Metal-Based Catalysts for Vegetable Oil Epoxidation, ACS Sustainable Chemistry & Engineering, 10(23) (2022) 7426-7446

[4] T. Salmi, A. Freites Aguilera, P. Lindroos, L. Kanerva, Mathematical modelling of oleic acid epoxidation via a chemo-enzymatic route–From reaction mechanisms to reactor model, Chemical Engineering Science, 247 (2022) 117047

[5] D. Zhao, J. Feng, Q. Huo, N. Melosh, G. H. Fredrickson, B. F. Chmelka, G. D. Stucky, Triblock copolymer syntheses of mesoporous silica with periodic 50 to 300 Ångström pores, Science 279(5350) (1998) 548-552

[6] T. Cogliano, R. Turco, V. Russo, M. Di Serio, R. Tesser, 1-H-NMR-based analytical method: A valid and rapid tool for the epoxidation processes, Industrial Crops and Products, 186 (2022) 115258

[7] F.P. Greenspan, D.G. McKellar, Analysis of aliphatic per acids, Analytical Chemistry, 20 (1948) 1061-1063

Keywords

Keywords

Epoxidation reaction, tall oil, heterogeneous catalyst, catalytic experiments.

Poster 6: Thermocatalytic Decomposition of Methane over Innovative Ordered Mesoporous Carbons and Carbon Black.

Simon De Langhe[1], Soroush Zareghorbaei[1], Hilde Poelman[1], Vladimir Galvita[1], Dirk Poelman[2], Joris W. Thybaut[1], Kevin M. Van Geem[1]*

1 Laboratory for Chemical Technology, Department of Materials, Textiles and Chemical Engineering, Ghent University, Ghent 9052, Belgium; 2 LumiLab, Department of Solid State Sciences, Ghent University, Ghent 9000, Belgium

**Corresponding author: kevin.vangeem@ugent.be*

Highlights

- Ordered mesoporous carbon has CMK9 higher space time yield and selectivity to H_2 compared to CBp2000.
- Ordered mesoporous carbons deactivate more rapidly compared to CBp2000.
- FWHM of C_{1s} XPS-peak governing parameter for carbon catalyst activity.

1. Introductionnntroduction

To enhance the cost-effectiveness and competitiveness of methane pyrolysis, it is crucial to develop a catalyst with a high activity per unit volume, high yield of hydrogen, and extended on-stream lifetime. However, the fast deactivation of the catalyst remains a significant challenge due to the substantial accumulation of carbon deposits on the catalyst surface during the methane decomposition reaction. Utilizing carbon catalysts helps to alleviate deactivation concerns attributed to coking, particularly prevalent in metal-based catalysts, as the carbon deposits become part of the catalytically active material, extending the catalyst lifetime. The activity and lifetime of the carbon catalyst, which exists in many different forms, highly depend on the carbon structure, with activated carbons (AC) and carbon blacks (CB) being frequently investigated [1]. Also other carbonaceous materials have been probed, such as carbon nanotubes, graphite, acetylene black, diamond powder, and fullerenes, but yield lower H_2 quantities compared to AC and CB [2]. Studies of Serrano et al. have shown that ordered mesoporous carbons (OMC's) with designated pore structures, i.e., CMK-3 and CMK-5, combine a high specific surface area and pore volume, and are able to accumulate a large quantity of carbon deposits, resulting in highly stable catalysts [3]. Therefore, in this study, innovative OMC's have been synthesized by hard- and soft-templating methods, characterized with N_2-physisorption, SEM-EDX and XPS, and tested alongside carbon black for the thermocatalytic decomposition of methane (TCDM) process in a fixed bed reactor to maximize hydrogen yields and the potentially valuable solid carbon by-product.

2. MethodsMethods

Carbon Black pearls 2000 (CBp2000) were delivered by Cabot Corporation, whereas three novel OMC's were synthesized in-house via the hard- and soft-templating technique. More specifically, for hard- templating, the mesoporous pore system of silica KIT-6 was filled with polymer via incipient wetness impregnation. For CMK8, the pores were completely filled, whereas for CMK9 partial filling was performed. In case of soft-templating, surfactant-stabilized silica colloids were enclosed with resin, resulting in a polymeric composite with a dense network of silica chains. Then, the samples were carbonized under an inert atmosphere, after which the silica material was etched to obtain carbon materials with a negative template structure. BET-surfaces and micro-/mesopore volumes were determined in a Micromeritics Tristar II apparatus. Further, the chemical state of the surface carbon analyzed by XPS (S-Probe Al Kα source, VG Surface Science Instruments). Activity tests were performed at 850°C and atmospheric pressure in a quartz fixed-bed reactor with a thermocouple axially placed inside the catalyst bed, composed of 0.1 g active material and 0.8 g SiC as inert dilute. A constant inlet gas feed of a CH_4/Ar (1:1 on molar basis) was ensured, corresponding to a weight hourly space velocity of 50 h^{-1}. Outlet concentrations of methane and hydrogen were determined by means of a mass spectrometer (Pfeiffer Vacuum OmniStar QMS 301), where argon was used as internal standard. Concentrations of CO, CO_2, C_2H_2, C_2H_6, C_2H_4, C_3H_8, C_3H_6, propyne, n-butane, i-butane, 2-butene and 1,3-butadiene were calculated by use of a Refinery Gas Analyzer (RGA) equipped with one FID- and two TCD-detectors. Here, methane and argon served as internal standards, respectively. Mass balances on carbon were closed within the experimental error range of ±1.5%.

3. Resultssand discussion

Figure 1 displays the space time yield (STY) of H_2 over time for three catalysts (CMK9, CMK8 and CBp2000) relative to the STY of CBp2000 in the TCDM process. Initially, CMK8 exhibits a similar STY compared to CBp2000, but it deactivates more rapidly. After 150 minutes, the STY diminishes to 40% of CBp2000's. Despite this decline, the selectivity towards H_2 remains more stable and drops from 90 to 86%. In contrast, CMK9 initially demonstrates a 30% higher STY than CBp2000. Only after 130 minutes, CBp2000 surpasses CMK9 in H_2 production per unit time and unit catalyst weight. Nonetheless, CMK9 maintains the highest selectivity towards H_2 throughout the entire testing period. Concerning the ethylene-to-ethane ratio, it is noteworthy that CBp2000 initially experiences an increase, stabilizing at a constant ratio of 4.7. Conversely, both CMK8 and CMK9 show a decreasing ethylene-to-ethane ratio, with CMK8 exhibiting a more pronounced decrease among the OMC's.

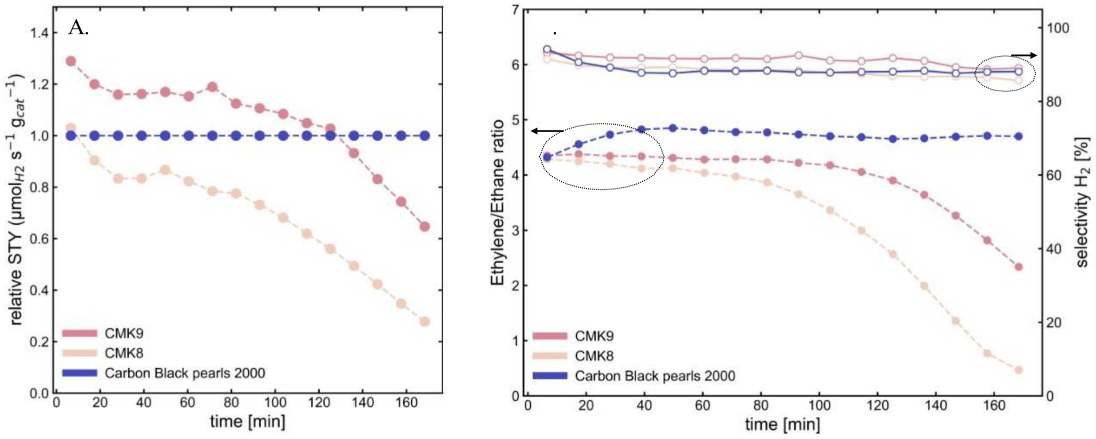

FiFigure 1.. (A.) Relative space time yield (STY) of CMK9, CMK8 and CBp2000 with respect to the STY of CBp2000, and (B.) Ethylene-to-Ethane ratio and selectivity towards to H_2 from methane conversion for CMK9, CMK8 and CBp2000 catalysts. Conditions: 850°C; 1 atm; CH_4/Ar 1:1; WHSV 50 h^{-1}.

N_2-physisorption measurements reveal that CMK9 exhibits a comparable BET-surface and pore volume to CBp2000, while these properties for CMK8 are considerably lower. Additionally, both CMK8 and CMK9 demonstrate a lower micropore-to-mesopore ratio, with values of 0.08 and 0.03, respectively, compared to CBp2000 (0.69). Last, XPS measurements, based on the FWHM of the C1s-peak, indicate that CMK9 possesses the highest number of defects in its carbon structure. These defects in the hexagonal polyaromatic graphene layers, such as mono- and di-vacancies, and Stone-Wales defects offer active sites for the TCDM reaction, which aligns with CMK9 displaying the highest initial STY.

4. Conclusionsnclusions

Based on activity tests, it is shown that the ordered mesoporous carbon CMK9 is a viable catalyst for the TCDM process, as it exhibits a higher initial STY and selectivity to H_2 compared to CBp2000. These results are in line with XPS measurements, showing that CMK9 has the highest number of defects of all three materials. In contrast with the BET-surface, pore volume, and micropore-to-mesopore ratio, the FWHM of the C1s-peak can therefore be considered as governing parameter for the activity of carbon catalysts for the TCDM process.

Referenceseferences

[1] D. P. Serrano, J. A. Botas, J. L. G. Fierro, R. Guil-Lopez, P. Pizarro, and G. Gomez, Fuel, 89, 6, 2010/06/01.
[2] I. Suelves, J. L. Pinilla, M. J. Lázaro, and R. Moliner, Chemical Engineering Journal, 140, 1-3, 2008/07/01.
[3] J. A. Botas, D. P. Serrano, R. Guil-López, P. Pizarro, and G. Gómez, International Journal of Hydrogen Energy, 35, 18, 2010/09/01.

Keywords

ordered mesoporous carbons; carbon black; methane pyrolysis.

Poster 7: Microkinetic analysis of acid gas conversion to COS by zeolite 13X

Raman Ghassemi[1], Soroush Zare Ghorbaei[1], Jeroen Lauwaert[2*], Marco Fabbiani[3], Ludovic Pinard[3], Valentin Valtchev[3], Joris Thybaut[1*]

1 Laboratory for Chemical Technology (LCT), Ghent University, Ghent, Belgium; 2 Industrial Catalysis and Adsorption Technology (INCAT), Ghent University, Ghent, Belgium; 3 Laboratory of Catalysis and Spectrochemistry (LCS), CNRS-ENSICaen-UniCaen, 14000 Caen, France

**Jeroen.Lauwaert@UGent.be; Joris.Thybaut@UGent.be*

Highlights

- Transient modelling of acid gas conversion to COS.
- Microkinetic model can describe the breakthrough times of compounds.
- Kinetic parameters for LHHW model are estimated.

1.Introductionoduction

Carbon dioxide emissions are a major contributor to climate change due to their role in the greenhouse effect. In 2018, global CO_2 emissions had risen to 37.1 Gt, mostly originating from fossil fuel combustion during transportation and industrial production [1]. Hence, the development of CO_2 utilization strategies is crucial to mitigate climate change. Various approaches for CO_2 conversion have been explored such as thermochemical and electrocatalytic technologies. However, currently available technologies for CO_2 conversion require highly pure CO_2 streams while many CO_2 streams contain impurities such as sulphur. Thus, transformation of H_2S containing CO_2 streams while avoiding additional separation steps remains a challenge. The e-CODUCT project aims at promoting an integrated treatment of acid gas streams (CO_2 + H_2S) through a two-step procedure. The first challenge in this respect represents the maximization of COS production from mixed CO_2 and H_2S streams by using zeolites as reactive adsorbents. Second, COS is decomposed into CO as a platform molecule and marketable sulphur in an electrothermal fluidized bed. This work focuses on the first stage of the process by developing a microkinetic model for the reaction of CO_2 and H_2S to produce water and COS on zeolite 13X catalyst. The microkinetic model provides the necessary insight into mechanistic understanding of the reaction which can provide a basis for future reactor and process design.

2. Methods An experimental investigation of acid gas conversion to COS using zeolite 13X is carried out in a fixed- bed reactor. An equimolar flow of H_2S and CO_2, diluted by nitrogen, is fed to the reactor at 45°C and 1.13 bar. The bed is loaded with 4 g of zeolite 13X, which has been pre-treated at 350° C under nitrogen flow.

Elementary-step modeling is conducted using a Langmuir-Hinshelwood-Hougen-Watson (LHHW) reaction mechanism and transient mass balances for gas phase and surface species. The model contains 10 adjustable parameters, i.e., the forward and reverse rate coefficients of the 5 considered steps. The system of equations is numerically solved using the method of lines.

3. Results and discussion Simulation results exhibit a good agreement with the experimental data, see Figure 1a. The model based on the LHHW mechanism can reproduce the breakthrough times of the various components involved. CO_2 is the first component to breakthrough, closely followed by COS. In addition, model adequately describes the CO_2 and COS rollup. The model nicely reproduces the experimentally observed higher retention capacity of the 13X for H_2S. Figures 2b,c,d, and e represent the evolution of active site coverages throughout the reactor length during the time on stream. In the apparent 'steady-state', i.e., after the CO_2 and COS breakthrough and roll-up, most of the active sites are occupied by H_2S and water coverage is slowly increasing, which can lead to the decrease in COS production. Additionally, the plots exhibit a spatial variation in surface coverages along the length of the reactor after pseudo-steady state is reached. At the end of experiment, near the packed-bed inlet, higher water coverages and lower H_2S coverages in comparison to the points closer to the reactor outlet could be observed, which reflects the changing distribution of surface coverages.

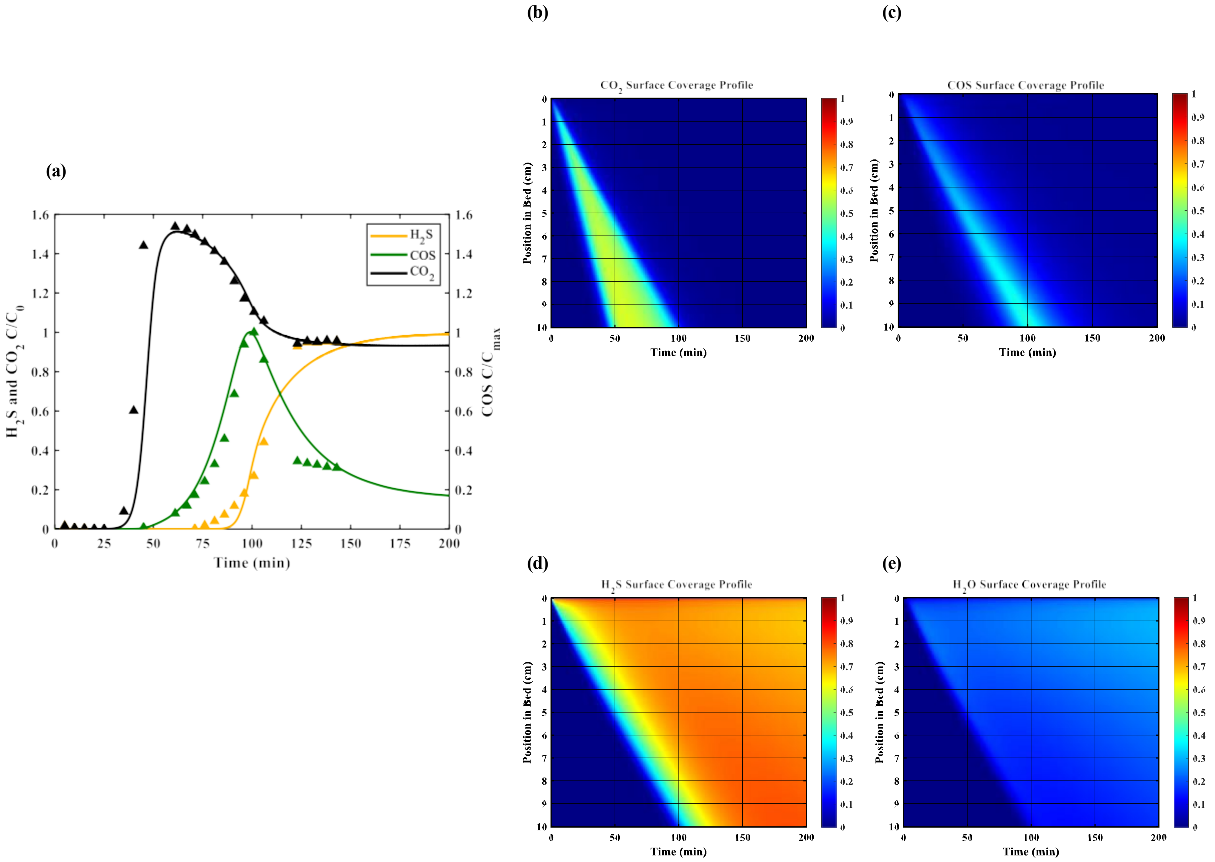

FFigure 1.. Results for the transient LHHW microkinetic model for acid gas conversion over zeolite 13X at 45°C, (a) comparing simulated results (lines) and experimentally obtained values (symbols) for the relative concentrations of H_2S, CO_2, and COS. (b) Surface coverage profile of CO_2, (c) COS, (d) H_2S, and (e) H_2O.

4. Conclusions Kinetic parameters estimated for the LHHW mechanism properly predict the experimental data from the transient fixed-bed reactor, accounting for breakthrough, rollup and pseudo-steady state of the components. The developed microkinetic model contributes to understanding acid gas conversion at a fundamental level and allows process optimization in future development.

References

[1] Z. Zhang, S.Y. Pan, H. Li, J. Cai, A.G. Olabi, E. J. Anthony, V. Manovic, Renew. Sust. Energ. Rev. 125 (2020) 109799

KeKeywords

Microkinetic modelling; Acid gas conversion; Zeolite 13X

Poster 8: Experimental and Numerical Assessment of Radial Thermal Behaviour of Chemical Looping Packed Bed Reactor

Ahmed Aman[1*], Ismaeel Ali[1], Vincenzo Spallina[1]

1 Department of Chemical Engineering and Analytical Science, University of Manchester, Manchester M13 9PL, United Kingdom

**Corresponding author: ahmed.aman@postgrad.manchester.ac.uk*

Highlights

- 2D chemical looping reactor model is validated with experimental results
- Temperature rise at centre of the reactor is twice than at the reactor wall
- Heat losses model calibrated against experimental temperature
- Redox heterogeneous reaction kinetics implemented and validated for Ni-based oxygen carriers

1. Introduction Chemical looping technology has attracted attention from academia and industry as intensified process due to its inherent separation function in the applications of carbon capture and hydrogen production. In this technology, a metal is oxidised with air reacted and then reduced with a fuel such as methane resulting a pure carbon dioxide stream, and eliminating the need for downstream carbon capture facilities. The redox process is overall exothermic and the heat can be utilised to drive endothermic reforming reaction to produce hydrogen. In order to operate at high pressure and remove the problem with solid circulation, chemical looping packed bed reactors have been proposed as alternative to fluidised bed reactors. This configuration has been studied experimentally and numerically by several researchers who demonstrated that the process is feasible for power generation and hydrogen production [1] [2]. Due to its dynamic nature, management of chemical looping packed bed temperature and heat is essential to maximise the process efficiency and minimise heat losses and thermal distribution across the reactor length and radius. Also, a heterogeneous temperature profile poses some issues on conversion and product selectivity which is relevant in presence of catalytic reactions or gas-solid reactions. This work provides a study at fundamental level on the impact of radial profile during high exothermic and endothermic reaction using Ni material as oxygen carrier. A two-dimensional pseudo-homogenous axially and radially dispersed model was developed to study the thermal behaviour of the packed bed. Different correlations for the mass and heat dispersion coefficients in axial and radial directions were assessed numerically to determine their impact on the bed 2-D model accuracy and performance.

2. MethodsMethods

The experimental setup consists of round tube packed bed reactor (OD x ID x L = 60 x 52 x 630 mm) made of special allow (253 MA), and placed inside external furnace to regulate the reactor temperature. Ni supported on $CaAl_2O_4$ (200 g) has been used as oxygen carrier, with a particle size of 2.0 – 2.8 mm and an overall bed length of 70 mm. To allow the gas to heat and mix, Al_2O_3 has been used as inert material before and after the reactive zone. The gas enters the reactor from the bottom and the flow is regulated by mass flow controller (Bronkhorst). After gas exits from the reactor top, it is air-cooled to allow steam to condense and then vented to atmosphere. Three thermocouple assemblies are inserted into the reactor from the top at different radial positions and fourth thermocouple assembly is inserted from the reactor bottom at the centre. Each assembly contains four type-K thermocouples, resulting in 16 measuring points across the reaction zone. In the experiments, the material oxidation was carried out with air, while the reduction was carried out with hydrogen. The experiments were conducted in cycles of oxidation, followed by heating, and then reduction. The oxidation reaction was conducted at temperatures of 500-600 °C, flow rates of 0.5-5 NLPM, and atmospheric pressure. On the other hand, the reduction was conducted at temperatures of 700-900 °C, flow rates of 0.5-2.5 NLPM, and atmospheric pressure. A two-dimensional pseudo-homogenous axially and radially dispersed model was developed using C++ programming language.

3. Results and discussion The experiments showed that reactions generate two temperature fronts, named reaction and heat fronts, which is line with previous work of other researchers. All researchers, who studied chemical looping packed bed reactors, have measured and simulated the two fronts in the axial direction in the reactor centre. The experiment showed that both reaction and heat fronts have radial and axial components. By calculating the temperature rise per second in the axial and radial direction, a maximum temperature rise is observed moving through the bed radially and axially. By plotting the maximum temperature rise time against its position in the bed, a linear correlation is developed for the axial temperature front and parabolic relationship is developed for the radial temperature front. The velocities of the two fronts can be determined both the axial and radial directions by taking the derivative of these correlations. These observations were used to validate 2-D model against both the reduction and oxidation cycles. Different mass and heat dispersion coefficient correlations were assessed to evaluate their impact on the model accuracy and speed.

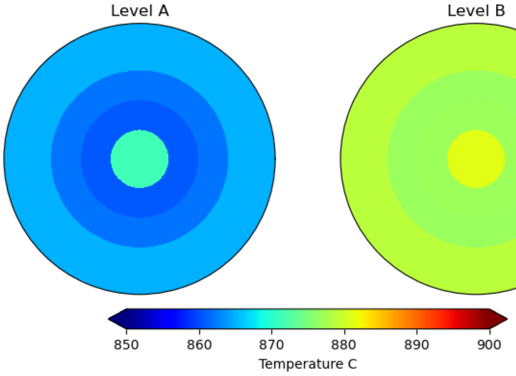

Figure 1.. Reactor temperature radial profiles at two axial locations based on experimental data at time 6015 second of reduction experiment

4. Conclusions The radial and axial thermal profile for chemical looping packed reactor has been developed based on experimental data for both oxidation and reduction of nickel-based oxygen carrier. The experimental data were utilised to measure the reaction and heat front velocities in both axial and radial direction, in addition to quantifying the heat losses in the radial direction. Two-dimensional axially and radially dispersed transient packed bed model was calibrated against the experimental data, and different dispersion coefficient correlations were evaluated.

5. Acknowledgements The authors acknowledge Saudi Aramco for sponsoring Ahmed Aman to conduct this research as part of his MSc Programme and TotalEnergies Onetech for the co-funding of the PhD project of Ismaeel Ali. Vincenzo Spallina acknowledges the Department of Energy Security and Net Zero in the framework of the Low Carbon Hydrogen Supply 2: Stream 1 Phase 2 Competition (TRN prj_579) (RECYCLE, HYS2304) for providing funding and support to the development of this study.

References

[1] P.A. Argyris, C. de Leeuwe, S.Z. Abbas, V. Spallina, Mono-dimensional and two-dimensional models for chemical looping reforming with packed bed reactors and validation under real process conditions, Sustain Energy Fuels 6 (2022) 2755–2770. https://doi.org/10.1039/d2se00351a.

[2] P. Alexandros Argyris, C. de Leeuwe, S.Z. Abbas, A. Amieiro, S. Poultson, D. Wails, V. Spallina, Chemical looping reforming for syngas generation at real process conditions in packed bed reactors: An experimental demonstration, Chemical Engineering Journal 435 (2022) 134883. https://doi.org/10.1016/J.CEJ.2022.134883.

KeywordsKeywords

Chemical Looping; Redox Catalysis; Reactor Design

Poster 9: CO and O2 Solubility in Different Mixtures of Ethanol, Acetonitrile and Water at High Temperatures and Pressures.

Maan Al Jurdi[1,2], Assaad Zoughaib[1*], Tetiana Krachko[2], Tawfiq Nasr Allah[2], Benoît Illy[2]

1 CES, Ecole de Mines Paris, PSL University, Paris 75000, France
2 Fairbrics, Villebon Sur Yvette 91140, France

**Corresponding author: assaad.zoughaib@minesparis.psl.eu*

Highlights

- Measure the solubility of CO and O_2 in different solvents.
- Regress solubility data into thermodynamic model on ASPEN plus.
- Determine vapor-liquid equilibria over a larger range of pressures and temperatures.

Introduction

Fairbrics is a French start-up opting to transform captured CO_2 into polyester in three main stages. As part of these different stages, we are developing heterogeneous catalysts that form complex three-phase catalytic systems consisting of a gas, liquid and solid catalyst phase. It is usual for these systems to face mass transfer limitations impacting the gas diffusion into the solvent medium followed by the diffusion into the surface of the catalyst where the reaction takes place. This prevents proper kinetic studies and catalyst optimization.

Even if there is an established solubility database for different gas-liquid pairings, for our specific system with CO or O_2, [1]-[5] insufficient data could be found for the range of operating high temperatures (100-200°C) or pressures (65-110bars) in solvents namely acetonitrile, ethanol or water. To overcome the latter, we define a new methodology that pairs the traditional calculations of gas diffusion with thermodynamic simulation models to cover the desired vapor-liquid equilibria of the Fairbrics process.

Methods

Studying mass transfer limitations, we need to calculate the diffusion effect at the level of gas dissolution into the solvent medium then the diffusion onto the surface of the catalyst to start the reaction.

To begin the testing, we needed to establish a protocol to work in known pressure and temperature conditions and record over time the dissolution evolving on our reactor setup and recording system.

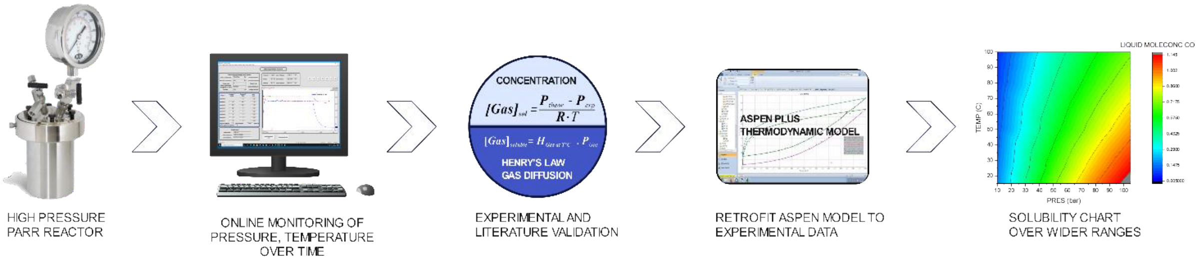

Figure 1. Reactor setup to Solubility chart process

The setup consists of a high-pressure Parr reactor that is connected to a computer software that does online recording and monitoring of the evolution of pressure, temperature and other interesting control parameters over time (Figure 1). These experiments are then interpreted, and the collected data relate the pressure changes over controlled temperature and time to deduce the gas concentration in the solvent mixture [6]. After referring to Henry's law for gas solubility of CO and O_2 and some literature values in known conditions, we will then have the corrected gas solubility over the studied system mix. Consequently, we need to assess the known thermodynamic model estimation of these gases on ASPEN plus and their behavior with the chosen liquids. As a result, we update the list of binary interaction parameters on ASPEN to change these gas liquid interactions in order to match up with the experimental results we have acquired ourselves. We noticed that even with the use of group estimation models like UNIFAC to deduce these types of interactions, data regression and parameters retrofitting is still needed to mimic the real experimental data. Finally, when the model is reproducing our lab data conditions, we can plot the extension of these gases' solubility over a wider pressure and temperature range.

Results and discussion

The pressure drop seen in the reactor setup has been evidently more noticeable at lower temperatures conditions for CO and O2, namely at higher partial pressures where the difference between the filling and end conditions are larger than the equipment measurement accuracy. We can also note that after the solubility testing of individual gases with similar reactor liquid portions, the addition of both gases simultaneously corresponds to the latter testing proving the point that the diffusion is not competitive. This means the total pressure drop can be cumulative, thus the gas concentration could be estimated for each gas species separately. However, one main challenge encountered is due to the small values of the Henry constants (ranging between 10^{-4} and 10^{-5} $mol.L^{-1}.bar^{-1}$) and for the studied case scale, the concentration change will be quite dependent on the overhead pressure in the dead volume to resupply the consumed gas in the liquid portion of the reactor. To overcome the issue with reading accuracy, we also used multiple independent equipment (reactor monometer, thermocouple, pressure transducer) in parallel to ensure our assumptions are more reliable.

Conclusions

We proposed an experimental protocol on our reactor setup which allows to measure the gas solubility and diffusion in our liquids. These results are then compared to the simulated results of the chosen thermodynamic package in ASPEN plus achieving an accuracy in solubility measurements of 5%. Finally, we can regress the binary interaction parameters to mimic the lab results and revalidate the assumed solubilities to cover a larger range and combination of reaction mixtures.

References

[1] L. C. A. Garzon, C. M. Romero, and A. F. Suarez, "Design and construction of an equipment for the determination of solubility of gases in liquids," AIChE Journal, vol. 63, no. 7, pp. 3105–3109, Jul. 2017, doi: 10.1002/aic.15637.

[2] M. Torli, L. Geer, G. M. Kontogeorgis, and P. L. Fosbøl, "Solubility of Syngas Components in Water, Acetic Acid, and Alcohol Using New Standard Fugacity Methodology," Ind Eng Chem Res, vol. 57, no. 49, pp. 16958–16977, Dec. 2018, doi: 10.1021/acs.iecr.8b03954.

[3] E. Wilhelm1 and R. Battino, "Thermodynamic Functions of the Solubilities of Gases in Liquids at 25°C," 1973. [Online]. Available: https://pubs.acs.org/sharingguidelines

[4] J. A. Campbell et al., "Preprints presented at the 71st annual AIChE meeting," Elsevier Pub. Co, 1973.

[5] S. P. Tonner, M. S. Wainwright, D. L. Trlmm, and N. W. Cant, "Avallable from Superintendent of Documents," 1983.

[6] W. M. Haynes, D. R. Lide, and T. J. Bruno, CRC Handbook of Chemistry and Physics 97 th Edition

Keywords

Gas Solubility; ASPEN simulation; diffusion

Poster 10: DPA synthesis: a feasibility study towards the continuous application

Francesco Taddeo[1]*, Federica Orabona[1,2], Domenico Licursi[3], Claudia Antonetti[3], Vincenzo Russo[1], Anna Maria Raspolli Galletti[3], Martino Di Serio[1]

1 Department of Chemical Sciences, University of Naples Federico II, Via Cintia, IT-80126 Naples; 2 Åbo Academy University, Laboratory of Industrial Chemistry and Reaction Engineering, Henrikinkatu 2, FI-20500, Turku/Åbo, Finland; 3 Department of Chemistry and Industrial Chemistry, University of Pisa, Via G. Moruzzi, IT-56124 Pisa.

**Corresponding author: francesco.taddeo@unina.it*

Highlights

- A catalytic screening was made for the synthesis of DPA/DPE.
- The selectivity towards p,p'-DPA/ p,p'-DPE was almost complete.
- A feasibility study for the continuous application was performed.

1. Introduction

Diphenolic acid (DPA) is emerging as a bio-based alternative to the toxic bisphenol A in the production of epoxy resins, polycarbonates, and isocyanate-free polyurethanes finding applications also as an additive in fire-retardant materials and painting formulations [1,2]. Typically, it is synthesized through the solvent-free condensation between two molecules of phenol and levulinic acid in the presence of a Brønsted acid catalyst. Mineral acids such as hydrochloric and sulfuric acid are conventionally used as homogeneous catalysts, anyway showing important disadvantages connected with their use, such as corrosion issues and intensive work-up within the wastewater treatment. Heterogeneous catalysts offer a more environmentally friendly alternative due to their safety and ease of separation from the reaction mixture.

Together with the formation of DPA, esterification of levulinic acid may occur as a side reaction, decreasing the selectivity to the desired product. New synthetic routes involving novel heterogeneous catalysts and substrates can be investigated. The reactivity of levulinic acid can be slowed by using ethyl levulinate instead of the acid, as the trans-esterification rate is typically slower than esterification with standard acid catalysts. Therefore, ethyl levulinate can be used as a substrate to improve selectivity. In this study, a catalytic screening was conducted to identify catalysts exhibiting the most promising performance in the reaction involving levulinic acid/ethyl levulinate and phenol. Various catalysts, including both homogeneous and heterogeneous were tested, focusing the attention both on commercial and synthetic ones. Among the catalysts commercially available, sulfuric acid, zeolites including H-Y Zeolite and β-Zeolite, and sulfonic acid resins i.e., Amberlite IR120, Dowex 50WX8, and Amberlyst-15 were tested. Additionally, synthetic catalysts, such as sulfonated hydrochars, were also considered. Therefore, a feasibility study was conducted to identify the catalyst with promising characteristics with the aim to perform the reaction in a continuous device.

2. Methods

The catalyst screening was conducted in a 100 mL two-necked glass flask. Levulinic acid (LA)/ethyl levulinate (EtLA) and phenol (PhOH) were loaded into the reactor and heated to the desired temperature before adding the catalyst to the system. Temperature was regularly monitored using a thermometer, while homogeneous mixing was achieved with a magnetic stirrer. Samples were collected every hour during the initial and final stages of the reaction to ascertain the steady-state condition. The catalytic screening was conducted fixing a temperature of 373 K, catalyst loading of 33 kg/m^3, PhOH:LA/EtLA molar ratio of 4:1, and a reaction time of 5 h. As for the continuous tests, a syringe pump was used to inject the reagents into the reactor, and a thermostated jacket allowed to keep constant the temperature throughout the experiment. The collected samples were analyzed through ^{1}H-NMR analysis.

3. Results and discussion

The synthesis experiments of DPA exhibited lower conversions when using heterogeneous catalysts compared to those achieved with sulfuric acid, possibly due to diffusion limitations. Specifically, ion exchange resins can be considered interesting catalysts for this reaction. In particular, Amberlyst-15 and Amberlite IR 120 emerged as the most promising catalysts, leading to the highest conversion and selectivity towards the desired product (p,p’-DPA) even if it was not extremely high. Using ethyl levulinate as reagent, very promising results were attained, with almost complete selectivity towards the desired product (p,p’-DPE), as showed in Figure 2. Similarly, also in the case of synthetic catalysts, interesting results were obtained.

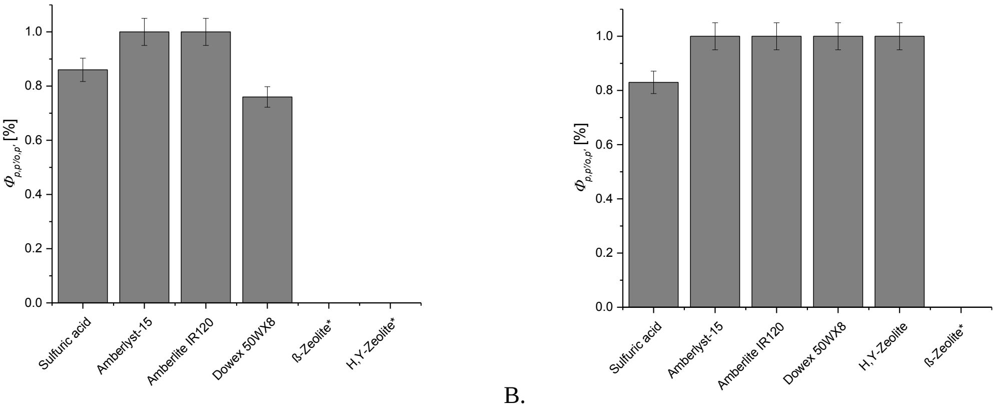

A. B.

Figure 2. Catalytic screening results starting from levulinic acid (A) and ethyl levulinate (B) fixing T = 373K, catalyst loading = 33 kg/m^3, PhOH:LA/EtLA = 4:1 mol/mol, t = 5 h.

4. Conclusions

The reaction between levulinic acid/ethyl levulinate and phenol was investigated for the synthesis of DPA/DPE. The attention was firstly focused on the catalytic screening, testing both homogeneous and heterogeneous catalysts, commercial and synthetic ones. It was verified that among the commercial heterogeneous catalysts, ion-exchange resins led to higher conversions and selectivity to the desired product, especially when using ethyl levulinate as reagent. Promising results were also achieved using synthetic catalysts. This preliminary study was therefore conducted with the aim of identifying the catalysts with best properties to be tested in a continuous reactor.

References

[1] Z. Qian, Y. Xiao, X. Zhang, Q. Li, L. Wang, F. Fu, H. Diao, X. Liu, Chem. Eng. J. 435 (2022) 135022.
[2] Z. Ma, C. Li, H. Fan, J. Wan, Y. Luo, B.G. Li, Ind. Eng. Chem. Res. 56 (2017) 14089–14100.

Keywords

Diphenolic acid; levulinic acid; ethyl levulinate; catalytic screening.

Acknowledgements

This study was carried out within the MICS (Made in Italy–Circular and Sustainable) Extended Partnership and received funding from the European Union Next-Generation EU (PIANO NAZIONALE DI RIPRESA E RESILIENZA (PNRR) –MISSIONE 4 COMPONENTE 2, INVESTIMENTO 1.3 –D.D. 1551.11-10-2022, PE00000004). This manuscript reflects only the authors’ views and opinions, neither the European Union nor the European Commission can be considered responsible for them.

Poster 11: Methanation of carbon dioxide on Co-containing catalysts based on aluminosilicates

Etibar Ismailov[2], Shahla Tagiyeva[1], Sevinj Osmanova[2,3*], Aygun Rustamova[2], Sevil Khalilova[2], Dilgam Tagiyev[2]

[1]*Institute of petrochemical Processes named after Acad. Yu.Mammadaliyev, 30, Khojali ave., AZ1025, Baku, Azerbaijan;*

[2]*Institute of Catalysis and Inorganic Chemistry named after Acad. M. Naghiyev 113, H.Javid ave., AZ1143, Baku, Azerbaijan;*

[3]*Khazar University 41, Mahsati Str., AZ1096, Baku, Azerbaijan*

email: sevinj.nasib.osmanli.26@gmail.com

Highlights

- Reduced in H_2 stream Co/aluminosilicates convert CO_2 to CH_4 at 573K and atmospheric pressure.
- Reduced Co/aluminosilicates contain superpara/ferromagnetic Co_3O_4 and “metallic” Co nanoparticles.
- Superpara/ferromagnetic particles catalyze the methanation of CO_2.
- Activity and selectivity of Co/aluminosilicates in CO_2 methanation depend on Al_2O_3/SiO_2 ratio.

1. Introduction

The involvement of carbon dioxide in chemical synthesis is currently considered as one of the possible options for replacing petroleum (fossil) raw materials with non-petroleum (alternative) ones. In this regard, expanding the scope of use of carbon dioxide as a starting reagent in chemical processes is an urgent task aimed at solving issues of environmental safety and rational use of CO_2. One of the promising and important methods of CO_2 utilization is hydrogenation reactions. However, the participation of a stable CO_2 molecule in chemical processes is hampered by the lack of effective catalysts that allow the hydrogenation of CO_2 with high yields and selectivity [1, 2].

This paper presents the results of a study of the phase composition, magnetic and catalytic properties of cobalt-containing Siral type aluminosilicates depending on the Al_2O_3/SiO_2 ratio in the methanation of carbon dioxide.

2. Methods

Catalysts with a cobalt concentration of 10 wt % (in terms of CoO) were prepared by impregnating Siral-type aluminosilicate with an Al_2O_3/SiO_2 ratio of 1,10,40 with cobalt nitrate $Co(NO_3)_2{\cdot}6H_2O$, followed by drying at 110-120 °C for 2 hours, calcination in air at 500 °C for 4 hours and reduction in a stream of hydrogen at 450 °C for one hour. Methanation reactions were carried out in a flow mode quartz reactor at the atmospheric pressure and 200, 300, 400 and 500 °C. The prepared catalysts was characterized by X-ray fluorescence spectrometer XGT 7000, Horiba, Japan, X-ray diffractometer XRD D2 and EMXmicro spectrometer, Bruker, Germany.

3. Results and discussion

The chromatographic analysis of the composition of gaseous products of CO_2 hydrogenation on Co/Siral-1 (Co/S-1), 10 (Co/S-10), 40 Co/C-40) catalysts shows that catalysts containing only cobalt, at a reaction temperature ≤ 573 K, generate at $T \geq 573$ K only methane and methane and no more than 1% carbon monoxide at 673K. The maximum methane yields -55, 41 and 33% are observed at a reaction temperature of 573 K, on Co/S-1, Co/S-10 and Co/S-40 catalysts, respectively, and with increasing SiO_2/Al_2O_3 ratio a decrease in methane output is observed. The dependence of the catalytic properties of these systems on the Al_2O_3/SiO_2 ratio is most likely associated with the textural features and acidic properties of the aluminosilicate base. The highest concentration of Lewis acid sites is observed for Siral-1 and 10 and the highest concentration of Bronsted acid sites for Siral-40 [3]. The values of the specific surface area and specific pore volume of Co-containing aluminosilicate samples

S-1,10,40, pre-calcined at 823 K in a stream of air and then reduced in a stream of hydrogen at 723 K for 1 hour, are 284; 343; 409 m^2/g and 0.46; 0.54; 0.63 in cm^3/g, respectively. The study of the elemental composition of 10% Co/S-1,10,40 samples by scanning at each of 4 randomly selected surface points using an X-ray fluorescence microscope allowed to determine the distribution of the active elements in the structure of catalyst. X-ray diffractometry of the phase composition of oxidized and reduced samples of the Co/Siral-10 catalyst shows that the calcined samples of the Co/S-1,10,40 catalyst are characterized by the presence of Co_2O_3, CoO, $CoAl_2O_4$ phases, and the reduced ones - Co_3O_4 and "metallic" Co. The average particle size of Co_3O_4, calculated from the characteristic peak with a 2θ value equal to 36.8° - according to the Debye-Scherrer equation equal to 20-25 nm. The evaluated average size of cobalt particles d(Co)and its dispersity, is respectively, $d(Co^o) = d(Co_3O_4) * 0.75$ =11-15nm and $D(\%) = 96/d(Co^o)$ = 8.7-6.4.

EMR spectra of Co-containing samples with an aluminosilicate base with different SiO_2/Al_2O_3 ratio equal to 1;10;40, Siral type, calcined in air for 4 hours and then reduced in a stream of hydrogen at 450°C for one hour (Figure 1, a-c) are a superposition of at least two signals - wide asymmetric with different average values of the g-factor (g_{av}), and narrow with a width of 42 mT and g_{av} value. equal to ~2.3 are characteristic to superpara/ferromagnetic nanosized particles.

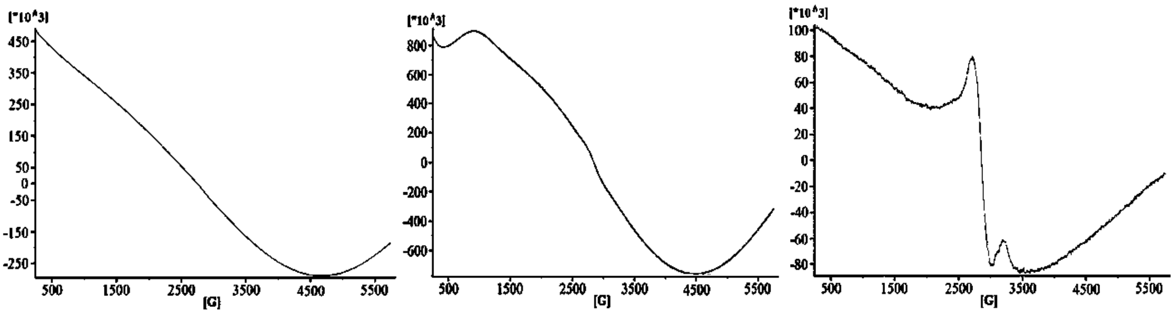

a) b) c)

Figure 1. EMR spectra recorded at room temperature of Co/Siral samples with SiO_2/Al_2O_3 ratio (1;10;40), calcined in air and then reduced in a stream of H_2 at 450°C for one hour: a) Co/S-1, b) Co/S-10 and c) Co/S-40

The line width and integrated signal intensity for all three samples change with decreasing temperature at which the spectra are recorded, and the integrated signal intensity increases by approximately 2 times. It was assumed sugested that these superpara/ferromagnetic particles of cobalt oxides (most likely Co_3O_4 and "metallic" cobalt) are catalytically active in the carbon dioxide methanation reaction: $2CO_2 + 5H_2 = CH_4 + CO + 3H_2O$ or in the form of separate stages:

$$CO_2 + 4H_2 \xrightarrow{k_1} CH_4 + 2H_2O; \quad CO_2 + H_2 \xrightarrow{k_2} CO + H_2O; \quad CO + 3H_2 \xrightarrow{k_3} CH_4 + 2H_2O$$

Based on a study of the kinetics of the CO_2 methanation reaction in the range of 573-773 K and the flow rate of the gas mixture in the range of 240-720 h^{-1} with a molar ratio of CO_2, H_2 and N_2 equal to 1:4:1.5, the values of k_1, k_2, k_3 and activation energy of reactions 1-3 were determined. It has been shown that during the reduction in a stream of hydrogen at a temperature of 450 °C of cobalt-containing samples pre-oxidized at 500 °C in air with an aluminosilicate base, highly dispersed superpara/ferromagnetic particles of oxide and "metallic" cobalt nanosizes are formed. It was shown that on these catalysts CO_2 is hydrogenated almost exclusively into methane with traces of CO (no more than 1% CO at reaction temperature $T \geq 573K$). Catalytic characteristics of these systems in the methanation reaction of carbon dioxide: $2CO_2 + 5H_2 = CH_4 + CO + 3H_2O$ significantly depends on the amount of superpara/ferromagnetic oxide and "metallic" cobalt particles and their ratio in the catalyst.

References

[1] M.A.Shah, A.L Shibiru, V. Kumar , V.Ch.Srivastava, Int. J. Green Energy. (2023) https://doi.org/10.1080/15435075.2023.2281330
[2] Sh.F.Taghiyeva, E.H. Ismailov, Chemicals problems. 4 (2020) 485–500.
[3] Sh.F. Taghiyeva, S.N.Osmanova, N.M. Aliyeva, E.H.Ismailov, Ukrainian Conf. with Intern. Participation. Chemistry, Physics and Technology of Surface, Kiev, Ukraine, 26-27 May, 2021, pp.156.

Keywords:
"Methanation", "CO_2", "Co/aluminosilicates", "superpara/ferromagnetic particles".

Poster 12: Surface Elemental and Phase Composition of MnOx-Na_2WO_4/SiO_2 Catalysts for Oxidative Coupling of Methane

Sevinj Osmanova[1,2*], Asif Mammadov[1,3], Etibar Ismailov[1], Dilgam Tagiyev[1], Michael Vorochta[4], Miquel Rodríguez[4], Tomáš Hrbek[4], Joris Thybaut[5]

[1]Institute of Catalysis and Inorganic Chemistry, 113, H.Javid Ave., AZ1143, Baku, Azerbaijan; [2]Khazar University 41, Mahsati Str., AZ1096, Baku, Azerbaijan;

[3]Azerbaijan Technical University, AZ1073, Baku, Azerbaijan;

[4]Charles University, Department of Surface and Plasma Sciences, Faculty of Mathematics and Physics, V Holešovičkách 747/2, 180 00 Prague 8, Czech Republic;

[5]Ghent University, Laboratory for Chemical Technology, Technologiepark 125, 9052 Ghent, Belgium.

E-mail: sevinj.nasib.osmanli.26@gmail.com

Highlights

- At OCM conditions Na_2WO_4 phase is in a molten state and covers SiO_2 granules.
- MnOx particles react with molten Na_2WO_4, forming catalytically active phases.
- Activity of MnOx-Na_2WO_4/SiO_2 in OCM is due to dynamics of surface elemental and phase composition.

1. Introduction

In the last few decades, selective oxidation of natural gas to C_{2+} hydrocarbons has attracted increased attention [1, 2]. Despite intensive research and development of technologies in this direction, the industrialization and practical application of oxidative condensation of methane (OCM) reaction is delayed. One of the main reasons for this is the lack of effective catalysts for this reaction. This report presents the results of a study of the surface elemental and phase composition of the MnOx-Na_2WO_4/SiO_2 catalysts for OCM reaction.

2. Experimental methods

MnOx-Na_2WO_4/SiO_2 samples were synthesized using tetraethoxysilane, citric acid, triethanolamine, manganese $Mn(CH_3COO)_2{\cdot}4H_2O$ and tungsten $Na_2WO_4{\cdot}2H_2O$ salts as precursors, characterized by XPS (EnviroESCA system, SPECS Surface Nano Analysis, GmbH), SEM/EDS (Phenom ProXG6, Thermo Scientific), XRD (MiniFlex 300/600, Rigaku) methods and tested as OCM reaction catalysts at 700–900 °C and atmospheric pressure.

3. Results and discussion

XPS spectra (Fig.1) and SEM/EDS data of MnOx-Na_2WO_4/SiO_2 catalyst calcined at 850°C before and after the OCM reaction show the changes in surface elemental composition of MoOx-Na_2WO_4/SiO_2 samples and in distribution of Na, Mn, W in the catalyst structure after influence of reaction mixture. XRD data show that the MnOx-Na_2WO_4/SiO_2 samples consist of MnOx, Na_2WO_4, $MnWO_4$ and SiO_2 phases. At the reaction temperature (750–850°C), one of these phases – Na_2WO_4 is in a molten state (the melting and decomposition temperature of Na_2WO_4 are 696 and 1200°C, respectively) and covers the surface of crystalline SiO_2 (cristobalite and/or tridymite). It was stated that catalytic activity of the samples decreases ~ 15% after 10 hours for catalyst operation with CH_4/O_2~4 mix at 800°C. The Ulich equation: $\Delta G_T^0 = \Delta H_T^0 - T\Delta S_{298}^0 - \Delta C_{P,298}^0 T\left[\ln\left(\frac{T}{298}\right) + \frac{298}{T} - 1\right]$ (1) in computer version: ΔG_T^0(kJ/mol)= 199-0.202*x-0.0235*x*(ln(x/298)+298/x-1), where x=T (2), was used to calculate the temperature dependence of the Gibbs free energy of reaction (3)

$MnO_2+Na_2WO_4+SiO_2 \xrightarrow{770-1500\,K} Mn_2O_3+ Na_2SiO_3 + MnWO_4+ O_2\uparrow$ (3), where $\Delta G_T^0; \Delta H_T^0; \Delta S_{298}^0$ - free energies, enthalpies and entropies of reaction, $\Delta C_{P,298}^0$- the difference between the molar isobaric heat capacities of the products and reactants. Calculation of the temperature dependence of the Gibbs free energy of reaction (1) according to equation (2) shows that beginning from 900 K the Gibbs free energy of reaction (3) acquires negative values and in the range of 900–1500 K reaction (3) is directed to the right.

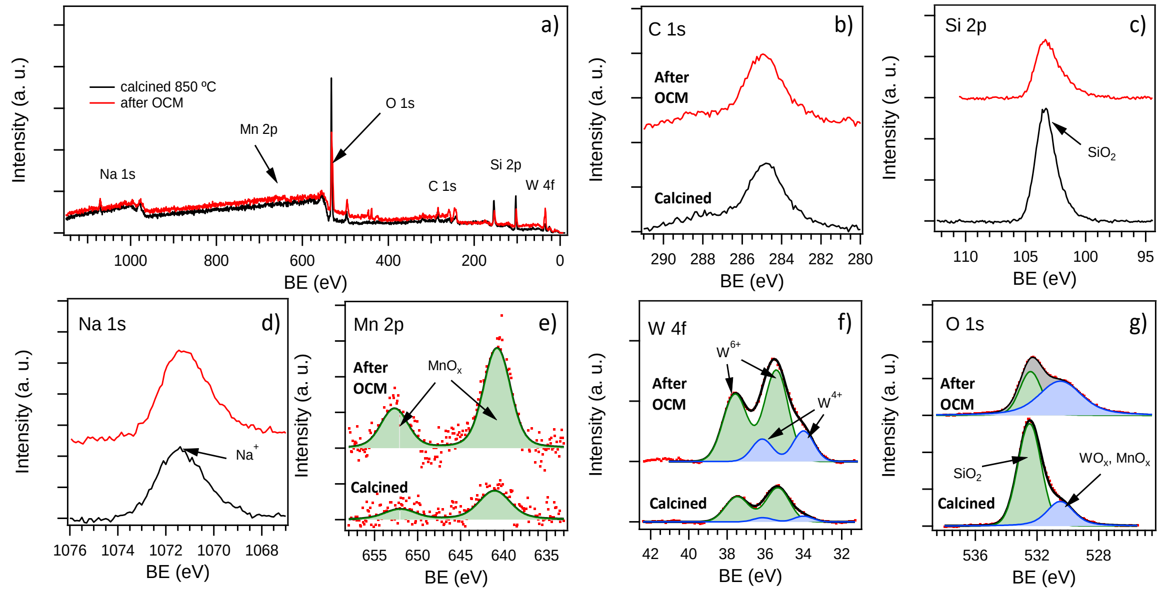

Figure 1. XPS spectra of 0.8Na3.2W2Mn/SiO_2 catalyst calcined for 2 hours in air at 850 °C before and after OCM reaction at 800 °C . Survey (a), C 1s (b), Si 2p (c), Na 1s (d), Mn 2p (e), W 4f (f), and O 1s (g)

MnO_2 is stable up to 803 K and starting from this temperature decomposes: $4MnO_2 = 2Mn_2O_3+O_2\uparrow$ (4). If we take into account the size dependence of the melting temperature of MnOx and use the Gibbs-Thomson equation: $T^m(r) = T^m(1-\frac{A}{r})$, where $A = 2\sigma_{s-l}/\Delta H^m \rho_s$, where all notations are generally accepted, we obtain that the values of the melting temperature for MnO and Mn_3O_4 particles with the sizes 5-10 nm are in the range of 1600-1400K. The curves of the melting temperature dependence of MnOx particles on their size show that under OCM conditions (700-900 °C) they are in a solid state. It should be noted that at typical OCM temperatures (>700°C), the Na_2WO_4 phase melts and the reaction $Mn_2O_3+2Na_2WO_4 + 2SiO_2 = 2MnWO_4 + 2Na_2SiO_3 + 0.5O_2\uparrow$ (5) is possible. The reaction proceeds with the reduction of Mn^{3+} ions to Mn^{2+}.

4. Conclusions

Based on XPS, SEM/EDS and XRD data, it is shown that under OCM conditions, the reaction mixture $CH_4/O_2 \geq 2$ notably changes the surface elemental and phase composition. Under these conditions, Mn_2O_3 and/or Mn_3O_4 particles react with molten Na_2WO_4, forming catalytically active phases.

Acknowledgments

This research was supported by the European Union's Horizon 2020 research and innovation program under grant agreement No.814557.

References

[1] C. Karakaya, R.J. Kee, Energy Combust. Sci. 55 (2016) 60-97 https://doi.org/10.1016/j.pecs.2016.04.003
[2] L. Pirro, Pedro S.F. Mendes, B. Kemseke, B.D. Vandegehuchte, G.B. Marin, J.W.Thybaut, Catal. Today. 365 (2021) 35-45. https://doi.org/10.1016/j.cattod.2020.06.084

Keywords

“MnOx-Na_2WO_4/SiO_2 catalyst”, “OCM”, “surface elemental”, “phase composition”.

Poster 13: Numerical Modelling of Mass Transfer in Multiphase Microreactors

Mohammad Anzar Hussain[1]*, Raghvendra Gupta[1,2]

1 Department of Chemical Engineering, Indian Institute of Technology Guwahati, Assam, India; 2 Center for Nanotechnology, Indian Institute of Technology Guwahati, Assam, India

**Corresponding author: m.anzar@iitg.ac.in*

Highlights

- Numerical model to simulate mass transfer in two phase flows inside microreactors.
- Rigorous validation of numerical model against mass transfer under forced convection problem.
- Simulation of two phase flows for different values of Reynolds (50-250) and Schmidt numbers (0.1-20).
- Grid independence study reveals large values of Schmidt number require higher quality mesh.

1. Introduction

Microreactors are continuous flow reactors having characteristic dimensions in micrometers. They are often used to carry out heat- and mass-transfer limited multiphase transport operations because of their high interfacial area density. Examples include biodiesel production inside microreactors [1], carbon sequestration using microreactors [2], etc. Conducting experiments inside microreactors is a challenging task, often requiring expensive non-intrusive measurement techniques. Investigation of hydrodynamics and mass transfer phenomena associated with gas-liquid and liquid-liquid two phase flows can be performed by modeling them using computational fluid dynamics (CFD) cheaply and with relative ease. We perform CFD simulations for hydrodynamics and mass transfer associated with gas-liquid and liquid-liquid two phase flows inside microreactors for different values of Reynolds and Schmidt numbers.

2. Methods

The Volume of Fluid (VOF) method [3] is most popular interface tracking method used by commercial (i.e. Ansys Fluent) as well as open source (i.e. OpenFOAM) CFD software packages for the modeling of two phase flows. It is based on single fluid formalism that involves solving only a single set of conservation equations for both phases, while the interface between them is tracked using an additional advection equation for volume fraction (α). The distribution of phase inside computational domain is identified by using volume fraction (α) defined by Equation (1). Single set of conservation equations for mass and momentum for incompressible Newtonian phases is given by Equations (2) and (3).

$$\alpha = \begin{cases} 0 \ \forall \text{ phase 1} \\ 1 \ \forall \text{ phase 2} \end{cases} \tag{1}$$

$$\boldsymbol{\nabla} \cdot \boldsymbol{v} = 0 \tag{2}$$

$$\rho\left(\frac{\partial v}{\partial t} + \boldsymbol{v} \cdot \boldsymbol{\nabla} \boldsymbol{v}\right) = -\boldsymbol{\nabla} p + \mu \boldsymbol{\nabla}^2 \boldsymbol{v} + \rho \boldsymbol{g} + \boldsymbol{F_\sigma} \tag{3}$$

The conservation equations are solved inside computational domain for volume fraction weighted average density (ρ) and viscosity (μ) defined by Equations (4) and (5).

$$\rho = \rho_1 \alpha + \rho_2 (1 - \alpha) \tag{4}$$

$$\mu = \mu_1 \alpha + \mu_2 (1 - \alpha) \tag{5}$$

where the subscripts 1 and 2 indicate the bulk properties associated with first and second phases respectively. Identification of the distribution of the phases and the interface between them is performed using an advection equation given by Equation (6).

$$\frac{\partial \alpha}{\partial t} + \nabla \cdot (\alpha \boldsymbol{v}) = 0 \tag{6}$$

The surface tension forces between the phases at the interface is modeled using continuum surface force (CSF) model [4] given by Equation (7). The interface curvature (κ) is computed using Equation (8).

$$\boldsymbol{F_\sigma} = \sigma \kappa \nabla \alpha \tag{7}$$

$$\kappa = \nabla \cdot \frac{\nabla \alpha}{|\nabla \alpha|} \tag{8}$$

A single conservation equation for species concentration is given by Equation (9). It is solved in the computational domain for volume fraction weighted average values of j^{th} species concentration (C_j) and mass diffusivity (D_j) defined by Equations (10) and (11). It also includes an additional flux term ($\boldsymbol{\phi_j}$) to model the concentration discontinuity and flux continuity at the interface, given by Equation (12).

$$\frac{\partial C_j}{\partial t} + \nabla \cdot (C_j \boldsymbol{v}) = \nabla \cdot (D_j \nabla C_j + \boldsymbol{\phi_j}) \tag{9}$$

$$C_j = C_{1j}\alpha + C_{2j}(1 - \alpha) \tag{10}$$

$$D_j = D_{1j}\alpha + D_{2j}(1 - \alpha) \tag{11}$$

$$\boldsymbol{\phi_j} = -D_j \left(\frac{C_j(1 - He)}{\alpha + He(1 - \alpha)} \right) \nabla \alpha \tag{12}$$

3. Results and discussion

Figure 1 shows the volume fraction and concentration distribution inside computational domain corresponding to a 0.5 mm circular cross section gas-liquid microreactor. The value of volume fraction $\alpha = 1$ corresponds to the liquid phase, while $\alpha = 0$ corresponds to gas phase. Gas and liquid phases are introduced into the cylindrical computational domain in a coannular arrangement, with a central gas core. Gas phase is introduced in the computational domain containing a species that diffuses inside the liquid phase. Liquid phase enters the inlet annulus without species.

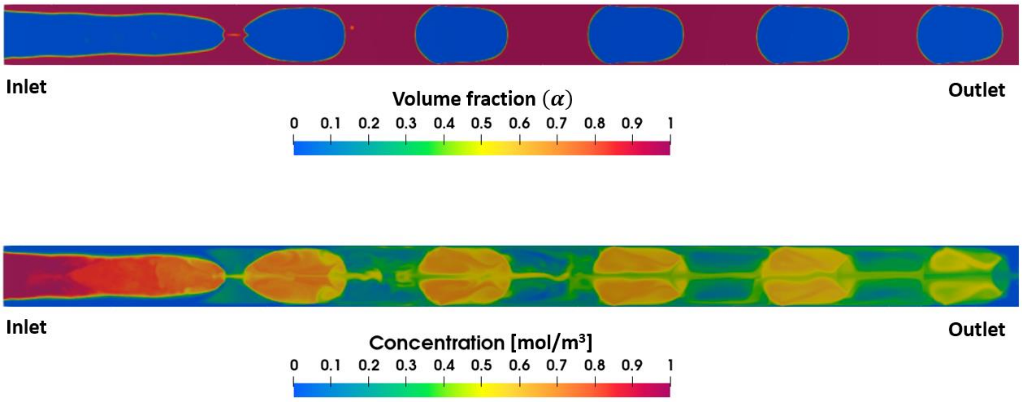

Figure 1. Volume fraction (top) and concentration (bottom) color plots.

References

[1] Rahimi M, Aghel B, Alitabar M, Sepahvand A, Ghasempour HR, "Optimization of biodiesel production from soybean oil in a microreactor," *Energy Conversion and Management*, vol. 79, pp. 599-605, 2014.

[2] Ganapathy H, Steinmayer S, Shooshtari A, Dessiatoun S, Ohadi MM, Alshehhi M, "Process intensification characteristics of a microreactor absorber for enhanced CO2 capture," *Applied Energy*, vol. 162, pp. 416-427, 2016.

[3] Hirt CW, Nichols BD, "Volume of fluid (VOF) method for the dynamics of free boundaries.," *Journal of Computational Physics*, vol. 39, no. 1, 1981.

[4] Brackbill J, Kothe D, Zemach C, "A continuum method for modeling surface tension," *Journal of Computational Physics*, vol. 100, no. 2, 1992.

Keywords

Mass transfer, Microreactors, Two phase flows, Computational Fluid Dynamics

Poster 14: Kinetics of α-terpineol reactivity under heterogeneous catalysis with heteropolyacid

Anna Rejzková[1]*, Marek Plachý[1], Eliška Vyskočilová[1]

1 Department of Organic Technology, University of Chemistry and Technology Prague,
Technicka 5, 166 28 Prague 6, Czech Republic

**Corresponding author: rejzkovn@vscht.cz*

Highlights

- The work is by principles of green chemistry (biorenewable, heterogenous catalyst, green solvent).
- Phosphotungstic acid was chosen as a suitable catalyst for the impregnation of a support.
- 1,8-Cineol as one key product was formed with a selectivity 15-26 % in ethyl acetate.

1. Introduction

Recently, there has been an effort to choose a raw material based on renewable resources. One of the many options is the use of essential oils from plants that are rich on monoterpenes and its derivates – monoterpenoids [1]. α-Terpineol is the most abundant isomer of terpineol present in essential oils. It can be found in lavender and leaves of conifer, cajeput tree, bitter orange tree, and some herbs, e.g., basil and oregano [2,3]. Thanks to its lilac scent, it is often used as a fragrance in soaps, perfumes, and cosmetics [2]. α-Terpineol also has a wide spectrum of biological activity, e.g., its antioxidant, anticancer, antihypertensive, and also has insecticidal properties described [3].

Under acid catalysis of α-terpineol reactivity, a lot of products are formed, namely dehydration products (limonene, α-terpinene, γ-terpinene, terpinolene), cyclization products (1,4-cineol, 1,8-cineol) and isomerization products (γ-terpineol, terpinen-4-ol). 1,8-Cineol and 1,4-cineol are the most interesting and abundantly used in industry. Significant solvent effects on selectivity were observed. In acetone, 1,4-cineol was produced more selectively compared to other products under homogeneous catalysis using phosphotungstic acid [4].

This work aimed to study solvent effects on α-terpineol reactivity using heterogenous catalysts - supported heteropolyacids. Firstly, testing of heteropolyacid under homogeneous conditions was performed. After choosing a suitable heteropolyacid, it was impregnated on support – silicas. The prepared catalysts were characterized. The selectivity for 1,8-cineol and 1,4-cineol was influenced by the interaction between the heterogenous catalyst and solvent.

2. Methods

Catalyst preparation. Fumed silica and mesoporous silica MCM-41 were used as supports. Silicas were impregnated by heteropolyacid from water solution. The impregnation proceeded for 24 h, water was evaporated, and a catalyst was dried.

Reaction arrangement. The terpineol transformation was performed in a 25 mL two-necked round bottom flask with a condenser heated in an oil bath on a magnetic stirrer and vigorous stirring. The catalyst was separated from the collected samples of the reaction mixture by neutralization (homogeneous) or centrifugation (heterogeneous). The organic layer was diluted, and the composition was analyzed by GC-FID with a non-polar column. Compounds were identified using GC-MS.

Kinetics calculation. The conversion and selectivity were calculated based on the composition of the reaction mixture, which was found out by GC-FID. For the calculation of the kinetic model, the program MATLAB was used. Reaction rate constants and activation energies were evaluated.

3. Results and discussion

The reaction course using homogeneous catalysts in ethyl acetate with chosen heteropolyacids (silicomolybdic – HSiMo, phosphomolybdic – HPMo, phosphotungstic – HPW) is described in Figure 1. The weight of HPW corresponds to 0.5 mol. %, HSiMo and HPMo 0.8 mol.%. The fastest was the reaction using HPW. The dependence of selectivity on conversion is also depicted in Figure 1. Limonene and terpinolene were formed in the highest amount (21-42 % and 27-31 % resp.). 1,8-Cineol was produced with selectivity 15-26 %. α-Terpinene, and γ-terpinene were formed with maximal selectivity 13 % and 8 %. 1,4-Cineol and other isomers of terpineol were produced in trace amounts.

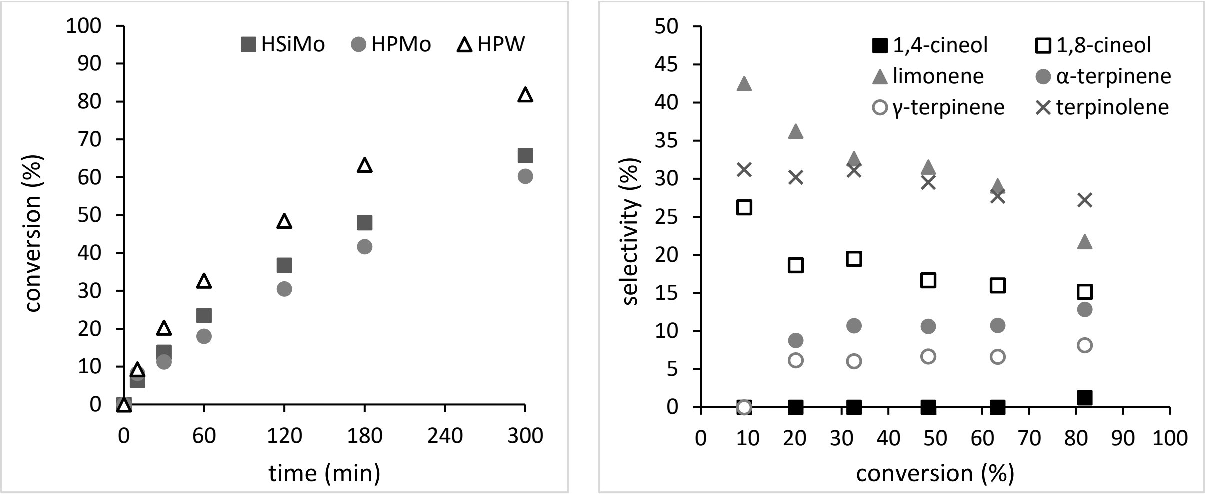

Figure 1. Reaction course of homogeneous catalysts testing (1 g α-terpineol, 10 wt.% catalyst, 5 ml ethyl acetate, 50 °C): left – dependence of conversion of α-terpineol on time with used heteropolyacids, right – dependence of selectivity for significant products on conversion on α-terpineol with phosphotungstic acid

HPW was impregnated on fumed silica and MCM-41. The prepared heterogeneous catalysts were characterized and used in the reaction of α-terpineol in various green solvents (methyl acetate, ethyl acetate, dimethyl carbonate etc.) for study of the interaction between catalyst and solvent. The reaction course with a heterogenous catalyst was slower but with similar selectivity, and the main advantage was the simple separation of the catalyst from the reaction mixture. Finally, the reaction mechanism was described, and kinetics parameters (reaction rate constant and activation energy) were calculated.

4. Conclusions

Based on testing of heteropolyacids activity, HPW was chosen as a suitable for the impregnation of silica support. Limonene, terpinolene, and 1,8-cineol were produced with a selectivity higher than 15 % for each. 1,4-Cineol was formed in trace amounts. HPW was impregnated on fumed silica and MCM-41 in various contents of HPW. We have also studied the influence on the interaction between the heterogenous catalyst and solvent, especially green ones.

References

[1] M. Dvořáková, I. Valterová, T. Vaněk, Chem. Listy 105 (2011) 839-845
[2] H. Surburg, J. Panten, Common Fragrance and Flavour Materials: Preparation, Properties and Uses, Wiley, 2006
[3] C. Khaleel, N. Tarabanca, G. Buchbauer, Open Chem. 16 (2018) 349-361
[4] E. J. Leão Lana, K. A. da Silva Rocha, I. V. Kozhevnikov, E. V. Gusevskaya, J. Mol. Catal. A-Chem. 259 (2006) 99-102

Keywords
α-Terpineol; biorenewable; heterogeneous catalysis; heteropolyacid.

Poster 15: New method of group characterization gas-liquid flow and its application in gas-liquid stirred tanks

Haoliang Wang[1], Xiangyang Li[2], Jingcai Cheng[1*], Chao Yang[1, 3*]

1 State Key Laboratory of Petroleum Molecular & Process Engineering, CAS Key Laboratory of Green Process and Engineering, Institute of Process Engineering, Chinese Academy of Sciences, Beijing, China;

2 College of Chemical Engineering, Sichuan University, Chengdu, China;

3 School of Chemical Engineering, University of Chinese Academy of Sciences, Beijing, China

**Corresponding author: jccheng@ipe.ac.cn; chaoyang@ipe.ac.cn*

Highlights

- A new method of group characterization of gas-liquid flow is proposed.
- Hydrodynamic behaviors of bubbles with different groups are investigated and analyzed.
- Actual flow regime of the system is the superposition of multiple dissimilar flow patterns.

1. Introduction

In the existing measurement techniques (e.g., PIV, LDV) for gas-liquid flow, the time-averaged bubble velocity is obtained by averaging instantaneous bubble velocities in a sampling period at a measuring location [1]. However, the experiments indicate that the bubble dynamics (such as velocity direction, velocity slip) significantly depend on the bubble sizes as shown in Figure 1(a). It is still a challenge to characterize the bubble behaviors more precisely in a gas-liquid reactor.

The objective of this work is to experimentally investigate bubble hydrodynamics in a stirred tank using polydisperse particle inline image method (PPIIM) newly developed in our recent work [2]. The dynamics of bubbles decomposed by bubble size is then comprehensively analyzed and new method of group characterization is proposed.

2. Methods

The experiment is conducted in a Plexiglas stirred tank (T=282 mm) stirred by a Rushton impeller (D=1/3T). The impeller speeds are ranged from 300 rpm to 500 rpm and the gas volumetric flowrate varies from 0.5 m^3/h to 1.5 m^3/h. The PPIIM is adopted to measure the polydisperse bubble dynamics, including bubble size, trajectory and slip velocity.

3. Results and discussion

The dynamic characteristics of bubbles are remarkably varying depending on the bubble size. Further considering the similarity of bubble dynamic behaviors in a certain size range, a new method of group characterization of gas-liquid flow is introduced. The basic idea is that the bubbles are divided into several groups based on the velocity slip and relaxation time as shown in Figure 1(b). Then the mean velocity of every group is determined respectively by averaging instantaneous bubble velocities.

According to the principle, three size groups ($G_1 \leq 0.6$ mm, 0.6 mm$<G_2\leq$2.2 mm, 2.2 mm$<G_3$) are demarcated, and every group exhibits very different flow patterns in a stirred tank. For group G_1, the follow-up characteristics of bubbles along the liquid flow are excellent. Two bubble motion loops respectively above and under the impeller disc are formed, in addition to another secondary circulation loops above the impeller. This group G_1 can be considered as pseudo-homogeneous. With respect to the group G_2, slightly upward inclination flows of bubbles are shown at the impeller discharge stream. Gas recirculation in the upper region disappears and becomes incomplete in the lower region. Meanwhile, for group G_3, the impeller discharge stream of bubbles is more inclined upward. And gas recirculations in the upper and lower bulk regions are absent. Compared with the flow pattern by averaging all sized

bubbles, the regime of the system is essentially the result of the superposition by these three patterns. Obviously, these outcomes notably align more closely with physical reality.

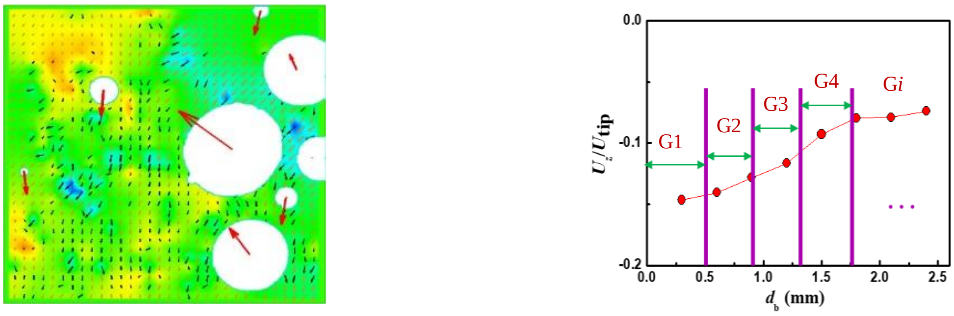

(a) **(b)**

Figure 1. (a) Snapshot of velocities for different bubble size, (b) scheme of the new group characterization method.

4. Conclusions

In order to accurately characterize the gas-liquid flow, a method of group characterization is proposed in this work. According to similarity of bubbles, three size groups (G1≤0.6 mm, 0.6 mm<G2≤2.2 mm, 2.2 mm<G3) are demarcated in gas-liquid stirred tanks. The results show that every group exhibits very different flow patterns and the apparent flow pattern of the system is essentially the result of the superposition by these patterns. In the following work, the LES simulation coupling with the population balance model (PBM) will be conducted to validate this new method further.

Acknowledgements

National Key Research and Development Program (2022YFC3902701), National Natural Science Foundation of China (22208346, 21938009, 22178326), and CAS Project for Young Scientists in Basic Research (YSBR-038) are gratefully acknowledged.

References

[1] G. Montante, D. Horn, A. Paglianti, Gas-liquid flow and bubble size distribution in stirred tanks. Chem. Eng. Sci. 63.8 (2008) 2107-2118.

[2] H.L. Wang, L.Yang, X.Y. Li, J.C. Cheng, C. Yang, Polydisperse particle inline image method and its application onto gas-liquid flow in a stirred tank. AIChE J. (2024) e18398. DOI: 10.1002/aic.18398.

Keywords

Multiphase reactor; Stirred tank; Bubble dynamic behaviors; Image-based method

Poster 16: Olefins Cracking by Zeolites Prepared from Valorized Refinery Waste

Our team is investigating the potential use of a refinery waste as a solvent to synthesize zeolites as an active component for industrial catalysts and adsorbents. Utilization of the refinery waste allows to reduce processing costs, valorizes the waste-derived solvent and modifies the resulting properties of the produced zeolites, which in turn reduces the zeolite synthesis cost. Understanding the catalytic performance of the zeolites prepared using the waste solvent is the objective of this study, which investigates the conversion of 1-hexene and 2-methyl-2-butene (2M2B) at various process operating conditions over zeolites prepared as a function of different silica-to-alumina ratios (SARs) and refinery waste loading levels.

Six zeolites synthesized using the refinery waste were prepared and characterized in terms of acidity, morphology, and textural properties. The impact of zeolite composition and properties on conversion and selectivity is examined and compared with commercial counterparts with similar SARs. The zeolites synthesized with the refinery waste achieved 80% 1-hexene conversion approaching 60% propylene selectivity, outperforming commercial zeolites (52%). However, 2M2B cracking exhibits slower reaction rates and enhanced oligomerization cracking, resulting in lower conversion (46–61%) and propylene selectivity (22–29%). Notably, the zeolite prepared at a 30% refinery waste loading having a sol-gel SAR of 50 shows the best performance among the all refinery waste-based zeolites in terms of stability and selectivity, with results comparable to the commercial zeolites. Notably, that the refinery waste-based zeolites possess larger crystals and higher acid site density compared with the commercial zeolites leading, generally, to a decreased stability. These findings enhance the understanding of the applicability of utilizing refinery waste-based zeolites in industrial processes and guide the development of improved refinery waste-based catalysts for petrochemical applications.

PosterPoster 17: A combined experimental and kinetic modeling study on low- and intermediate-temperature oxidation of trimethoxymethane e-fuel

Gilles Dossche[1], Kevin De Ras[1], Olivier Herbinet[2], Frédérique Battin-Leclerc[2], Maarten Sabbe[1], Kevin M. Van Geem[1]*

1 Laboratory for Chemical Technology (LCT), Ghent University, Technologiepark-Zwijnaarde 125, 9052, Ghent Belgium; 2 Laboratoire Réactions et Génie des Procédés, CNRS-Université de Lorraine, 1 Rue Grandville, 54000 Nancy, France

**Corresponding author: Kevin.Vangeem@ugent.be*

Highlights

- New experimental data for the oxidation of trimethoxymethane in a jet-stirred reactor
- Oxidation of trimethoxymethane starts at 600 K
- Main products include CH_4, CO, CO_2, C_2H_6, C_2H_4 and dimethyl carbonate
- Detailed kinetic model to unravel the experimental observations

1. Introduction

The development of different technologies to reduce greenhouse gas emissions and to evolve toward a more circular carbon economy is currently advancing at a high pace due to the rising and detrimental effects of climate change. One of the key areas is the transportation sector, which is responsible for nearly a quarter of the global energy related CO_2 emissions. Due to the limited energy density of current state-of-the-art batteries, electrification of heavy-duty transport, such as airplanes, ships and trucks, is expected to be impractical, if even technically feasible. Hence, e-fuels, i.e., fuels that can be produced from CO_2 and water using renewable electricity as primary energy source, are expected to be an important, sustainable alternative. Trimethoxymethane (TMM), the smallest branched oxymethylene ether (OME), is an example of a highly promising novel type of e-fuel. These OMEs are a family of chemical species composed of a chain of oxymethylene units (-CH_2O-). Their beneficial combustion properties, such as reduced emissions of toxic and pollutant products, have already been reported in detail in the literature. Substantial scientific research has already been conducted for the oxidation of linear OMEs [1]. In this study, new experimental data have been acquired for the low- and intermediate-temperature oxidation of TMM in a jet-stirred reactor for two equivalence ratios. A detailed kinetic model, based on first principles, has been used to explain the observed experimental trends.

2. Methods

New oxidation experiments have been performed in an isothermal quartz jet-stirred reactor [2] under highly diluted conditions (He), for two equivalence ratios, i.e., $\varphi = 1.0$ and 2.0, over the temperature range of 500-1000 K, at a pressure of 1.07 bara and an average residence time of 2 seconds. Three online gas chromatographs (GCs) were used for the characterization of the reactor effluent composition: a GC equipped with a carbosphere packed column and a thermal conductivity detector, a GC equipped with a PLOT-Q capillary column and a flame ionization detector, which is preceded by a methanizer, and a GC equipped with an HP-5ms capillary column and a flame ionization detector. A fourth GC, equipped with either a PLOT-Q or an HP-5ms capillary column, was used for the identification of the reactor effluent products. A detailed kinetic model for the pyrolysis and oxidation of TMM, constructed with the in-house developed automatic kinetic model generation framework Genesys [3], was used to elucidate the experimental observations.

3. Results and discussion

For both equivalence ratios, the decomposition of TMM starts at approximately 600 K and reaches nearly full conversion around 850 K, as depicted in Figure 1. The main products detected in the reactor effluent include CH_4, CO, CO_2, C_2H_6, C_2H_4 and dimethyl carbonate (DMC). For an equivalence ratio of 1.0, CO and CO_2 are formed from 600 and 575 K onwards, while CH_4 is only formed above 700 K. The effluent mole fraction of the latter reaches a maximum around 900 K, after which it decreases again.

C_2H_6 and C_2H_4 are formed from 650 and 725 K, respectively, and reach a maximum around 875 and 925 K. Compared to OME-2, which has the same chemical formula as TMM, the effluent concentrations of hydrocarbons, such as C_2H_6 and C_2H_4, are found to be substantially higher. DMC is an important reaction intermediate which is formed from 600 K onwards via among others the β-scission of a tertiary TMM-derived radical. The effluent mole fraction of DMC reaches a quasi-constant value between 675 and 825 K, and finally monotonously decreases at higher temperatures. The relatively high effluent mole fractions of DMC again indicate that the decomposition chemistry of TMM is fundamentally different from that of OME-2. Minor products include C_3H_8, C_3H_6, methyl acetate and dimethoxymethane. Similar trends are observed for an equivalence ratio of 2.0, see Figure 1. However, the effluent mole fractions of C_2H_4 and C_2H_6 are found to be higher, which could be expected for a fuel-rich mixture. Moreover, instead of decreasing, the effluent mole fraction of CH_4 remains quasi constant above 900 K.

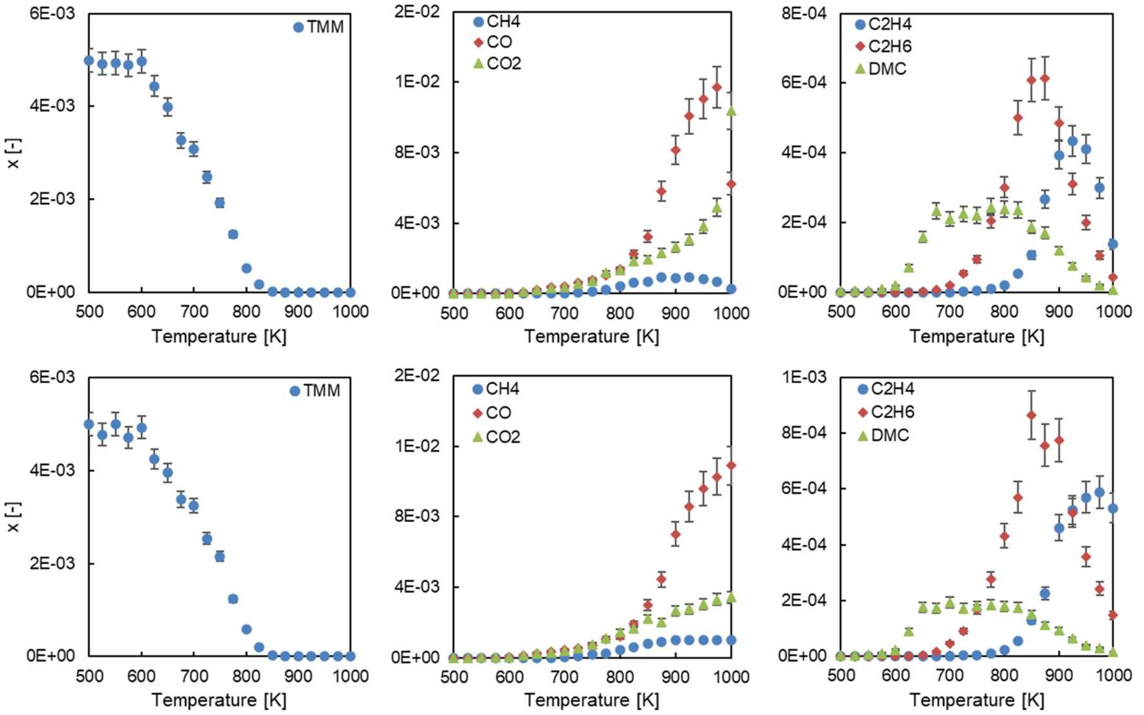

Figure 1: Measured effluent mole fractions of TMM (left), CH_4, CO and CO_2 (middle) and C_2H_4, C_2H_6 and DMC (right) as a function of temperature (500-1000 K) for the oxidation of TMM at an equivalence ratio of 1.0 (top) and 2.0 (bottom) in a jet-stirred reactor. The experiments are done for a mean residence time of 2 seconds and a pressure of 1.07 bara.

4. Conclusions

New experimental data have been acquired from a jet-stirred reactor to capture the low- and intermediate-temperature oxidation of TMM. The oxidation of TMM starts at approximately 600 K and reaches nearly full conversion around 850 K. The major products include CH_4, CO, CO_2, C_2H_6, C_2H_4 and DMC. The relatively high effluent concentrations of C_2H_6, C_2H_4 and DMC indicate that the decomposition chemistry of TMM is fundamentally different from that of OME-2.

References

[1] K. De Ras *et al.*, "A detailed experimental and kinetic modeling study on pyrolysis and oxidation of oxymethylene ether-2 (OME-2)," *Combustion and Flame,* vol. 238, 2022, doi: 10.1016/j.combustflame.2021.111914.

[2] O. Herbinet and G. Dayma, "Jet-Stirred Reactors," in *Cleaner Combustion*, (Green Energy and Technology, 2013, ch. Chapter 8, pp. 183-210.

[3] N. M. Vandewiele, K. M. Van Geem, M.-F. Reyniers, and G. B. Marin, "Genesys: Kinetic model construction using chemo-informatics," *Chemical Engineering Journal,* vol. 207-208, pp. 526-538, 2012, doi: 10.1016/j.cej.2012.07.014.

Keywords

Trimethoxymethane; Oxidation; Jet-stirred reactor; Kinetic modeling; E-fuel.

Poster 18: Optimal design and experimental test of a reactor used for the biooxidation of refractory gold ores

Yanzhen Chen[1], Guangji Zhang[1]*, Jiale Guo[2], Chao Yang[1]*

1 State Key Laboratory of Biochemical Engineering, CAS Key Laboratory of Green Process and Engineering, Institute of Process Engineering, Chinese Academy of Sciences, Beijing, 100190, China; 2 Hefei University, School of Biology, Food and Environment, Hefei 230601, China.

**Corresponding author: gjzhang@ipe.ac.cn (Guangji Zhang), chaoyang@ipe.ac.cn (Chao Yang)*

Highlights

- Designed a stirred tank equipped with draft tube and microbubble generator.
- The biooxidation rate in the designed reactor is higher than the former.
- The new reactor improved the solids suspension and oxygen transfer rate.
- Bacterial growth and metabolism are better with gentle stirring in this reactor.

1. Introduction

Biooxidation is considered as the most promising technology for pre-treatment of refractory gold ores prior to the recovery of gold by cyanidation. Currently, many commercially successful biooxidation plants are running in several countries. Due to the slow oxidation rate, the large scale continuous stirred tank reactors (CSTR) are adopted in these plants for getting longer residence time[1-2]. However, the solids sedimentation is inevitable in these large scale stirred tank reactors, which results in higher pulp density at the tank bottom. On the other hand, the gas utilization rate is low in this kind of gas dispersed systems[3-4].

2. Methods

For achieving better reaction efficiency, a stirred tank equipped with draft tube and microbubble generator is designed. The new reactor is tested by biooxidation of arsenic-bearing gold concentrate with the mixing strain containing *Leptospirillum ferrooxidans* and *Acidithiobacillus caldus* used in all experiments. Eh, pH, dissolved oxygen concentration and total arsenic concentration are monitored and the volumetric mass transfer coefficient $k_L a$ is measured in different biooxidation stages.

3. Results and discussion

The biooxidation experiment results showed that the redox potential (Eh) rise rate and the oxygen uptake rate (OUR) slowed down with the increasing pulp density, implying that the friction from the random motion of ore grains will influence the bacteria significantly. Experimental data showed that the biooxidation rate is higher in the reactor equipped with draft tube and microbubble generator at the 25% pulp density. The dearsenization reaches 70% in 6 days in contrast to 8 days in the former stirred tank.

4. Conclusions

The new reactor is thought capable to improve the solids suspension and oxygen transfer rate with gentle stirring and introducing microbubbles.

Acknowledgment: This work was supported by the National Key Research and Development Program (2022YFC2105302).

References

[1] D. E. Rawlings, Trans. Nonferrous Met. Soc. 18 (2008) 1311–1318
[2] M E. Ly Arrascue, J V Niekerk, Hydrometallurgy. 83 (2006) 90–96
[3] J Lueske, K Kar, L Piras, J Pressler, Chem Eng Technol. 38 (2015) 1993–2001
[4] S. S. D. Jesus, J M Neto, R. M. Filho. Biochem Eng J. 118 (2017) 70–81

Keywords

biooxidation of refractory gold ores; stirred tank; draft tube; microbubble

Poster 19: **Acidity requirement and reaction pathway for the dehydration of 1,3-butanediol to 1,3-butadiene over ZSM-22**

Loïc Eloi[1,2], Jeroen Poissonnier[2], Dhanjay Sharma[1], Maarten K. Sabbe[1,2], Joris W. Thybaut[2] and An Verberckmoes[1]*

1 Industrial Catalysis and Adsorption Technology, Ghent University, 9000 Ghent, Belgium

2 Laboratory for Chemical Technology, Ghent University, 9052 Zwijnaarde, Belgium

**Corresponding author: An.Verberckmoes@Ugent.be*

Highlights

- Successful hydrothermal synthesis of HZSM-22 with varying Si/Al ratio & without any impurities
- HZSM-22 crystals exhibit a uniform needle-like morphology with comparable textural properties
- Influence of acid properties of HZSM-22 is being investigated for 1,3-butanediol dehydration

1. Introduction

The transition towards a carbon-neutral and circular society requires the production of bulk chemicals to shift from fossil feedstocks to bio-based ones. 1,3-Butadiene (BD) is a key building block in the chemical industry and its main application is associated with the production of synthetic rubbers. BD is currently obtained as a by-product during naphtha steam cracking (4-5 wt% yield) in ethylene plants, which poses an impact on the environment. Moreover, lighter feedstocks are being used in ethylene plants, i.e. shale gas, which reduces the BD supply. Therefore, an on-purpose BD production is required to meet the increasing BD demand and the need for a more sustainable chemical industry [1]. The selective dehydration of 1,3-butanediol (1,3-BDO), requiring two consecutive dehydration steps, is a greener alternative to obtain BD and is currently being investigated over solid acids. However, one drawback of this process is that one of the intermediates, 3-buten-1-ol (3B1OL), is prone to cracking and generates propylene and formaldehyde, negatively impacting the BD selectivity. Lee et al. [2] studied different topologies and concluded that 3B1OL is subjected to intramolecular hydrogen bonding in bigger pores (HZSM-5) hampering further dehydration and limiting the BD yield, typically below 60%. In contrast, smaller pores (HZSM-22) inhibited this phenomenon, increasing the BD yield to 65% in a continuous fixed-bed reactor at 300°C. In this present work, commercially available as well as self-synthesized HZSM-22 with varying Si/Al ratio (45-100) are thoroughly characterized and the catalytic performance for the dehydration of 1,3-BDO is assessed in a continuous fixed-bed reactor.

2. Methods

Commercially available NH_4-ZSM-22 was purchased from ACS Material LLC and calcined to obtain its protonic form. The self-synthesized zeolites were prepared via a hydrothermal synthesis procedure and ion-exchanged to obtain HZSM-22 [3]. The topology, morphology, composition, and physicochemical properties are determined via XRD, SEM-EDX, ICP-OES, N_2-sorption, and NH_3-TPD, respectively. The gas-phase dehydration reactions will be investigated in a high-throughput kinetics set-up, in a set of parallel continuous flow fixed-bed reactors using a 20 wt% of 1,3-BDO in 1,4-dioxane as feedstock. The experiments will be performed between 250-300°C, at varying space times (5-210 kg.s/mol) to cover the entire conversion range, and at a total pressure of 5 bar.

3. Results and discussion

As depicted in Figure 1a, the XRD patterns of the self-synthesized zeolites exhibit characteristic diffraction peaks corresponding to the ZSM-22 topology without any impurities, indicating a successful synthesis. SEM images of commercial HZSM-22 (Figure 1b) revealed aggregates of small needle-like crystals with dimensions ranging from 300-500 nm. In contrast, the self-synthesized materials display a consistent needle-like morphology, with crystals measuring 5 µm in length and widths ranging from

100-500 nanometers (Figure 1c). Furthermore, as displayed in Table 1, the self-synthesized materials exhibit a higher specific surface area and pore volume compared to c-HZSM-22. Since commercial HZSM-22 has a similar Si/Al ratio as HZSM-22 (45), c-HZSM-22 can be used as a benchmark to investigate the influence of the textural and morphological properties on the dehydration of 1,3-BDO. Moreover, by varying the Si/Al ratio in the self-synthesized materials, the acid properties were altered, while maintaining comparable textural properties (Table 1). The influence of the acid properties on the dehydration of 1,3-BDO is being investigated through catalytic experiments to get insight into the catalyst design and to improve the BD. It is expected that a higher Si/Al ratio, i.e. HZSM-22 (100), would result in less cracking of 3B1OL, and therefore, a higher BD yield.

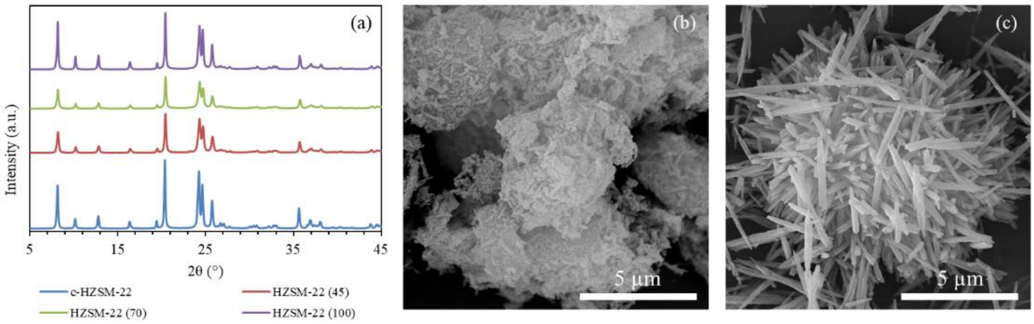

Figure 1. (a) XRD patterns of the zeolites studied in this work, (b) SEM image of c-HZSM-22, and (c) of HZSM-22 (45).

Table 1. Physicochemical properties of the materials studied in this work.

Sample	**N_2-adsorption**		**Acidity, NH_3 uptake (µmol/g)**			**Total acidity (µmol/g)**	**Si/Al^{EDX}**
	S_{BET} (m^2/g)	$V_{tot.}$ (cm^3/g)	Weak	Medium	Strong		
c-HZSM-22	182	0.12	98	97	107	302	43
HZSM-22 (45)	271	0.14	80	97	110	287	47
HZSM-22 (70)	295	0.14	48	56	102	206	63
HZSM-22 (100)	301	0.14	30	35	75	140	104

4. Conclusions

In this work, HZSM-22 with varying Si/Al ratio and a needle-like morphology are prepared via a hydrothermal synthesis approach. The synthesized zeolites do not contain any impurities, consist of crystals with dimensions of 5 µm, and exhibit comparable textural properties, allowing to investigate the influence of the acidic properties on the dehydration of 1,3-butanediol to butadiene. Commercially obtained HZSM-22 is used as a benchmark and to investigate the textural and morphological properties on the dehydration reaction, since c-HZSM22 has a lower specific surface area, and pore volume and consists of smaller crystals with dimensions of 300-500 nm compared to HZSM-22 (45). The materials are being investigated in a continuous flow fixed-bed reactor at temperatures between 250-300 °C and varying space times to cover the entire conversion range.

References

[1] E.V. Makshina, M. Dusselier, W. Janssens, J. Degrève, P.A. Jacobs, B.F. Sels, Chem. Soc. Rev., 43 (2014) 7917-7953.
[2] J.H. Lee, S.B. Hong, Appl. Catal. B Environ., 280 (2021) 119446.
[3] M. Zhai, W. Wu, E. Xing, Y. Zhang, H. Ding, J. Zhou, Y. Luo, J. Liu, K. Zhu, X. Zhu, Chemical Engineering Journal, 440 (2022) 135874.

Keywords

HZSM-22; 1,3-butanediol dehydration;1,3-butadiene; catalyst development

Poster 20: Hydrolysis of an emerging contaminant using an immobilized laccase scaffold fabricated by 3D technology

Carola Bahamondes[1*], Paula Garín,[1] Isabel Cáceres[1]

1 Departamento de Biotecnología, Universidad Tecnológica Metropolitana, Santiago,

**Corresponding author: c.bahamondesd@utem.cl*

Highlights

- Design and 3D printing of a polylactic acid reactor.
- Immobilization of laccase enzyme in the previously functionalized polylactic acid reactor.
- Hydrolysis of oxytetracycline using the reactor with the immobilized enzyme.

1. Introduction

Currently, the usefulness of enzymes in different bioprocesses worldwide is mainly limited by their stability and cost, which has led to the research and development of processes that use some immobilization method.

Recently, three-dimensional (3D) printing has enabled a breakthrough in the design and fabrication of complex structures through the fused deposition modeling (FDM) process [1], achieving the rapid creation of prototypes with complex geometries, especially those with internal structures, porous structures, and channels, without loss of material. This technology can be applied to fabricate supports for immobilizing enzymes. In the last decade, polylactic acid (PLA) filaments have gained popularity as a thermoplastic source for use in 3D printing in multiple areas, due to their advantages over other materials, such as their biodegradability, biocompatibility, low cost, high availability and mechanical strength; in addition to their ease of printing, gloss and multicolor appearance. Despite these advantages, PLA is a hydrophobic material, with absence of functional groups, being necessary to make chemical modifications that allow the union between the material and the enzyme.

The objective of the research developed was the immobilization of the laccase enzyme in a prototype bioreactor printed with 3D technology, using PLA functionalized with chemical groups that allowed the binding of the enzyme, to apply it in the reduction of the emerging pollutant oxytetracycline.

2. Methods

A network-like structure was printed with 3D technology, using a 1.75 mm natural colored 3D850 PLA filament SMARTFIL. This device was subjected to a chemical modification, first an aminolysis reaction was carried out [2], obtaining amino groups and then an activation with glutaraldehyde [3], to allow the covalent bonding between the enzyme and the support. The correct functionalization of the material was corroborated with the use of FTIR infrared spectroscopy and immobilization by the determination of activity with the ABTS substrate, determining the immobilization yield [4]. The bioreactor with immobilized laccase obtained was used to hydrolyze the antibiotic oxytetracycline, analyzing supernatant samples at different times using an HPLC system.

3. Results and discussion

A disc shaped lattice type device was printed and subjected to different chemical modifications. The aminolysis allowed the successful incorporation of amino groups into the structure, optimizing the reaction conditions with Diaminohexane at 40°C for 15 minutes. Subsequently, the conditions to activate the support were optimized by adding 15% glutaraldehyde for 16 hours at 30°C. Finally, the best conditions were found to immobilize the enzyme, using a pH of 4.5 and 20°C, obtaining a scaffold with approximately 6.5 mg of laccase per gram of PLA and an immobilization yield of 74.5% with a retained activity of 65.1%.

The bioreactor with immobilized enzyme was used to hydrolyze the antibiotic oxytetracycline at different pH and a temperature of 20°C. The best results are obtained at pH 6, with a percentage of hydrolysis close to 70% at 48 hours of reaction.

4. Conclusions

Conditions were optimized to functionalize the surface of a PLA scaffold and immobilize the laccase enzyme, with an immobilization yield close to 75%. The device obtained allowed the hydrolysis of about 70% of oxytetracycline in aqueous solution.

References

[1] S. Y. Jun, A. Elibiary, B. Sanz-Izquierdo, L. Winchester, D. Bird, A. McCleland. IEEE T. Comp. Pack .Man Tech.(2018). 8, 2227-2235.

[2] F. Gonçalves, R. Bentini, M. Burrows, A. Carreira, P. Kossugue, M. Sogayar, and L. Catalani.(2015). Materials 8, 408–23.

[3] M. Vera, G. Nyanhongo, G. Guebitz, and B. Rivas. (2020). Arabian Journal of Chemistry 13, 4218–27.

[4] Z. Gao, Y. Yi, J. Zhao, Y. Xia, M. Jiang, F. Cao, H. Zhou, P. Wei, H. Jia, X. Yong X.(2018). Bioresour Bioprocess. 5, 27C.A. de Araujo Filho, D. Mondal, S. Haase, J. Wärnå, K. Eränen, J.P. Mikkola, T. Salmi, Chem. Eng. Sci. 149 (2016) 277–295.

Keywords

Immobilized enzyme, hydrolysis of oxytetracycline, bioreactor, PLA scaffold

Poster 21: Investigating deactivation and kinetics of levulinic acid hydrogenation on titania supported ruthenium catalysts

Adarsh Patil[1], Amin Delparish[1], Remy Creemers[1], John van der Schaaf[1] and M.F. Neira d'Angelo[1*]

1 Laboratory of Chemical Reactor Engineering, Sustainable Process Engineering group, Chemical Engineering and Chemistry, Technische Universiteit Eindhoven, P.O. Box 513, 5600 MB, Eindhoven, The Netherlands

**Corresponding author: M.F.Neira.dAngelo@tue.nl*

Highlights

- Cause of deactivation - sintering, coking, leaching and ruthenium oxidation state investigated
- Deactivation kinetics higher at lower operating temperatures.
- Leaching and coking not observed. Sintering and changing oxidation state dominant phenomena.
- First order kinetics of levulinic acid hydrogenation upon catalyst stabilization after initial deactivation.

1. Introduction

Successful substitution of traditional industrial commodities derived from non-renewable sources with renewable counterparts has been one of the primary focus in recent years. Lignocellulosic biomass sourced through agricultural and forestry residues, waste streams from paper and pulp mills to produce alternate chemicals can help accomplish this. Among a multitude of chemicals that can be obtained from these sources, γ-valerolactone (GVL), produced via levulinic acid (LA) hydrogenation, can be used as a solvent and fuel additive. The hydrogenation of LA typically takes place under aqueous phase conditions. Recent trends on ruthenium-catalyzed LA hydrogenation have led to a variety of catalytic supports being used. Amongst these, TiO_2 has shown promising catalytic activity albeit suffering from deactivation. This work utilizes typical industrial conditions (T>100°C) to investigate stability and LA hydrogenation kinetics upon full deactivation of the catalyst. Slower deactivation kinetics are prevalent at higher operating temperatures. On doubling the ruthenium loading (from 1 to 2 wt.%), the catalytic activity upon full deactivation surpasses twice its value (from 10 to 53%). This was attributed to first-order dependence on LA with a deactivated Ru (2 wt.%)/TiO_2 at 100 and 200°C.

2. Methods

Ru/TiO_2 was synthesized using incipient wetness impregnation techniques with $RuCl_3$ as the ruthenium precursor. Catalytic activity testing was performed in a packed bed reactor with upflow conditions. The samples at reactor outlet were analyzed using HPLC (Zorbax Phenyl reversed phase 4.6*250mm column) and UV/vis detector. Ruthenium oxidation state was calculated using XPS on fresh and spent catalyst samples, TEM and TGA were used to analyze particle size distribution and coking of the samples, respectively.

3. Results and discussion

Figure 1 shows the drop of catalyst activity over a period of five hours. The deactivation rate is highest for 100°C and decreases with temperature. This is in stark contrast with sintering as the main cause of deactivation, since this phenomenon would otherwise be favored at high operating temperatures and high partial pressures of water. . On the other hand, evidence of some degree of sintering was observed using TEM for particle size distribution measurements. While TEM results show a 60% decrease in specific surface area of active metal particles, a 90% drop in catalytic activity is observed. In addition, an increase in Ru^0 content with longer time on stream suggests in-situ reduction and change in the catalytic structure with reaction time. Besides, no ruthenium was detected with ICP analysis of the liquid reaction sample; and no significant differences in the TGA curves of spent catalysts from different time-on-streams.

To determine the effect of ruthenium loadings on deactivation kinetics, active metal loading was initially doubled (i.e., from 1 to 2wt.%) and later, total catalyst mass was doubled (i.e., from 100 to 200 mg) while maintaining ruthenium loading at 1wt.%. Both the catalytic beds showed significantly slower deactivation kinetics (0.023-0.025 vs. 0.219 hr^{-1} with 100 mg 1wt% Ru/TiO_2) with an observed LA conversion of 51-53% upon stabilization of catalytic activity after initial deactivation.

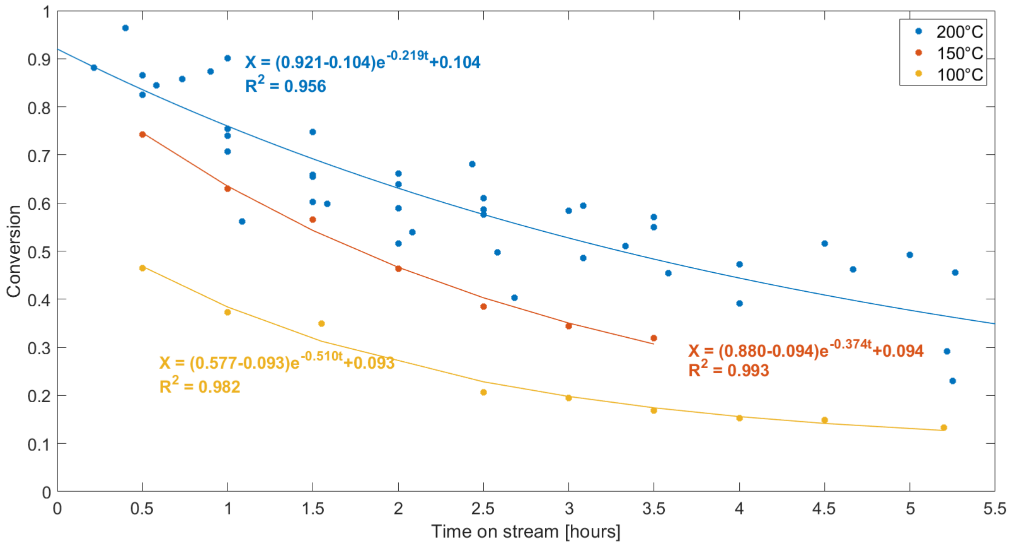

Figure 1. Deactivation of 1wt% Ru/TiO_2 (100 mg) at different temperatures with 2wt% LA in water. Flowrate - 1 mL/min of 2wt% LA and 40 NmL/min H_2.

4. Conclusions

We have shown that at higher operating temperatures (at 200°C), the deactivation rate of titania-supported ruthenium catalysts is slower than that observed at lower temperatures (at 100 and 150°C). Sintering and changes in the ruthenium oxidation state are the primary causes for deactivation in aqueous phase LA hydrogenation. We report a first-order dependence on LA for the aqueous phase hydrogenation kinetics valid from 100 to 200°C. This is applicable for catalysts stabilized after initial deactivation and not at the beginning of the catalyst lifespan. Decoupling the rate of sintering and changing ruthenium oxidation state might be beneficial in optimizing reaction and catalytic parameters for LA hydrogenation.

References

[1] Abdelrahman, O.; Heyden, A.; Bond, J. Analysis of Kinetics and Reaction Pathways in the Aqueous-Phase Hydrogenation of Levulinic Acid To Form -Valerolactone over Ru/C. ACS Catalysis 2014, 4, 1171–1181

Keywords

Deactivation, hydrogenation, sintering, kinetics

Poster 22: Investigations on nickel-based catalysts for the reverse water gas shift reaction.

Elina Mkrtchian[1], Ilaria Rizzardi[1], Marcello Pagliero[1,2], Andrea Pastorino[1], Camilla Costa[1,2], Antonio Comite[1,2]*

1 Department of Chemistry and Industrial Chemistry, University of Genoa, Via Dodecaneso 31, 16146 Genoa, Italy; 2 National Interuniversity Consortium of Materials Science and Technology (INSTM), Florence, Italy

**Corresponding author: antonio.comite@unige.it*

Highlights

- Comparison of different methods of synthesis of Ni/Al_2O_3 catalysts.
- Characterization of active metal specie by advanced electron microscopy.
- Competition of methanation and reverse water gas shift.

1. Introduction

CO_2 utilization is a growing field of research since it is an important option to contribute to the challenge of lor or neutral carbon economy. The Reverse Water Gas Shift reaction (RWGS) based on the use of green hydrogen by renewables is of interest [1] since it results in the formation of CO which is a molecule more active and prone to be more easily converted to other chemicals as for example methanol:

$$\mathrm{CO_2 + H_2 \rightleftharpoons CO + H_2O} \qquad \Delta H_r^\circ = 41.2\ \mathrm{kJ\ mol^{-1}}$$

Nickel catalyst promote both the RWGS reaction and the methanation reaction. In addition, RWGS reaction affects the product selectivity of another important process aimed at CO_2 utilization like the dry reforming one. The understanding of the factors affecting the product selectivity of Ni based catalyst is relevant due the wide use of such metal for developing industrial catalysts. In the present work carried out under the PNRR project NEST, Ni catalyst were prepared either using conventional impregnation routes or a combination of sol-gel chemistry and nanoparticle formation (e.g. either precipitation and green reduction synthesis) to evaluate the effect of the size of the active metal as well as its arrangement within the support, and their activity was assessed in a fixed bed microreactor.

2. Methods

Supported Ni catalysts were prepared by dry impregnation of commercial alumina with nickel nitrate solution. γ-alumina was obtained by aqueous precipitation from an aluminum nitrate solution and the corresponding boehmite sol was obtained by peptization at 90°C for several hours. The Ni nanoparticles were generated by reduction with glucose either before its addition to the boehmite sol or directly during the peptization step (Fig. 1). Iron as metal dopant was explored. The catalysts were characterized by physisorption with N_2 at 77K, infrared spectroscopy and electron microscopy (FESEM and S/TEM equipped with EDS mapping). The microreactor was a quartz tube filled with about 50mg of catalyst heated with an electrical mini-furnace. After the reactor water is condensed before sending the stream to a gaschromatograph set-up to ensure the detection of H_2, CO, CH_4 and CO_2. In each testing run the temperature was varied between 450°C and 650°C. Some catalysts were tested also in the dry reforming reaction to evaluate their tendency to carbon formation.

Figure 1. a) Nickel nitrate precursor solution, b) reduced Ni nanoparticles, c) boehmite sol, d) coprecipitated Ni-boehmite sol.

3. Results and discussion

The impregnation method affected the specific surface area of the support which for the catalyst resulted lower. On the other side the supported Ni was easily accessible at the reactants although its crystallite size was affected by the impregnation conditions. Glucose showed to be an effective reducing agent for the formation of the Ni nanoparticles either starting from the nickel nitrate solution or from the coprecipitated nickel and aluminium hydroxide. The formation of methane decreased by increasing the temperature above 470°C while in the same temperature range the CO yield increased. The temperature where the RWGS reaction become more important changed by varying the nickel loading and the synthesis method and on the presence of Iron as dopant.

4. Conclusions

Nickel catalysts in the RWGS reaction are affected by the competition with the methanation reaction. Catalyst preparation methods, dopant, crystallite size of the active metal as well as its confinement in the narrow pore structure affect the selectivity. In particular, the metal crystallite confinement can be advantageous during dry reforming to limit the carbon filaments formation.

References

[1] J. Gandara-Loe, E. Portillo, J.A. Odriozola, T.R. Reina, L. Pastor-Pérez, K-Promoted Ni-Based Catalysts for Gas-Phase CO_2 Conversion: Catalysts Design and Process Modelling Validation. Front Chem. 18 (2021) 785571

Keywords
Reverse water gas shift; Nickel catalyst; electron microscopy of catalysts.

Poster 23: Numerical modelling of gas-liquid flow in mesoscale reactors using periodic boundaries

Isabel S. Fernandes[1,2], Madalena M. Dias[1,2], José C. B. Lopes[1,2], Ricardo J. Santos[1,2]*

1 LSRE-LCM - Laboratory of Separation and Reaction Engineering – Laboratory of Catalysis and Materials, Faculty of Engineering, University of Porto, Rua Dr. Roberto Frias, 4200-465 Porto, Portugal Affiliation and address; 2 ALiCE - Associate Laboratory in Chemical Engineering, Faculty of Engineering, University of Porto, Rua Dr. Roberto Frias, 4200-465 Porto, Portugal

**Corresponding author: rsantos@fe.up.pt*

Highlights

- NETmix surpasses most state-of-the-art technology for mixing and heat transfer.
- Two-phase flow in NETmix was modelled using CFD simulations with a novel reduced geometric model.
- LoopNUB uses periodic boundary conditions to simulate the entire reactor's network.
- Shadowgraph technique was applied to characterise the flows experimentally.
- LoopNUB reduces the NUB CFD model for flow simulation in NETmix by 2.3 fold.

1. Introduction

NETmix is a mesosized static mixer that consists of a network of mixing chambers interconnected by channels that promotes high-intensity mixing due to its topology [1]. This reactor is having a fast industrial uptake, first introduced for the continuous large-scale production of nanosized crystal materials and, more recently, due to outstanding heat and mass transfer capabilities, for multiphase flow applications, such as the formation of CO_2 hydrates [2]. The NETmix reactor has been studied using computational fluid dynamics (CFD) simulations validated by experiments. Fonte et al. [3] introduced the model NETmix Unit Block (NUB) to simulate the flow in NETmix. This model considers a central region of the network and applies translational Periodic Boundary Conditions (PBCs) in the sidewalls. After statistical analysis of turbulent scales, it was concluded that the flow dynamics in a NUB composed of at least nine rows and three columns is suitable for describing the flow dynamics in NETmix. This NUB geometry has been used for CFD modelling of NETmix rectors for single-phase [4] and liquid-liquid [5] flows. The successive split and recombining of flow contributes to an intense fluid renewal around the two phases' interface, enhancing the mass transfer rates. The good performance of this mixer in multiphase applications motivated in depth studies. However, the CFD simulations are time-consuming as large data sets are needed to fully characterise the flow dynamics. This work presents the development of a novel CFD model based on a reduced geometry to simulate gas-liquid flows in NETmix.

2. Methods

A 2D two-phase model based on an Euler-Euler approach with the Volume of Fluid method (VOF) was developed using the CFD software ANSYS/Fluent. The VOF model was used to track the dynamic evolution of the interface between the two phases. The new model - the LoopNUB - considers, in addition to the PBCs in the sidewalls, PBCs between the inlets and outlets of the geometry, comprising four rows and three columns.

The working fluids considered were air at 20 ºC and atmospheric pressure and liquid water under the same operating conditions. A surface tension value of 73 $mN\cdot m^{-1}$ was considered between the phases. The wettability was defined by a wall contact angle of 60.5°, measured experimentally inside a water drop on a Polymethyl methacrylate (PMMA) plate. Upstream vertical flows were accounted for in the analysis. The air phase volume fraction was fixed at 0.45 for all cases, and different pressure gradients, Δp^*, were considered between the inlets and outlets of the model to determine the transitional flow regimes. Shadowgraph was applied to experimentally characterise gas-liquid flows and validate the CFD model using a transparent PMMA NETmix composed of seven rows and nine columns. Processing algorithms were developed using ImageJ and Matlab to determine the bubble size and phase hold-up.

3. Results and discussion

The pressure gradient was varied from 10-500 kPa·m^{-1} while maintaining equal the volume of the two phases inside the mixer. The CFD air volume fraction contour maps were analysed. Figure 1a shows the results for Δp^* of 25 and 500 kPa·m^{-1}, where it is observed the dispersion of air bubbles within the water.

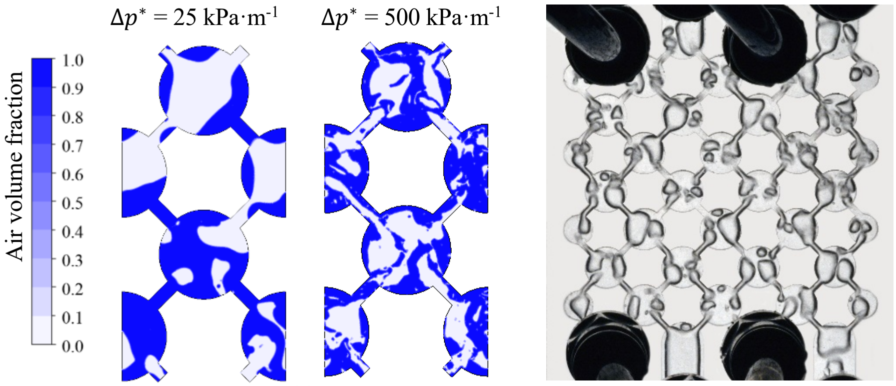

$\Delta p^* = 25$ kPa·m^{-1} $\Delta p^* = 500$ kPa·m^{-1}

(a) (b)

Figure 1. Air-water flow in NETmix (a) CFD volume fraction maps of water-air flow using LoopNUB (water – dark blue, air – white) for $\Delta p^*= 25$ and 500 kPa·m^{-1}, (b) shadowgraph result ($Re_{air}=76$, $Re_{water}= 605$).

A slug flow with large bubbles was noted for the smallest Δp^* tested (e.g. $\Delta p^*= 25$ kPa·m^{-1} – Figure 1a). The large dimension of the bubbles indicates that the surface tension is dominant over inertial forces. With the increase of Δp^*, the inertial forces increase and overtake the surface tension; therefore, the air structures become smaller and more random in shape. This is well predicted by the Weber number. For higher Δp^*(e.g. $\Delta p^*= 500$ kPa·m^{-1} – Figure 1a), the large bubbles became unstable and collapsed, leading to a churn flow with chaotic oscillation. Figure 1b shows the shadows of air bubbles as dark rings with bright interiors under the same flow conditions as the CFD result for $\Delta p^*= 25$ kPa·m^{-1} in Figure 1a. The experimental results corroborate the flow patterns predicted by the 2D CFD model. A mean equivalent drop diameter (compared with a spherical drop) of 2.48 ± 2.00 and 2.33 ± 2.21 was obtained for experiments and CFD, respectively; the values differ by less than 6%, which validates the CFD model.

4. Conclusions

Various flow regimes were modelled using the 2D LoopNUB model, varying the in/out pressure gradient. The increase in pressure gradient intensifies the flow chaoticity, resulting in a reduction in bubble size. The transition from slug to a highly disordered churn flow was observed. The shadowgraph imaging technique enabled the identification of the air-water interfaces. The agreement between experimental and 2D CFD results regarding flow patterns and bubble size distribution validated the use of LoopNUB for modelling the two-phase flow in NETmix reactors. The reduction of the simulation domain using LoopNUB will enable a faster technological development of NETmix.

References

[1] J.C. B. Lopes, P.E. M. S. C. Laranjeira, M. M. G. Q. Dias, A.A.A. Martins, Network mixer and related mixing process, US 8434933 (2013).

[2] M.F. Costa, C.M. Teixeira, A.M. Lopes, J.P. Araújo, M.M. Dias, R.J. Santos, J.C.B. Lopes, Carbon Capture and Storage Toward Industrialization: A Novel Continuous Process for the Production of Carbon Dioxide Clathrates, Energy Technol. 10(6) (2022).

[3] C.M. Fonte, M.E. Leblebici, M.M. Dias, J.C.B. Lopes, The NETmix reactor: Pressure drop measurements and 3D CFD modeling, Chem. Eng. Res. Des. 91(11) (2013).

[4] J. Matos, R.J. Santos, M.M. Dias, J.C.B. Lopes, Mixing in the NETmix Reactor, Front. Chem. Eng. (2021).

[5] I.S. Fernandes, M.S.C.A. Brito, Y.A. Manrique, M.M. Dias, J.C.B. Lopes, R.J. Santos, Experimental and Numerical Characterisation of Two-Phase Flow in NETmix Reactors, Chem. Eng. Process. (2023).

Keywords

Multiphase flow; CFD; NETmix; LoopNUB

<u>Poster 24:</u> Membrane utilization for intensified CO_2 conversion to MeOH based on multisite microkinetic modelling of $Cu/ZnO/Al_2O_3/MgO$

Anže Prašnikar[1]*, Andraž Pavlišič [1], Marija Sarić [2], Damjan Lašič Jurković [1], David Bajec[1], Matic Grom[1], Blaž Likozar[1]*

1 Department of Catalysis and Chemical Reaction Engineering, National Institute of Chemistry, Ljubljana 1001, Slovenia; 2 Energy & Materials Transition, TNO, Petten 1755, Netherlands

**Corresponding authors: anze.prasnikar@ki.si, blaz.likozar@ki.si*

Highlights

- Membrane-enhanced CO_2 conversion investigated
- State of the art multisite microkinetic model used for catalyst description.
- Determined deviations during scale-up to multitubular membrane reactor

1. Introduction

To achieve a carbon-neutral future, reducing CO_2 emissions is crucial, with potential sequestration in aquifers. CO_2 can be utilized to close the carbon loop using renewable and nuclear energy, with methanol as a key product in carbon capture and utilization (CCU). Methanol can serve as a biofuel, sourced from biomass or CO_2 from industries, using fewer H_2 molecules than for the preparation of other compounds like formaldehyde or methane. Multistep processes are involved in converting CO_2 to other compounds like elemental carbon or formic acid. Focus on methanol production through thermocatalytic CO_2 conversion is favored over other methods due to selectivity. Understanding catalyst dynamics, particularly in Cu-ZnO systems,[1] is crucial for efficient methanol synthesis. Experimental validation is necessary to confirm active site structures and optimize reaction conditions.

We here engaged in fundamental modeling of experimental data to develop practical tools for CO_2 conversion assesment. Utilizing these insights, we utilized a multisite microkinetic model, which was applied to simulate a multitube membrane-enhanced reactor for methanol synthesis. This model allows us to examine the impacts of crucial parameters during the scale-up process.

2. Methods

The input stream to the multi-tubular membrane reactor (8.6 kg of catalyst) is divided among seven membranes (SPEEK-PI on Al_2O_3, total area 0.25 m^2), each yielding two outlet streams (permeate and retentate) which were combined at the reactor exit. The gas streams were analysed with gas chromatography. The microkinetic modelling of reactor is performed in the software CERRES, developed at NIC. The multi-tubular reactor is simulated by treating it as a single-tube with a larger membrane surface area with the amount of catalyst as used in the experiment. For the membrane reactor model, we included convection and permeation through the membrane for each selected component, together with reaction phenomena such as adsorption and desorption of species on the catalytic surface along with catalytic surface microkinetic reactions on $Cu/ZnO/Al_2O_3/MgO$ catalyst.[2] In addition, CFD (computational fluid dynamics) calculations performed in OpenFoam were used to determine concentration polarization on the membrane.

3. Results and discussion

The experimental findings revealed higher CO_2 conversion and methanol yield compared to gas conversion alone in a packed bed reactor. While there was a good correlation between experimental and modeling trends (Figure 1d), the membrane reactor's performance fell short of a previously validated theoretical model developed in CERRES. To investigate this, we examined several factors: non-isothermal operation, non-uniform permeance across membranes, radial gas dispersion from reactor to membrane walls, and uncertainties in gas composition and temperature measurements. The permeance of membranes in this parallel system varied significantly, with flow rates through membranes ranging from 5% to 25% (Figure 1b). This variation affected flow distribution among parallel sections (Figure

1c) and overall synthesis rate (Figure 1a). At lower inlet flow rates into the multitubular reactor, differences in permeance had a greater impact: methanol synthesis rate decreased by 3% while CO synthesis rate increased by 1%.

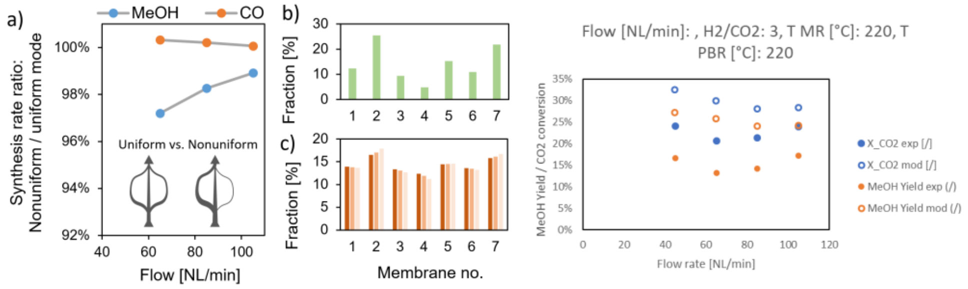

Figure 1 a) Effect of nonuniform membrane permeability on overall synthesis rate. **b)** Flow fraction through each membrane. **c)** Inlet flow rate distribution into each single-tube after variable permeability correction of membranes. **d)** Comparison of the microkinetic model results with experimental data.

The primary factor significantly affecting reactor performance is likely the low radial dispersion, which refers to the radial transport from reactor walls to the membrane. Computational fluid dynamics simulations illustrated a notable methanol molar fraction gradient (10%) across the reactor radius (Figure 2). Additional simulations will provide a more precise understanding of the reactor's performance impact.

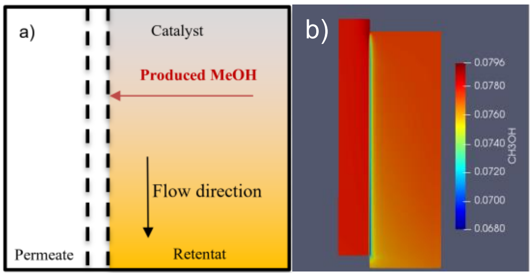

Figure 2 a) Scheme of the part of membrane reactor. For efficient MeOH membrane reactor operation the produced MeOH in any part of reactor should travel fast enough to the membrane walls (and than permeate through). **b)** Simulation results showing large gradient of MeOH molar fraction (10%) across the reactor radius.

4. Conclusions

We utilized CERRES software to model a multitubular membrane reactor for enhanced MeOH synthesis, revealing consistent trends between experimental and modeled data. Notably, we identified radial transport from reactor walls to the membrane as a critical factor influencing catalyst activity. These findings shed light on the critical steps of MeOH synthesis and suggest opportunities for enhancing reactor design and operation to intensify CO_2 conversion.

References

[1] van den Berg, R.; Prieto, G.; Korpershoek, G.; van der Wal, L. I.; van Bunningen, A. J.; Lægsgaard-Jørgensen, S.; de Jongh, P. E.; de Jong, K. P. (2016). Structure sensitivity of Cu and CuZn catalysts relevant to industrial methanol synthesis. Nat. Commun., 7, 13057.

[2] Prašnikar, A.; Jurković, D. L.; Likozar, B. (2021). Reaction Path Analysis of CO_2 Reduction to Methanol through Multisite Microkinetic Modelling over Cu/ZnO/Al2O3 Catalysts. Appl. Catal. B Environ., 292, 2.

Keywords

Membrane reactor; microkinetic modelling, CO_2 conversion, reaction intensification

Poster 25: Single Pellet String Reactors – Theoretical Study on Heat and Mass Transport Limitations based on the CO_2 Methanation

Christian Bauer[1,2,*], Tabea Gros[1,2], Olaf Hinrichsen[1,2]

1 Technical University of Munich, School of Natural Sciences, Lichtenbergstr. 4, 85748 Garching, Germany
2 Technical University of Munich, Catalysis Research Center, Ernst-Otto-Fischer-Str. 1,85748 Garching, Germany
**Corresponding author: ch.bauer@tum.de*

Highlights

- Evaluation of internal and external mass transfer in Single Pellet String Reactors
- Identification of the hotspot formation and its evaluation with changing flow rate
- Dependency of the reactor performance on the pellet string length

1. Introduction

The single pellet string reactor (SPSR) has shown potential for testing different catalyst shapes as a scaled-down version of a fixed-bed reactor [1]. The reactor tube has a diameter that closely matches the diameter of the catalyst pellets. The main goal of this study is to examine the scalability of different single pellet string lengths with respect to external mass transfer limitations. The exothermic CO_2 methanation over a Ni-based catalyst serves as the model reaction. Reactive CFD modelling is used to get insights into the SPSR system with the highest level of detail. The reliability of the model is shown by comparing the simulative studies with experimental results.

2. Methods

Reactive CFD simulations are conducted by a fully resolved multi-region model. In the fluid phase, conservation of total mass, momentum, species and energy is ensured. The porous catalyst pellets are fully resolved in terms of heat and mass transfer by Fick's law or Fourier's law. The model is implemented in OpenFOAM v2006 as steady-state solver. The kinetic model by Xu and Froment [2], which serves as the source term for heat and species in the catalytic reaction, has been refitted to powder measurements of crushed pellets. Our spherical catalyst pellets were prepared by impregnating Al_2O_3 pellets with a nickel-nitrate solution, resulting in a nickel loading of 20 wt.-%. For all cases, a stoichiometric molar feed gas ratio of $H_2/CO_2 = 4/1$ was used for the reaction. All feed gas flow rates result in a particle Reynolds number below 50 which allows the assumption of laminar flow conditions. Internal mass transfer resistance can be evaluated by efficiency factors. The efficiency factor of a species, which is evaluated for each pellet, is defined by the ratio of its volume averaged formation rate and its surface averaged formation rate. The temperature uptake in the pellets due to the exothermic reaction and the heat transfer resistance is postprocessed as well. Moreover, the deviation from plug-flow conversion is evaluated by section wise 1D modelling of the SPSRs. In this attempt the maximum temperature of a pellet and its efficiency factor for methane production is passed to the corresponding section in the 1D model. In this way the effects of internal mass transfer resistance and of heat transfer are assumed to be compensated. The deviation between 1D and CFD modelling are then assumed to result from non-ideal transport phenomena in the gas phase.

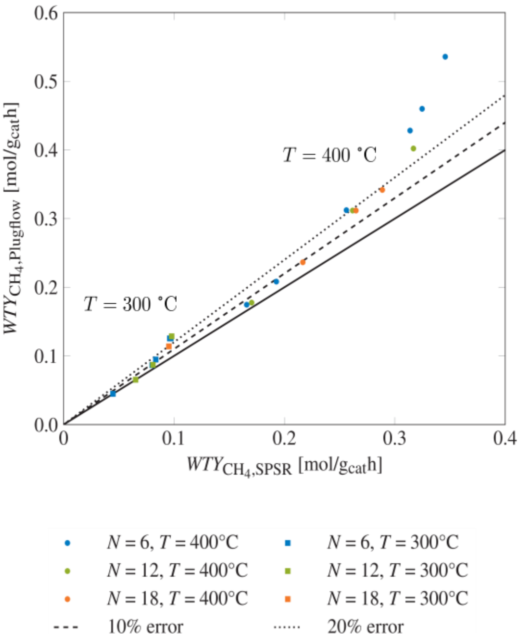

Figure 1. Comparison of methane weight time yield between section wise 1D plug-flow modelling and reactive CFD modelling of SPSRs with different lengths.

3. Results and discussion

In general, conversion results of SPSRs with different lengths show that under laminar flow conditions a 12 pellet and an 18 pellet SPSR result in nearly the same performance at the same GHSV while a 6 pellet long SPSR shows less carbon dioxide conversion and methane production. This can also be indicated in figure 1 where the deviation from plug-flow conversion is evaluated. By comparing the methane production, a 6-pellet long SPSR deviates the most. In any case the higher the methane production rate, which is related to a higher GHSV at constant temperature, the more a SPSR deviates from plug-flow behavior. This can be ascribed to the external mass transfer resistance which becomes dominant with increasing flow rate. Figure 2 supports this finding as it shows the Damköhler number for methane production in a 6 pellet SPSR. Damköhler numbers above unity indicate that mass transport is dominant. In this context, the first pellets in a SPSR are more influenced by external mass transport than the last ones. However, with decreasing flow rate more pellets are operating in the kinetic regime as the Damköhler numbers dropping below unity. This indicates that for spheres the SPSR is a suitable reactor to reach plug-flow behavior at lower flow rates.

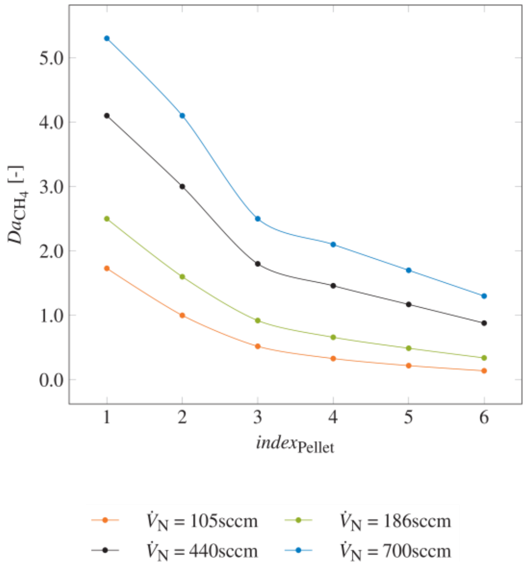

Figure 2. Damköhler numbers for methane production in a 6 pellet SPSR at different flow rates. The pellets are counted in ascending order in flow direction.

4. Conclusions

For the investigated system a 12 pellet SPSR is sufficient to yield results which are independent of the pellet number at constant GHSV in the laminar flow regime. The internal mass transfer resistance is evaluated by the effectiveness factor which relates the surface reaction rate with the mean reaction rate of each sphere. Relatively high surface temperatures due to the exothermicity of the methanation reaction and the limited diffusion rate due to the small pores of our pellets result in quite low effectiveness factors for methane production. By comparing the results of section wise 1D modelling of the SPSRs and reactive CFD modelling we address the deviations to non-ideal mass transport in the gas phase. With increasing flow rate, the deviations also increase which means external mass transfer becomes relevant. This can also be found by the evaluation of the Damköhler number for each component. More pellets operate in the mass diffusion regime at higher flow rate while most pellets in the SPSR operate in the kinetic regime at lower flow rates.

References

[1] J. Fernengel et al., Chem. Eng. J. 373 (2019) 1397–1408.
[2] J. Xu. and G. F. Froment, AIChE Journal 35 (1989) 88–96.

Keywords

Single Pellet String Reactor; Heat and Mass Transfer Limitations; CO_2 Methanation; Reactive CFD Modelling

<u>Poster 26::</u> Coalescence and rebound of bubbles in gas-liquid dispersed systems: experiments and theory

Runci Song[1], Jie Chen[1,2], Luchang Han[3], Chao Yang[1,2]

[1]*State Key Laboratory of Petroleum Molecularand Process Engineering, CAS Key Laboratory of Green Process and Engineering, Institute of Process Engineering, Chinese Academy of Sciences, Beijing 100190, China*

[2]*School of Chemical Engineering, University of Chinese Academy of Sciences, Beijing 100190, China*

[3]*School of Chemical Engineering, Xiangtan University, Xiangtan, Hunan 41105, China*

Abstract: Bubble collisions often occur in gas-liquid dispersion systems, and the collision results have a significant impact on the bubble size distribution and flow field structure of the system. However, current research on bubble collision is still limited, and its dynamics are unclear. We have investigated the bubble's behavior at different collision velocities via experiments, simulations, and modeling. Experiments show that the collision outcome can shift from coalescence to rebound as the collision velocity increases. A novel model that simultaneously considers the bubble approach, deformation, and film drainage processes was developed. Unlike previous models, this model can not only predict bubble coalescence but also rebound, thus predicting the critical collision velocity. The theoretical and experimental results are in good quantitative agreement. Also, a direct numerical simulation of the bubble collision process was carried out, which captured the motion characteristics of the bubbles well. The necessity of considering bubble deformation in the model was verified by analyzing the energy evolution during the collision process. Our work provides new insights into the modeling of bubble coalescence, and the newly developed model helps to improve the accuracy of gas-liquid reactor simulations.

Keywords: Bubble collision; Coalescence and rebound; Mechanism model；Deformation

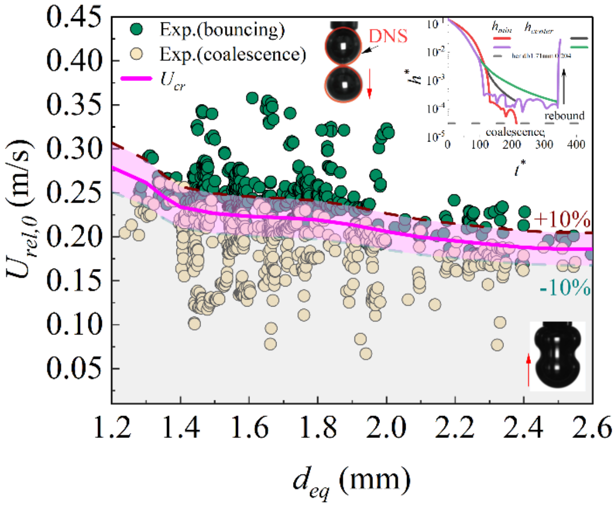

Figure 1: Comparison between experimental measurements (dot), model predictions (U_{cr}) and direct numerical simulations (bubble contour) of bubble collisions

Acknowledgment: This work was supported by the National Key Research and Development Program (2023YFC3903901) and the National Natural Science Foundation of China (22078320, 22035007, 21676224).

Poster 27: Comparative Study of Conventional and Ozone-assisted Catalytic Oxidation of Methane using Mn/Hydroxyapatite Catalyst: Introducing a Novel Setup

Reza Monjezi[1], Alexandra Bouriakova[1], Karen Leus[2], Philippe M. Heynderickx[3,4], Pascal Van Der Voort[5], Rino Morent[2], Joris W. Thybaut[1,*]

1 Laboratory for Chemical Technology, Ghent University, Technologiepark 125, B-9052 Ghent, Belgium; 2 Research Unit Plasma Technology, Ghent University, St-Pietersnieuwstraat 41, 9000 Ghent, Belgium; 3 Ghent University Global Campus, 119-5 Songdomunhwa-Ro, Yeonsu-Gu Songdo Incheon 406-840, South Korea; 4 Department Green Chemistry and Technology, Ghent University, Coupure Links 653, 9000 Ghent, Belgium; 5 COMOC-Center for Ordered Materials, Organometallics and Catalysis, Department of Chemistry, Ghent University, Krijgslaan 281-S3, 9000 Ghent, Belgium

**Corresponding author: Joris.Thybaut@UGent.be*

Highlights

- CH_4 CCO over Cu/HAP indicated a high temperatures requirement.
- LoPOx setup enabled comparison of CH_4 CCO and OzCO, offering controlled experimental conditions.
- Mn/HAP possessed higher O_{ads} (4 X) compared to Cu/HAP.

1. Introduction

In recent decades, the increase in emissions of volatile organic compounds (VOCs) has posed profound environmental and health challenges. Conventional catalytic oxidation (CCO), which employs oxygen (O_2) as the oxidant, is recognized as an efficient approach to reduce VOC emissions. However, this approach necessitates high operational temperatures, leading to energy efficiency constraints. As a promising alternative, ozone-assisted catalytic oxidation (OzCO) offers the advantage of effectively eliminating VOCs at lower temperatures (below 150 °C). Employing ozone (O_3) as an oxidant in OzCO introduces a crucial sensitivity to pressure, thus requiring precise control of the reaction's total pressure [1], a factor that has been overlooked in existing literature. Moreover, a comparison between the efficiency of CCO and OzCO in VOC abatement remains inadequately explored. As part of the present work, a novel experimental setup is introduced, specifically designed to acquire intrinsic kinetic data for both CCO and OzCO under precisely-controlled, near-ambient pressure conditions. Methane (CH_4), a highly stable light alkane, is used as a model compound for this investigation. The Mn/hydroxyapatite (Mn/HAP) catalyst was chosen based on the superior activity of MnO_x in the OzCO reaction, ascribed to pronounced reducibility, multiple oxidation states, and excellent performance in O_3 decomposition. This work aims to compare Mn/HAP catalyst performance for the CH_4 CCO and OzCO and investigate the impact of operating conditions, including total pressure, on CH_4 OzCO performance.

2. Methods

A hydroxyapatite (HAP) support was prepared via co-precipitation using $Ca(NO_3)_2.4H_2O$ and $NH_4H_2PO_4$ precursors. Two monometallic catalysts (Cu/HAP and Mn/HAP), each containing 10 wt% metal, were synthesized using wet impregnation. The synthesized materials were characterized using O_2-TPD.

A novel custom-built setup, denoted as Low-Pressure Ozone-assisted Oxidation (LoPOx), was employed to evaluate intrinsic catalytic performance at precisely-controlled pressure conditions. The LoPOx setup is meticulously designed to operate at near-ambient pressure conditions, accommodating both vapor-phase and liquid-phase VOCs, within a concentration range of 1000 to 5000 ppmv, reflecting typical VOC concentration levels encountered in both indoor and outdoor environments. The setup integrates an O_3 generator to convert O_2 into O_3, alongside several MFCs making it possible for the simultaneous feeding of various reactants. The LoPOx setup features a fixed-bed reactor (L=500 mm, ID= 9 mm), equipped with a thermocouple (OD=3.2 mm) positioned within the reactor to precisely monitor the temperature of the catalyst bed. This reactor's temperature range spans from low temperatures (50 to 150 °C) where O_3 thermal decomposition is minimal, up to 600 °C for CCO experiments. An outstanding feature of the LoPOx system is its capability to maintain the total reactor pressure at nearly atmospheric levels, a functionality rarely found in OzCO experimental setups. The LoPOx setup is equipped with an O_3 analyzer, gas chromatograph (GC), and mass spectrometer (MS) for real-time analysis of component concentrations spanning from ppm to percentage levels, both in transient and non-transient conditions.

3. Results and discussion

Kinetic experiments on CH_4 CCO using Cu/HAP have been performed as a benchmark (shown in Figure ***1***a), resulting in a 40% conversion of CH_4 at a space time amounting to 535 $kg_{cat}\ s\ mol_{CH_4,0}^{-1}$. These findings highlight the temperature demand to accomplish CH_4 total oxidation.

The O_2-TPD profile shown in Figure 1b revealed that 4 times more surface adsorbed oxygen (O_{ads}) is present on Mn/HAP than on Cu/HAP. These highly active O_{ads} species play a pivotal role in the VOC OzCO reaction by targeting adjacent VOC molecules and cleaving C-H bond [2], thereby significantly enhancing the CH_4 OzCO performance. Additionally, the MnO_x catalysts possess easily accessible multiple oxidation states, contributing to the best capacity for O_3 decomposition, thus resulting in superior performance in OzCO reaction [1]. The combined effect of the increased O_{ads} species and multiple oxidation states of MnOx underscore the superior activity of Mn/HAP catalyst, potentially overcoming the constraints observed with the benchmark catalyst in the CH_4 OzCO reaction. Comparative studies of CH_4 CCO and OzCO using Mn/HAP are ongoing to more effectively evaluate the performances of CCO and OzCO techniques.

The LoPOx setup is currently being used for the verification of the intrinsic kinetic regime at conditions where the reaction rate is the highest. Subsequently, it is aimed to compare the efficiency of CH_4 CCO and OzCO approaches utilizing Mn/HAP catalyst by determining the T_{50} value, representing the temperature required to achieve 50% conversion. Following this comparison, the study will investigate the effect of total pressure fluctuations, mirroring atmospheric pressure changes throughout the year (0.95 to 1.05 bara), on the O_3 decomposition and the CH_4 OzCO performance.

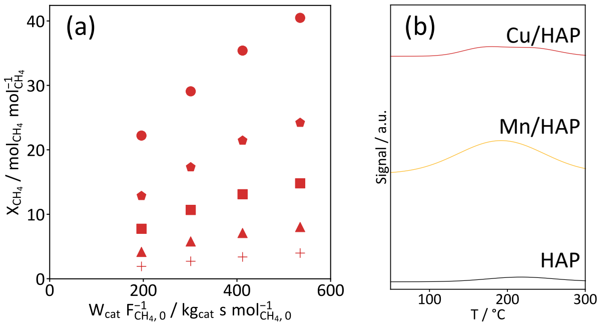

Figure 1. (a) CH_4 conversion (X_{CH_4}) vs. $W_{cat}F_{CH_4,0}^{-1}$ over Cu/HAP catalyst in CCO at T=350 (+), 375 (▲), 400 (■), 425 (⬟), and 450 °C (●). (b) O_2-TPD profiles.

4. Conclusions

CH_4 CCO using Cu/HAP indicated a high temperature requirement in this approach. The Mn/HAP possessed 4 times higher amount of O_{ads} compared to Cu/HAP catalyst, making it an excellent choice for comparative study between CH_4 CCO and OzCO. The novel LoPOx setup was crucial in investigating the performances of CH_4 CCO and OzCO over Cu/HAP and Mn/HAP catalysts, offering precise control over reaction conditions.

References

[1] F. Lin, Z. Wang, Z. Zhang, Y. He, Y. Zhu, J. Shao, D. Yuan, G. Chen, K. Cen, Chemical Engineering Journal 382 (2020)

[2] B. Liu, J. Ji, B. Zhang, W. Huang, Y. Gan, D.Y.C. Leung, H. Huang, J Hazard Mater 422 (2022).

Keywords

Volatile Organic Compounds; Catalytic Ozonation; Mn catalyst

Poster 28: A FACILE BIOMASS CARBON-BASED COMPOSITE FOR APPLICATION IN ELECTROCHEMISTRY

Cristina M. S. G. Baptista[1,*], Christopher M. A. Brett[2], Marcelino L. Gimenes[3], Mara Heloisa N. O. Scaliante[3], Wanderson da Silva[2], Wardleison M. Moreira[1,3]

[1]CERES, Department of Chemical Engineering, University of Coimbra, 3030-790 Coimbra, Portugal
[2]Department of Chemistry, CEMMPRE, University of Coimbra, 3004-535 Coimbra, Portugal
[3]PEQ, Department of Chemical Engineering, State University of Maringá, Maringá, Paraná, Brazil
**Corresponding author: cristina@eq.uc.pt*

Highlights

- Tannin and Kraft black liquor blends synthesized a low-cost carbon-based electrode material.
- The presence of a variety of functional groups enhances the novel electrode electrochemical properties.
- The electrode has excellent cycling stability, with no significant loss of specific capacitance after 1000 cycles.
- The proposed electrode promoted electrochemical oxidation of acetaminophen and bisphenol-A.

1. Introduction

A consequence of increasing global industrialization is the generation of waste, which has caused a significant environmental impact. In this context, biorefinery has gained considerable importance for improving renewable waste management. Renewable wastes, such as biomass, have high availability and low cost, are environmentally friendly and recyclable, and can also be used as raw materials in developing new biobased materials. Among all the biomass wastes, lignocellulosic biomass is an accessible and abundant renewable carbon source. It can produce new biomass-derived carbon-based materials (BCP) with improved functional, mechanical, and electrochemical properties and high thermal stability. BCP electrodes have excellent properties, low cost, easy preparation, and renewable surface. A simple, environmentally friendly electrode from BCP can be obtained by blending it with biomacromolecules, such as chitosan.

The present work proposes a new BCP by hydrothermal processing of condensed tannin and integral Kraft black liquor. The integral Kraft black liquor pH is around 12–14 and is directly mixed with the tannin extract solution. The basic medium favors breaking the condensed tannin hydrogen bonds, decreasing the viscosity of the solution to an operational range. Then, the direct use of Kraft black liquor decreases the viscosity of the tannin extract, improving its processability, reducing the processing costs of effluent generation, and saving process time. The synthesized BCP was blended with chitosan, producing a BCP-chitosan composite used to fabricate BCP electrodes. The BCP and the BCP-chitosan composite were characterized, and the electrochemical properties of the new BCP electrode (BCE) were studied by cyclic voltammetry (CV) and electrochemical impedance spectroscopy (EIS). Finally, the new BCE was also assessed for sensing applications, illustrated by acetaminophen (APAP) and bisphenol A (BPA) determination using square wave voltammetry (SWV).

2. Methods

A reflux system was used to synthesize the BCP, as discussed by Moreira et al. (2021)[1]. Briefly, the synthesis occurred by first hydroxymethylating the integral Kraft black liquor with formaldehyde. A tannin solution was prepared in a sodium hydroxide aqueous solution and incorporated into the hydroxymethylated black liquor to be blended. After these steps, the hydroxymethylated blend was crosslinked inside a stainless steel/PTFE autoclave under hydrothermal conditions. The BCP-chitosan composite was then prepared by mixing the chitosan acetic solution and the BCP powder. The new BCP electrode (BCE) was made by packing the BCP-chitosan paste into a plastic tube, and a copper disc plus wire was inserted on the rear side to establish electrical contact. Then, the surface was mechanically smoothed, and the excess carbon paste was removed with filter paper without further pretreatment. Electrochemical measurements were carried out in a conventional electrochemical cell with a rear copper plate as a working electrode (BCE), a Pt wire as a counter electrode, and an Ag/AgCl (3 M KCl) electrode as a reference. Voltammetric experiments were performed with an Ivium CompactStat potentiostat (software version 2.024, Ivium Technologies, Netherlands). Electrochemical impedance measurements were carried out with a Solartron 1250 Frequency Response Analyzer coupled to a Solartron 1286 electrochemical interface using ZPlot 2.4 software (Solartron Analytical, UK).

3. Results and discussion

The new material was characterized, and its potential application as an electrode material was assessed. Cyclic voltammetry, square wave voltammetry, and electrochemical impedance spectroscopy were used to characterize the system.

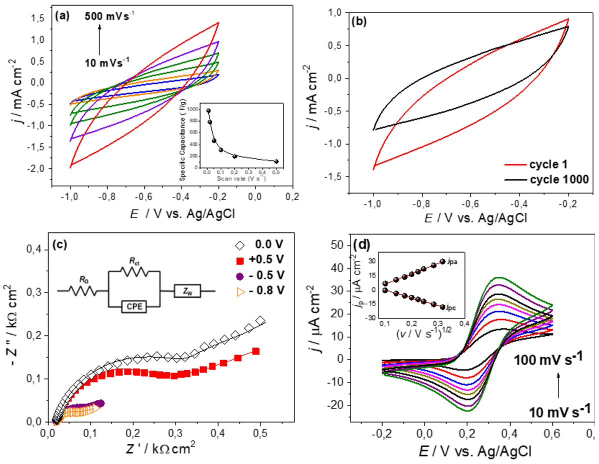

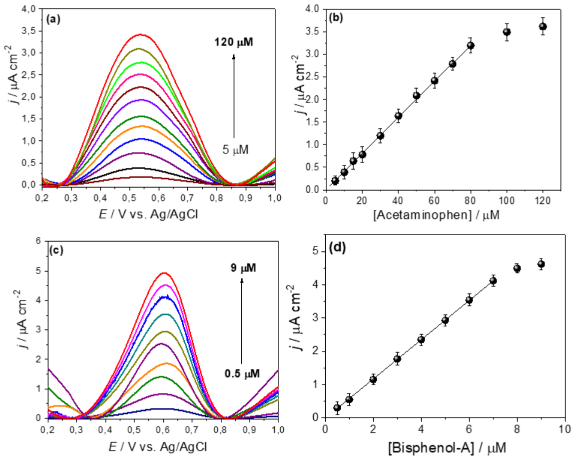

Figure 1. Electrochemical characterization of BCE ((a) to (c)) carried out in a 6.0 M KOH aqueous electrolyte. (a) cyclic voltammetric curves at different scan rates, inset: Specific capacitance calculated from cyclic voltammetric curves at different current densities; (b) Cycling stability measurements of the BCE; (c) Complex plane impedance spectra at BCE; (d) Determination of electroactive area from cyclic voltammetric curves of 5 mM $K_3[Fe(CN)_6]$ in 0.1 M KCl at different scan rates, inset: dependence of the anodic and cathodic peak current densities, j_{pa} and j_{pc}, on the square root of the scan rate ($v^{1/2}$).

Figure 2. (a) SWV curves for various concentrations of acetaminophen (APAP) at BCE in 0.1 M phosphate buffer solution (pH 7.0); (b) Relationship between the oxidation peak current and the concentration of APAP; (c) SWV curves for various concentrations of bisphenol A (BPA) at BCE in 0.1 M phosphate buffer solution (pH 7.0); (d) Relationship between the oxidation peak current and the concentration of BPA. SWV conditions: 50 Hz frequency, 50 mV amplitude, 25 mV s^{-1} scan rate, 0.5 mV step potential.

The quasi-rectangular shape voltammograms of the novel electrode resembled those of a typical electrical double-layer capacitor. The electrode has excellent cycling stability, with no significant loss of specific capacitance after 1000 cycles and promoted electrochemical oxidation of acetaminophen and bisphenol-A with good reproducibility and excellent selectivity.

4. Conclusions

A biomass carbon-based polymer was successfully synthesized under hydrothermal conditions using Kraft black liquor and tannin as phenolic precursors. Afterward, the material was blended with chitosan to produce a biomass carbon-based electrode, which presented no apparent redox peaks in the 6.0 M KOH electrolyte solution. After 1000 cycles, its specific capacitance remained at 92% of its initial value. As an electrochemical sensor for acetaminophen and bisphenol A, the oxidation peak currents after 30 days were 96.5% and 95% of the initial value, respectively. The good reproducibility and repeatability of the synthesized electrode demonstrate its feasibility as an alternative, sustainable, and low-cost material in electrochemical applications.

References

Moreira, W.M., Viotti, P.V., Vieira, M.G.A., Baptista, C.M.S.G., Scaliante, M.H.N.O., Gimenes, M.L., Colloids Surfaces A Physicochem. Eng. Asp. 608 (2021), 125597.

Keywords

Biomass; Hydrothermal carbonization; Capacitors; Electrochemical sensor.

Poster 29: Characterization and modelling of an innovative Elastic Foam-bed Reactor (EFR) for gas-liquid(-solid) multiphase applications

Laura TRICAS*, Pascal FONGARLAND, Régis PHILIPPE, David EDOUARD
CP2M, Université Lyon 1, CNRS, CPE 3 Rue Victor Grignard, 69100 Villeurbanne, France
** laura.tricas@univ-lyon1.fr*

Highlights

- Study of a “new family” of reactor
- High G-L mass transfer rate for a low energy consumption.
- Up to 75% increase in G-L mass transfer coefficient when compared to fixed bed mode
-

1. Introduction

Process intensification sets a challenge in chemical industry, particularly in multiphase systems where reactor performance often dictates process efficiency. Several physical phenomena can influence the productivity but the most important are heat and mass transfer.

In a process intensification objective, several strategies were developed to overcome these issues. Among them, one consists in the use of millimeter-scale structured internals to replace dense packed beds (monoliths, open cells solid foams or static mixers [1]), inert or coated with an active catalyst layer. Another one consists in the use of unsteady and/or periodic operations (siphon reactor, rotating packed beds, oscillating reactors, etc. [2]). However, these solutions can be difficult to implement and may not be suitable for complex fluid flows.

In this context, the study proposes the exploration of a 'new family' of reactors, recently described in the literature: the Elastic Foam-bed Reactor (EFR) [3]. This concept exploits the mechanical properties of an elastomeric structured internal (PU foams) to promote G-L mass transfer efficiency when submitted to periodic compression/decompression cycles with a low energy input, as illustrated in figure 1. The combination of two foams on each side of a crankshaft, in phase opposition, ensures a constant volume operation. The mechanical movement undergoes by the local fluid flow and foam material structure, contribute to an effective mixing, nearly decorrelated from fluid flowrates. Such elastomeric structure can be functionalized by soft chemistry via a polydopamine film [4].

2. Methods

To characterize the reactor in countercurrent gas-liquid flow (Figure 1.b.), an experimental methodology is implemented for the measure of three effective parameters in a multiphase reactor: (i) liquid and gas retention, (ii) pressure drop, and (iii) gas-liquid transfer.

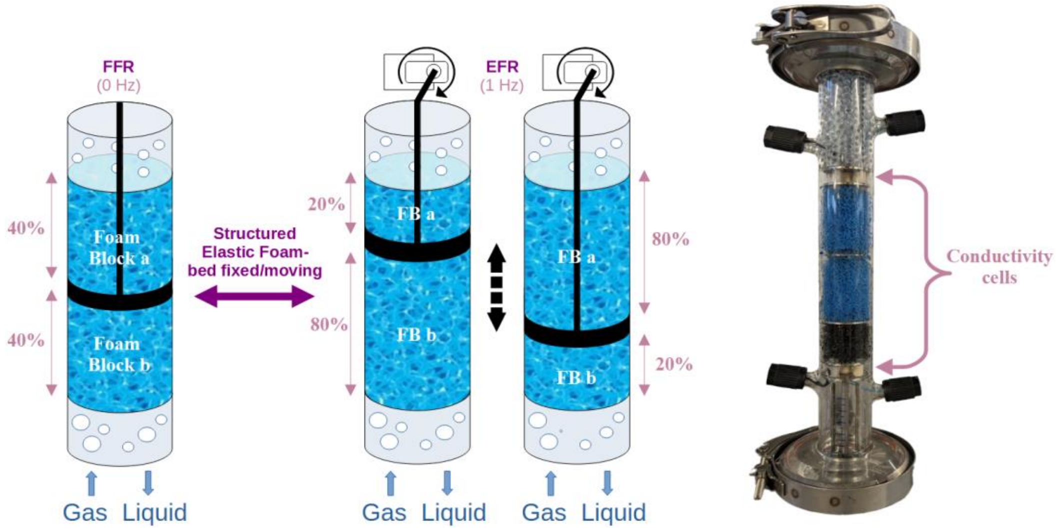

Figure 1. a: Diagram of the two operating modes (FFR and EFR) b: Photograph of the reactor

Each of these parameters is evaluated for the two reactor operating modes: (I) fixed bed mode (Fixed Foam-bed Reactor), in which the foams are not deformed over time (crankshaft with a frequency of 0Hz), and (II) dynamic bed mode (Elastic Foam-bed Reactor, crankshaft frequency of 1Hz), Figure. 1, a. This approach allows the comparison between the EFR and FFR efficiency [3]. The liquid retention ($\varepsilon_l(t)$) is obtained by the tracer method (a KCl solution in Dirac is followed by conductimetry) Figure 1, b. The pressure drop is measured using two manometers, located upstream and downstream of the catalytic bed. Finally, the overall gas-liquid mass transfer (K_la) is estimated using O_2 stripped by N_2 in deionized water measured by an oxygen probe, Figure. 2.

3. Results and discussion

By assuming a plug flow behavior in the liquid phase, the concentration balance of O_2 in the liquid phase ($C(z,t)_l$) is given by the following PDE:

$$\frac{\partial \varepsilon_l(t) * C(z,t)_l}{\partial t} = D_{ax_l}\frac{\partial^2 C(z,t)_l}{\partial z(t)^2} - u_l\frac{\partial C(z,t)_l}{\partial z(t)} + K_l a\left(\frac{C(z,t)_g RT}{H} - C(z,t)_l\right)$$

It should be noted that the packing (elastic foams) undergoes deformations during the crankshaft cycles and therefore the liquid retention and the spatial variable z vary over time.

The experiments are conducted in steady-state conditions, and the flow is considered as an ideal piston flow. As a first approximation, the gas velocity is considered negligible [3]. Under these conditions, the K_la can be estimated using the following relation:

$$K_l a = \ln\left(\frac{\frac{C_g^{in}RT}{H} - C_l^{in}}{\frac{C_g^{out}RT}{H} - C_l^{out}}\right)$$

$$avec\ C_g^{out} = C_g^{in} + \frac{u_L}{u_G}\left(C_l^{in} - C_l^{out}\right)$$

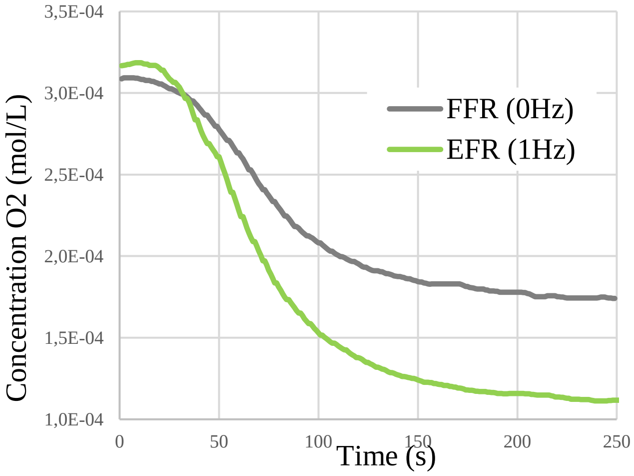

Figure 2. Evolution of the concentration of O_2 in saturated water (in equilibrium with air) stripped by N_2 with, the gas and liquid velocities of $8.0*10^{-3}$ m/s.

4. Conclusions

Under similar gas and liquid flow conditions, the FFR mode achieves a K_la of approximately $4.24*10^{-2}$ s^{-1}, whereas the EFR mode achieves a K_la of $7.38*10^{-2}$ s^{-1}, which means an improvement of 75% of the mass transfer between the two modes.

The full comparison between static and dynamic modes will be detailed for various flowrates during the conference. Future work will be dedicated to the impact of various parameters in the dynamic operation (foam structure, frequency, amplitude, etc.).

References

[1] C.P. Stemmet, M. Meeuwse, J. Van der Schaaf, B.F.M. Kuster, J.C. Schouten, Gas–liquid mass transfer and axial dispersion in solid foam packings, Chemical Engineering Science, 62, 5444, 2007.
[2] K.D.P. Nigam, F. Larachi, Process intensification in trickle-bed reactors, Chemical Engineering Science, 60, 5880, 2005.
[3] M. Michaud, F. Bornette, E. Rautu, S. H. More, M. Leonardo Martinez Mendez, L. Jierry, D. Edouard, Unprecedented continuous elastic foam-bed reactor for CO2 capture, Chemical Engineering Journal, 452, 138604, 2023.
[4] L. Birba, Mousses Élastomères En Polyuréthane Comme Supports Catalytiques Structurés Pour l’intensification de Procédés Chimiques, Polymères, 2021.

Keywords

Process intensification; multiphase reactor; elastic structured catalytic bed; gas-liquid mass transfer.

Poster 30: Computational Benchmark for Vanadium Oxide Clusters in Oxidative Dehydrogenation of Propane

Dilan Tunçer, Elisabete Maria Tangerino Pinto, Sara Santos, Max Bols, Mark Saeys*

Laboratory for Chemical Technology (LCT), Department of Materials, Textiles and Chemical Engineering (MaTCh), Faculty of Engineering and Architecture, Ghent University, Technologiepark 125, 9052 Ghent, Belgium

**Corresponding author: Mark.Saeys@UGent.be*

Highlights

- Hybrid functionals are suitable for calculating vanadium structures in the gas phase. The B3LYP level with a Def2TZVP basis set is suitable for geometry optimization and to obtain Raman frequencies at reasonable computational cost. Single point energies are then best derived with a CCSD(T) method.
- In mono- and dinuclear clusters, the V^{3+} oxidation state is thermodynamically unstable relative to the V^{+5} and V^{+4}. This suggests a redox couple between the +5 and +4 oxidation states drives catalytic cycles.
- The thermodynamics of the polymerization of vanadium monomers revealed that the formation of dimers from monomers is favorable, especially for polymerization of identical ion structures.

1. Introduction

Propylene production through the oxidative dehydrogenation of propane (OPDH), employing oxidants like O_2 and CO_2, has attracted considerable attention due to its several advantages over traditional industrial propane dehydrogenation processes. Utilizing CO_2 offers the added benefit of consuming a greenhouse gas and preventing product overoxidation. Research into active and selective catalysts for this process is ongoing. Vanadium, supported on various materials, emerges as a promising catalyst due to its abundance, low toxicity, and versatile redox properties [1]. Its catalytic activity arises from its ability to readily transition between oxidation states 3+, 4+, and 5+, facilitating a redox cycle [2].

Computational simulations have garnered attention to design more effective catalysts, offering insights into their activity, selectivity, and stability [3]. As an initial step towards computational simulations of vanadium catalysts for oxidative dehydrogenation of propane (OPDH), it is imperative to benchmark the methods. This study reports a comparative analysis using various computational methods and basis sets.

2. Methods

Density functional theory (DFT), MP2 and coupled cluster (CC) methods were performed using ORCA [4]. Monomer and dimer structures of vanadium clusters were examined under standard conditions through gas phase simulations. Hybrid (B3LYP, M06-2X, PBE) and pure (M06-L and MN15-L) functionals were used for DFT calculations. In coupled cluster methods, CCSD, CCSD(T) and DLPNO-CCSD(T) with two basis sets (Def2TZVP and Def2QZVP) were used. The effect of each method and basis set were assessed for geometry optimization, single point energy calculations, and frequency analysis for all geometries.

3. Results and discussion

For the optimization of the structures' geometries, B3LYP/Def2TZVP is preferred, giving favorable performance at low cost in optimizing geometries and deriving Raman frequencies. For energies, a subsequent single point CCSD(T) or DLPNO-CCSD(T) calculation is recommended. These calculations demonstrate that the instability of the vanadium +3 oxidation state impedes a sequential net two electron reduction of the propane substrate. More favorable would be two repeated transitions between +5 and

+4 oxidation states, either at two different vanadium sites or with intermittent regeneration. This would suggest dimers would be more suitable for catalyzing the two-electron propane to propene reaction.

In the conversion of propane to propylene, dimers hence exhibit greater catalytic activity than monomers. For instance, in $(V^{V}O(OH)_2)_2(\mu\text{-}O)$, the presence of two active V=O bonds facilitates consecutive hydrogen abstractions (Figure 1). On the dimers, the initial hydrogen abstraction presents the largest barrier, as confirmed by our calculations.

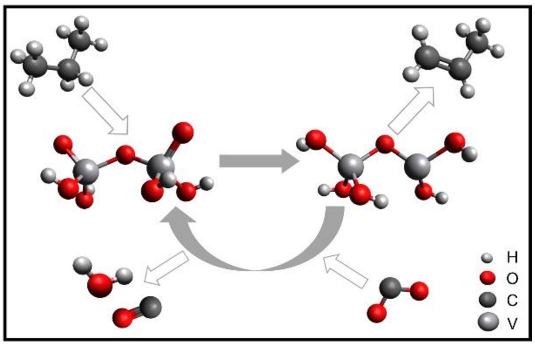

Figure 1. Reduction cycle on vanadium dimer clusters in ODHP.

4. Conclusions

A comprehensive benchmark study on vanadium clusters, covering both monomer and dimer forms, began with initial geometry optimization using various theoretical methods. Hybrid DFT functionals outperformed others in describing the geometry of vanadium clusters. The M06-2X functional demonstrated superior accuracy compared to CCSD. Finally, CCSD(T)/Def2QZVP emerged as a suitable CC level, with DLNPO-CCSD(T)/Def2-QZVP as a balanced alternative.

References

[1] M. G. Rigamonti, M. Shah, T. G. Gambu, M Saeys, M. Dusselier ACS Catal. 12, 15, 9339–9358 (2022)

[2] Y. L. Shan, H. Sun, S. Zhao, P. Tang, W. Zhao, J. Ding, W. Yu, L. Li, X. Feng, D. Chen, ACS Catal. 12, 5736−5749 (2022)

[3] E. Lontchi, M. M. Mason, M. Vasiliu, D. A. Dixon, Phys. Chem. Chem. Phys. 25, 8355-8368 (2023)

[4] F. Neese, F. Wennmohs, U. Becker, C. Riplinge, J. Chem. Phys. 152, 224108 (2020)

Keywords

Vanadium oxide catalyst, oxidative propane dehydrogenation, ab-initio calculations, density functional theory.

PostePoster 31: MICS: Green and sustainable products & materials from non-critical and secondary raw sources

M. Di Serio[1*], F. Orabona[1], F. Recupido[2], F. Taddeo[1], G.C. Lama[2], L. Verdolotti[2], V. Russo[1]
1 Università di Napoli 'Federico II', Department of Chemical Sciences, Napoli, Italy
2 Institute for Polymers, Composites and Biomaterials (IPCB-CNR), CNR, Portici, Italy

**Corresponding author: diserio@unina.it*

Highlights

- Bio-based non isocyanate polyurethane foams are presented.
- Review on green and sustainable products for NIPU synthesis.
- Chemical and technological aspects were treated.

1. Introduction

The Neapolitan Industrial Chemistry Laboratory (NICL) of the Department of Chemical Sciences of the University of Naples Federico II is a key player in the MICS (Made in Italy–Circular and Sustainable) Extended Partnership, on the synthesis of green and sustainable products & materials from non-critical and secondary raw sources, with the aim to synthesize non-isocyanate polyurethane foams (NIPUs).

Polyurethane (PU) foams represent a wide class of polymeric materials, having implications in different sectors from automotive, packaging, cushioning/bedding to construction building. However, their synthesis requires the use of oil-based components, mostly harmful and toxic isocyanate components. On this account, NIPUs foams have been indicated as suitable candidates to replace conventional PUs, where foams can be obtained through "non-isocyanate" routes such as aminolysis between 5 or 6 membered ring-cyclic carbonates (5CCs and 6 CCs) and diamines or transurethanization between carbamates and diamines. A sketch of the possible routes is reported in Figure 1 [1].

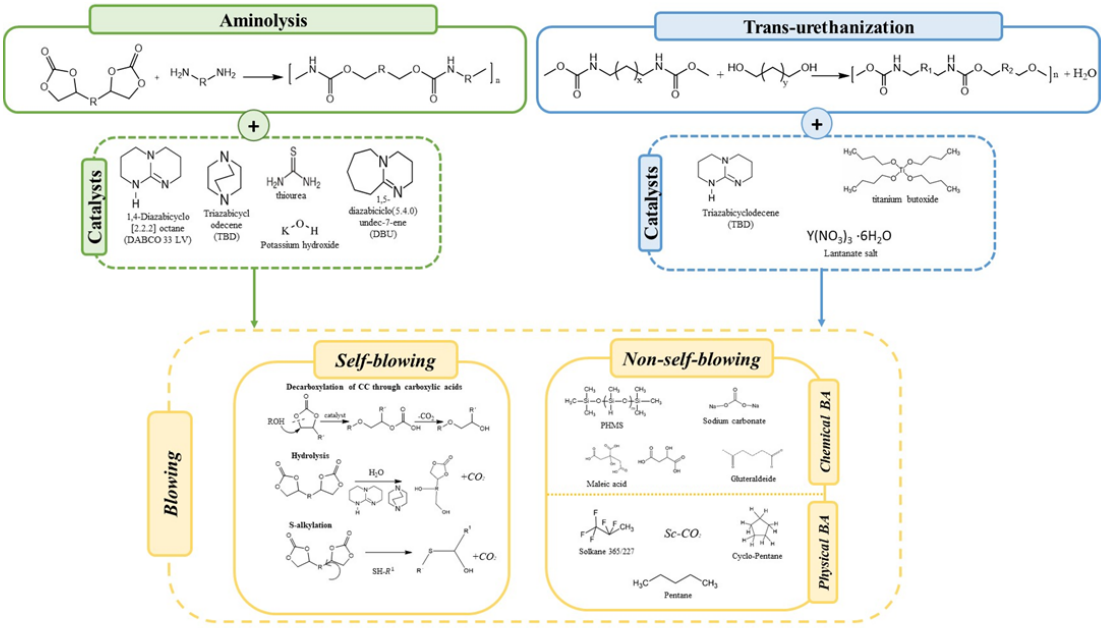

Figure 1. Main polymerization and blowing routes to obtain NIPU foams. Taken from [1].

In the present work, details on the different strategies are provided.

2. Conclusions

During the last decade, NIPU foams have gained considerable attention as alternatives to isocyanate PU-based foams owing to the chief environmental concerns associated with the use of isocyanate compounds. Aminolysis and trans-urethanization have been presented as environmentally friendly strategies for the synthesis of NIPU-based materials. In the first cases, 5-CCs from renewable sources (e.g., vegetable oils, lignin, sugars) have been widely selected owing to their versatility and low environmental footprint. Although less studied, carbamates have also appeared as possible "green" precursors of NIPUs via the trans-urethanization route. Diamines (derived also from sustainable sources e.g., cadaverine, putrescine and the commercial PriamineTM) are co-monomers to both CCs and carbamates and can be obtained sustainably through e.g., fermentation of sugars. To get foamed materials, polymerization occurs simultaneously with blowing reaction, which can be aided using chemical or physical BAs (non-self-blowing) or via self-blowing routes (s-alkylation or hydrolysis). Conventionally, harsh process conditions i.e., temperatures higher than 100°C and long curing times are often necessary; this represents an important limitation in upscaling on larger scales.

Promising results have been recently achieved using self -blown PHU foams, obtained using water as a blowing agent and with a relatively short gelling time e.g., 30 min. which opens the possibility to implement such materials on industrial scales in the future. Therefore, it is also worth stating that, the development and optimization of new routes conducted at lower temperature conditions will be included, including the optimization of membered ring-CCs- CCs e.g., 6CCs, which, at present, are found to be more reactive and harder to control than 5CCs.

Moreover, a few studies have pointed out the reprocessability of NIPU foams through diol-based CANs and to depolymerize such materials at their end life by upcycling them into new-generation foams or in thermoplastic films. On the contrary with conventional PU foams, NIPU foams present primary and secondary hydroxyl groups, which makes the reprocess much easier. Contextually the evaluation of the environmental impact of NIPU precursors and foams through LCA is also little investigated. In this sense, several affords will be required to comprehensively provide relevant information on the material life cycle stages from selection/extraction of precursors 'building blocks to service lifetime and end-life of foams, by pointing out possible environmental burdens.

References

[1] F. Orabona, F. Recupido, F. Taddeo, G.C. Lama, T. Salmi, M. Di Serio, L. Verdolotti, V. Russo, submitted to ACS SusChemEng 2024.

Keywords

NIPU; MICS; green and sustainable chemistry.

Acknowledgements

This study was carried out within the MICS (Made in Italy–Circular and Sustainable) Extended Partnership and received funding from the European Union Next-Generation EU (Piano Nazionale Di Ripresa E Resilienza (PNRR) –Missione 4 Componente 2, Investimento 1.3 –D.D. 1551.11-10-2022, PE00000004). This manuscript reflects only the authors' views and opinions, neither the European Union nor the European Commission can be considered responsible for them.

Poster 32: GCM development to predict liquid organic hydrogen carrier properties and to evaluate energetically their hydrogenation/dehydrogenation cycle.

Javier Álvarez-Valcarce, Antonio Tabernero, Eva M. Martín del Valle

Department of Chemical Engineering, University of Salamanca, Spain

Hydrogen is considered one of the most promising energy carriers for different applications. However, its use in the industry is still difficult due to different phenomena, starting with its storage. In this context, liquid organic hydrogen carriers (LOHCs) have been proposed as an alternative to classical methods to storage hydrogen. The use of LOHCs is based on the hydrogenation/dehydrogenation reaction of organic compounds. LOHCs´ properties are important concerning their future use for hydrogen storage. In this respect, a group contribution model (GCM) has been developed to estimate the properties (normal boiling point, normal melting point, heat liquid capacity, standard enthalpy of formation and the partition coefficient octanol-water) of potential LOHCs. The obtained deviations in the predictions were always lower than 10%, highlighting the accuracy of this fast methdology. This GCM was also used to perform mass and energy balances of several unknown LOHCs hydrogenation/dehydrogenation processes to evaluate mainly the energy involved in a computational way, proposing the implementation of an organic ranking cycle to decrease the energy requirements. These results can be used to perform an initial selection of a compound to be used as a future LOHC, assessing also a potential energy integration in the general hydrogenation/dehydrogenation process.

Poster 3Poster 33: Single Bubble Rise in Marinized Fluidized Beds

Athena Adabi, Ali Akbar Sarbanha, Seyed Mohammad Taghavi, Faïçal Larachi*

*Department of Chemical Engineering, Université Laval, 1065 Avenue de la Médecine, Québec, Québec G1V 0A6, Canada (*Corresponding author: faical.larachi@gch.ulaval.ca)*

Highlights

- Bubbles shrink after reaching 1/3 height in vertical beds.
- Bed tilt creates channels, altering bubble trajectories.
- Vertical deviations reduce minimum fluidization.
- Bubble dynamics altered by swell-like bed oscillations.

1. Introduction

Given today's global concerns regarding greenhouse gas emissions [1], the shipping industry is poised to improve its environmental impact by utilizing fluidized bed technology, echoing its adoption in the 1980s as an effective emission control solution for coal-fired marine boilers, driven by the remarkable heat and mass transfer capabilities of fluidized beds [2]. Although the transition to diesel engines resulted in a period of stagnation in the advancement of marine fluidized bed technologies, the potential of these systems, especially bubbling fluidized beds, has remained largely untapped. Although recent research has delved into rolling fluidized beds in the fast fluidization regime for marine exhaust treatment [3,4], our prior investigations have primarily focused on bubbling fluidized beds [3]. This study is the first to address the dynamics of individual bubbles in this context. The integration of fluidized bed technology into the marine environment presents a significant challenge, which is exacerbated by the six degrees of freedom motion of ships (Figure 1-a). Swell induces significant changes in the orientation of shipboard objects relative to gravity, resulting in pronounced dysfunction and instability in shipboard fluidized beds. This study investigates the local characteristics of a fluidized bed, including porosity and local minimum fluidization conditions, under marine swells by examining the behavior of a solitary bubble rising within a non-vertical and rolling beds. This approach does not attempt to alter the bed geometry, but rather aims to improve our understanding of the fundamental parameters affecting the stability of rolling fluidized beds through the detailed study of single bubble dynamics. The significance of this research lies in its in-depth investigation of the local bed characteristics induced by single bubble behavior, providing new insights that could lead to advancements in the effectiveness of marine emission control technologies. Here, we aim to provide a fundamental understanding that could pave the way for the optimization of bubbling fluidized bed systems for the adsorption of SO_X, NO_X, particulate matter, and potentially CO_2, by exploiting the unique dynamics of single bubbles under the challenging conditions presented by ocean waves.

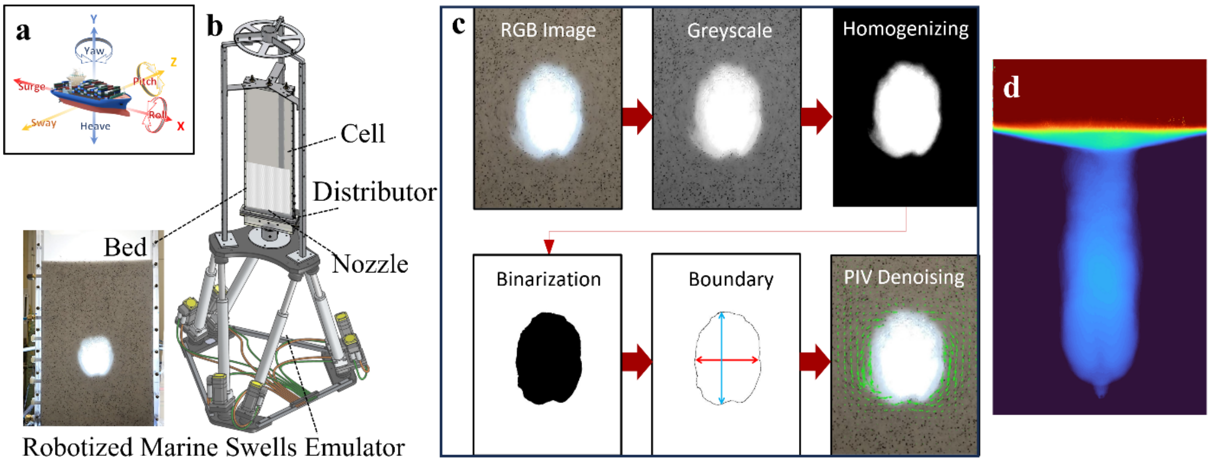

Figure 1. (a) six degrees of freedom motion of ships, (b) Setup assembly, (b) Coupled PIV-DIA steps, (c) Time-averaged bubble induced void fraction

2. Methods

To achieve precise replication of sea swell conditions, the experimental setup involved a transparent cuboidal cell, measuring 26 x 85 x 2 cm^3, specially designed to support a quasi-two-dimensional fluidized bed, as illustrated in (Figure 1-b). This cell, filled with Geldart-B class expandable polystyrene beads (EPS)—noted for their cut size range of 0.85 to 1 mm, high sphericity of 0.98, density of 1095 kg/m^3. Five nozzles, strategically placed just above the distributor and each equipped with a solenoid valve, were controlled by software designed to inject bubbles of uniform size across each transversal quintile of the bed. Bubble injection is performed when the bed is in a state of minimum fluidization, ensuring precision and uniformity of the process. To accurately simulate sea swell conditions, the fluidized bed cell itself was mounted on a hexapod platform. This arrangement allowed the simulation of sea swell motion through precise manipulations along the robot's X, Y, and Z axes, with each direction of motion clearly color-coded in red, blue, and orange, respectively. Using the Particle Image Velocimetry-Digital Image Analysis (PIV-DIA) technique, this study conducted a comprehensive investigation of bubble dynamics, covering aspects such as size, shape, and rising velocity, as well as the behavior of the granular phase around each bubble (steps shown in Figure 1-c,d). This sophisticated experimental design and methodological approach allowed a comprehensive analysis of bubble behavior and granular phase dynamics in a controlled environment that closely mimics the complex conditions of sea swells.

3. Results and discussion

Experimental results show that in a standard vertical fluidized bed, bubbles rise at a constant size after release until they reach about one-third of the height of the bed. At this point, due to a reduced pressure drop, gas escapes more freely from the bubble into the porosity of the bed, causing the bubble size to decrease slightly. Specifically, Figure 1-D shows the behavior of bubbles emanating from the central nozzle and illustrates the time-averaged bubble width at various heights within the bed, indicating a uniform phenomenon across this specific nozzle location. In an inclined bed configuration, changing the angle of inclination disrupts the minimum fluidization state of the bed, resulting in channel formation at the top and an expanding dead zone at the bottom. Bubbles closer to the formed channel are quickly drawn in and experience rapid shrinkage, while bubbles at the bottom may either avoid the dead zone or disintegrate due to gas escaping from the bubble edge into the porosity of the bed. This results in a significant deviation in the trajectory of the bubbles and a change in their shape from vertical ellipsoidal to horizontal, which impedes their upward mobility and significantly enhances transverse mixing of solids. This effect is attributed to the potential for cluster movement around the bubble perimeter under minimal fluidization conditions. Under rolling conditions, the bubble dynamics oscillate throughout the cycle between those observed in vertical and inclined configurations, with the continuous amplitude variation promoting enhanced particle mixing. The distribution of the bubble aspect ratio, as a measure of fluidization quality, was also analyzed.

4. Conclusions

This study investigated the hydrodynamics of a single bubble under the influence of non-verticality and oscillations using non-intrusive direct vision techniques. It was observed that deviations from verticality resulted in a lack of minimum fluidization, prompting a detailed examination of both bubble and solid phase behavior. By understanding the intricate dynamics of individual bubbles when subjected to complex conditions similar to sea swells, this research aims to inform future optimizations of fluidized bed technologies for environmental applications.

References

[1] P.E. Stalker, Rev. Marit. Transp., Geneva, 2021.
[2] S. Hamahira, Y. Miyaji, S. Yutani, Y. Hashimoto, J. Mar. Eng. Soc. Jpn. 18(11) (1983) 856-866.A.C.
[3] A.A. Sarbanha, F. Larachi, S.M. Taghavi, Chem. Eng. Sci. 280 (2023) 119041.
[4] T. Zhao, X. Ding, Z. Wang, Y. Zhang, K. Liu, Eng. Appl. Comput. Fluid Mech. 15(1) (2021) 210-221.

Keywords

Marine Fluidized bed; Single Bubble; PIV-DIA; Fluidization

Poster 34: Kinetics and reaction mechanism of limonene epoxidation with hydrogen peroxide promoted by Al_2O_3

Rosa Turco[1]*, Wander Perez Serna[2], Federica Orabona[1,2], Martino Di Serio[1], Kari Eränen[2], Dmitry Murzin[2], Vincenzo Russo[2], and Tapio Salmi[2]

1 Department of Chemical Sciences, University of Naples Federico II, Via Cintia, IT-80126 Naples

2 Laboratory of Industrial Chemistry and Reaction Engineering, Åbo Akademi – Turku/Åbo, FI-20500

**Corresponding author: rosa.turco@unina.it*

Highlights

- Al_2O_3 was found to be active in limonene epoxidation with hydrogen peroxide
- Information on reaction kinetics was retirved
- A reaction mechanism was proposed

1. Introduction

The epoxidation of double bonds is a very important and studied reaction because it provides valuable compounds. Usually, soluble, and heterogeneous derivatives of transition metals are used as epoxidation catalysts. The epoxidation of terpenes confers valuable fragrances, food additives and monomers [1]. Limonene is one of the most common terpenes because it is produced by more than 300 plants. This compound is extracted from citrus oil (30,000 tons per year) and is widely used as a raw material [2]. Limonene can be used in cosmetics and as a flavoring to mask the bitter taste of alkaloids. The epoxidation of limonene in the presence of homogeneous and heterogeneous catalysts provides isomeric mono and diepoxides [3, 4,]. Diepoxides can be transformed into particularly valuable polymeric materials.

The selective transformation of organic compounds into their oxygenated derivatives using truly leaching-resistant heterogeneous catalysts and green oxidants is a challenging goal of oxidative catalysis. Hydrogen peroxide is a clean and atom-efficient oxidant that produces water as the only by-product. Alumina was demonstrated to be very active in double bonds epoxidation allowing to reach high selectivity to the desired epoxy-compound [5].

The aim of the present work is the kinetic investigation and determination of the reaction mechanism of limonene epoxidation with hydrogen peroxide promoted by Al_2O_3. A rigorous kinetic investigation was conducted using the most active and selective catalyst using a fed-batch reactor. Different reaction conditions were varied to verify their influence on the reaction rates that lead to the formation of different limonene oxide isomers.

The collected data were interpreted with reliable reactor model to allow the determination of the main kinetic parameters needed for a future scale-up of the operation.

2. Methods

All the experiments were conducted in a standard jacketed fed batch reactor, of the capacity of 0.25L. Limonene was dissolved in ethyl acetate as solvent, and pre-heated at the desired temperature level under stirring. The catalyst was then added in fine powdered form. At this moment, an aqueous solution of hydrogen peroxide (60wt.%) was fed at a fixed flowrate to the reactor through a syringe pump for a given time. The starting-up of the pump represented the exact moment when the reaction started. Liquid samples were periodically withdrawn and analyzed both via GC-MS and iodometric titration to measure the evolution of the concentration of each component along the experimental time.

3. Results and discussion

The experimental results collected at different temperature were useful to determine the activation energy value for each reaction involved within the network. Figure 1A demonstrates that limonene consumption rate increases with temperature, while 1,2-limonene oxide concentration decreases because of the occurrence of ring opening reactions.

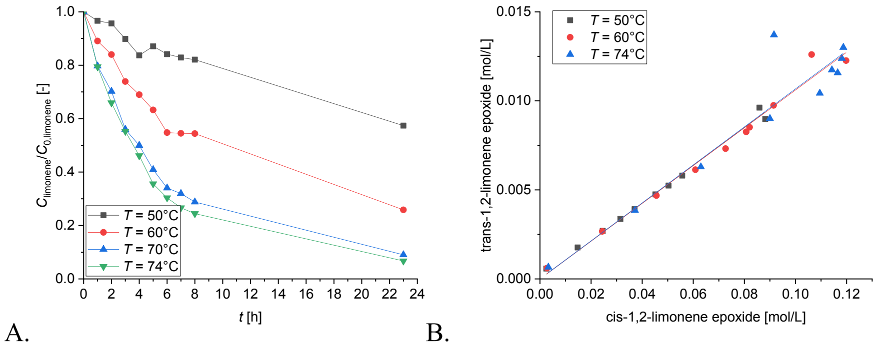

Figure 1. Temperature effect on: A. limonene consumption; B. isomers distribution.

Figure 1B clearly shows that the ratio between cis and trans isomers of 1,2-limonene oxide is kept constant along the experimental time, demonstrating that there is no equilibrium interchange between the two isomers, but the are formed via a parallel mechanism. Figure 1B clearly indicates that the two reactions leading to the two isomers are characterized by the same activation energy values, as the diagonal lines obtained at different temperatures always overlap.

Starting from all the collected results, a Langmuir-Hinshelwood rate expression was proposed for each chemical reaction, taking into consideration all the qualitative results obtained, Equation 1.

$$r_j = \frac{k_j c_l c_{H_2O_2}}{\left(1 + K_l c_l + K_{H_2O_2} c_{H_2O_2} + K_{H_2O} c_{H_2O}\right)^2} \qquad (1)$$

4. Conclusions

The limonene epoxidation reaction mechanism was investigated, and a kinetic study was conducted, allowing to find original information not reported yet in the scientific literature.

References

[1] J.L. Bicas, A.P. Dionisio, G.M. Pastore, Chem. Rev. 109 (2009) 4518-4531.
[2] P. Gallezot, Catal. *Today 121* (2007) 76-91.
[3] D. Naróg, A. Szczepanik, A. Sobkowiak, Catal. Lett. *120, (2007)* 320-325.
[4] D. Mandelli, Y.N. Kozlov, C.C. Golfeto, G.B. Shul'pin, Catal. Lett. 118 (2007) 22-29.
[5] A.J. Bonon, Y.N. Kozlov, J.O. Bahú, R.M. Filho, D. Mandelli, G.B Shul'pin, J. Catal. 319 (2014) 71-86.

Keywords
Limonene epoxidation; kinetics; Al_2O_3; hydrogen peroxide.

Poster 35: Post-Plasma Catalytic Toluene Abatement over Mn-Cu based Oxides Supported on Hydroxyapatite

Anastasiia Gromova[a,†,*], Jean-Marc Giraudon[b], Jean-Francois Lamonier[b], Maryam Nilkar[a]
Karen Leus[a], Mikhail Gromov[a], Christophe Leys[a], Nathalie De Geyter[a], Rino Morent[a]

[a] Research Unit Plasma Technology (RUPT), Department of Applied Physics, Faculty of Engineering and Architecture, Ghent University, Sint-Pietersniewstraat 41B, 9000 Gent, Belgium.

[b] Université de Lille 1 Sciences et Technologies, Unité de Catalyse et Chimie du Solide, UMR CNRS 8181, Bât. C3, Cité Scientifique, 59655 Villeneuve d'Ascq, France

[*] Corresponding author: Anastasiia.Gromova@UGent.be

Highlights

- HAP greatly boosts the oxidation of downstream fragments, increasing CO_x selectivity.
- The presence of bi-metallic oxides on the HAP positively impacts the overall process performance.
- The $Mn_{10}Cu_{10}HAP$ (1:2) catalyst demonstrates maximum toluene conversion, CO_2 selectivity, and O_3 removal.

1. Introduction

The rapid growth of the chemical industry has significantly increased VOC (volatile organic compound) emissions, worsening indoor air quality in suburban and urban areas and introducing hazardous pollutants that pose serious health risks. The main challenge is efficiently purifying air with low concentrations of VOCs, which are difficult to remove with traditional methods.

Among various techniques developed to address this issue, non-thermal plasma (NTP) has emerged as an effective tool for removing low-concentration VOCs, utilizing highly energetic electrons and reactive species like nitrogen and oxygen radicals. However, NTP alone faces challenges such as low energy efficiency, incomplete oxidation, and the formation of toxic by-products. To overcome these limitations, combining NTP with catalytic processes known as plasma-catalysis has shown promise. Plasma-catalysis enhances VOC removal efficiency, controls by-product formation, increases complete oxidation, and reduces energy consumption, advancing NTP technology for air purification [1].

This research focuses on the decomposition of VOCs using NTP combined with catalysis in a post-plasma-catalysis (PPC) process arrangement. A multi-pin-to-plate DC corona discharge reactor was used, along with catalysts such as Cu, Mn, and Cu/Mn binary oxides on hydroxyapatite (HAP) support (hereafter called catalyst). The optimal catalyst was selected based on its ability to remove toluene, destroy ozone (O_3), and achieve high total oxidation into CO_2 and H_2O under varying specific input energies (SIE) and catalytic bed temperatures.

2. Methods

The experimental setup was previously detailed in our earlier work [2]. The conditions used in this study included a gas flow rate of 1 L/min, an initial toluene concentration of 150 ppm, an SIE range of 100-350 J/L, and a catalytic bed temperature of 100-200 °C. Catalysts, including HAP support, Mn_xHAP, Cu_xHAP and Mn_xCu_xHAP (where x- is different wet percentages), were thoroughly characterized using ICP-OES, XRD, N_2-adsorption, and XPS as explained in previous studies [3]. The downstream gas phase was analyzed using Fourier-transform infrared spectroscopy (FTIR), and the concentrations of the effluent gases were used to calculate toluene conversion ($[C_7H_8]_{conv}$), CO_x ($CO+CO_2$) selectivity (S_{COx}) and O_3 removal capacity [2], [4], [5].

3. Results and discussion

The experiments were conducted in 3 different system configurations, namely plasma alone, plasma + HAP, and plasma + catalyst, to distinguish the effects of each. Toluene abatement using plasma alone was observed to be between 30% and 57% within an SIE range of 150-350 J/L. The selectivity towards CO_x increased from 8% to 15%, indicating that the process leads to partial oxidation of toluene, with fragmentation being a significant outcome. In plasma + HAP experiments, raising the HAP temperature from 100°C to 200°C led to a 7% to 20% improvement in toluene reduction compared to plasma alone scenario. The CO_x selectivity reached 57% at 200 °C with an SIE of 350 J/L. Although catalysts based on copper oxide (Cu_xHAP) and manganese oxide (Mn_xHAP) showed good results individually, combining Cu and Mn oxides on the HAP surface provided the best performance in terms of toluene and ozone removal efficiencies, as well as selectivity towards CO_2, as demonstrated in Figures 1a and 1b. Based on these results and the catalyst characterization before and after the PPC process, the roles of Cu and Mn were elucidated and summarized (see Figure 1c). Copper oxides act as electron mediators, offering active sites for VOC adsorption and interaction with reactive species generated by plasma, facilitating ozone decomposition into reactive oxygen species (ROS). Meanwhile, manganese oxides, with their ability to transition between oxidation states, enhance oxidation reactions by providing active sites and promoting electron transfer between reactants. Therefore, the combination of Cu and Mn significantly improves VOC breakdown into less harmful substances and effectively catalyzes the oxidation of VOCs and the decomposition of O_3.

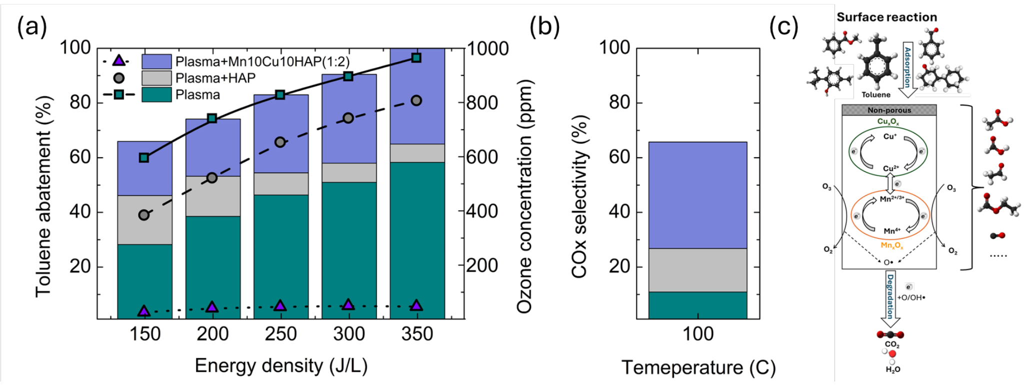

Figure 1. (a) Effect of SIE on toluene abatement efficiency and O_3 concentration in plasma-alone system (at room temperature) and PPC system (100 °C), (b) CO_x selectivity at 350 J/L and 100 °C in the catalytic reactor, highlighting the contribution of plasma, HAP, and $Mn_{10}Cu_{10}HAP(1:2)$ catalyst, and c) possible pathways of toluene degradation on the surface of bimetallic catalysts.

4. Conclusions

This study focuses on the post-plasma catalyst process for toluene removal using Mn, Cu, and Mn-Cu-based oxides supported on hydroxyapatite. The contributions of each involved process, including plasma alone, the catalytic effect of HAP, and the metal catalysts, were defined. The results showed that the PPC process considerably enhances overall reaction rates through a synergistic effect achieved by combining non-thermal plasma with the $Mn_{10}Cu_{10}HAP(1:2)$ catalyst. Plasma decomposes toluene *via* reactive species (achieving up to 60% conversion but with low selectivity towards CO_x, about 15%), while the catalyst, aided by stable oxidative species from plasma (O_3), improves catalytic oxidation (reaching 100% conversion with CO_x selectivity of 60%). The experiments demonstrated that Cu and Mn metal oxides interact strongly with plasma-generated reactive species, offering high surface area and stability. These interactions help tailor the reaction pathways, resulting in enhanced catalytic activity and improved overall process efficiency.

References

[1] M. Qu, Z. Cheng, Z. Sun, D. Chen, J. Yu, and J. Chen, "Non-thermal plasma coupled with catalysis for VOCs abatement: A review," Sep. 01, 2021, *Institution of Chemical Engineers*. doi: 10.1016/j.psep.2021.06.028.

[2] J. Van Durme, J. Dewulf, W. Sysmans, C. Leys, and H. Van Langenhove, "Abatement and degradation pathways of toluene in indoor air by positive corona discharge," *Chemosphere*, vol. 68, no. 10, pp. 1821–1829, 2007, doi: 10.1016/j.chemosphere.2007.03.053.

[3] M. Ibrahim, M. Labaki, N. Nuns, J. M. Giraudon, and J. F. Lamonier, "Cu−Mn Hydroxyapatite Materials for Toluene Total Oxidation," *ChemCatChem*, vol. 12, no. 2, pp. 550–560, Jan. 2020, doi: 10.1002/cctc.201901336.

[4] S. K. P. Veerapandian, Z. Ye, J. M. Giraudon, N. De Geyter, R. Morent, and J. F. Lamonier, "Plasma assisted Cu-Mn mixed oxide catalysts for trichloroethylene abatement in moist air," *J Hazard Mater*, vol. 379, Nov. 2019, doi: 10.1016/j.jhazmat.2019.120781.

[5] D. Chlala, J. M. Giraudon, N. Nuns, M. Labaki, and J. F. Lamonier, "Highly Active Noble-Metal-Free Copper Hydroxyapatite Catalysts for the Total Oxidation of Toluene," *ChemCatChem*, vol. 9, no. 12, pp. 2275–2283, Jun. 2017, doi: 10.1002/cctc.201601714.

Keywords

Plasma-catalysis; VOCs degradation; Toluene; Metallic and bimetallic oxide catalysts; Selectivity.

Poster 36: Optimizing Photocatalytic Reactor Design for Enhanced Indoor VOC Decomposition

Hadis Mortazavi Milani, Ewoud Cosaert, Dirk Poelman*

LumiLab, Department of Solid State Sciences, Ghent University, 9000 Ghent, Belgium

**Corresponding author: Dirk.Poelman@UGent.be*

Highlights

- A photocatalytic reactor has been designed to optimize the photocatalytic reaction rate and efficiency.
- A TiO_2/PVDF photocatalytic membrane decomposes ethanol in less than 4 minutes.
- The quick breakdown of ethanol allows for tracing the reaction intermediates.

1. Introduction

The indoor environment where people spend much of their time significantly can impact public health, as it can harbor numerous air pollutants. Volatile organic compounds (VOCs) are prevalent indoor pollutants with the potential to cause cancer, neurological disorders, and respiratory ailments [1]. Various methods, including catalytic combustion, membrane separation techniques, bioprocesses, and photocatalysis, have been developed to address this issue [2]. Photocatalysis, using semiconductors like TiO_2, has proven to be effective in decomposing pollutants while consuming minimal energy [3]. This study aims to optimize photocatalytic efficiency by developing an innovative photocatalytic reactor and tracking the resulting reaction intermediates.

2. Methods

The study involved the photocatalytic decomposition of ethanol in a quartz tube batch reactor with a volume of 0.3 L (Fig. 1). A photocatalytic membrane, containing TiO_2 particles, was fixed to the surface of a stainless steel tube within the reactor. The quartz tube was illuminated with UV light from 48 UV LED lamps positioned on all four sides, generating a total output power of 17 W at 365 nm. The resultant photocatalytic decomposition of ethanol was analyzed using a quadrupole mass spectrometer (QMS) manufactured by Hiden Analytical Ltd. in Warrington, U.K. The QMS continuously monitored time-dependent gas samples from the reactor chamber. The photocatalytic membrane was made using poly(vinylidene fluoride-co-hexafluoropropylene) (PVDF-HFP M.W. = 400000) and 1-Methyl-2-pyrrolidone (NMP), both sourced from Sigma-Aldrich Co. P25 TiO_2 particles, which have a composite structure of rutile and anatase, were procured from Evonik Germany. AR-grade (≥ 99.9%) ethanol was used as a model pollutant in the tests. With a mixture of 150 wt.% TiO_2 to PVDF, a TiO_2/PVDF membrane was created using the nonsolvent-induced phase separation method (NIPS).

3. Results and discussion

The degradation of 13500 ppm (10 μL) of ethanol under UV light was used to evaluate the photocatalytic activity of the membrane. The findings showed that the TiO_2/PVDF membrane could efficiently decompose all ethanol in less than 4 minutes, as shown in Fig. 2. Equations 1–5 describe the multi-step breakdown process that was indicated by the detection of intermediates due to the high decomposition rate. The stepwise oxidation of ethanol ultimately yields carbon dioxide and water as final products. When exposed to ultraviolet light, electrons from TiO_2's valence band are driven to the conduction band, where they combine with oxygen to generate superoxide (${}^{\bullet}O_2^-$). This superoxide then reacts with adsorbed ethanol molecules on the membrane's surface to oxidize them into acetaldehyde. The acetaldehyde undergoes sequential transformation into acetic acid, which then decomposes into formaldehyde, and finally into formic acid. Each of these stages represents a step in the gradual breakdown of ethanol, resulting in final products in about 10 minutes. However, formic acid is an exception, as it is not fully decomposed after a 10-minute photocatalytic reaction.

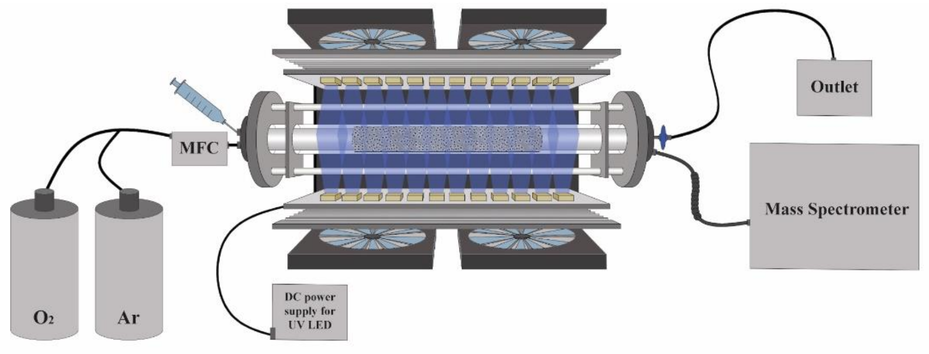

Figure 1. Schematic experimental setup for photocatalytic measurement.

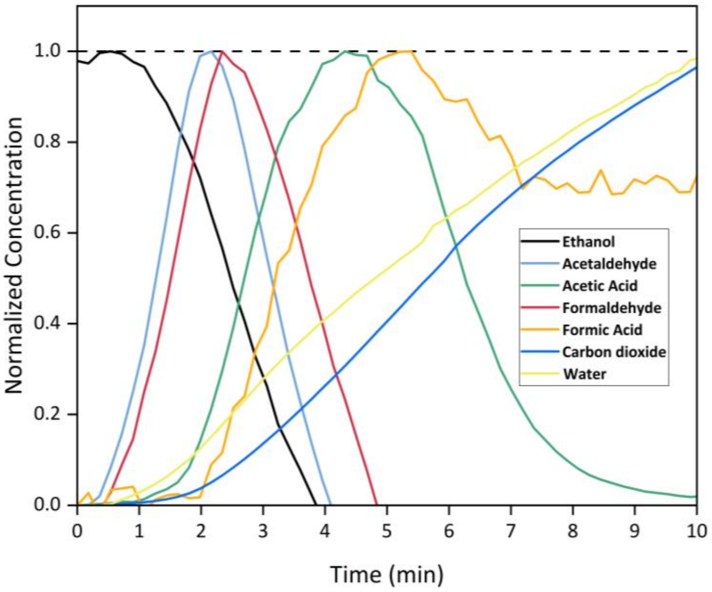

Figure 2. Photocatalytic decomposition of ethanol.

$$\mathrm{CH_3CH_2OH + 0.5\ O_2 \rightarrow CH_3CHO + H_2O} \quad (1)$$

$$\mathrm{CH_3CHO + 0.5\ O_2 \rightarrow CH_3COOH} \quad (2)$$

$$\mathrm{CH_3COOH + O_2 \rightarrow HCHO + CO_2 + H_2O} \quad (3)$$

$$\mathrm{HCHO + 0.5\ O_2 \rightarrow HCOOH} \quad (4)$$

$$\mathrm{HCOOH + 0.5O_2 \rightarrow CO_2 + H_2O} \quad (5)$$

4. Conclusions

The design of the photocatalytic reactor has proven to be successful in achieving a high level of photocatalytic efficiency, leading to enhanced VOC decomposition through the use of the TiO_2/PVDF membrane. This presents a feasible solution for mitigating indoor air pollutants. The rapid breakdown of ethanol allows for a comprehensive examination of the ensuing reaction stages, encompassing all intermediate products.

References

[1] E. Cosaert, C. Wolfs, S.D. Lambert, G.J. Heynderickx, D. Poelman, Molecules 26 (2021) 6584
[2] I. Cimieri, H. Poelman, J. Ryckaert, D. Poelman, J. Photochem. Photobiol., A 263 (2013) 1-7
[3] S. Wang, H.M. Ang, M.O. Tade, Environ. Int. 33 (2007) 694-705

Keywords
photocatalytic reactor; air purification; VOCs; TiO_2

Poster 37: BHET hydrolysis kinetics in a batch reactor

Riccardo Tesser[1*], Vincenzo Russo[1]

1 Department of Chemical Sciences, University of Naples Federico II, Via Cintia, IT-80126 Naples
**Corresponding author: riccardo.tesser@unina.it*

Highlights

- BHET was partially hydrolyzed in a batch reactor.
- A reaction mechanism was proposed and verified.
- The collected data were interpreted describing the product distributions.

1. Introduction

Polyethylene terephthalate (PET) can be considered nowadays one of the most abundant polymers produced in the chemical industry. The recycling and disposal of this polymer is still an open issue, as several technologies were proposed: i) thermal degradation, ii) hydrolysis and repolymerization [1,3]. Both from an environmental and economic perspective, the second route is surely more promising, as the used PET bottles could undergo to a chemical recycling where the polymer could be first hydrolyzed/glycolyzed and then used as raw material (i.e., monomer) to produce PET again. Glycolysis of PET is one among the most promising and efficient chemical depolymerization route and brings, after suitable purification steps, to a pure BHET (bis(2-hydroxyethyl) terephthalate). This monomer is less reactive than the traditional one (TPA, terephthalic acid), in PET synthesis, and a partial hydrolysis of BHET could increase its reactivity [3].

The aim of the present work is to investigate the BHET hydrolysis reaction kinetics, proposing a possible reaction mechanism that was able to describe the experimental data collected in a batch system.

2. Methods

The hydrolysis experiments were conducted using a stainless-steel autoclave of 150mL, operating under nitrogen pressure of 12bar, to keep all the reaction mixture in the liquid phase. The reactor was loaded with a fixed amount of BHET, water and catalyst (Sb_2O_3). Experiments were conducted varying both the reaction temperature (T=160-200°C) and the water content (2.5-12.5wt.%). Samples were withdrawn periodically and analyzed via HPLC-UV detector to retrieve the product distribution, and by acid-base titration to retrieve the content of free carboxylic acids. The collected data were interpreted assuming that BHET can be hydrolyzed in an in-series mechanism, also including the possible condensation and esterification steps. In detail, the following reaction scheme was considered.

1) $B + W \rightleftarrows M + G$ $\quad r_1 = k_i \cdot C_B \cdot C_W$
2) $M + W \rightleftarrows A + G$ $\quad r_2 = k_i \cdot C_M \cdot C_W$
3) $D + W \rightleftarrows MD + G$ $\quad r_3 = k_i \cdot C_D \cdot C_W$
4) $B + D \rightleftarrows T + G$ $\quad r_4 = k_p \cdot C_B \cdot C_D$
5) $2B \rightleftarrows D + G$ $\quad r_5 = k_p \cdot C_B^2$
6) $M + B \rightleftarrows D + W$ $\quad r_6 = k_e \cdot C_B \cdot C_M$
7) $MD + B \rightleftarrows T + W$ $\quad r_7 = k_e \cdot C_{MD} \cdot C_B$
8) $D + MD \rightleftarrows TE + W$ $\quad r_8 = k_e \cdot C_D \cdot C_M$
9) $D + M \rightleftarrows T + W$ $\quad r_9 = k_e \cdot C_D \cdot C_{MD}$
10) $D + A \rightleftarrows T + W$ $\quad r_{10} = k_e \cdot C_D \cdot C_A$
11) $B + DEG \rightleftarrows BD$ $\quad r_{11} = k_t \cdot C_B \cdot C_{DEG}$
12) $2G \rightleftarrows DEG + W$ $\quad r_{12} = k_d \cdot C_G^2$

As revealed, 12 reactions were considered, involving only 5 kinetic constants, as it was assumed that the similar reactions occur with the same rate constant.

The following mass balance equation was imposed and solved within MATLAB R2023b environment.

$$n_{tot}\frac{dx_i}{dt} = V_L \sum_{j=1}^{12} \upsilon_{i,j} \cdot r_j \tag{1}$$

3. Results and discussion

For each experiment, the evolution of the molar fraction of the chemical components was obtained vs the experimental time. In every case, BHET concentration was observed to decrease with time, leading to the formation of a distribution of products. An example is reported in Figure 1, where the experimental data collected fixing a reaction temperature of 160°C and a reactant loading of BHET=70g, H_2O=10g, and Sb_2O_3=0.1g are reported.

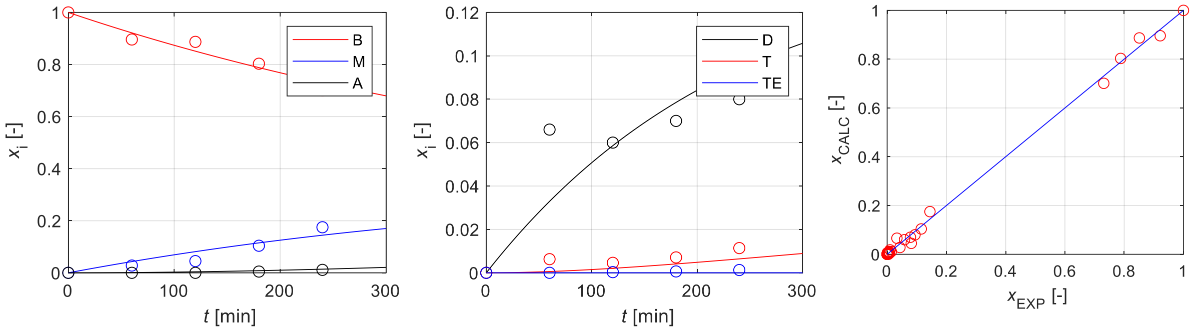

Figure 1. Example of kinetic data interpretation for a BHET hydrolysis experiment conducted at 160°C, using 70g BHET and 10g H_2O, with a catalyst amount of Sb_2O_3=0.1g. x_i: molar fraction of generic component *i*. B: BHET, M: MHET, A: terephthalic acid, D/T/TE: dimer/trimer/tetramer.

The collected data were interpreted using the reaction scheme reported in the methods section. An example of agreement between the experimental and the calculated data is reported in Figure 1, where it is possible to appreciate the overall agreement also via a dedicated parity plot. As revealed, the agreement can be considered satisfactory.

4. Conclusions

The BHET hydrolysis kinetics was investigated in a batch reactor, varying a wide range of operation conditions (i.e., temperature and reactants loading content). A reaction mechanism was proposed and tested on the collected data, showing the ability to correctly interpret the data of the whole experimental matrix. In perspective, the model could be tested to optimize the BHET hydrolysis in view of PET recycling technology.

References

[1] M. D. De Dios Caputto et al., Chemical upcycling of poly (ethylene terephthalate) waste: Moving to a circular model. Journal of Polymer Science, 60,24 (2022), 3269-3283.
[2] N. A. S. Suhaimi et al., Recycling of polyethylene terephthalate wastes: A review of technologies, routes, and applications. Polymer Engineering & Science, 62,8 (2022) 2355-2375.
[3] T. E. Long; John Scheirs (ed.). Modern polyesters: chemistry and technology of polyesters and copolyesters. John Wiley & Sons, 2005.

Keywords

BHET hydrolysis; PET recycling; kinetics; modeling.

Poster 38: CFD simulations and surrogate modeling approach of photocatalytic reactor for ethanol oxidation

Mohammad Rusydi Fatahillah[1], Quinten Nijs[1], Geraldine J. Heynderickx[1]*

1 Laboratory for Chemical Technology (LCT), Department of Materials, Textiles, and Chemical Engineering, Ghent University, Belgium

**Corresponding author: Geraldine.Heynderickx@UGent.be*

Highlights

- 3D CFD model VOC oxidation in a continuous photocatalytic reactor.
- DOM to simulate UV radiation from LEDs.
- UV LEDs radiation combined with mechanistic reaction model.
- 1D PFR surrogate model development.

1. Introduction

Indoor air is often contaminated with various Volatile Organic Compounds (VOCs), classified as hazardous pollutants. VOCs can be emitted indoors through activities such as cooking, decorating materials such as paint and flooring, and consumer products used for cleaning and disinfecting. Prolonged exposure to VOCs, even at low concentrations, has been linked to serious health issues, including cancer [1].

To effectively meet the needs for indoor VOC abatement, it is crucial to develop technologies that are fit for treating airflows with low VOC concentrations, keeping in mind that energy consumption needs to be low. Conventional methods of VOC removal, such as thermal oxidation, consume lots of energy and are often less efficient or easy to use at very low concentrations. Photocatalytic reactors have emerged as a promising technology to tackle these challenges, as confirmed by Ginestet et al., who studied the use of a photocatalytic reactor to treat air in aircraft cabins [2]. Photocatalytic reactors utilize a UV light source to activate a catalyst, such as TiO_2, that will oxidize VOCs into less harmful compounds and ultimately result in total oxidation into CO_2. The introduction of photocatalytic technology addresses the urgent need for new VOC abatement technology and aligns with broader sustainability goals like developing advanced oxidation technologies that can utilize green electricity as power source.

In this work, a 3D Computational Fluid Dynamics (CFD) simulation of an annular photocatalytic reactor equipped with modern ultra-violet (UV) light-emitting diodes (LEDs) (365 nm) is performed. The reactor is used to treat an airflow with low ethanol (a VOC) concentration, using TiO_2 as a photocatalyst. The first goal of this study is to develop a comprehensive 3D CFD model to simulate a photocatalytic reactor using the Discrete Ordinate Model (DOM) for simulating UV LEDs. A second goal is to propose and validate a computationally efficient 1D surrogate model, making use of a dimensional reduction approach.

2. Methods

The CFD simulated geometry, shown in Figure 1, is based on an experimental setup used by our project partner, LumiLab of UGent. Two cylinders are positioned in a rectangular box. The wall of the outer cylinder is made of transparent quartz, while the wall of the inner cylinder is coated with the photocatalyst, TiO_2. The transparent quartz wall separates the annular reacting gas zone from the ambient air in the rectangular block. On the sidewalls of the rectangular block, four UV LED strips, containing 12 LEDs each, are attached, resulting in a total of 48 LEDs. A low ethanol concentration gas feed flows through the annular compartment (8.75 mm hydraulic diameter and 320 mm length). For the CFD simulation, a computational grid of 1.3 million cells is applied to the entire geometry.

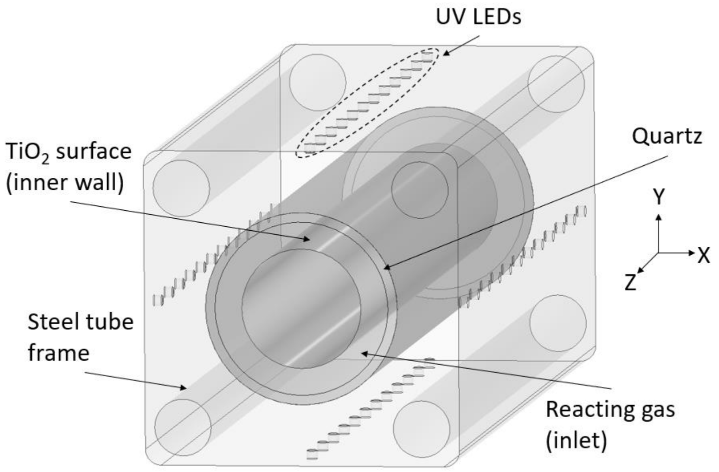

Figure 1. Simulated photocatalytic reactor geometry

All 3D CFD calculations are carried out with ANSYS Fluent 2021 R2, using double precision mode and a coupled pressure-velocity scheme. The pressure-based solver is selected to solve the governing equations, which include conservations for mass, momentum, energy, and species. A reactive source term is added to the conservation equations for the computational cells adjacent to the inner wall only, as the TiO_2 photocatalyst is applied to the inner wall of the annular ring. This layer of cells is referred to as the reaction zone. Boundary conditions are imposed. The inlet of the annular reactor is specified as a mass-flow rate inlet, while the outlet is specified as a pressure outlet. No-slip wall boundary conditions are imposed at the reactor walls.

To account for the UV radiation physics of the LEDs, CFD simulations of the photocatalytic reactor incorporate DOM to solve the Radiative Transfer Equation (RTE). DOM is increasingly used in CFD modeling of photocatalytic reactors due to its capability to simulate radiation from a surface emitted in a conical form, transmitted through a transparent material, accounting for specular reflections, and anisotropic scattering if needed [3]. For the proposed geometry, the UV LEDs are modeled with a conical emission having a 45-degree viewing angle from the specified surfaces.

To account for the reaction chemistry, a reaction mechanism and kinetic model are implemented as User-Defined Function (UDF). The reaction chemistry is based on the Langmuir-Hinshelwood mechanism, as proposed by Nimlos et al. [4]. It describes a five-step serial degradation mechanism, including the sequential formation of acetaldehyde, acetic acid, formaldehyde, formic acid, and CO_2. The effect of UV radiation on reaction rates implied in the reaction zone is accounted for by assuming the reaction rate coefficient (k_i) to depend on the incident radiation.

A surrogate modeling approach assuming the reactor to be a 1D plug flow reactor (PFR) is developed to reduce the computational costs of 3D CFD simulations. The surrogate model development is based on applying dimensional reduction, as illustrated in Figure 2. Dimensional reduction principles are mainly used for the purpose of design optimization, as they help eliminate irrelevant variables from the problem description [5]. The key dimensional reductions in this study are applied to both the radiation model and the hydrodynamics model. First, a relationship between the UV LED power output (I_{LED}) and the incident radiation in the reaction zone (I_{TiO_2}) is determined. This relation simplifies the computationally intensive 3D radiation calculations by using an area-averaged incident radiation ($\bar{I}_{TiO_2}$) on the photocatalyst surface. The latter value accounts for the effect of radiation intensity on reaction rates (R_i). This simplification is feasible and acceptable due to the absence of light scattering and minimal radiation absorption in our computational domain. It allows for the reduction of the RTE to Beer-Lambert's law, as supported by previous studies [6]. Second, the axial gas velocity in the reaction zone (u_z) is extracted from the results of the hydrodynamics model in the 3D CFD calculations. It is justified since the flow in the annular chamber can almost immediately be assumed as a fully developed flow and thus predominantly governed by the axial gas velocity component.

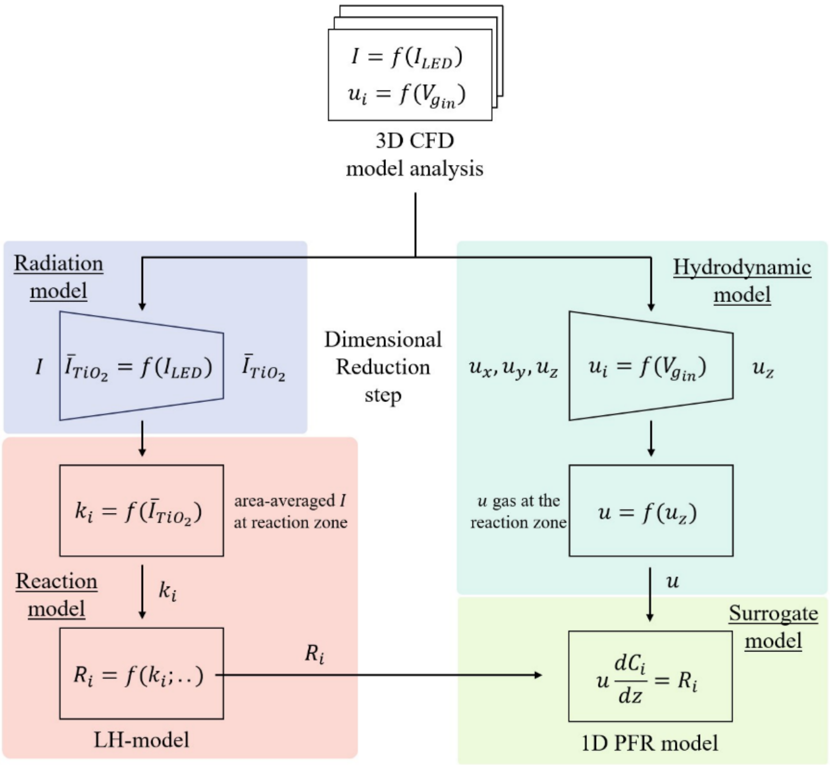

Figure 2. Illustration of the surrogate modeling approach

3. Results and discussion

First, 3D CFD simulations are performed using different directional discretizations as DOM settings to solve the RTE. For a 15x15 discretization with ten pixelation, significant numerical deviation due to ray-effect (distorted incident radiation) is no longer observed, as shown in Figure 3 [7]. The results for 5×5 and 10×10 directional discretization appear to have low precision, as concluded from the observed segregation of the UV radiation beam within the computational domain. The 15×15 discretization is selected as it provides sufficient accuracy while requiring less computational costs than the 20×20 configuration. Additionally, the results indicate that the incident radiation on the inner cylindrical wall is highest when the distance to a UV LED on the outer cylindrical wall is smallest, as expected. Using DOM can be computationally expensive, not only in terms of computational time but of storage capacity as well [8]. Using a 15×15 directional discretization in the proposed modeling takes approximately 18 seconds for one iteration on a 2×48-core AMD EPYC 7552 with a 250 GB RAM HPC cluster. A steady-state calculation may take up to 3 or 4 hours. Furthermore, a 22.4 GB data file storage capacity is needed for each simulation.

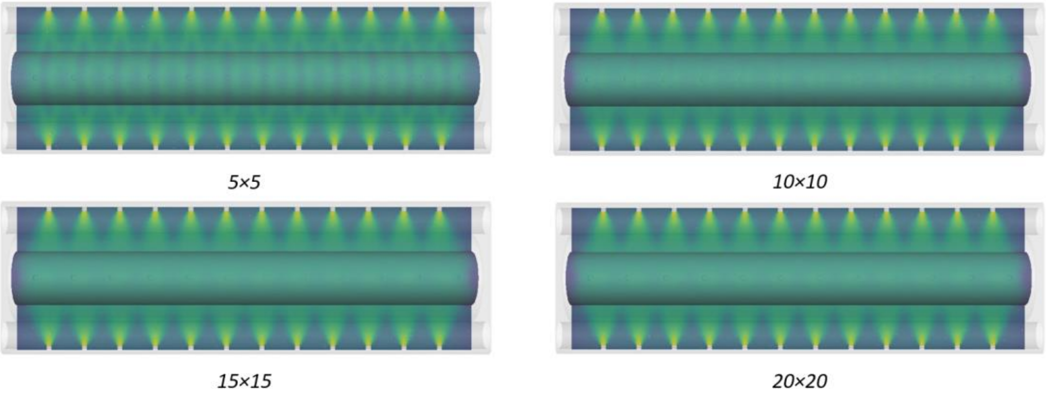
5×5

10×10

15×15

20×20

Figure 3. Incident radiation contour plot showing 2D cut (YZ-plane) and inner wall

Figure 4(a) shows a 2D cut (through the center of a LED strip, YZ-axes plane) for the ethanol mole fraction obtained from a 3D CFD simulation using the validated kinetic model of Nimlos et al. [4]. The simulation is carried out with a gas inlet flowrate of 10^{-3} m^3 min^{-1} (1 l min^{-1}) containing 202 ppm ethanol, fed at ambient pressure and temperature. In the reaction zone, the average incident radiation is calculated to be 17 W m^{-2}, corresponding to the conditions established by Nimlos et al. [4].

Figure 4(a) shows that a slight radial gradient of the ethanol concentration in the annular ring is observed for nearly all axial positions. This must be attributed to the dynamic changes in both diffusional transport and ethanol reaction rate. Ethanol diffuses from the bulk phase to the reaction zone, where it is converted. Both steps are clearly depicted in Figure 4(b), which shows the axial ethanol concentration profiles in the bulk and the reaction zone. The ethanol concentration in the bulk phase is higher than in the reaction zone, resulting in diffusional transport from the bulk phase to the reaction zone. The ethanol concentration profile in the bulk phase is seen to decrease quite linearly. In the reaction zone, the decrease in the ethanol concentration profile fluctuates as a consequence of varying reaction rates due to varying incident radiation. The strongest reductions are observed at the position of the 12 dotted vertical lines, corresponding to the position of each of the 12 UV LEDs on the strip. The ethanol concentration profiles near the inlet and outlet of the reactor behave differently, caused by low ethanol degradation due to lower UV illumination, as observed in Figure 3.

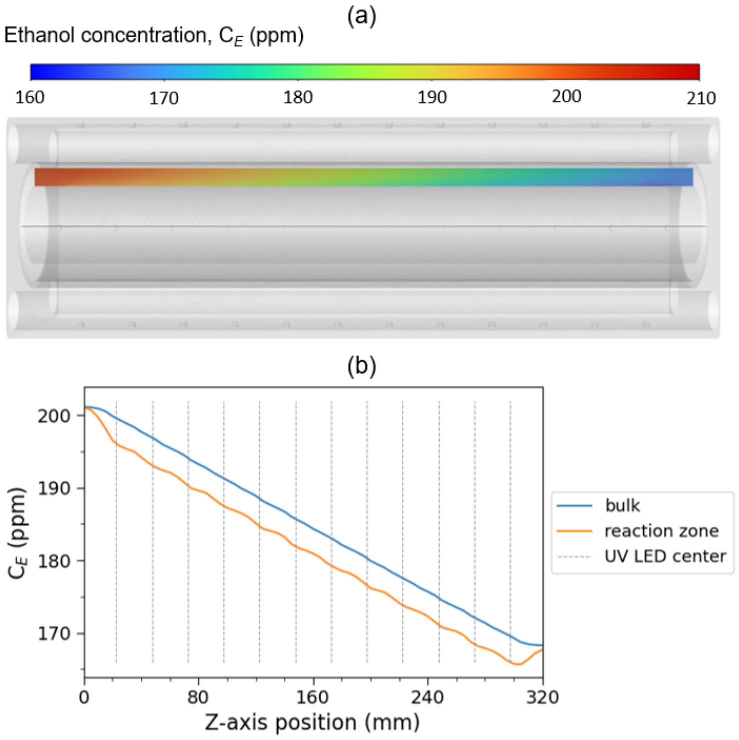

Figure 4. (a) 2D contour (through LED center, YZ-plane) of ethanol concentration in the annulus; (b) axial ethanol concentration profile (locally averaged) for bulk phase zone and reaction zone

Using insights from comprehensive 3D CFD simulations, a simplified 1D PFR model is developed as a surrogate model (see Figure 2). Calculations using the surrogate model are performed using an average incident radiation of 17 W m^{-2} in the reaction zone. The surrogate model is written in Python and executed in a 2x4-core Intel i7-1185G7 laptop with 16 GB RAM. A steady-state calculation per case is performed for a total of 2 seconds and requires 576 KB of file storage. Consequently, the 1D model reduces the computational time by a factor of 7,200 and storage space by a factor of 38,800 per case.

Figure 5(a) shows the ethanol and acetaldehyde concentration profiles as a function of reactor length. Other species are not shown as their concentration remains below one ppm. The values for the 3D simulations are mass-weighted average values in a radial plane, covering both the bulk phase and the reaction zone concentrations. The 3D CFD and 1D PFR ethanol and acetaldehyde concentrations show good quantitative agreement. In Figure 5(b), ethanol conversions for varying gas inlet volumetric flowrates (fixed 202 ppm ethanol inlet concentration) and for varying ethanol inlet concentrations (fixed volumetric inlet gas flowrate 10^{-3} m^3 min^{-1}) are compared for 1D and 3D modeling. The results indicate that the ethanol conversion obtained using the 1D model aligns well with the results obtained in the 3D simulations, particularly when the volumetric gas inlet flowrate varies. Ethanol conversion is seen to decrease with increasing volumetric gas inlet flowrate. The latter is due to the reduction in contact time. For increasing ethanol inlet concentration in a constant gas flow, the conversion decreases due to the decreasing space time (the amount of catalyst remains constant). Overall, ethanol conversion calculated using the 1D and 3D models is seen to be less good, especially at low ethanol inlet concentrations. The discrepancy is most likely due to a decreasing concentration gradient in radial direction for the 3D simulation, resulting in a lower diffusional rate of ethanol. In the 1D surrogate model, radial uniformity is assumed. The effect of assuming radial uniformity on simulation results reduces with increasing ethanol concentrations.

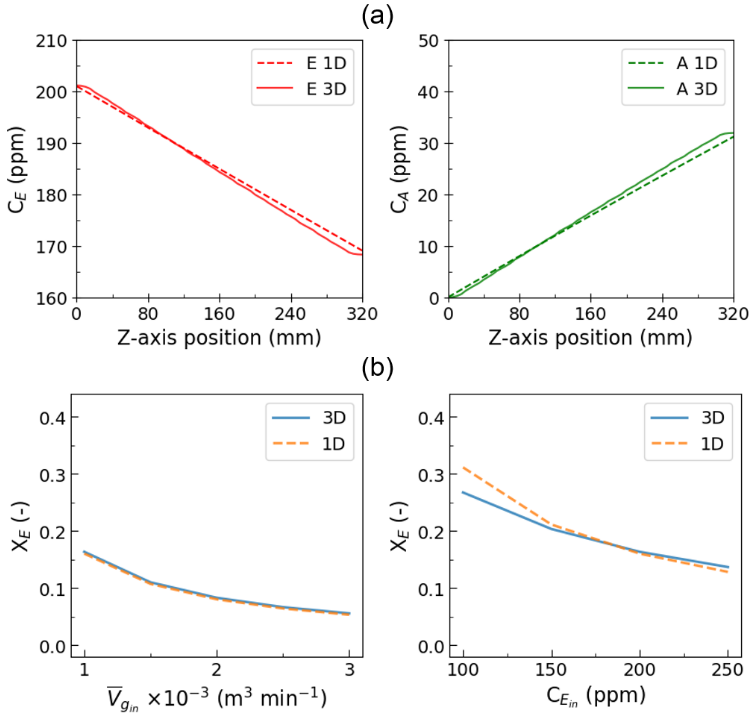

Figure 5. 3D CFD and 1D surrogate model. (a) Axial ethanol and acetaldehyde concentration profiles; (b) Ethanol conversion as a function of volumetric gas inlet flowrate (202 ppm ethanol concentration) and ethanol inlet concentration (10^{-3} m^3 min^{-1} gas flowrate)

4. Conclusions

In this study, a 3D CFD model to simulate a photocatalytic reactor using UV LEDs and a TiO_2 photocatalyst used to remove ethanol, a VOC, is developed. The model uses DOM to solve the RTE, while a validated 5-step reaction model with Langmuir-Hinshelwood kinetics accounting for the UV incident radiation on the photocatalyst, is included as UDF. Additionally, a 1D surrogate model is developed using the dimensional reduction approach. Model validation learns that ethanol concentration and conversion profiles obtained with the 1D surrogate model agree well with the 3D CFD model results. The surrogate model significantly reduces computational costs associated with simulating photocatalytic reactors and is valuable for conducting sensitivity analyses or process optimization studies more efficiently.

References

[1] A. Mozaffar, Y.-L. Zhang, Atmospheric Volatile Organic Compounds (VOCs) in China: a Review, Curr. Pollut. Rep. (2020) 250-63

[2] A. Ginestet, D. Pugnet, J. Rowley, K. Bull, H. Yeomans, Development of a new photocatalytic oxidation air filter for aircraft cabin, Indoor Air (2005) 326-34

[3] C. Casado, J. Marugán, R. Timmers, M. Muñoz, R. van Grieken, Comprehensive multiphysics modeling of photocatalytic processes by computational fluid dynamics based on intrinsic kinetic parameters determined in a differential photoreactor, Chem. Eng. J. (2017) 368-80

[4] M. R. Nimlos, E. J. Wolfrum, M. L. Brewer, J. A. Fennell, G. Bintner, Gas-Phase Heterogeneous Photocatalytic Oxidation of Ethanol: Pathways and Kinetic Modeling, Environ. Sci. Technol. (1996) 3102-10
[5] A. Viswanath, A. I. J. Forrester, A. J. Keane, Dimension Reduction for Aerodynamic Design Optimization, AIAA J. (2011) 1256-66
[6] Y. Boyjoo, M. Ang, V. Pareek, Some aspects of photocatalytic reactor modeling using computational fluid dynamics, Chem. Eng. Sci. (2013) 764-84
[7] B. Hunter B, Z. Guo, Numerical smearing, ray effect, and angular false scattering in radiation transfer computation, Int. J. Heat Mass Transfer (2015) 63-74
[8] M. R. Fatahillah, E. Cosaert, H. M. Milani, D. Poelman, G. J. Heynderickx, Numerical and experimental study of an annular photocatalysis reactor to remove VOC in air, 14th European Congress of Chemical Engineering and 7th European Congress of Applied Biotechnology (ECCE & ECAB), 2023

Keywords

Computational Fluid Dynamics; Photocatalytic reactor; Volatile Organic Compounds

Poster 39: Ligand Engineered In-MOFs with Tuned Band Structure for Enhanced Photocatalytic CO_2 Reduction

Geqian Fang[1], Vitaly Ordomsky[1]*, Andrei Khodakov[1]*

1 CNRS, Centrale Lille, Univ. Artois, UMR 8181 - UCCS − Unité de Catalyse et Chimie du Solide, Univ. Lille, Lille F-59000, France

**Corresponding authors: vitaly.ordomsky@univ-lille.fr; andrei.khodakov@univ-lille.fr*

Highlights

- Tuning the band structure of In-MOFs by ligand engineering
- CO_2 photocatalytic reduction performance is directly proportional to Band gap of In-MOFs-$(NH_2/H)_x$
- High CO_2 photoreduction yield of 738.4 μmol g_{cat}^{-1}

1. Introduction

The increasing CO_2 emissions from fossil fuel consumption have contributed significantly to global environmental changes. Photocatalytic conversion of CO_2 into valuable chemicals, such as CO and CH_4, has emerged as a promising approach to address both energy needs and environmental challenges. The photocatalytic reduction of CO_2 is a complex multi-electron process that can yield a variety of products. Therefore, precise control over the number of electrons involved in the reduction is crucial for selectively generating desired products. While metal oxides or metal/oxide catalysts are commonly used in CO_2 reduction, these semiconductor structures are often limited by their simplicity, making it challenging to fine-tune their band structures. As a result, the enhancement of photoconversion efficiency remains constrained.

Compared to other materials, MOFs exhibit well-defined structures, excellent light absorption capabilities, and efficient charge carrier separation, making them outstanding candidates for photocatalysis. In this work, we employed ligand engineering to selectively tune the band structure of In-MOFs-$(NH_2/H)_x$ while maintaining consistent geometric structures across the catalysts. This approach allowed us to precisely control the CO_2 reduction process. Among these catalysts, In-MOFs-H demonstrated the highest band gap and achieved the highest CO_2 photoreduction yield (738.4 μmol g_{cat}^{-1}), surpassing the performance of other reported metal oxide catalysts.

2. Methods

Synthesis of the Photocatalysts. In-MOFs-$(NH_2/H)_x$ was prepared according to a reported solvothermal procedure. $In(NO_3)_3 \cdot xH_2O$ and H_2BDC and/or NH_2BDC were dissolved in DMF. The mixture was then transferred to a 100 mL Teflon-lined autoclave, sealed in a stainless-steel autoclave, and heated at 100 °C for 5 h. After cooling to room temperature, the white solid products were centrifuged and washed with DMF and acetone. Finally, the In-MOFs-$(NH_2/H)_x$ sample was obtained after drying at 120 °C for 12 h.

Catalyst Characterization. The ultraviolet–visible diffuse reflectance spectroscopy (UV-vis DRS) analysis was performed on a PerkinElmer Lambda 650S spectrometer, with an integrating sphere covered with $BaSO_4$ as a reference. The X-ray powder diffraction (XRD) patterns of catalysts were collected using the PANalytical Empyrean X-ray diffractometer with a Cu-Kα radiation source (40 kV and 30 mA). The morphology of the MOFs was characterized using a JSM-7800F Scanning electron microscope (SEM) with an accelerating voltage of 30.0 kV.

Catalytic Test. Typically, 10 mg of catalyst, 20 mL of water, and 1 mL of triethanolamine were added to a 220 mL photoreaction vessel, and then the reaction system was filled with high purity CO_2 (99.999 %) and maintained at r.t. with a recirculating water system. The light source was a 500 W Xe lamp. After photocatalytic reactions, the gaseous products were analyzed by a gas chromatograph (PerkinElmer Clarus 580 GC) equipped with a PoraBOND Q and a ShinCarbon ST 100/120 columns, as well as a thermal conductive detector and a flame ionized detector.

3. Results and discussion

Characterization techniques (XRD, SEM, UV-vis, etc.) have confirmed that the band structure of In-MOFs can be precisely tuned. As shown in Figure 1a, SEM analysis indicates that both In-MOFs-$(NH_2/H)_x$ and their derived In_2O_3 maintain a similar rod-like morphology. The XRD results reveal that, due to the introduction of ligands, In-MOFs only exhibit characteristic peaks of In_2O_3 at low degree (Figure 1b). Notably, In-MOFs-$(NH_2/H)_x$ with different ligands still retain the same geometric spatial configuration. Compared to In_2O_3, the introduction of the NH_2 ligand reduces the band gap to 2.59 eV, while the H ligand increases it to 3.02 eV (Figure 1c). As depicted in Figure 1d, pure In_2O_3 produces only 43 μmol μmol $g_{cat}{}^{-1}$ of methane, but after introducing the NH_2 ligand, the methane yield increases by 2.3 times, reaching 101 μmol $g_{cat}{}^{-1}$. As the proportion of H_2BDC increases, the CO_2 reduction products (CH_4, CO, C_2H_6) also gradually increase, reaching a maximum of 738.4 μmol $g_{cat}{}^{-1}$ on the In-MOFs-H catalyst. These results clearly demonstrate that the band structure of In-MOFs can be selectively tuned through ligand engineering, enabling precise control over their photocatalytic performance in CO_2 reduction.

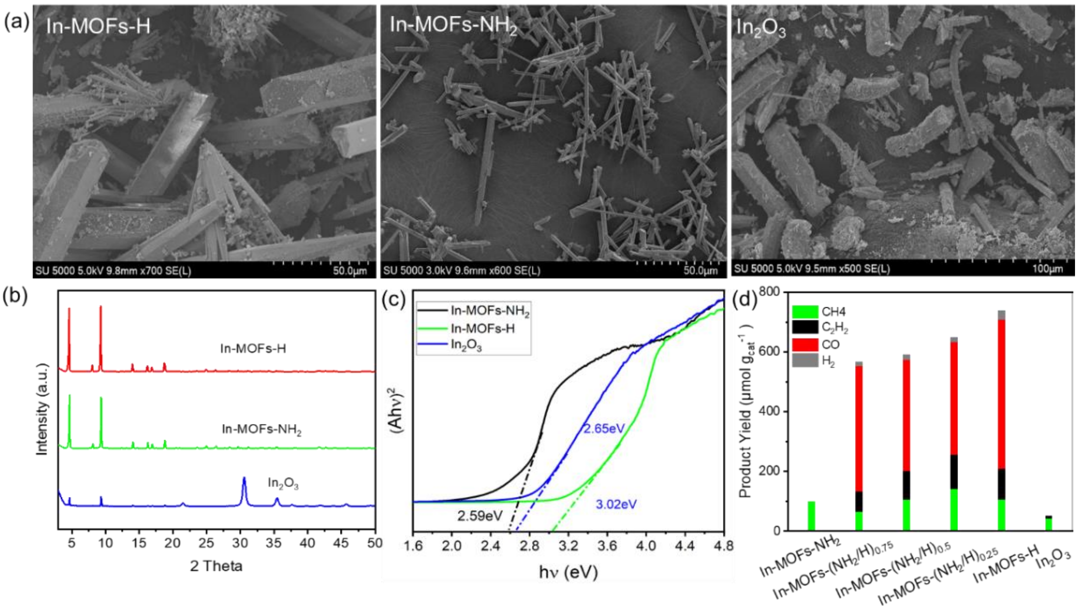

Figure 1. (a) SEM, (b) XRD, (c) Energy gap, (d) Photocatalytic CO_2 reeducation performance over In-MOFs-$(NH_2/H)_x$ and In_2O_3

4. Conclusions

In this study, we demonstrated that ligand engineering can be effectively used to selectively tune the band structure of In-MOFs-$(NH_2/H)_x$ while maintaining consistent geometric structures across the catalysts. This precise control of the band structure significantly impacts the photocatalytic performance in CO_2 reduction. Among the catalysts studied, In-MOFs-H exhibited the highest band gap and the greatest CO_2 photoreduction yield, outperforming other reported metal oxide catalysts. Characterization confirmed that the introduction of specific ligands could finely adjust the band gap, thereby enhancing the photocatalytic efficiency. The results highlight the potential of ligand engineering as a powerful tool for optimizing the photocatalytic properties of MOFs, paving the way for more efficient CO_2 reduction processes.

References

[1] Sun, Q.; Zhu, Y.; Zhong, X.; Jiang, M.; Fan, Y.; Yao, J. ACS Appl. Mater. Interfaces 2022, 14, 53904−53915.

Keywords

In MOFs-X; Ligands engineering; Energy structure; Photocatalytic CO_2 reduction.

Poster 40: Stoichiometric selective carbonylation of methane to acetic acid by chemical looping

Yinghao Wang[1*], Chunyang Dong[1,2], Mariya Shamzhy[3], Yury G. Kolyagin[1], Jeremie Zaffran[1], Andrei Y. Khodakov[1] and Vitaly V. Ordomsky[1]

1 UCCS–Unité de Catalyse et Chimie du Solide, Université de Lille, CNRS, Centrale Lille, ENSCL, Université d'Artois, UMR 8181, Lille, France.

2 Department of Chemistry, The University of Hong Kong, Hong Kong, China.

3 Department of Physical and Macromolecular Chemistry, Faculty of Science, Charles University, Hlavova 2030/8, 12843 Prague, Czech Republic

**Corresponding authors: Yury.Kolyagin@univ-lille.fr; Jeremie.Zaffran@cnrs.fr; snowflakelost@126.com; Andrei.Khodakov@univ-lille.fr; Vitaly.Ordomsky@univ-lille.fr*

Highlights

- Chemical looping strategies for methane activation and conversion
- Selective synthesis acetic acid from methane and carbon monoxide
- Pt-single atoms sites over TiO_2-supported heteropolyacid.

1. Introduction

Conversion of methane to valuable products is one of the main challenges of modern chemistry. Acetic acid (AcOH) is a key chemical reagent in industry[1], produced nowadays by the carbonylation of methanol over homogeneous Rh and Ir catalysts[2]. Here, we propose a chemical looping approach for highly selective stoichiometric synthesis of AcOH by oxidative carbonylation of methane with CO using single-site Pt over isolated phosphotungstic anions compensating positively charged titania (Pt-HPW-TiO_2). The reaction proceeds by methane activation, which coincides with reduction of platinum species in the presence of CO at 423 K and results in surface acetates attached to TiO_2. Subsequent hydrolysis by water releases AcOH at ambient temperature. Spent Pt-HPW-TiO_2 is then regenerated to the initial state by subsequent calcination in air. This approach provides an opportunity for selective synthesis of AcOH (99 %) from methane and carbon monoxide under mild conditions. A high concentration of AcOH (1.1 wt %) in aqueous solution can be obtained at a methane conversion of 4.5 %.

2. Methods

The material for the carbonylation of methane to acetic acid was prepared by co-impregnation of an aqueous solution of tungstophosphoric heteropolyacid (HPW) together with metal salt to obtain 0.2 wt% of metal with subsequent calcination at 250 °C and removal of excess of HPW by washing of the catalyst and drying[3].

3. Results and discussion

We uncovered selective synthesis of AcOH by chemical looping over nanocomposites containing HPW, TiO_2 and several metals (**Figure 1b-c**). The reaction has been performed in the multi-cycle mode. The first cycle involved treatment of dry material in batch reactor in the mixture of CH_4 and CO with ratio CH_4/CO = 15 at the total pressure of 15 bar and at 175 °C for 2 h. After analysis of the gas phase products, the reactor was opened and water has been added with further analysis of the liquid solution by NMR. The solid material was filtered out and calcined in the flow of air at 250 °C before the next cycle. After optimization of composition, Pt-HPW/TiO_2 nanocomposite exhibited an acetic acid productivity of $14.6 \cdot 10^{-7}$ mol/g. Using large amounts of nanocomposite allowed highly concentrated acetic acid aqueous solutions to be synthesized.

Characterization shows that the catalyst is composed of cationic Pt single sites anchored by polyoxometalate clusters to TiO_2. The atomic-resolved HAADF imaging showed HPW highly dispersed isolated Keggin-type clusters (**Figure 1a**). The oxidized PtO_x is required to activate of methane by dissociation of the C-H bond with simultaneous coupling with CO to form acetate. The role of heteropolyacid is relevant to stabilization of single atom reduced Pt, providing oxygen transfer to TiO_2

for stabilization of acetate and hydrolysis of acetate. The role of TiO_2 is in capturing of acetate to form Ti-O-Ac species for subsequent hydrolysis. Isotopic labeling tests with the ^{13}C labeled reactants confirm that the methyl groups are derived from CH_4, while acyl groups of AcOH are produced from CO. The NMR spectra of liquid phase by using $H_2{}^{17}O^{17}$ demonstrated no ^{17}O in acetic acid.

The O atom previously linking Pt to TiO_2 diffuses to locate further as a surface adatom, hence allowing CO to bind a vacant Pt atom with CH_4 physisorbed nearby. Then, in a concerted mechanism, we simultaneously observe C-H breaking in CH_4 molecule, C-C bonding between CH_4 and CO, C-O bonding between CO and the O adatom at the surface from PtO_x and O-H bonding between the O adatom and the H resulting from C-H scission in CH_4, leading to the formation of surface acetate. The acetates are then removed from the surface via hydrolysis (**Figure d**). The recyclability of the material has been verified by several cycles with intermediate regeneration by air calcination.

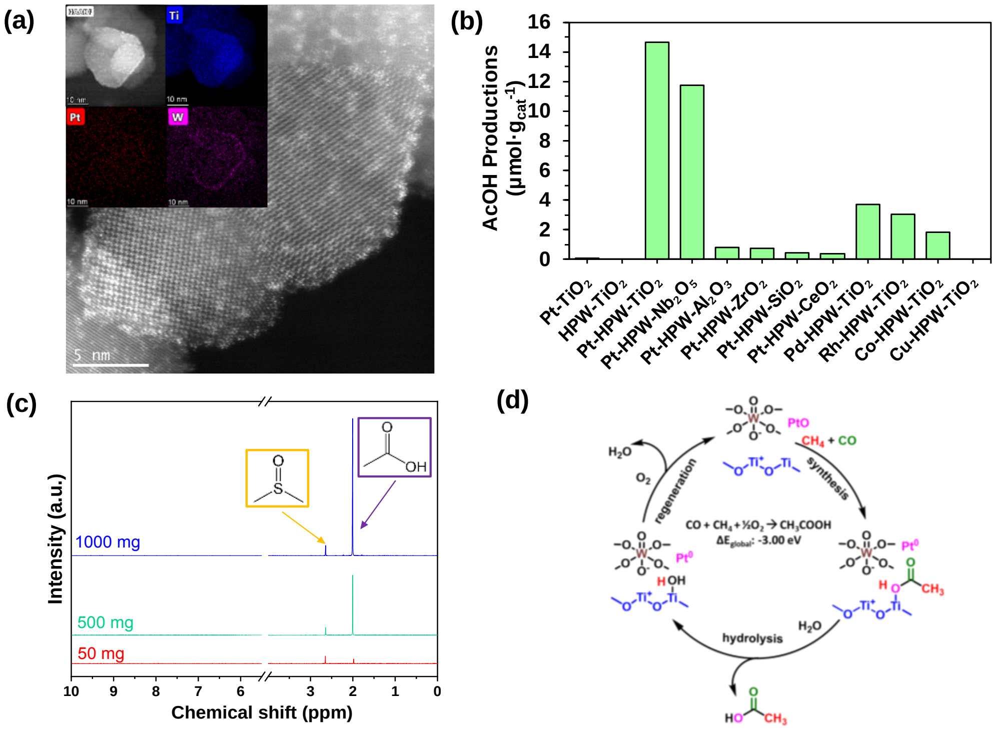

Figure. (a) Atomic-resolved HAADF-STEM image of Pt-HPW/TiO_2, (b) Amount of acetic acid which produced by per gram of different catalysts, (c) NMR of high concentration acetic acid synthesized in water (d) Scheme of the reaction.

4. Conclusions

We demonstrated a new chemical looping strategy for the selective synthesis of AcOH by oxidative carbonylation of methane. Synthesis of AcOH in the amount corresponding to 1.5 atoms of Pt, with a 99% liquid-phase selectivity and yielding the AcOH solution with a high concentration was achieved over Pt-HPW-TiO_2 nanocomposite. A combination of isotope labelling and in-situ characterization suggests that CH_4 is activated by oxidized Pt and reacts with a CO molecule yielding an acetyl group over TiO_2 surface. The acetyl group is then extracted by water to form an AcOH solution, and the sample should be calcined afterwards to regenerate PtO_x sites for the new reaction cycle. The proposed strategy enables producing high acetic acid concentrations in aqueous solution from methane and CO under mild reaction conditions.

References

1. Periana, et al. *Science* **2003**, *301* (5634), 814-818.
2. Q. Yuan, et al. *J. Catal.* **2005**, *233* (1), 221-233.
3. X. Yu, et al. *Nat. Energy* **2020**, 5, 511–519

Keywords:
Methane activation; Chemical loop; Acetic acid; High selectivity

Poster 41: Preparation and Testing of Inconel based Pd-AG membranes in Electrified reactor for enhanced Hydrogen Separation

Anusha Yajurvedi[1], Patrice Perreault[1]*

1 University of Antwerp, Blue App – ElectrifHy, Olieweg 97, 2020 Antwerp Belgium

**Corresponding author: patrice.perreault@uantwerpen.be*

Highlights

- Preparation of Pd-Ag membrane by Electroless pore-plating method.
- Testing of membrane up to 40 bar
- Testing of membrane at temperature up to 700 °C.
- Installation of membranes in an electrothermal fluidized bed reactor.

1. Introduction

Hydrogen is the fuel for the future, however in the most of cases other than electrolysis it is generated with byproducts like CO, CO_2, C_2H_4, C_2H_6, etc. The selective separation of hydrogen from the mixture of gases is major challenge. The process efficiency of conventional hydrogen purification techniques like PSA, TSA and cryogenic distillation is often low and they are bulky and energy-intensive. Membrane technology of H_2 purification offers an advantage because it can run continuously to create ultra-pure hydrogen. Pd-alloy membrane membrane's high hydrogen selectivity, permeance, chemical, and thermal durability, makes it ideal choice for hydrogen separation . However, Pd alone experiences hydrogen embrittlement at low temperature (573 K), necessitating alloying with other metals. Ag has a dominant position among all alloying metals due to its improved H_2 permeance and low cost membrane because of its high weight ratio.

2. Methods

This research focuses on the synthesis and evaluation of Pd-Ag membranes synthesized via the electroless pore-plating method. The membrane designed for the hydrogen separation, will be developed on porous Inconel tube of 150 mm length and 8 mm inner diameter with 2 mm of wall thickness to leverage its high temperature stability, mechanical strength and corrosion resistance. The electroless pore-plating method will be used to synthesize the membrane. The hydrazine base reducing agent will kept inside the tubular porous Inconel support, while the metal solution will retain in the bath outside of it. Additionally, while plating, hydrazine concentration will be regulated according to the metal redox potential. Testing will be conducted in an electrothermal reactor under extreme conditions, operating at up to 40 bar and 700 °C.

3 . Conclusions

Th electrified reactor will aim to enhance the hydrogen separation efficiency by optimizing the energy input and reducing the operational costs and it will also provide the valuable insights in to the advancement of membranes for efficient hydrogen separation, with significant implications for clean energy technologies.

References

[1] Mardilovich PP, She Y, Ma YH, Rei MH. Defect free palladium membranes on porous stainless-steel support. AIChE Journal 1998; 44: 310

Keywords

Pd-Ag membrane, Electroless Pore-Plating, Membrane Separation, Hydrogen Membrane

Poster 42: Effective modeling of transport limitations in catalytic filter wall

Jan Němec[1], Marie Plachá[1], Petr Kočí[1]*

1 University of Chemistry and Technology, Prague; Technická 5, Praha 166 28, Czech Republic

**Corresponding author: petr.koci@vscht.cz*

Highlights

- Extension of 1D+1D model of a catalytic filter.
- Transport limitation in both catalytic coating, and free pores.
- Realistic conversion profiles.
- Prediction of reactant slip at high flow rates.

1. Introduction

Traditional automotive catalytic converters and particulate filters can be combined into catalytic particulate filters (CPF) which are able to convert harmful gases and capture the particulate matter simultaneously. CPF is a monolith with a honeycomb structure with each channel plugged at one end, forcing the gas to permeate through the porous wall. Macroscopic 1D+1D model is commonly used to predict the behavior of the device under various conditions. Pore-scale simulations of gas transport and reactions inside the porous structures can be conducted using a 3D model that incorporates the realistic structure of the wall obtained through X-ray microtomography (XRT). The 3D profiles can also be used to evaluate the effective parameters of the wall (e.g. permeability) for input into the 1D+1D model.

Study of conversion in 1D+1D model requires further thoroughness. The 3D simulations reveal that gas flowing through the wall tends to use free pores and bypass the catalytic centers which are often only reachable by diffusion, which may become a limiting factor for the reactions.

2. Methods

The macro-scale 1D+1D model assumes 1D plug flow in the channels, and 1D transport through the wall. The processes are described by mass, enthalpy, and momentum balances. To account for potential transport limitations in the wall, the corresponding component balance equation must be adjusted.

In this work, we consider both possible contributions to the diffusion limitations: the diffusion of the components inside the catalytic coating (between its surface and active sites), and the diffusion between the coating surface and the gas flowing inside the free pores. The study was conducted considering the reaction of $CO + ½ O_2 \rightarrow CO_2$ on Pt/Al_2O_3 catalyst with a Langmuir–Hinshelwood rate law:

$$r = \frac{k\, y_{\mathrm{CO}} y_{\mathrm{O_2}}}{(1 + K y_{\mathrm{CO}})^2}.$$

To describe the transport limitation inside the coating, effectiveness factor η is used. The reaction-diffusion equation with this kinetics does not have an analytic solution. However, it was shown that studying its asymptotic behavior can provide insight into the problem in cases of a strong inhibition. This work examines the relevance of utilizing first-order kinetics relations for catalyzed reactions and possibilities of combining this approach with the asymptotic relations.

The driving force for the transport in the free pores is the concentration difference between the bulk gas and the coating surface. A new set of concentration values have introduced to describe the pore-coating boundary. The reaction term of the component balance equation of the wall is replaced by a mass transfer term. This heterogeneous approach must be accompanied by a new component balance equation describing the gas inside the transfer and the reaction.

The fitted parameter for each of the contributions is appropriate diffusion length. Their value can be estimated by comparing the 1D conversion profiles against the spatially averaged profiles from the pore-scale 3D model.

3. Results and discussion

The study results indicate that all the considered approaches provide reasonable results for low CO concentration when inhibition is negligible, Figure 1a. However, increasing the CO concentration has a significant impact on the first-order relations, as they overestimate the significance of the diffusion limitation, Figure 1b. The importance of the limitation in the free pores is evident from the light-off curves. Only the heterogeneous model can predict the reactant slip which has been previously observed at high flow rates in the experiments, Figure 2a.

The proportion of the two contributions, i.e. the values of diffusion lengths (Figure 2b), can be evaluated this way by fitting the concentration of the slipped reactant, or theoretically by thorough XRT analysis of the porous structure and the coating distribution.

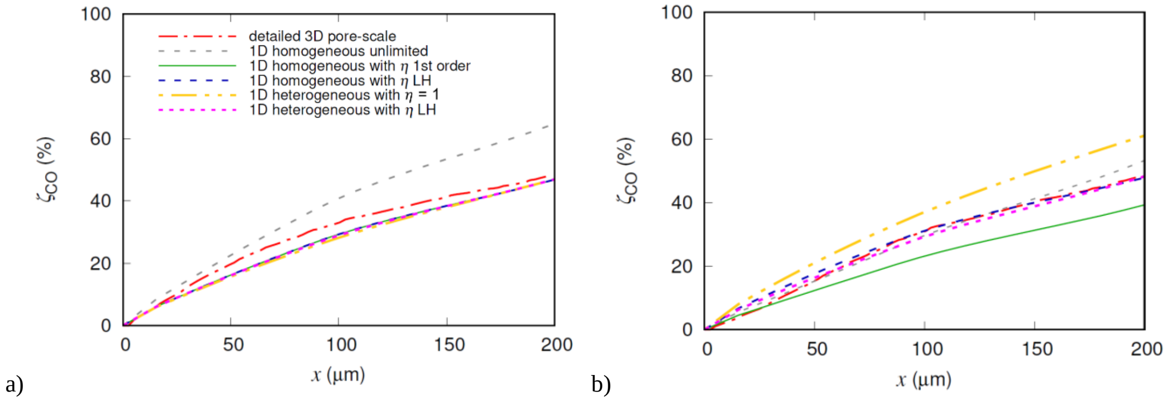

Figure 1. Selected CO conversion profiles over catalytic filter wall at temperature near T_{50}.
(a) $y_{\mathrm{CO}} = 0.001, y_{\mathrm{O_2}} = 0.05$; (b) $y_{\mathrm{CO}} = 0.01, y_{\mathrm{O_2}} = 0.05$

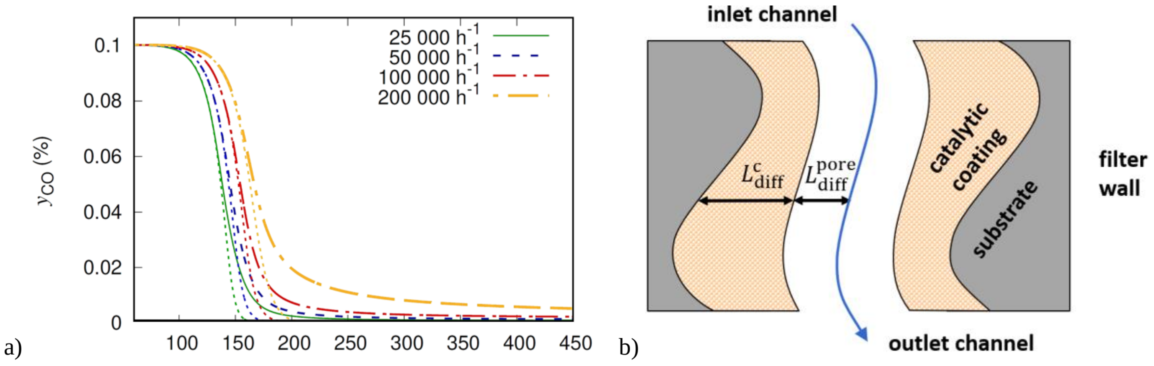

Figure 2. (a) CO light-off curves calculated for $y^{\mathrm{in}}_{\mathrm{CO}} = 0.001, y^{\mathrm{in}}_{\mathrm{O_2}} = 0.05$ at different gas hourly space velocities using heterogeneous model with effectiveness factor; dotted lines show unlimited homogeneous model results.
(b) Schematics of diffusion limitations in the filter wall.

4. Conclusions

The 1D+1D model of a catalytic filter can be extended to consider diffusion limitations inside porous wall, which can improve predictions of reactant conversion [1]. The model takes into account diffusion limitation in both the gas inside the free pores and in the catalytic coating. Macroscopic simulations can effectively describe the filter's performance with little computational demand by using the averaged micro-scale structure of the wall. The predicted reactant slip at increased flow rates (Figure 2b) agrees well with the observations from lab reactor experiments [2].

References

[1] J. Němec, M. Plachá, P. Kočí, Chem. Eng. J. 461 (2023), 141847.
[2] R. Pečinka, M. Blažek, R. Knopp, P. Kočí, A. York, Chem. Eng. Sci. 260 (2022), 117876.

Keywords

Heterogeneous catalysis; exhaust gas aftertreatment; catalytic particulate filter; mathematical modeling.